Final Report

MarsExplore

Gravity Mapping of Mars Powered by Quantum Sensing

DSE Group 10

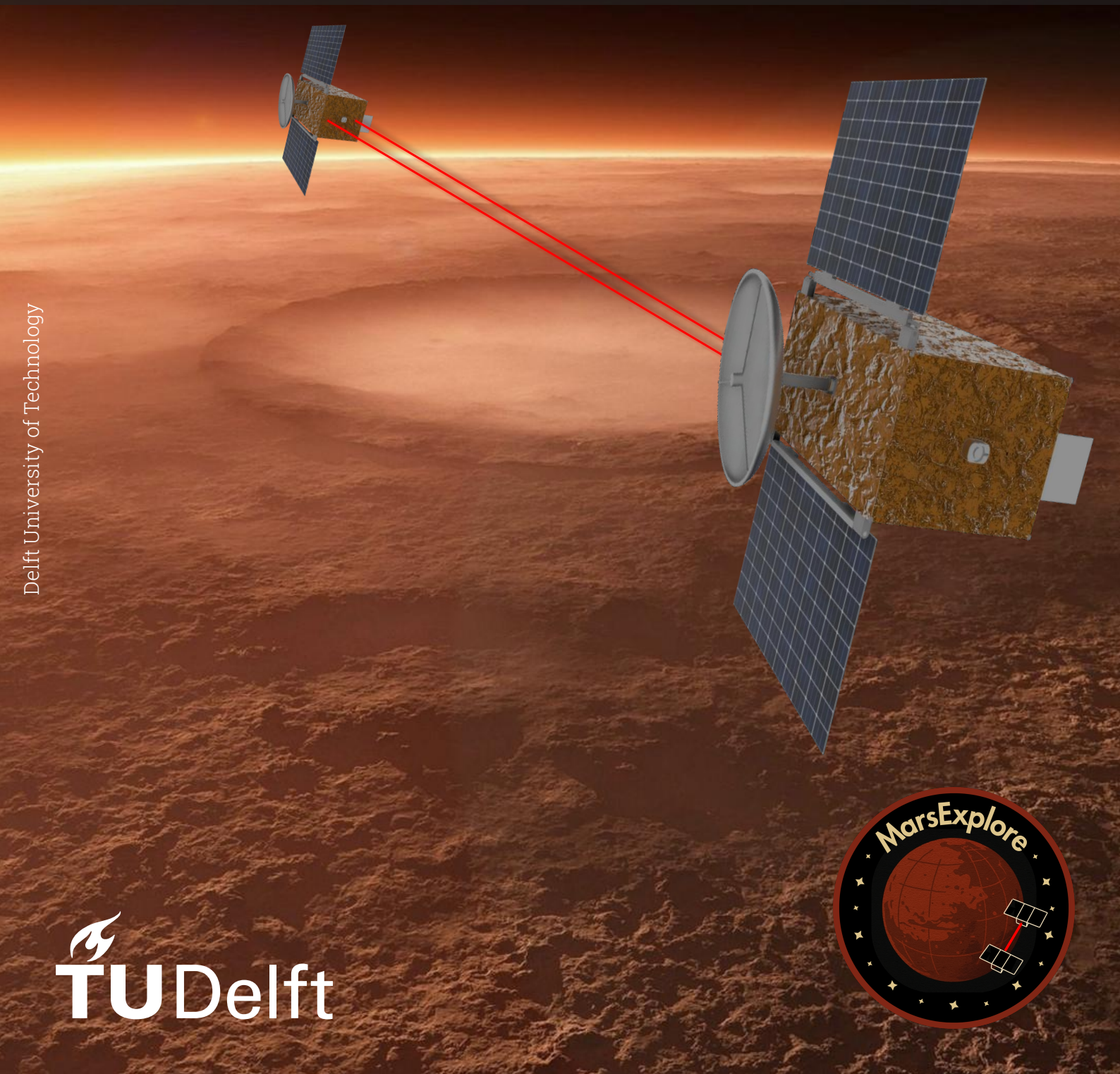

Delft University of Technology

TU Delft

MarsExplore

Final Report

by

Group 10

Name	Student Number
Yasmine Mafoutsis	5687969
Santiago Armada Gamboa	5691311
Pablo Garcia-Conde Ortiz	5692458
Viktor Hazenoot Raddum	5732115
Marco Insinga	5733197
László Jirkovszky-Bari	5754216
Bern Sluis	5759412
Gaia Barocco	5763517
Veronica Fossa	5779960
Mito Apfelstedt	5799716

Tutor: Bart Root
Coaches: Francesco Orefice, Sasha Vlaskin

Project Duration: April 2025 – June 2025

Version	Date	Authors	Description
1.0	18/06/2025	All	Produced Final Report draft.
2.0	24/06/2025	All	Produced finalised Final Report.

[1] Cover background available at: `https://www.techspot.com/news/84142-nasa-insight-lander-detects-marsquakes-red-planet.html` (Accessed: 19 June 2025).

Contents

List of Abbreviations and Symbols

List of Abbreviations

ADCS	Attitude Determination and Control Subsystem
CaC	Cost at Completion
CAI	Cold Atom Interferometer
CAV	Optical Cavity
CDHS	Command and Data Handling Subsystem
CMT	Centre of Mass Trim Assembly
CoM	Centre of Mass
DDI	Development Difficulty Index
DED	Design Engineering Difficulty
DLR	German Aerospace Centre
DSE	Design Synthesis Exercise
ECSS	European Cooperation for Space Standardization
EPS	Electrical Power Subsystem
ESA	European Space Agency
FBS	Functional Breakdown Structure
FFD	Functional Flow Diagram
HGA	High-Gain Antenna
IMSS	Integrated Mission System Simulator
IRU	Iodine Reference Unit
LAS	Laser Source
LCA	Life Cycle Assessment
LGA	Low-Gain Antenna
LRI	Laser Ranging Interferometer
USO	Ultra Stable Oscillator
XFS	Xenon Feed System
BOL	Begin of Life
EOL	End of Life
LRP	Laser Ranging Processor
MGS	Mars Global Surveyor
MLI	Multi-Layer Insulation
MRO	Mars Reconnaissance Orbiter
MTI	Mars Transfer Injection
NASA	National Aeronautics and Space Administration
OBA	Optical Bench Assembly
OBC	Onboard Computer
OBE	Optical Bench Electronics
OMIS	Optomechanical Inertial Measurement Unit
PCDU	Power Control and Distribution Unit
QCD	Quasi-Circular Depression
QPR	Quadrant Photoreceiver
RAMS	Reliability, Availability, Maintenance, and Safety
SOT	State of Technology
SST	Satellite-to-Satellite Tracking
TCS	Thermal Control System
TMA	Triple Mirror Assembly
TRL	Technology Readiness Level
TT&C	Telemetry, Tracking & Command

List of Symbols

Φ	Gravitational field
r, R	Radius
d	Diameter
a	Semi-major axis
T	Orbital period
V	Velocity
E	Energy
θ	Latitude
ϵ	Error
ρ	Density
G	Gravitational constant
t	Time
ϵ	Strain
I_{sp}	Specific Impulse
I	Moment of inertia
D	Drag
m	Mass
α	Accommodation coefficient
α	Absorptivity
μ	Mass ratio
r	Speed of incident molecule
C_D	Drag coefficient
t_w	Required rear wall thickness
S	Standoff distance
σ	Stress
E	Elastic modulous
η	Efficiency
P	Power
Q	Heat
T	Temperature
ε	Emissivity

Executive Overview

Project Goal

The objective of the project is to design an ESA M-Class requirement compliant mission to map the gravity field of the planet Mars. A planet's gravity field informs on its internal structure, together with shifts and dynamics within its density. By comparing these to Earth's dynamics, both the Earth's and Mars' dynamics can be understood better, allowing for deeper insights into phenomena such as climate change, seismic activity, seasonal variations or volcanic eruptions. Furthermore, potential locations of subsurface water and ice deposits to support an eventual landing party can be found.

In the Midterm Report, a mission concept was chosen that involves two spacecraft. In order to determine the gravitational field, the distance between them is measured over time, as gravitational changes affect the spacecraft. The effect of gravity is isolated by measuring other disturbing effects on the spacecraft with a cold-atom interferometer, a novel quantum sensing payload that acts as an accelerometer.

Science Overview

On Mars, a precise gravity map can help understand the unknown formation of specific regions of the planet, better landings and orbit insertions, and perform predictions of both Mars' and Earth's atmosphere. MarsExplore measures the static gravity field of Mars, monitors temporal variations in this, analyses perturbations in Mars' gravity field due to external bodies, and analyses seasonal changes of Mars' polar caps to better understand their influence on Mars' geophysical system.

MarsExplore aims to find and analyse several geological phenomena. These are:

- Subsurface aquifers: the high surface temperature of Mars does not allow water to stay in a liquid state, however, liquid water could be found at depths of 2-20 km.
- Quasi-Circular Depressions: circular depressions on Mars' surface, and beneath, can contain rich materials and provide insight into potential asteroid impacts.
- Volatile-rich sediments: reservoirs such as ancient mud volcanoes potentially preserve records of early Martian environmental conditions. On Earth, mud volcanoes often host microbial ecosystems, making their Martian counterparts promising targets in the search for biosignatures.
- Mantle Dynamics: by monitoring seasonal and long-term gravity changes, the martian mantle can be understood in more depth.
- Mars Atmosphere: the Martian atmosphere is thin and primarily composed of carbon dioxide, and it plays a dynamic role in seasonal and annual cycles. It is strongly affected by seasonal changes of CO_2 and water polar caps. Better models for the Martian atmosphere can help understand seasonal variations.

Market Analysis

MarsExplore will be proposed to the upcoming ESA Medium-Class (M-class) Mission Call. Analysing the competitors and MarsExplore's uniqueness is important to win the proposal. The criteria used by the experts to select the best mission are: science value, scientific feasibility, timeliness, and complementarity with other projects.

ESA's long-term interest in habitability and eventual human exploration of Mars increases the possibility for additional complementary missions, particularly in gravity mapping, which is a currently unexplored domain. This is one of MarsExplore's main unique selling points. Especially its pioneering in the quantum technologies domain fills a critical science gap, as current gravity models

of Mars. Quantum technology is a large up-and-coming domain, with recent investments by the European Commission of over 50 million euros.

MarsExplore has several direct competitors, from countries all around the globe. The M-Matisse mission has been identified as the most direct competitor of MarsExplore, due to its focus on Mars exploration. The ORACLE mission proposes studying Mars' performing gravity field as well. The fact that multiple scientific teams are proposing similar missions highlights the importance of this exploration initiative.

Payload

Numerous payload instruments are included for the mission. Firstly, the Laser Ranging Interferometer (LRI) is used to measure the distance between the two spacecraft. This laser is stabilised with an Iodine Reference Unit, and the laser link is acquired with a sensor that detects the neighbouring spacecraft called MiniCAS.

The cold-atom interferometer measures the accelerations on the spacecraft very precisely, in addition to the OMIS accelerometers. This allows for isolation of the effects of gravity on the satellites, against the effects of drag for example. Finally, a set of masses called the CMT is moved to stabilise the spacecraft measurements. These instruments present a new and improved way of performing gravity science which has never been done before, highlighting the uniqueness of the MarsExplore mission.

Mission Design

The Ariane 62 rocket is selected as the launcher for the mission, to be launched from Guiana Space Center near October 8th 2041. The spacecraft will be put on a transfer trajectory to Mars, where they will arrive 8 months later. Upon arrival, the spacecraft will capture into Mars orbit and perform an aerobraking manoeuvre to lower their orbit without expending fuel, over a span of 3 months. Arriving in the final desired orbit, the spacecraft will spend 2 more months analysing the health of the spacecraft, and deploying all the instruments. Science operations will then last one Martian year, which equates to 1.9 Earth years. Then, the spacecraft will be decommissioned by placing them on a higher graveyard orbit, that will remain stable for the next 200 years, and will not interfere with other Mars missions.

Spacecraft Design

The spacecraft design dives deeper into the design of each subsystem.

Propulsion

The propulsion subsystem is responsible for all manoeuvres required, including orbit insertion and station keeping. A hybrid propulsion system is employed, with bipropellant and electric thrusters being used.

ADCS

The Attitude Determination and Control Subsystem (ADCS) determines the attitude of the spacecraft and orients it according to the needs of other subsystems. The main design driver of the ADCS is how accurately it has to point the spacecraft. Based on these requirements the spacecraft will make use of star trackers and gyroscopes during science mode, and sun sensors and horizon scanners during safe mode. For attitude control, the ADCS will employ cold gas thrusters with gaseous nitrogen as the propellant

TT&C

A dedicated communications subsystem is designed in order to allow communication with Earth at all times. This includes 1.6 m antennas on both spacecraft, to allow communication with Earth in case

one of them breaks. As a result, the science data can be safely transmitted back to Earth.

CDHS
The spacecraft contains an onboard computer that carries out all commands received from Earth and links all the subsystems.

Thermal
The thermal subsystem is responsible for maintaining all instruments at the correct temperature. It consists of heaters, thermometers, radiators and heat blankets.

Electrical Power Subsystem
The electrical power subsystem (EPS) is responsible for generating and supplying the entire spacecraft with power. It achieves this by being equipped with two solar array wings. Furthermore, it has three Lithium-ion batteries (two for redundancy). The distribution is managed by the Power Control and Distribution Unit (PCDU). The main design driver of the EPS is the power required by all the spacecraft components, which sizes the solar array, along with the large peak power burst required by the electrical propulsion subsystem, which mainly sizes the battery.

Structures Subsystem
The primary function of the Structures Subsystem is to house and protect all spacecraft components from mechanical loading, radiation, magnetic fields and space debris. Its design is driven by loads acting at the ending phase of launch, as well as by the slenderness of the structure's stiffening elements. The resulting structure is a semi-monocoque thin walled cuboid: it measures (3 m x 1.7 m x 1.2 m), it is made from Aluminium, and is stiffened by a total of 8 stringers.

Design Overview
Budgets
The final design has a dry mass of **691.4 kg** and a wet mass of **1124 kg**. Further it will have a spacecraft power of **842 W** at end of life. The cost at completion of the spacecraft will be **716 M€**, which can be split into the various mission activities as seen in Figure 1. It should be noted that this is exceeds the requirement by ESA. As such additional funding from government agencies such as NLR and DLR should be pursued.

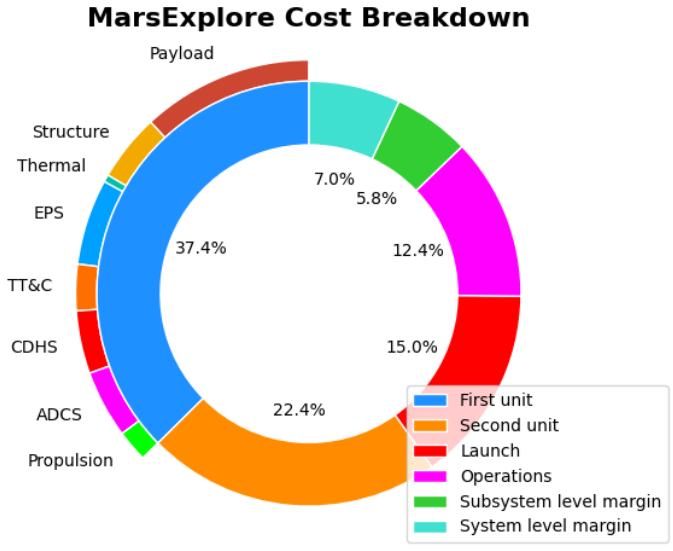

Figure 1: Cost breakdown into all mission activities

Internal and External Configuration

The internal and external views of the spacecraft are presented below.

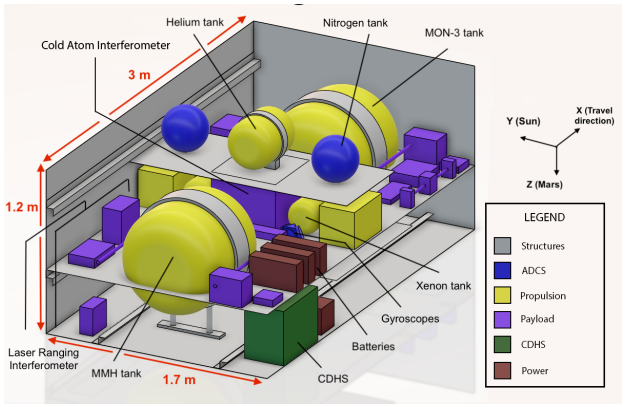

(a) Internal configuration viewed isometrically

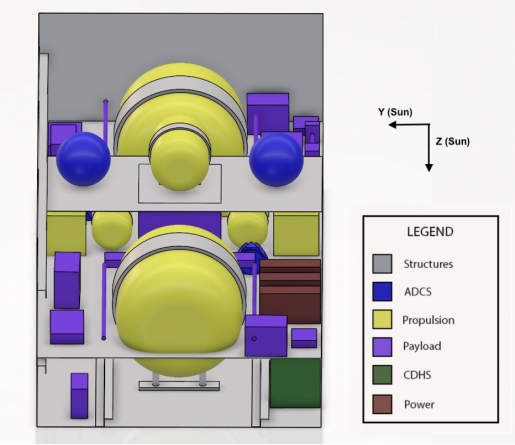

(b) Internal configuration viewed in the flight direction

Figure 2: Comparison of internal configurations from two viewpoints

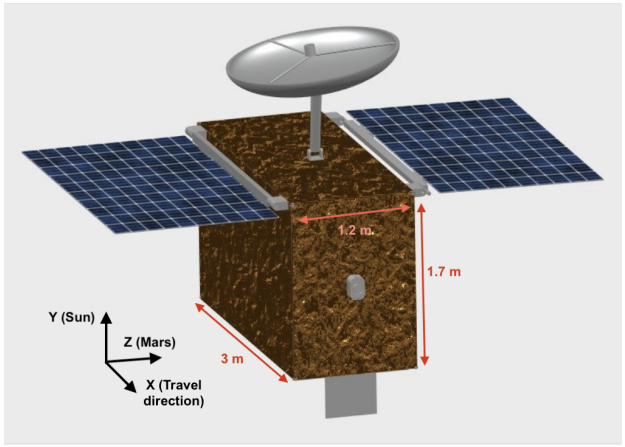

(a) External configuration viewed isometrically

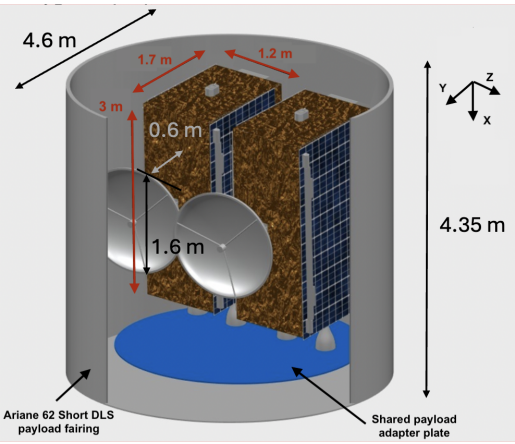

(b) External configuration viewed in the Ariane 62 launcher, undeployed

Figure 3: Comparison of external configurations, deployed and undeployed in launcher

Verification and Validation

The Verification & Validation Plan uses the V-model. Product verification focuses on achieving the system and subsystem requirements using:

1. Inspection: visual assessment conducted in ISO Class 8 cleanrooms, inspection ensures compliance with design documentation.
2. Analysis: models simulate system behaviour where physical testing is impractical employing advanced software.
3. Demonstration: physical setups confirming basic system functions.
4. Testing: structural, functional, thermal and integration tests were conducted at system level and a comprehensive list of subsystem-specific tests were developed at subsystem level. These

will be carried out in facilities such as ESA's HYDRA, LSS, and other specialised labs. The DLR Institute of Space Propulsion will be used for the bipropellant propulsion subsystem.

Product validation focuses on the mission-level objectives using the Integrated Mission System Simulator (IMSS) and the Ground Segment Testbed (GST). This is done through:

- End-to-End Testing (E2E): two main E2E tests simulate operations over a Martian year to verify static and temporal gravity field mapping respectively.
- Scenario-Based Testing: special scenarios like communication blackout and atmospheric drag variability are tested.

Lastly, model verification will ensure code correctness via code review, unit and system testing, through tools like Pytest. In terms of model validation, model predictions are made with inputs from data from heritage missions and the difference between the model output and the actual data is discussed.

Concluding Remarks

This report aimed to justify the final detailed spacecraft design as well as the final mission design. Through the thorough analysis, calculations, research, and modelling, this aim was realised, resulting in a justified spacecraft design and mission design.

Further design iterations are recommended to optimize the design and increase mission robustness. The current concept involves multiple mission phases. Specifically, the aerobraking phase and end-of-life could be better determined in order to better size the spacecraft to withstand critical phases. a kick stage for orbit insertion, as well as a third satellite for communication, could be considered. Discussions between planetary scientists and payload manufacturers must take place to determine the required sensitivity of the LRI. Finally, the cost estimation can be improved by adopting a bottom-up methodology.

1 Introduction

As Mars continues to garner increased scientific interest, there is a need to gain a deeper understanding of the planet's development history and internal processes. Research suggests that Mars' surface would have had an abundance of water in the past. It is expected that subsurface reservoirs still hold liquid water and volatile-rich sediments, which could give important insight into possible life on the Red Planet, in the past and present, and also bring invaluable knowledge for future exploration of Mars. Another key point of attention is the presence of mantle activity, which could explain the Tharsis Rise and Crustal Dichotomy, or the seasonal behaviour of the CO_2 ice at the poles and the effect of the Martian moons [1]. These areas of interest require an improved understanding of the static and dynamic Martian gravity fields to an unprecedented level of accuracy. Fortunately, advancements in quantum sensing offer the accuracy necessary to resolve these gravity anomalies, improving upon the success of previous Earth gravity missions such as GRACE, GRACE-FO, and GOCE, which have yet to be carried out on another planet.

The mission objective is to design an ESA M-Class-compliant mission to map the static and dynamic gravity field of the planet Mars, demonstrating the effectiveness of novel quantum sensing instruments, with a group of 10 people over 10 weeks. The mission shall launch in 2041 on a European launcher, with a total cost of 670 million euros. This report aims to justify the final detailed spacecraft design as well as the final mission design.

The current report builds upon the Midterm Report, which considered Doppler tracking, gravity gradiometry, and two Satellite-to-Satellite Tracking (SST) concepts [2]. The first is akin to the GRACE-FO mission and is characterised by a Laser Ranging Interferometer (LRI) and an electrostatic accelerometer in its payload. The second also includes an LRI but incorporates a cold-atom interferometer (CAI) instead to measure non-gravitational disturbances. The Midterm Report concludes that the optimal configuration is a dual-satellite SST mission using an LRI and CAI. This design was selected based on a weighted trade-off considering mass, power, risk, cost, static and dynamic gravity field resolution, and sustainability, and validated by sensitivity analysis. The preferred orbit is a 212 km sun-synchronous dawn/dusk orbit with a 30-sol repeat cycle, inserted via aerobraking and a mid-course inclination change to minimize ΔV.

The science goals are covered in Chapter 2. Chapter 3 presents the market analysis, detailing the mission-relevant stakeholders and markets. The science acquirement methodology is explained in Chapter 4. The mission design, in Chapter 5, explains all mission phases and the mission functional analysis. The spacecraft design is justified at the subsystem level in Chapter 6. An overview of the final design is provided in Chapter 7. The verification and validation of the mission are justified in Chapter 8. The compliance matrix, project design and development logic, and additional risks can be found in the appendix.

2 Science Objective

Gravity is one of the nature's most fundamental forces. A gravitational field is present in all corners of the universe and is deeply rooted in the workings of reality. Gravity exploration methods depend on the identifying discrepancies in density between geological features and their surroundings. The magnitude of the gravity field is determined by measuring the disturbances acting on a test mass [3]. Such an instrument is know as a gravimeter.

On Earth, gravity space missions such as GOCE [1], GRACE [2], and GRACE-FO [3] helped with the understanding of our planet through observations of the variations in the hydrological cycle, measurements of ice losses of glaciers, quantification of sea level changes, detection of water droughts and changes in the water held in the major river basins, and much more.

The gravitational field is described by the potential field Φ. At a point above the planet's surface, with spherical coordinates r, latitude θ, and longitude ϕ, it can be expressed as a sum of Legendre functions:

$$\Phi(r,\theta,\phi) = \left(\frac{\mu}{r}\right)\left(1 + \sum_{l=2}^{l_{\max}}\left(\frac{R}{r}\right)^{l}\sum_{m=0}^{l} F_{l,m}(\theta,\phi)\right) \tag{2.1}$$

where μ=GM is the monopole moment, R is a reference radius, and

$$F_{l,m}(\theta,\phi) = P_{l,m}[\sin\theta]\left(C_{l,m}\cos(m\phi) + S_{l,m}\sin(m\phi)\right) \tag{2.2}$$

where P_{lm} are the Legendre polynomials of degree l and order m, and C_{lm} and S_{lm} are the spherical harmonic coefficients.[4] The higher the order l, the smaller the spatial scale. The variations in the areoid (= Martian reference surface from which elevations are measured) height can be fully described by the spherical harmonic coefficients C_{lm} and S_{lm}, referred to as Stokes coefficients. It is this set of coefficients that is estimated from the satellite measurements. [5] Spherical harmonics are mathematical functions used to describe variations on a sphere, organized by the two parameters degree and order. The degree represents the level of spatial resolution of the spherical harmonic function, while the order represents the number of wave-like variations around the planet's longitude, in the east-west direction [6]. A higher d/o corresponds to smaller-scale features on the planet's surface. For example, a d/o of 1 describes very large, global features, while higher d/o values capture finer details.

Satellite-based gravity data must be corrected before geophysical interpretation. The Free-Air Correction compensates for the altitude of the observation point, acknowledging that gravity weakens with height. The Bouguer Correction adjusts for the gravitational attraction of the rock mass between the measurement point and sea level. Applying these corrections isolates subsurface mass anomalies and allows accurate recovery of a planet's gravitational structure.

Mars' gravity field provides critical insights into its internal structure and seasonal processes. Figure 2.1 helps visualize the detectable features of Mars, and shows how MarsExplore would dramatically push the boundaries of what can be observed.

[1] https://www.esa.int/Enabling_Support/Operations/GOCE(Accessed 17/06/2025)
[2] https://earth.esa.int/eogateway/missions/grace(Accessed 17/06/2025)
[3] https://gracefo.jpl.nasa.gov/(Accessed 17/06/2025)

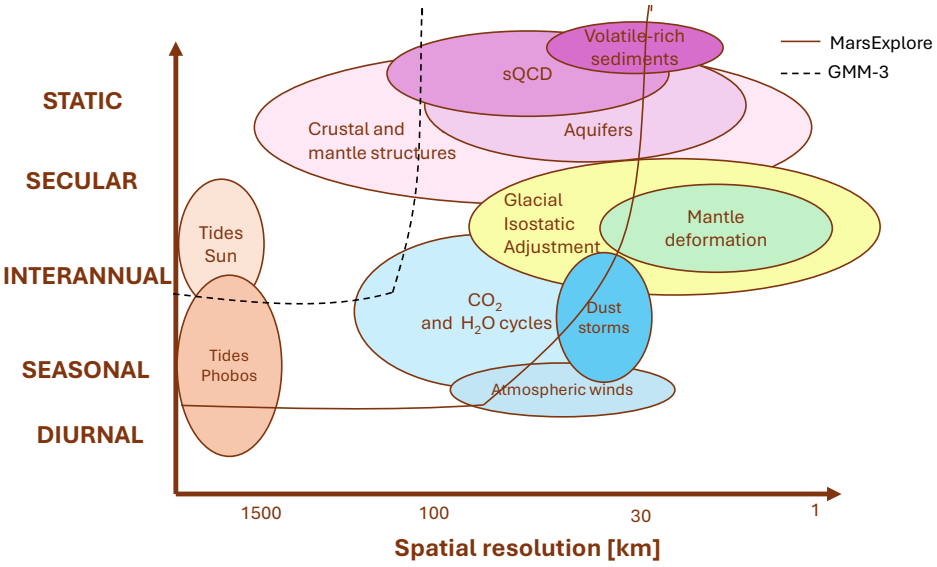

Figure 2.1: Temporal and spatial scales of gravity field detectable by MarsExplore

The planet's average surface gravity is 3.728 m/s^2, 38% of Earth's, but variations reveal hidden subsurface features such as subsurface water and crustal thickness. Gravity maps allow for the inside of a planet to be observed. On Mars, a precise gravity map can help understand the unknown formation of specific regions of the planet, better landings and orbit insertions, and perform predictions of both Mars' and Earth's atmosphere. The current gravity field maps of the Red Planet are derived using Doppler and range tracking data from three NASA spacecraft in orbit around Mars: Mars Global Surveyor (MGS), Mars Odyssey (ODY), and the Mars Reconnaissance Orbiter (MRO). Slight differences in Mars' gravity change the trajectory of a spacecraft and alter the signal being sent from the spacecraft to the Deep Space Network, allowing for the gravity field to be reconstructed. The current map, visible in Figure 2.2, has a resolution of around 120 km and helps interpret how the Martian crust has evolved throughout its history. [4]

[4] `https://www.jpl.nasa.gov/news/new-gravity-map-gives-best-view-yet-inside-mars/`

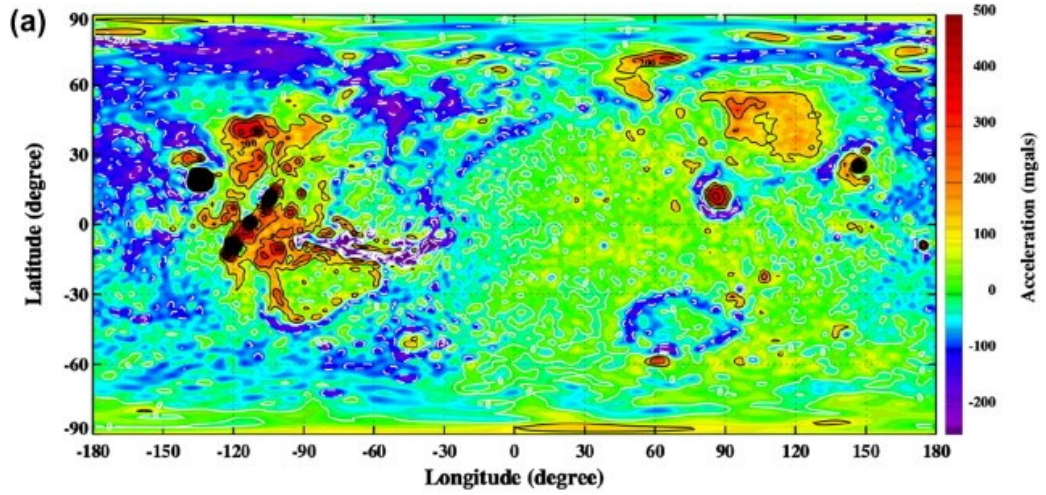

Figure 2.2: Surface gravity anomalies complete to degree and order 90 with respect to the reference ellipsoid (f = 1/196.9, Re = 3397 km) [7]

The unanswered questions that the MarsExplore gravity mission wants to address are:

- **SQ1** *Is there liquid water beneath the surface of Mars? If so, where is it located, and what are its depth and spatial extent?*
- **SQ2** *Are there volatile-rich subsurface sediments on Mars, and how are they distributed geographically?*
- **SQ3** *How does the mass and orbital motion of Phobos influence Mars' gravity field?*
- **SQ4** *Where are the stealth Quasi-Circular Depressions located, and what are their characteristics?*
- **SQ5** *Is the Martian mantle still geologically active?*
- **SQ6** *What are the driving mechanisms behind the seasonal polar caps changes?*
- **SQ7** *How do gravity waves influence the atmospheric dynamics and winds?*

These scientific questions translate into clear mission objectives, which MarsExplore aims to achieve.

- **SO1** Map the static gravity field of Mars (target resolution: higher than 120 km) to identify subsurface mass anomalies, supporting the investigation of subsurface water, volatile-rich sediments, and stealth impact features. (Addresses SQ1, SQ2, SQ4)
- **SO2** Monitor temporal variations in Mars' gravity field with an accuracy of 0.018 μGal/year to detect changes related to mass redistribution in the mantle, polar caps, and atmosphere. (Addresses SQ5, SQ6, SQ7)
- **SO3** Analyse the perturbations in Mars' gravity field induced by Phobos and seasonal changes of polar caps to better understand their influence on Mars' geophysical system. (Addresses SQ3, SQ6)

Each main area of research has to be analysed in detail, and the expected signals have to be estimated to define a list of requirements derived from the Scientific Questions.

2.1. Measured Signal

Qualitative estimates of the achievable static field resolution can be derived from the error covariance analysis presented in [4]. The satellite-to-satellite tracking is the methodology used in the MarsExplore mission, and its accuracy can be calculated using:

$$\sigma_l^{\text{sat-sat}} = \left(\frac{\varepsilon}{\sqrt{N}}\right)\left(\frac{1}{nr}\right)\left(\frac{r}{R}\right)^l F_l \tag{2.3}$$

$$F_l^{\text{sat-sat}} = \frac{l}{\sqrt{2+4l+4l^2}} \cdot \frac{1}{|\sin(\gamma/2)|} \tag{2.4}$$

where N is the number of observations, each of accuracy ϵ, resulting in the error estimate σ, at degree l. R is the radius of the planet, in this case Mars, r the distance of the satellite from the centre of mass, and n the mean motion of the satellite's orbit around Mars [4]. An example can be observed in Figure 2.3, where three different ϵ values have been plotted. This value strongly influences the sensitivity of the measurements. Moreover, a longer mission duration is essential for observing time-variable gravity signals, which require a very small error in low frequencies.

The oscillating behaviour observed in Figure 2.3 is caused by the factor $\frac{1}{2|\sin l\gamma/2|}$, where γ is the inter-satellite angle. This factor goes to infinity at $l = 2\pi k/\gamma$, where k is a positive integer. SST is effectively insensitive to the effect of gravity at such wavelengths since there is no differential acceleration between the two spacecraft [4]. To avoid this problem, the spacecraft separation has to be set in a way that avoids these singularities. A separation of 58 km between the satellites would avoid these singularities.

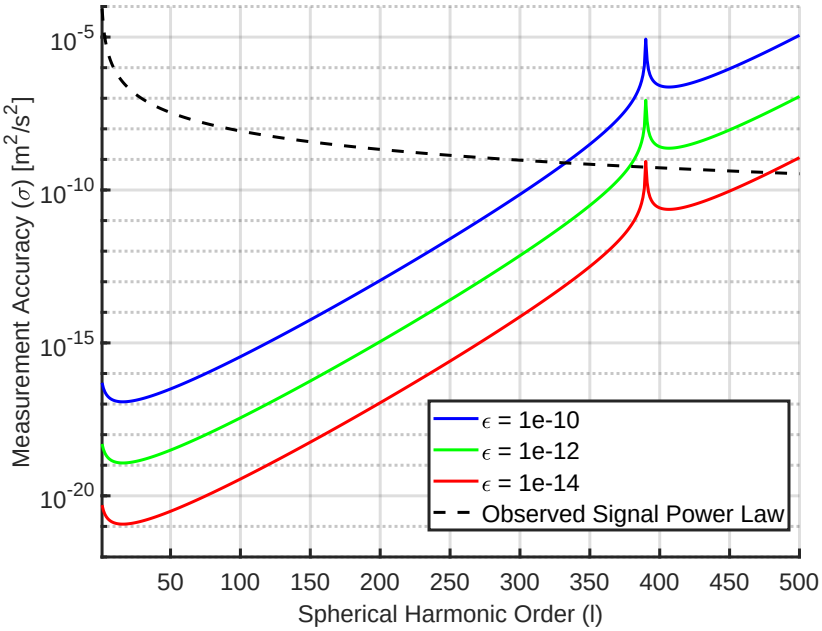

Figure 2.3: Estimated gravity signal error for 1 Martian year SST measurements with LRI + CAI payload and different optical error links. Frequency of measurements 10 Hz, altitude 212 km

In Figure 2.3 the black dotted line represents the observed signal power law, which for Mars is $RMS[\Phi_l] = \frac{8.5\times10^{-5}}{l^2}$ and quantifies the expected strength of the gravity signal at a specific spatial scale. This is the square root of the mean variance per degree, which is a one-dimensional error measure, [8], derived from the degree variance through Equation 2.5.

$$RMS_l = \sqrt{\frac{V_l}{2l+1}} \tag{2.5}$$

Here, V_l indicates the degree variance or error power per degree. The intersection between the black line and the error curve indicates the highest accuracy of the static gravity field that can be reached. The ϵ value of 10^{-14} represents the highest accuracy in measurements. Current models estimate an error of 10^{-10} [9]. Other sources estimate an achievable error value of 10^{-12} [9, 10]. The required optical link error is closely linked to the spacecraft's payload capabilities and directly sets the

performance requirement for the ranging noise of the Laser Ranging Interferometer (LRI), which is commonly expressed in units of $\mathrm{nm}/\sqrt{\mathrm{Hz}}$. Achieving low noise levels depends on the satellite's ability to minimize pointing noise and on the thermal noise environment, which needs to be minimized especially at low frequencies [11].

2.2. Aquifers

Addresses Science Question 1

Water is one of the fundamental prerequisites for life as we know it on Earth, and its presence is a key indicator in the search for potentially habitable environments. On Mars, the detection of subsurface aquifers could provide critical evidence of past or even present water activity, with profound implications for planetary science, astrobiology, and future human exploration.

The high surface temperature of Mars does not allow water to stay in a liquid state and the current understanding of the subsurface thermal gradients suggests that liquid water is stable at depths of kilometres, in ranges from 2–7 km in the equatorial regions and 11–20 km near the poles [12], as shown in Figure 2.4. Deep environments with liquid water on Mars are likely similar to those found in Earth's subsurface, where the majority of microbial terrestrial biomass resides. Currently, a thin layer of liquid water, about 20 km wide, in the South Pole of Mars is hypothesised to lie beneath a 1.5 km-thick part of the polar ice cap [13]. Moreover, some crater lakes filled with groundwater could exist below the surface, across 100 km [14].

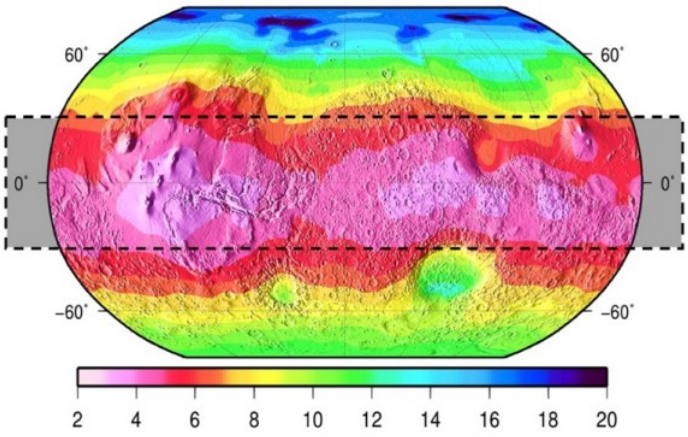

Figure 2.4: Groundwater depth map [km] [12]

In order to produce requirements to detect the subsurface liquid water, named aquifers, the expected signal has to be modelled. To do so, a model that randomly allocates a specific number of aquifers on Mars and generates the degree of variance has been used. The degree variance denotes the total error power of a certain degree l. The model inputs are:

- Number of aquifers to allocate;
- Depth;
- Density;
- Size;
- Altitude of observation (orbit altitude for satellite measurements);
- Resolution.

To realistically predict the signal of aquifers, the density of water has been assumed to be 1271 kg/m^3, which is consistent with a dust proportion of 15% by volume [15]. Subsequently, three depths have

been assumed as 3 km, 11 km, and 20 km, consistent with estimates by Stamenkovic [12]. The size of the presumed aquifers is the biggest uncertainty. One example of the degree variance and the gravity signal predicted by this model is presented in Figure 2.5.

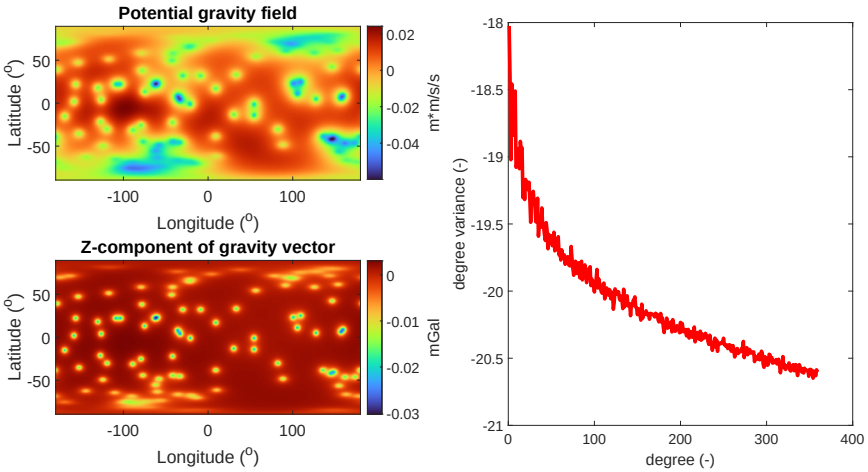

Figure 2.5: Predicted gravity signal of 100 Aquifers, 5 km in Size, 100 m in thickness, and 2 km deep.

In Figure 2.6, the measurement accuracy of Doppler observations and SST is compared. Using Doppler measurements alone, the aquifer signals are barely detectable. In contrast, SST provides much higher resolution, allowing for clearer visibility of the aquifers and revealing their spatial distribution in greater detail. As expected, deeper aquifers produce a weaker gravity signal, making them more challenging to detect.

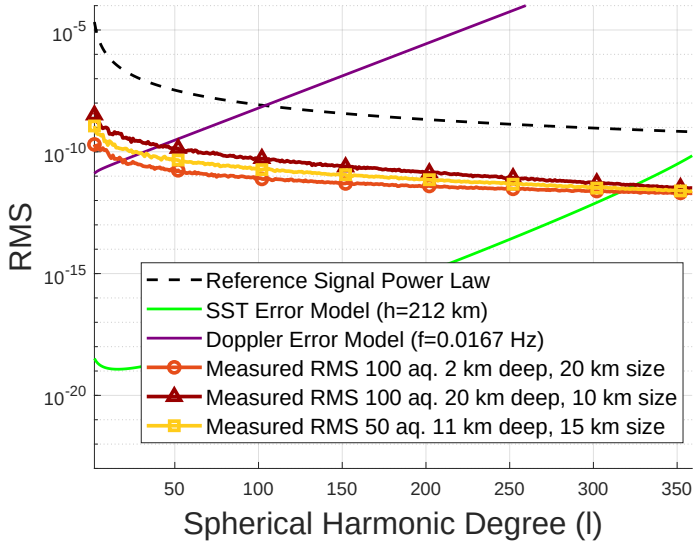

Figure 2.6: Measurement of aquifers' accuracy versus degrees (1 Martian year)

2.3. Quasi-Circular Depressions

Addresses Science Question 4

Quasi-Circular Depressions (QCDs) are defined as any depression of Mars' surface that appears to be somewhat circular. Some of these are obvious impact craters, others are large circular fractures which are theorised to cover buried impact craters, and others have no corresponding visible structural

feature on the surface and are called stealth QCDs (sQCD) [16]. These are theorised to be the surface representation of completely buried impact craters. The Mars Orbiter Laser Altimeter (MOLA) yields a high-precision topographic data set and identifies many sQCD across Mars [17]. It can map sQCD in a 7-110 km range diameter, and more than four hundred are found, especially located in the northern lowlands [16]. The northern lowland surface is considerably younger than the southern highlands. It is determined that an older lowland basement is buried under a younger cover material, which has to be around 20 km thick to account for the present-day topography [17].

sQCDs are mainly composed of outflow channel sediments, such as mud, sand, dust, volatile-rich mantle, silt, sedimentary deposit, and fluvial deposit [17]. Outflow channel sediments are sinuous incisions containing streamlined islands that can be thousands of kilometres long and hundreds of kilometres wide, with depths reaching 2.5 km, and densities from 2900 kg/m^3 (basalt) to 1200 kg/m^3 (volcanic ash)[18, 19]. Martian dust has a density of 2730 kg/m^3, while Martian sand has a density of 1000 kg/m^3. Moreover, QCDs have a thickness of 2.8±0.6 km, so this can also be assumed for sQCDs [20, 21]. The same model as for aquifers can be used to estimate the signal of sQCDs. An example is presented in Figure 2.7, where two different sQCDs are plotted. It is relevant that the difference in composition is better detectable at higher d/o; therefore, the higher resolution the mission has, the more the material of QCDs can be identified with precision.

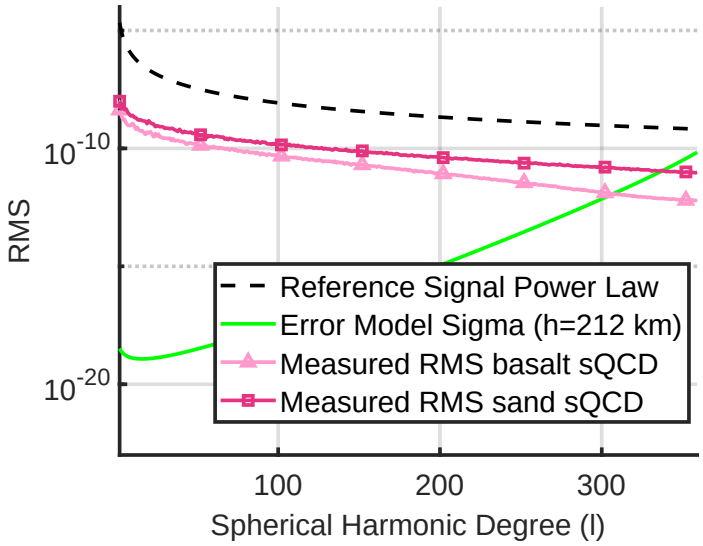

Figure 2.7: Predicted gravity signal of 100 QCDs, 2.8 km thick and 20 km deep.

2.4. Volatile-Rich Sediments

Addresses Science Question 2

Numerous landforms observed on Mars, particularly in Utopia Planitia and Acidalia Planitia, have been interpreted as evidence of volatile-rich sediment reservoirs, potentially in the form of ancient mud volcanoes. These features are believed to result from the mobilisation and eruption of subsurface, volatile-laden sediments—processes similar to terrestrial mud volcanism. Such activity might have enabled the transport of deep materials to the surface, potentially preserving records of early Martian environmental conditions. On Earth, mud volcanoes often host microbial ecosystems, making their Martian counterparts promising targets in the search for biosignatures [1].

Utopia Planitia, a vast lowland basin, hosts a range of landforms fractured rises (5–50 km wide), elliptical mounds (2–12 km wide, up to 200 m high), pitted cones (<300 m high, about 6.4 km wide), and expansive depressions (10–6800 km^2 in area). [22] These morphologies suggest weak enclosed

materials, which might have been triggered by seismic or tectonic activity [22]. Many of the mounds indicate repeated eruptive events by displaying lobes and central pits. Such volatile-rich sedimentary systems may offer critical insight into the geologic, hydrologic, and potential biologic evolution of Mars.

To estimate the gravity signal produced by these volatile-rich sediments, the same model used for sQCDs and aquifers is used. The density is assumed to be the same as the sediments of Earth, where mineral-rich/organic-poor soils have densities in the range of 2400-2900 kg/m^3 and mineral-poor/organic-rich sediments have densities between 1000-1500 kg/m^3 [23].

2.5. Mantle Dynamics, Temporal Changes, Phobos, and Polar Caps

Addresses Science Questions 3, 5 and 6

Mars has two moons, Phobos and Deimos, which are thought to be captured asteroids. Phobos is closer to Mars, and it is not perfectly spherical. The uneven mass distribution interacts with Mars' gravity field and alters its gravitational pulls. This causes periodic oscillation in Phobos' rotation angle and the orbit's periapsis to drift. Its orbital period around Mars is 0.32 days [5] and needs to be accounted for in the measurements. Determining the frequency dependence of Phobos can provide further constraints on both Mars' interior and evolution [24]. Moreover, the masses and orbits of Phobos and Deimos need to be accounted for in the gravity field recovery process. The dynamics of the Martian moons, unlike atmospheric density, are well constrained and predictable, allowing for not polluting the gravity recovery [25].

The second-degree Love number, k_2, quantifies how much a planetary body deforms gravitationally in response to tidal forces, such as the one exerted by Phobos or the Sun. k_2 depends on the internal structure, mainly the density, rigidity, and viscosity of the mantle and core, and it reflects how responsive the planet is to external gravity. To estimate the error in the k_2 measurements, Equation 2.6 is used [4].

$$\sigma_{k_l} = \left(\frac{\varepsilon}{\sqrt{N}}\right)\left(\frac{1}{nr}\right)\left(\frac{r'}{R}\right)^l (2l+1)\frac{GM}{GM_p}\left(\frac{r_p}{R}\right)^{l+1} F_l \tag{2.6}$$

where r_p is the distance to the perturbing body from the centre of the body that is being perturbed, M_p is the mass of the perturbing body, and the other parameters are the same as the ones used in Section 2.1. This analysis shows that with the LRI + CAI configuration, the longer wavelengths of the Sun's effect on k_2 are visible, whereas they are not detectable with the Doppler effect. Any of the three values of ϵ allow for this precision. This enables a better estimation of the Love number and the interior structure of the mantle. Beyond tidal forcing, Mars exhibits significant temporal variations in its gravity field due to seasonal redistribution of mass, primarily driven by CO_2 and H_2O. These, during the Martian summer, sublimate from the polar ice caps and are transported towards the equator, decreasing the mass at the pole and increasing it at lower latitudes. As a consequence, the gravity field flattens. This process is inverse during the winter, and the mass exchange between poles is estimated to be $4 \cdot 1015$ kg [1]. The observed pattern is more complex than current general circulation models predict and suggests additional contributing processes such as subsurface mass movement or viscoelastic crustal responses [26].

The CO_2 forms permanent ice sheets with a thickness of approximately 2 km, covering areas with a diameter of roughly 1000 km and 400 km on the Northern and Southern polar caps, respectively [1]. One way to measure the position of Mars around the Sun is the solar longitude, L_s, which is a seasonal clock of the planet. The Martian year is divided into 360°. The maximum accumulations of ice at the poles have been observed at $L_s \approx 155°$ in the South and $L_s \approx 140°$ in the North [27]. There are two or three significant oscillations per Martian year of the thickness of these ice sheets, which makes it necessary to take measurements for at least one full Martian year. The cycle repeats

[5] https://sci.esa.int/web/mars-express/-/31031-phobos

every $L_s \approx 120°$, leading to a good sampling frequency of approximately $L_s \approx 15°$, based on the Nyquist criterion. Taking at least eight samples per Martian year allows for accurate capture of the seasonal variations, corresponding to sampling approximately every 28 Martian days (sols). Therefore, scheduling repeat orbits every 30 sols ensures sufficient temporal resolution to monitor seasonal changes while maintaining sufficient surface coverage.

Moreover, recent observations captured a slow rate of crustal deformation under the north polar ice cap of about 0.13 mm per year [28]. The north polar cap is likely only a few million years old; therefore, it is currently the only Martian surface feature massive enough to produce measurable deformations. To detect these changes, the Bouguer equation is used. This is based on the assumption of an infinite horizontal slab of uniform density and reduces the gravity value accordingly, partially counteracting the free-air correction [3]. The attraction of an infinite plate of thickness h is described by Equation 2.7.

$$\Delta g_B = 2\pi\rho h G \left(\frac{R}{r}\right)^{l+1} \tag{2.7}$$

where G is the gravitational constant of the planet, ρ the difference between the density of the material and the planet's crust, R the radius of the planet, r the distance from the centre of the planet to the observation point (R + depth of the anomaly), and l the degree of the spherical harmonic term. Assuming a deformation results in using a ρ value of -3550 kg/m^3, which is the negative of the Martian mantle density, which is the one deforming over time. The signal expected and the precision required can be visualised in Figure 2.8, where a precision of 0.0182 μGal/yr is desired for a mission duration of one Martian year. By calculating the total RMS noise with $\sqrt{\sum \sigma^2}$, when using the smallest optical link error of 10^{-14}, the accuracy achieved is 0.3734 μGal/yr, which is not sufficient to detect this deformation. This accuracy can be reached after 5 Martian years of science data gathering.

Personal communication with PhD students from TU Delft, suggested that in the range of RSM values of 10^{-19}-10^{-23}, temporal changes of Martian gravity field can be observed. Figure 2.9 shows that an optical link error of 10^{-14} is required to be able to detect temporal changes in the Martian gravity field. These lines have been plotted using the equations described by Bills et al. over time, and degree 2 [4].

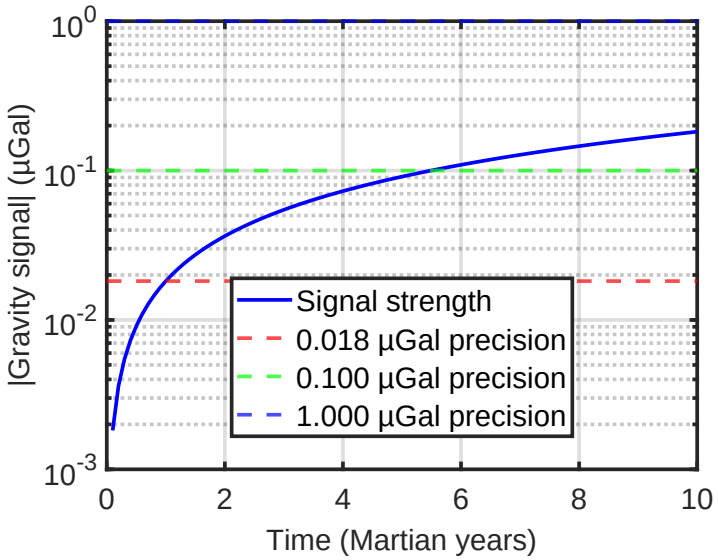

Figure 2.8: Temporal signal detectability analysis

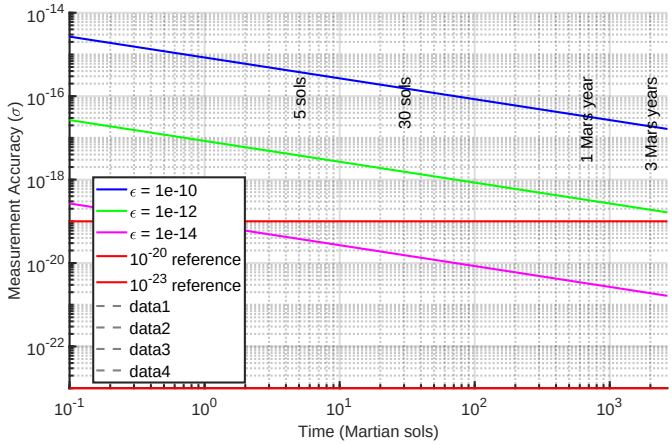

Figure 2.9: Measurement accuracy versus time, $l = 2$

In summary, the combined analysis of tidal Love numbers and time-variable gravity harmonics on Mars offers insight into the planet's internal dynamics. By monitoring seasonal and long-term gravity changes, the Martian mantle can be better constrained, as well as the interaction between surface-atmosphere processes and deep interior responses.

2.6. Mars Atmosphere

Science Question 7

The Martian atmosphere is thin and primarily composed of carbon dioxide, and it plays a dynamic role in seasonal and annual cycles. One of the most significant processes is the condensation and sublimation of CO_2 at the poles, described in Section 2.5. The pressure variations and atmospheric winds introduce changes in the Length Of Day (LOD) and excite polar motion, affecting the planet's rotation dynamics [29]. Mars experiences, like Earth and Venus, axial angular momentum variations. These are driven by seasonal atmospheric mass redistributions, specifically of CO_2 and water cycles explained in Section 2.5. As a consequence of Mars' eccentric orbit, the southern winter is approximately 30 days longer than the northern one. This results in a dominant semi-annual signal in the planet's axial angular momentum [30]. In addition, there is a daily variation in the spherical coefficient C_{22} in a range between -6·10^{-11} and 3·10^{-11}, and a 6-7 day periodicity attributed to planetary atmospheric waves, which further affect the angular momentum [31, 30].

One of the consequences of these variations is a measurable fluctuation in LOD. Dust loading plays a critical role in this context, enhancing atmospheric tides and affecting wind patterns. Dust storms have been observed only during southern spring and summer and have not been modelled with adequate precision. Dust storm amplitudes vary from different mission data, and require more precise models [32]. High-precision gravity missions can detect atmospheric pressure anomalies. Data reveals pressure oscillations with periods ranging from tens of minutes to a few hours, which are strongest during early morning and late evening hours, and they intensify in the latter half of the Martian year [29]. High-sensitivity accelerometers allow for reconstruction of atmospheric models, as has been done using GOCE data by Doornbos et al. [33]. Tri-axial accelerometers measure along-track deceleration due to drag, as well as cross-track components that help isolate orientation and aerodynamic effects. By comparing repeat orbits, where the gravitational signals remain consistent, any differences in accelerometer data can be attributed to changes in atmospheric winds and pressure.

2.7. Science Tools

By considering the different cases discussed before and the main deviations, the expected gravity signals in μGal are: aquifers -741.66 to -74.56; sQCD -2393.00 to -175.10; volatile-rich sediments -69.19

to -46.13, temporal variations during one Martian year -0.0182. These are shown in Figure 2.10, where the expected signals of the analysed phenomena are summarised. Moreover, Table 2.1 summarises the tools used to estimate said values.

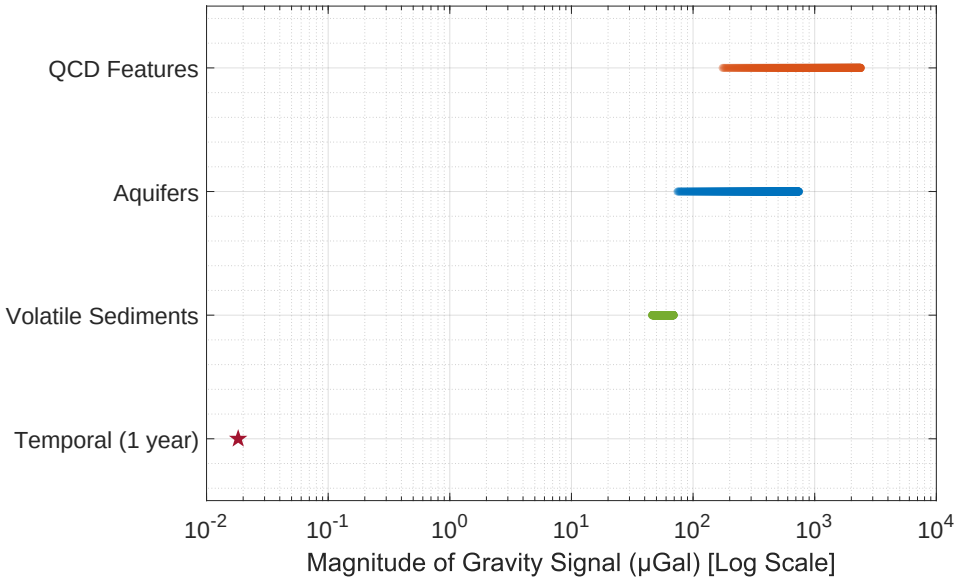

Figure 2.10: Comparison of Martian subsurface gravity signals

Table 2.1: Science Tool Breakdown

Document Name	Model Description	Input	Output
do_model_epsilon.m	Plot [4] equations and estimated the error of the measurements.	Satellite altitude, separation, frequency of measurements, number of observations, optical link error	RMS estimate for different inputs
expected_signals.m	Prints the expected signals produced by different Mars phenomena	Density, thickness, depth and satellite altitude	μGal signal
plot_k2.m	Plots error in measurements of Phobos and Sun tides.	Distance of Phobos and Sun from Mars	RMS estimates for Phobos and Sun tides.
plot_temporal.m	Plots error of measurements over time and checks what accuracy can be achieved	Reference RMS lines, parameters used for SST measurement	Accuracy of measurements over time.
run_aquafers.m	Randomly allocates a specific number of aquifers on Mars and generates the expected degree variance	Number of aquifers to allocate, depth, density, size, altitude of observation, resolution	Degree variance

2.8. Science Requirements

The analysis of the science questions and objectives leads to the derivation of precise science requirements, which define the expected performance of the gravity field measurements of MarsExplore. These requirements guide the following design and ensure the scientific return needed to study mantle dynamics, gravity variations, and other hidden features on Mars.

Updated ID	Old ID	Description	Verification
MIS-SCI-1.1	UR-SUB-PAY-2.4.2.2.1	The static gravity field of Mars shall be measured to a resolution of at least 360 d/o.	Analysis
MIS-SCI-1.2	UR-SUB-PAY-2.4.2.2.2	The temporal gravity field of Mars shall be measured to a resolution of at least 30 d/o.	Analysis
MIS-SCI-1.3	UR-SUB-PAY-2.4.2.2.2	The temporal gravity field of Mars shall be measured as a 30 sol timeseries.	Analysis
MIS-SCI-1.3.1	UR-SUB-PAY-2.4.2.2.2	The orbiter shall pass over the same points on the surface of Mars at least once every 30 sols.	Analysis
MIS-SCI-1.4	SUB-PAY-2.4.2.2.3	The temporal gravity field of Mars shall be measured to a sensitivity of at least 0.018 μGal/year.	Analysis
MIS-SCI-1.5		The mission shall analyse gravitational fluctuations with periods up to 1 Martian year at least.	Review of Design
MIS-SCI-1.5.1		The orbiter shall perform science measurements for at least 1 Martian year.	Review of Design
MIS-SCI-1.6		The mission shall gather gravity data on at least 95% of the Martian surface.	Analysis
MIS-SCI-1.6.1		The orbiter shall have an orbital inclination between 85 and 95 degrees.	Analysis
MIS-SCI-1.7		The measurements shall have at minimum a root-mean-square amplitude of 10^{-20}.	Analysis
MIS-SCI-1.7.1		The optical link error of the measurement shall be at least 10^{-14}.	Analysis
MIS-SCI-1.7.2		The separation of the two satellites shall be at most 58 km.	Analysis
MIS-SCI-1.8		The payload shall be capable of measuring acceleration along three orthogonal axes.	Analysis

3 Market Analysis

MarsExplore project is developed as part of the Design Synthesis Exercise (DSE), the final project of the Bachelor of Aerospace Engineering at Delft University of Technology. It has been initiated by Assistant Professor Bart Root, who proposed the concept to submit it for the upcoming ESA Medium-Class (M-class) Mission Call[1].

3.1. Competitor Analysis and Unique Selling Point

In 2021, ESA finalised the long-term plan for its science programme, the Voyage 2050[2], which outlines the agency's vision for space science over the coming decades. To fulfil said goals, ESA has published the competitive Medium and Fast Mission calls. The criteria used by the experts to select the best mission are: science value, scientific feasibility, timeliness, and complementarity with other projects[3].

Out of the last three candidates for the previous Mission call, the M-Matisse mission has been identified as the most direct competitor of MarsExplore, due to its focus on Mars exploration. The final selection of this mission could reduce the likelihood of ESA supporting another Mars-centric mission in the near future. On the other hand, the opposite may be true, as ESA utilises spare flight equipment in mission development to reduce costs and timelines[4]. ESA's long-term interest in habitability and eventual human exploration of Mars increases the possibility for additional complementary missions, particularly in gravity mapping, which is a currently unexplored domain. This should be highlighted as one of MarsExplore's unique selling points. The MarsExplore mission is well aligned with both ESA's Voyage 2050 objectives and the European Commission's strategic goals on quantum technologies. As outlined in ESA's white paper on Quantum Technologies in Space, quantum sensors offer unprecedented sensitivity for gravity field measurements [34]. A review of literature shows that most proposed quantum-gravity missions focus on large-scale cosmic structures or dark matter. Therefore, a gravity-focused mission like MarsExplore fills a critical scientific gap, as current models lack dynamic effects.

The European Commission shows a strong commitment to advancing quantum technologies (QT). Large investments have been announced, such as €40 million to boost research into quantum technologies, of which €25 million will be invested for the creation of a pan-European network of quantum gravimeters, which are gravity sensors[5]. Projects such as the EU Quantum Flagship and Horizon Europe initiatives are actively developing space-grade quantum gravimeters. For example, the CARIOQA-PMP (Cold Atom Rubidium Interferometer in Orbit for Quantum Accelerometry – Pathfinder Mission Preparation) project[6] collaborates with many companies such as Exail.

The ORACLE mission proposes studying Mars' climate, surface, and interior by performing gravity field measurements with instruments used in the GRACE and GRAIL missions [35]. This mission does not incorporate quantum technologies, making MarsExplore a more innovative mission. It should again be noted that this is a unique selling point of the mission. The fact that multiple scientific teams are proposing similar missions highlights the importance of this exploration initiative, making it more likely for ESA to prioritise such missions. International agencies are also pursuing similar paths. For instance, in 2024, NASA initiated a focused effort to develop a Quantum Gravity Gradiometer (QGG)

[1] https://www.cosmos.esa.int/web/call-for-missions-2025 (Accessed on 01/05/2025)

[2] https://www.cosmos.esa.int/web/voyage-2050/white-papers (Accessed on 01/05/2025)

[3] https://www.esa.int/Science_Exploration/Space_Science/Final_three_for_ESA_s_next_medium_science_mission#M-Matisse%20anchor (Accessed: 29/04/2025)

[4] https://www.esa.int/Science_Exploration/Space_Science/How_a_mission_is_chosen (Accessed: 29/04/2025)

[5] https://digital-strategy.ec.europa.eu/en/news/commission-invests-eu112-million-ai-and-quantum-research-and-inn 29/04/2025)

[6] https://cordis.europa.eu/project/id/101081775(Accessed on 29/04/2025)

pathfinder instrument, targeting a demonstration flight by 2030[7]. Meanwhile, the French government space agency CNES is conducting the GRICE study (GRadiométrie à Interféromètres quantiques Corrélés pour l'Espace) to evaluate the usage of cold atom technologies for gravity measurements around Earth [9]. The strong competition from international countries, such as the USA, China, and Canada, calls for a coordinated European effort towards the development of QT in and for space [34], as well as offers a wide range of possible collaborators. Overall, the originality, timeliness, and technological ambition of MarsExplore make it a strong candidate for ESA's future mission portfolio.

3.2. Market Overview

MarsExplore aims to apply to the ESA Mission call, which would cover 670 M€. These might suffice for the mission, but, realistically, finding additional funders would significantly increase the quality of the mission. To assess the market opportunity, three progressively narrower scopes can be analysed:

- **Total Addressable Market (TAM)**: the overall revenue opportunity available for a product or service within a defined market [8].
- **Serviceable Addressable Market (SAM)**: the portion of TAM that a company can realistically target and serve, based on its resources and capabilities [9].
- **Serviceable Obtainable Market (SOM)**: the share of SAM that a company can realistically capture, considering competition and its own strengths. [10]

MarsExplore operates at the intersection of three key markets:

- The global Space Industry;
- The Quantum Technology Market;
- The Gravity Sensor and Gravitational Data Market.

The TAM estimate is approximately €130 billion for 2024 and €150 billion for 2030, considering some overlaps and space-specific relevance. This estimate includes institutional space budgets (civil and defence), which reached €122 billion in 2024, along with the public space budget in Europe, amounting to €12.6 billion. In addition, private investments in space reached €7 billion in 2024 [36].

The global space launch services market is projected to reach €38.4 billion (converted from USD 41.31 billion) by 2030, growing at a Compound Annual Growth Rate, or CAGR, of 14.6% from 2024 to 2030[11].

The global quantum technology market is expected to reach €1.75 billion in 2025 (converted from USD 1.88 billion), and is projected to grow to €4.55 billion by 2029 (converted from USD 4.89 billion)[12]. The global gravity sensor market size was valued at approximately €83.7 million in 2024 (converted from USD 0.09 billion), and is forecasted to grow to around €214 million by 2033 (converted from USD 0.23 billion), with a CAGR of 11.4% from 2025 to 2033[13].

The SAM narrows down the market availability, given the mission's focus on Mars gravity mapping using quantum technology. Only a fraction of the space budget is dedicated to Mars and science missions relevant to MarsExplore. It can be assumed that around 10% of ESA's budget is dedicated to planetary science and Mars (= €1-1.3 billion). A 10% fraction of the quantum investments can

[7] https://esto.nasa.gov/quantum/ (Accessed on 29/04/2025)

[8] https://swoopfunding.com/uk/business-glossary/total-addressable-market/(Accessed 17/06/2025)

[9] https://swoopfunding.com/au/business-glossary/serviceable-addressable-market/(Accessed 17/06/2025)

[10] https://simplicable.com/new/serviceable-obtainable-market(Accessed 17/06/2025)

[11] https://www.grandviewresearch.com/press-release/global-space-launch-services-market (Accessed 17/06/2025)

[12] https://www.rdworldonline.com/quantum-industry-sees-rapid-growth-in-2025-report-finds/ (Accessed 17/06/2025)

[13] https://www.businessresearchinsights.com/market-reports/gravity-sensor-market-110348 (Accessed 17/06/2025)

be assumed for space mission (= €0.3 billion) and the same fraction for gravity sensors dedicated to Mars missions (= €0.1 million). From this, the total estimation SAM is €1.7 billion. The SOM reflects the realistic portion of the market that MarsExplore could capture within its operational time frame. An approximate value would be €940 million. This includes approximately €670 million in funding from ESA, up to €200 million from NASA, around €20 million from European quantum technology initiatives, and an estimated €50 million from the gravity sensor market and related scientific applications.Figure 3.1 illustrates the estimates of the available market for the MarsExplore mission and its future growth.

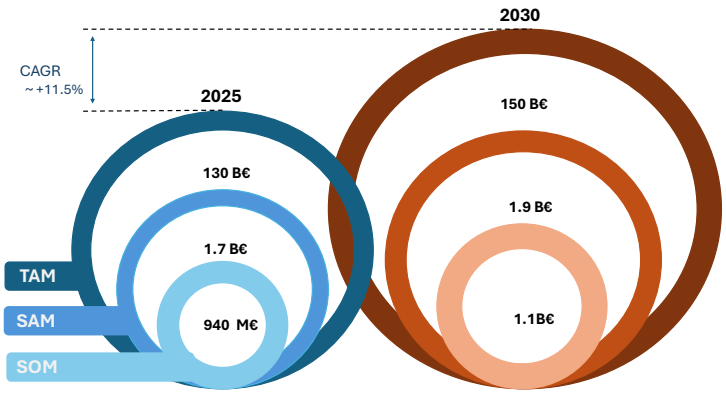

Figure 3.1: Extension and growth estimation of the MarsExplore market

3.3. SWOT Analysis

The market analysis leads to the generation of a SWOT (Strengths, Weaknesses, Opportunities, and Threats) table, Table 3.1.

Table 3.1: SWOT Analysis of the MarsExplore Mission

Strengths	**Weaknesses**
• Technology demonstration of quantum gravimeter • Pathfinder for deep-space quantum tech. in general • Unprecedented accuracy in Martian gravitational field mapping • Gathers data for atmospheric, hydrology, and mantle dynamics research on Mars • Mature spacecraft components and proven mission architecture • Mission aligns with ESA's Voyage 2050 long-term science themes • Mission aligns with European Commission goals for quantum technologies	• Unproven cold-atom gravimetry in deep space (miniaturization, robustness) • Desired accuracy might be unachievable • High mass, volume, and power consumption of quantum devices • Unknown operational challenges in Mars orbit • Limited global expertise; requires strong industrial-academic consortia
Opportunities	**Threats**
• Potential partnership with NASA/JPL (e.g., QGGPf) • Collaboration with CNES and GRICE for Earth validation • Reusable instrument concept for Moon, Venus, or icy moons • Growing European interest and funding in quantum space payloads • Addition of secondary payload to reduce cost and mission risk	• Technology may not reach TRL 6, risking ESA rejection • ESA may consider quantum tech too risky for Mars • Competing Mars M-class proposals may appear safer • Delays/failures of GRICE or CARIOQA-QKD may lower confidence • Risk of cost overruns • Shift in ESA/EU priorities away from Mars

3.4. Stakeholder Analysis

In Table 3.1, it is shown that the mission has a strong alignment with key stakeholders, such as the EU and ESA interests under strengths, and their priorities under threats, or partnerships with NASA under opportunities. Therefore, the success of the MarsExplore mission concept depends on the

engagement and alignment of a variety of stakeholders. The stakeholders can be identified as key stakeholders, who directly and significantly influence the project, and other stakeholders. The key stakeholders are the Tutor (Assistant Professor Bart Root) and ESA. The Tutor is the initiator of the MarsExplore concept and supervisor of the DSE. Dr. Bart Root plays the primary role in defining the technical direction and objectives of the mission. ESA is the target organization for the M-Class mission proposal, which is the constraint posed by the Tutor. ESA serves both as the funding agency and the mission authority. Their evaluation criteria and requirements for the mission directly shape the project's structure.

Other stakeholders identified are TU Delft, EU, NASA, the scientific community, the quantum technology, gravitational data and space industries, and the general public. TU Delft provides the academic framework for the project, offering facilities, technical mentoring, and visibility. The EU is an indirect but influential stakeholder; its funding and policy frameworks support the maturation of quantum sensing technologies. The scientific community is the primary audience for the scientific output of MarsExplore; therefore, their needs are indirectly guiding the mission. The quantum technology industry is a stakeholder as it is in its best interest that a quantum sensing mission is successful; the same can be said for the space industry and gravitational data industry.

The general public holds a vested interest in space exploration, which captures the imagination, and can influence political and funding support for space missions and enhance ESA's outreach objectives. However, public interest can be increased through science communication efforts that increase their engagement with the mission, represented by the arrow in Figure 3.2. For example, this could be done through a competition with schools to implement their own secondary payload, marketing, buying a "ticket" to go on the spacecraft, or engraving names on the spacecraft through a competition. Finally, collaboration between MarsExplore and NASA's goals could open doors for joint technology development or future mission integration. This stakeholder analysis has been simplified in Figure 3.2, where the influence and the interest that each stakeholder has on the project outcome can be visualised. The stakeholders in the yellow box are the primary stakeholders and should be given the highest priority and attention.

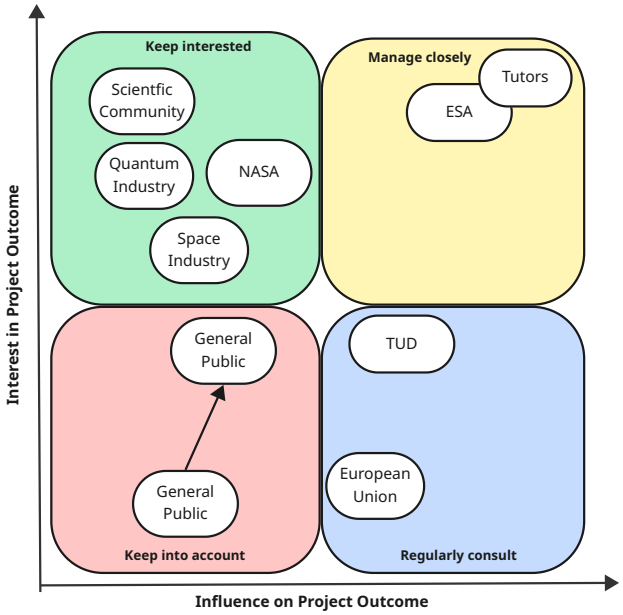

Figure 3.2: Stakeholder Map

3.5. Market Analysis Requirements

The following mission requirements are derived from the market analysis.

Updated ID	Old ID	Description	Verification
MIS-ESA-2.1	ESA-SYS-1.3.1.1	The mission shall have a Cost at Completion ceiling of 670 million euros at 2025 economic conditions.	Review of Design
MIS-ESA-2.2		The mission shall launch no earlier than 2041.	Review of Design
MIS-ESA-2.3	ESA-SUB-PW-1.1.1.3	The mission shall not incorporate Radioisotope Thermoelectric Generators.	Review of Design
MIS-ESA-2.4	UR-SYS-2.1.1.1	Launch shall be performed with an ESA launcher.	Review of Design
MIS-ESA-2.5		The mission shall comply with the COSPAR Policy on Planetary Protection.	Review of Design
MIS-ESA-2.6	ESA-MIS-1.1.1.1	All mission activities shall comply with ESA's 2024/2041 Green Agenda standards.	Review of Design
MIS-ESA-2.7	UR-SYS-2.6.8.1.1	All critical technologies shall be at a Technology Readiness Level of 6 according to the ISO scale by the end of the mission's definition phase.	Review of Design
MIS-UR-3.1	UR-MIS-2.6.5.1	All normal subsystems of the mission shall incorporate double redundancy.	Review of Design
MIS-UR-3.2	UR-MIS-2.6.5.2	All critical subsystems of the mission shall incorporate triple redundancy.	Review of Design
MIS-UR-3.3	UR-MIS-0	The mission shall demonstrate the use of quantum technologies for interplanetary space missions.	Demonstration

4 Payload

MarsExplore is an SST mission, similar to GRACE, GRACE-FO, and GRAIL, where the changes in the distance between two orbiters are measured to extract gravitational field data[1]. The effect of gravitational disturbances is isolated with the use of an accelerometer or inertial measurement unit, which can detect all non-gravitational effects on an inertial reference, thus isolating the gravity signal's contribution to the changes in inter-satellite range. MarsExplore represents the first time that the SST concept is applied in the context of an interplanetary mission, bringing unique insights into how the overall spacecraft, particularly the payload, must be designed. The relevant mission requirements considered in the payload design are listed below.

Relevant Mission Requirements – Payload	
MIS-SCI-1.1	The static gravity field of Mars shall be measured to a resolution of at least 360 d/o.
MIS-SCI-1.2	The temporal gravity field of Mars shall be measured to a resolution of at least 30 d/o.
MIS-SCI-1.3	The temporal gravity field of Mars shall be measured as a 30-sol timeseries.
MIS-SCI-1.8	The payload shall be capable of measuring acceleration along three orthogonal axes.
MIS-UR-3.1	All normal subsystems of the mission shall incorporate double redundancy.
MIS-UR-3.3	The mission shall demonstrate the use of quantum technologies for interplanetary space missions.

The functions to be performed by the payload, identified in the mission functional analysis of Section 5.1, are as follows.

- F.4.3 Perform Scientific Measurements
  - F.4.3.1 Activate Payload
  - F.4.3.2 Measure Non-Gravitational Disturbances
  - F.4.3.3 Measure Total Disturbances
  - F.4.3.4 Measure with Secondary Payload

4.1. Laser Ranging Interferometer

The Laser Ranging Interferometer (LRI) follows from the technology demonstration used on GRACE-FO [37] with minor adjustments; this time serving as the main science instrument for inter-satellite ranging. As a result, redundancy in the LRI is a much more important consideration than in GRACE-FO. During laser interferometry, one LRI unit must act as a reference, with its laser stabilised against an optical cavity, whereas the other half of the LRI unit, on the other spacecraft, acts as a secondary unit, whose phase is locked on to that of the incoming reference laser [38]. The LRI is made up of the following components[2] [37].

- Laser Source (LAS): this is where the laser, used in the laser interferometry, is first produced. It emits 25 mW of light and has a wavelength of 1064 nm.
- Optical Bench Assembly (OBA): part of the laser then travels into the OBA, where it is routed and pointed. The OBA also includes the Fast Steering Mirror (FSM), which is responsible for the finest pointing of the laser, towards the other spacecraft, and the quadrant photoreceiver (QPR), whose measured phase signal represents the measured change in spacecraft distance.
- Optical Bench Electronics (OBE): the OBE provides power to the FSM, QPR and OBA, working alongside the Laser Ranging Processor to control the LRI.

[1] `https://grace.jpl.nasa.gov/mission/grace-fo` (accessed 16 June 2025)
[2] `https://gracefo.jpl.nasa.gov/laser-ranging-interferometer/` (accessed 16 June 2025).

- Optical Cavity (CAV): the other part of the laser travels to the optical cavity, responsible for stabilising the laser frequency in short timescales, typically in the second or minute timeframe [39, 40]. This is needed as changes in laser frequency are indistinguishable from changes in inter-satellite distance; thus, the frequency is required to be very stable to ensure scientific measurements are accurate.
- Triple Mirror Assembly (TMA): the TMA routes the beam throughout the spacecraft in a racetrack configuration. It acts as a corner-cube reflector, in essence, three perpendicular mirrors that reflect a beam in the direction it came from. Its vertex is placed to coincide with the accelerometer inertial reference and spacecraft centre of mass (CoM), thus turning the path length into the distance between the spacecraft CoM. The laser is redirected from the TMA into the outgoing baffle, where it is sent to the other spacecraft.
- Laser Ranging Processor (LRP): the LRP measures the phase of the laser interferometer signal from the QPR, outputting the interference measurements. It is also responsible for controlling the laser frequency and commanding the FSM.
- Baffles: the baffles are small tubes, approximately 2.5 cm in diameter[3]. The incoming travels through one baffle, is directed into the OBA, and is then sent into the TMA. The TMA directs it around the spacecraft, into the other baffle, which transmits it to the other baffle, which directs it to the other satellite.

As one of the main science instruments, in compliance with **MIS-UR-3.1**, redundancy is a key consideration for the LRI. On GRACE-FO, the LRI served as a technology demonstrator and hence incorporated limited redundancy. Instead, the redundancy strategy suggested in [11] has been adhered to, making the LRI fully double redundant, more specifically incorporating cold redundancy. Hot redundancy is incorporated in the QPR of the OBA. This is presented in Figure 4.1, where the RRU is the TMA, LAS is shown as a red and black box, ICU refers to electronics, and LSU is the CAV.

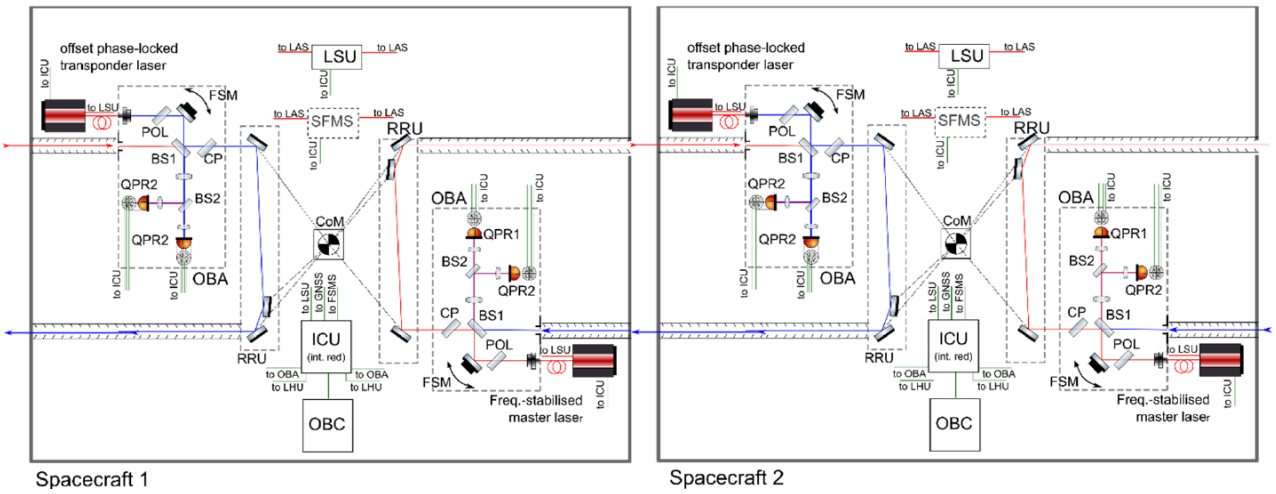

Figure 4.1: Laser Range Interferometer with Full Redundancy [11]

Essentially, this makes it such that one LRI unit is placed "forward-facing" (i.e. direction of travel) and one is placed "backward-facing" per spacecraft, whereas in GRACE-FO, only the forward-facing unit was incorporated. This not only allows the spacecraft to be even more symmetric, of which the significance is discussed in Section 4.5, but also greatly reduces the risk of failure. In case of single laser unit failure, the leading spacecraft, Isaac, can switch positions with the trailing spacecraft, Albert,

[3]Discussion with Alexander Koch, German Aerospace Center (DLR), expert on inter-satellite laser interferometry, on 27/05/2025.

as illustrated in Figure 4.2, such that the defective LRI unit is no longer in use. The forward-facing LRI is shown in red, the backward-facing in blue.

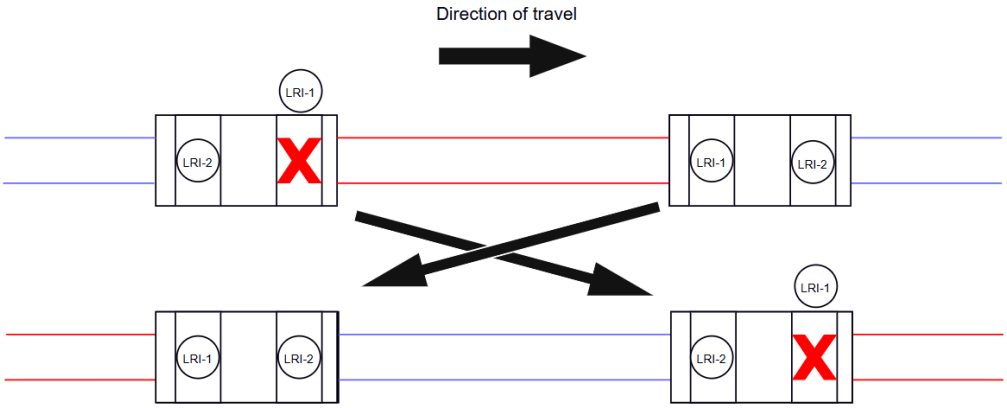

Figure 4.2: Laser Range Interferometer Redundancy Strategy

The presented LRI redundant configuration essentially doubles all components, with the exception of the CAV. Redundancy for the CAV is achieved by flying one per spacecraft, where only one is needed in the constellation [11]. Despite the new redundant configuration and overall payload architecture, the LRI can be considered to have a Technology Readiness Level (TRL) of 9 for "Flight Proven", given its usage on GRACE-FO.

With regards to the required optical link error discussed in Chapter 2, it remains a complicated procedure to estimate in the scope of this design exercise. For an example of a figure demonstrating the optical link error requirements for the LRI, one can refer to Figure 3 of [11]. As discussed Section 7.7, this requirement must be discussed by the scientists and payload manufacturers, to reach a common ground on the desired optical link error.

4.2. Iodine Reference Unit

A key consideration in the design of the payload for a planetary mission is how to determine the frequency of the laser with absolute knowledge. On the ground, the laser frequency can be easily determined with absolute knowledge. However, after launch, the LRI will transition from 1-g to microgravity, causing debending of the components and uncertainty in the laser frequency. This can, however, be determined from an external measurement of the inter-satellite range. On GRACE-FO, this is achieved through orbit determination with GPS satellite [41], which is not possible on Mars. Additionally, another point to consider is the long-term stability of the laser. While the CAV offers sufficient short-term frequency stability, it is highly unstable in the long term (> 100 s) due to temperature effects [40].

As a result, studies have suggested the incorporation of an absolute frequency reference, such as an iodine reference unit (IRU) [42, 40, 39], which is independent of the effects of debending or temperature as they rely on molecular spectroscopy. Therefore, an IRU has been included as one of the primary science instruments to stabilise the LRI in the long term. The power, mass, and volume estimates for the IRU have been extracted from those of the COMPASSO from the German Aerospace Center (DLR), one of the latest iodine clock space missions[4]. Similarly to the CAV, redundancy in the IRU is considered by implementing one unit per spacecraft, as only one is needed in the constellation[5]. Given

[4] `https://www.optica-opn.org/home/articles/volume_35/january_2024/features/timekeepers_in_space` (accessed 16 June 2025).

[5] Discussion with Alexander Koch, German Aerospace Center (DLR), expert on inter-satellite laser interferometry, on 27/05/2025.

that COMPASSO will fly on the ISS in the next 2 years[6], the TRL of the IRU can be considered to be an 8 for "Flight Qualified". Several IRUs are presented in Figure 4.3 for illustrative purposes [39].

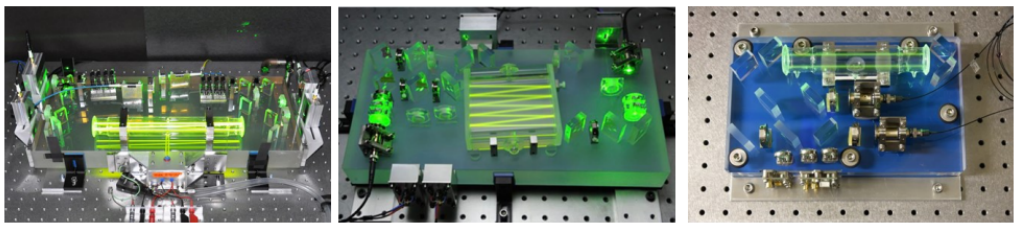

Figure 4.3: Example Images of Iodine Reference Units [39]

4.3. Cold Atom Interferometer

The cold atom interferometer (CAI) is one of the most novel additions to the payload, in comparison to past missions, having been identified numerous times as an opportunity to improve the science of current space gravimetry missions [9, 43]. It serves as the main accelerometer or inertial measurement unit for the mission. In a CAI, a cloud of Rubidium atoms in free fall is used as a test mass [9, 43]. This cloud of atoms is cooled to the nano- and pico-Kelvin scale to reduce its motion. The acceleration of this cloud of atoms is measured. As the cloud of atoms is placed very close to the spacecraft CoM, this allows the accelerations on the spacecraft CoM to be measured precisely.

The CAI is composed of the following components [9]:

- Physics Package (PP): the PP consists of a vacuum chamber with varying magnetic fields to manipulate the Rubidium atoms. It is surrounded by various layers of magnetic shielding.
- Laser source (LS): the LS produces the laser necessary to prepare the cold atoms and detect their state.
- Electronics Unit (EU): encompasses the electronics needed to operate the PP, such as the ion pump and magnetic field control.

Given the placement of the PP near the spacecraft CoM, it is very difficult to incorporate redundancy for it. This also imposes that the TMA vertex is aligned in all dimensions with the spacecraft CoM. However, double cold redundancy can simply be incorporated into the LS and EU[7]. Moreover, the redundancy of the inertial measurement of the spacecraft can be greatly enhanced by incorporating more accelerometers into the spacecraft. In particular, the CAI excels at acceleration measurements for low frequencies, so an accelerometer suited for high frequencies is a suitable choice for redundant accelerometers[7], leading into the next section.

An important consideration of the CAI is its axis. While ideally the CAI would measure accelerations in all axes, this is prohibitive for the mass, power, and cost budgets. As suggested by DLR and in other papers, the CAI will be implemented in an along-track configuration, to measure gravitational disturbances in the along-track direction[7] [9, 43]. The CAI's limited usage in space missions and current development efforts place it at a TRL of 5 for "Technology Demonstrator". An atom interferometer is illustrated in Figure 4.4 [44].

[6] `https://www.dlr.de/en/latest/news/2024/dlr-laser-clock-achieves-world-class-accuracy`, accessed 16 June 2025.

[7] Discussion with Christian Schubert, German Aerospace Center (DLR), head of Quantum Sensing, on 03/06/2025.

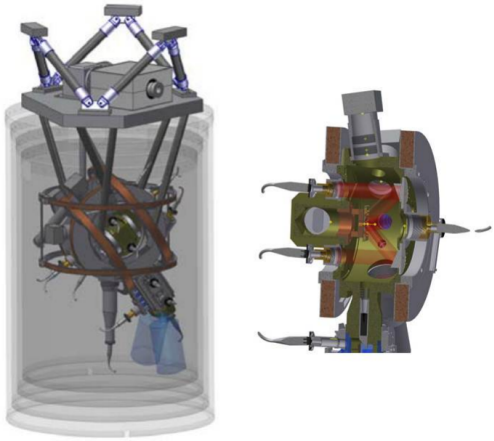

Figure 4.4: Example Image of an Atom Interferometer [44]

4.4. Optomechanical Inertial Measurement Unit

Optomechanical Inertial Measurement Units (OMIS) can be used to accurately measure frequencies with no calibration over a large frequency range [45]. OMIS consists of two small mirrors that act as an optical cavity. One is fixed, whereas the other is located on the movable test mass. When an acceleration is induced, the test mass moves, changing the length of the optical cavity, which is translated into an acceleration measurement in a single axis [45]. Their performance in higher frequencies, as well as their simplicity, and feasible mass, power, and volume characteristics, make them an attractive option for the mission. The application of OMIS for gravimetry has been widely considered [1, 45]. Therefore, an OMIS on each side of the CAI is included to measure along-track accelerations.

This not only brings additional science in higher frequencies, but also acts as a redundant accelerometer in the case of CAI failure. Additionally, two more OMIS are included to measure cross-track and nadir accelerations, bringing additional science to the mission, in compliance with **MIS-SCI-1.8**. An example of an OMIS is included in Figure 4.5 [46].

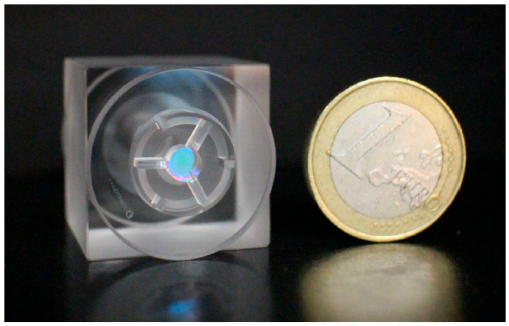

Figure 4.5: Example Image of an Optomechanical Inertial Measurement Unit [46]

4.5. Centre of Mass Trim Assembly

Given the strict CoM positioning requirements imposed by the science, it is necessary to ensure that the CoM coincides with the TMA vertex and CAI Rubidium atom cloud to the micrometer level [37] throughout the mission. The changing mass of the spacecraft throughout the mission, such as due to the depletion of propellant tanks, complicates this. To solve this, components that change in mass throughout the mission are positioned symmetrically about the spacecraft CoM, and importantly, a centre of mass trim assembly (CMT) is included. The CMT, also an instrument flown on GRACE-FO, consists of movable-mass mechanisms that can perform small shifts in the CoM in all 3 axes [37]. The

CMT flown on GRACE-FO can shift the CoM by at most ±1.9 mm along a single axis. However, since MarsExplore incorporates other movable elements not present on GRACE-FO, such as a high-gain antenna, it imposes that the range of mass trimming must be increased beyond 1.9 mm.

Firstly, it is determined that the antenna dish will at most need to shift by 33 degrees when pointing from Mars to Earth, causing an estimated change in its CoM of 0.27 m, after making some assumptions. When multiplied by the assumed proportion, it contributes to the dry mass. At the end of the mission, the spacecraft CoM shift is obtained, resulting in around a 2.5 mm shift. Thus, it is estimated that an improvement in the trim range capability of the CMT is needed, to about ±5 mm. This value has also been verified with the actual antenna dimensions and mass to be the same. Despite this, the CMT was already slightly adapted from GRACE to GRACE-FO to increase the trim range, so the development effort remains small. Given the slight adjustments needed, the TRL of the CMT can be considered to be 8 for "System Development". An example of a CMT model from a different study is shown in Figure 4.6 [47].

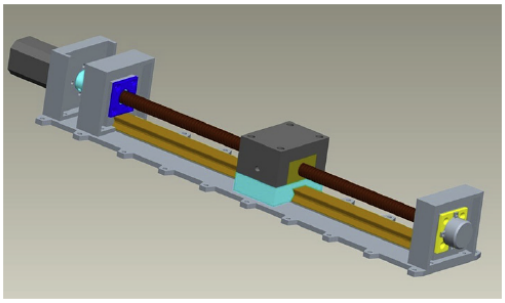

Figure 4.6: Example Image of a Centre of Mass Trim Assembly [47]

4.6. Miniaturised Constellation Acquisition System

The final payload instrument is the miniaturised constellation acquisition system (MiniCAS). MiniCAS is an optical system, comprised of an emitter and a receiver, that uses light to measure the relative orientation between two spatially separated platforms[8]. It is currently in development at the DLR and is particularly useful for constellation missions such as MarsExplore. MiniCAS works by projecting a wide-divergence beam, which passes through an aperture at the receiver, where it is collected in a focal-plane array sensor. By tilting the receiving spacecraft, it is possible to translate the tilt into beam displacement, and thus into relative spacecraft orientation down to microradian accuracy[8], more than sufficient for the mission.

In missions incorporating intersatellite ranging, such as with the LRI, the link acquisition procedure to acquire the laser (or other) link is crucial. On GRACE, the orienting of the spacecraft took several days every time that science mode needed to be entered, imposing a significant penalty on science operations and availability. On GRACE-FO, this was improved with the inclusion of the FSM. Once the spacecraft are pointing at each other within a narrow range, the FSM performs a scanning procedure over the area in which the receiving LRI may be located. This procedure can take up to 9 hours[3] [9].

On the other hand, the inclusion of MiniCAS in MarsExplore can reduce the link acquisition procedure to being almost instantaneous, depending more on attitude data processing onboard the spacecraft rather than actual scanning[8]. This first improves the availability of the mission, as well as reducing the risk of the link acquisition procedures, which is one of the highest-risk procedures of the mission.

MiniCAS is split into an emitter and receiver component. For basic operation, one emitter must be

[8] Discussion with Julia Desirée van den Toren, German Aerospace Center (DLR), on 03/06/2025.

[9] `https://gracefo.jpl.nasa.gov/news/128/lasers-in-space-grace-fo-tests-new-technology` (accessed June 17, 2025)

present on one spacecraft, and one receiver on the other. For redundancy, an emitter and a receiver are included on each spacecraft. Furthermore, given that MiniCAS is currently in development at DLR, its TRL is considered to be 5 for "Technology Demonstrator". The MiniCAS measurement principle is demonstrated in Figure 4.7[10].

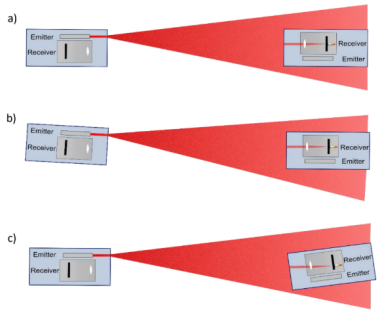

Figure 4.7: Miniturised Constellation Acquisition System Measurement Principle. a) Perfect Alignment, b) Tilt of the Emitting Spacecraft, c) Tilt of the Receiving Spacecraft

4.7. Payload Instrument Overview

The mass per payload component is presented in Table 4.2. A technology reduction factor of 0.8 is applied to account for miniaturisation efforts and technological improvements before launch. This is not applied to the CMT mass, as it would reduce the trim range.

Table 4.2: Estimated Mass of Payload Components per Spacecraft

Component	Amount	Mass per Unit [kg]	Total Mass [kg]	Source
Laser Ranging Interferometer (LRI)				
OBA (cold, hot QPR redundancy)	2	4.05	8.10	
OBE (cold)	2	2.25	4.50	
LRP	2	5.00	10.00	
LAS	2	0.61	1.22	
CAV	1	2.71	2.71	
TMA	2	1.62	3.24	
Baffles (cold)	2	0.57	1.14	
Subtotal			**31.47**	DLR[3]
Cold Atom Interferometer (CAI)				
Physics Package	1	45.00	45.00	
Electronics (cold)	2	5.00	10.00	
Laser Source (cold)	2	25.00	50.00	
Subtotal			**105**	[9]
Other Instruments				
Iodine Reference Unit	1	27.00	27.00	Optica-opn.org[4]
OMIS	4	0.50	2.00	
CMT	1	5.50	5.50	[37]
MiniCAS	1	7.00	7.00	DLR[10]
			Total Payload Mass	**177.97**
			Total After Technology Reduction Factor (× 0.8)	**143.50**

[10]Obtained from MiniCAS requirements document, shared by Julia Desirée van den Toren, German Aerospace Center (DLR), on 03/06/2025.

Similarly, the power per payload component is presented in Table 4.3. A technology reduction factor of 0.8 is applied to account for miniaturisation efforts and technological improvements before launch.

Table 4.3: Estimated Power of Payload Components per Spacecraft

Component	Amount	Power per Unit [W]	Total Power [W]	Source
CAI				
Physics Package	1	8.00	8.00	
Electronics (cold)	2	57.00	57.00	
Laser Source (cold)	2	96.00	96.00	
Subtotal			**161**	[9]
Other Instruments				
LRI (cold)	2	50.00	50.00	DLR[3]
Iodine Reference Unit	1	51.00	51.00	Optica-opn.org[4]
OMIS	4	5.00	20.00	
CMT	1	0.00	0.00	[37]
MiniCAS	1	10.00	10.00	DLR[10]
			Total Payload Power	**292.00**
			Total After Technology Reduction Factor (× 0.8)	**234.00**

Finally, the dimensions per payload component are included in Table 4.4.

Table 4.4: Dimensions of Payload Components per Spacecraft

Component	Amount	Dimensions per Unit [m]	Source
Laser Ranging Interferometer (LRI)			
OBA (cold, hot QPR redundancy)	2	0.25 × 0.15 × 0.20	DLR[3]
OBE (cold)	2	0.30 × 0.20 × 0.07	
LRP	2	0.25 × 0.15 × 0.25	
LAS	2	0.15 × 0.15 × 0.25	
CAV	1	0.08 × 0.25 × 0.25	
TMA	2	0.60 × 0.05 × 0.10	
Baffles (cold)	2	0.025 in diameter, length from TMA to edge	
Other Instruments			
CAI	1	0.493 x 0.493 x 0.493	[9]
Iodine Reference Unit	1	0.3 x 0.15 x 0.035	Optica-opn.org[4]
OMIS	4	0.02325 × 0.02325 × 0.00233	
CMT	1	0.6505 x 0.124 x 0.086	[47]
MiniCAS Emitter	1	0.10 × 0.20 × 0.10 0.10 x 0.20 x 0.20 receiver	DLR[10]
MiniCAS Receiver	1	0.10 x 0.20 x 0.20	DLR[10]

4.8. Cost

In order to estimate the payload cost, a reference value is found from literature. The main payload instruments, representing the most development and testing needed, are considered; that is, the LRI and CAI. As an initial estimate, this was found to be 60 M€ for the cold atom interferometer [48] and 25 M€ for the laser ranging instrument [49].

Following this, this estimate is improved by adding a margin based on TRL as described in *Space Mission Analysis and Design* [50] of 20%. As a result, the payload cost is estimated to be 102 M€ per spacecraft. However, for the second spacecraft, a learning curve is applied, detailed in Section 7.2.

4.9. Risk

While the payload is designed to achieve the scientific objectives of the mission, its successful operation is inherently subject to technical risks. These risks stem not only from the complexity of operating advanced instruments such as the laser ranging system and the cold atom interferometer, but also from the demanding requirements imposed across the spacecraft's subsystems.

To better assess the risk of the payload, the Development Difficulty Index (DDI) is used, evaluated using two metrics: the State of Technology (SOT) and the Technical Difficulty (DED). These metrics are chosen as they quantify the risks associated with the design and development phases of the project. The corresponding scales are presented in Table 4.5 and Table 4.6 respectively. The Development Difficulty Index (DDI) is defined by multiplying the SOT and DED as shown in Equation 4.1. The 0.1 added to both SOT and DED ensures that the numerator stays non-zero, preventing DDI from becoming zero. To normalize the result, the product is divided by the reference maximum values of the SOT and DED scales: 8 and 7, respectively.

$$\text{DDI} = \frac{(\text{SOT} + 0.1)(\text{DED} + 0.1)}{(8 + 0.1) \times (7 + 0.1)} \tag{4.1}$$

Table 4.5: State of Technology (SOT)

Rating	State of Technology (SOT)
0	Proven (flight) design
1	
2	Extrapolated from existing flight design
3	
4	Based on existing non-flight engineering
5	
6	Working laboratory model
7	
8	Feasible in theory

Table 4.6: Design Engineering Difficulty (DED)

Rating	Design Engineering Difficulty (DED)
0	Qualified off-the-shelf item which meets all requirements
1	Off-the-shelf item which requires qualification
2	Off-the-shelf item with minor modifications
3	Design effort required using standard components within spec
4	Poor alternatives and/or uses standard components beyond accepted spec level
5	Poor alternatives and/or new component development required
6	No alternative and/or major engineering development using existing knowledge
7	No alternatives and/or requires new or breakthrough advances

The consequence is defined as the effect of a full failure of the component, and it is assessed at the mission level. This analysis assumes conditions during science operations. The mission impact ratings are shown in Table 4.7.

Table 4.7: Mission Impact Ratings

Rating	Mission Impact
0.1	**Negligible:** Failure to meet the requirement would create inconvenience or non-operational impact. Reduction in technical performance.
0.5	**Marginal:** Failure to meet the requirement would result in degradation of the secondary mission. Minimal to small reduction in technical performance.
0.7	**Critical:** Failure to meet the requirement would degrade system performance to a point where mission success is questionable. Some reduction in technical performance.
0.9	**Catastrophic:** Failure to meet the requirement would result in mission failure. Significant degradation or non-achievement of technical performance.

The risk analysis results are shown in Table 4.8 and visualised in Figure 4.8.

Table 4.8: SOT/DED Ratings, Resulting Development Difficulty Index and Mission Impact for Key Payload Components

Item	SOT	DED	Development Difficulty Index	Mission Impact
LRI	2	3	**0.11**	**0.8**
CAI	5	4	**0.36**	**0.7**
Iodine Reference Unit	5	3	**0.27**	**0.6**
OMIS	5	3	**0.27**	**0.5**
CMT	1	3	**0.06**	**0.6**
MiniCAS	6	8	**0.86**	**0.1**

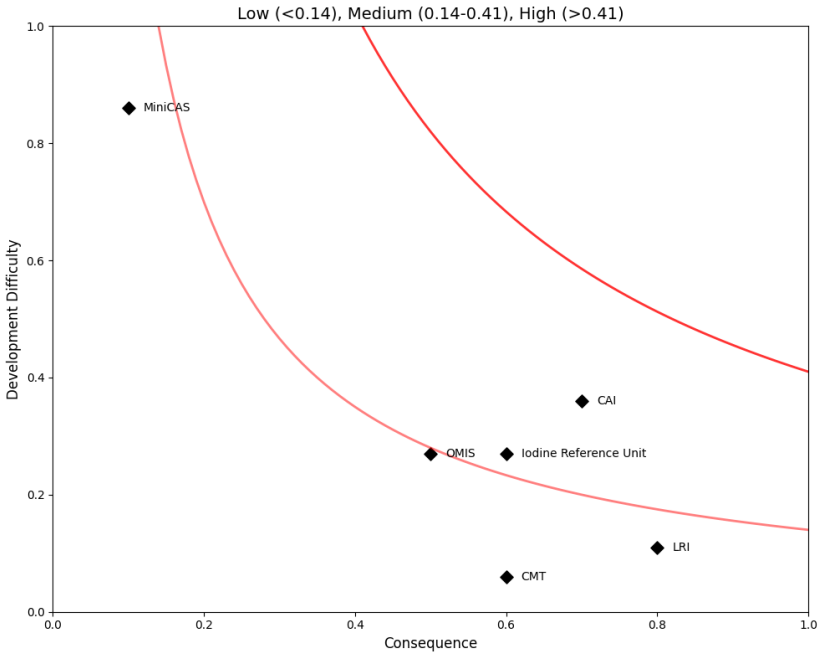

Figure 4.8: Payload Risk Map

4.10. Payload Requirements

This payload analysis resulted in system level requirements that will drive the design at subsystem level. These requirements are listed in the following table.

Updated ID	Old ID	Description	Verification	Source
SYS-PAY-4.1		The LRI laser source temperature shall not fluctuate by more than 0.1 K per orbit.	Testing	[37]
SYS-PAY-4.2		The LRI Triple Mirror Assembly temperature shall not fluctuate by more than 0.1 K per orbit.	Testing	[37]
SYS-PAY-4.3		The LRI cavity temperature shall not fluctuate by more than 1.5 K per orbit.	Testing	[37]
SYS-PAY-4.4		The CAI temperature shall not fluctuate by more than 0.1 K per orbit.	Testing	DLR[7]
SYS-PAY-4.5		The LRI temperature shall be kept within the range of 27–33 °C.	Testing	[37]
SYS-PAY-4.6		The CAI temperature shall be kept within the range of 20–23 °C.	Testing	DLR[7]
SYS-PAY-4.7		The spacecraft shall provide at least 0.1 mrad pointing accuracy in pitch when in nominal science mode.	Testing	DLR[3]
SYS-PAY-4.8		The spacecraft shall provide at least 0.1 mrad pointing accuracy in yaw when in nominal science mode.	Testing	DLR[3]
SYS-PAY-4.9		The spacecraft shall provide at least 0.25 mrad pointing accuracy in roll when in nominal science mode.	Testing	DLR[3]
SYS-PAY-4.10		The CAI shall be positioned in a single axis, along-track configuration.	Inspection	DLR[7]
SYS-PAY-4.11		The CMT shall provide a spacecraft trim capability of at least ±5 mm in the X and Y axes.	Testing	Derived
SYS-PAY-4.12		The CoM of the spacecraft shall be offset by less than 300 micrometers from integration to transfer orbit acquisition.	Demonstratior	[37]
SYS-PAY-4.13		The CoM of the spacecraft shall not change more than 100 micrometers over six months of science operations.	Analysis	[37]
SYS-PAY-4.14		The spacecraft shall not produce vibrations that render science data unusable for more than 1% of science operations.	Analysis	Derived
SYS-PAY-4.15		The spacecraft shall be able to provide 234 W to the payload throughout the mission.	Review	Derived
SYS-PAY-4.16	SUB-STRUC-2.6.1.3	The magnetic field external to the CAI shall be less than 10 mT.	Testing	[44]
SYS-PAY-4.17		The spacecraft shall be able to downlink all of the 3.7 Gbits of payload data generated every day.	Testing	[37]
SYS-PAY-4.18		The payload shall collect science data at a 10 Hz measurement rate.	Testing	DLR[3 7]
SYS-PAY-4.19		The absolute knowledge of laser frequency at time scales greater than 10,000 seconds shall have a fractional sensitivity of 10^{-8} or better.	Testing	[42, 40, 39]
SYS-PAY-4.20		The spacecraft shall have an absolute frequency reference, with stability of 10^{-14} for observation times > 100 s.	Testing	[42, 40, 39]

MarsExplore Mission

F.1 Design System

F.1.1 Outline Concepts

- F.1.1.1 Conduct Literature Study
  - F.1.1.1.1 Review heritage missions
  - F.1.1.1.2 Research scientific applications
  - F.1.1.1.3 Research payload
- F.1.1.2 Develop Mission Requirements
  - F.1.1.2.1 Perform stakeholder & market analysis
  - F.1.1.2.2 Create Requirement Discovery Tree
  - F.1.1.2.3 Perform requirement verification
- F.1.1.3 Estimate Initial System Budgets
  - F.1.1.3.1 Analyse effect of quantum payload
  - F.1.1.3.2 Create initial system budgets
- F.1.1.4 Identify Alternative Concepts
  - F.1.1.4.1 Create Design Option Tree
  - F.1.1.4.2 Perform feasibility analysis
  - F.1.1.4.3 Draw basic concept sketches
- F.1.1.5 Identify Subsystem Relationships
  - F.1.1.5.1 Create N2 chart
  - F.1.1.5.2 Identify critical interface points

F.1.2 Perform Concept Trade-Off

- F.1.2.1 Size Concepts
  - F.1.2.1.1 Estimate payload requirements
  - F.1.2.1.2 Determine preliminary dimensions
  - F.1.2.1.3 Size subsystems at high-level
- F.1.2.2 Perform Concept Risk Analysis
  - F.1.2.2.1 Create concept risk assessment chart
  - F.1.2.2.2 Evaluate concept risk levels
- F.1.2.3 Determine Trade-off Criteria
  - F.1.2.3.1 Select trade-off criteria
  - F.1.2.3.2 Select trade-off weights
- F.1.2.4 Perform Trade-Off
  - F.1.2.4.1 Create trade-off table
  - F.1.2.4.2 Perform trade-off sensitivity analysis

F.1.3 Design Subsystems in Detail

- F.1.3.1 Update Subsystem Relationships
  - F.1.3.1.1 Update N2 chart
  - F.1.3.1.2 Determine critical interface points
  - F.1.3.1.3 Create systems engineering interface
- F.1.3.2 Define Subsystem Requirements
  - F.1.3.2.1 Review existing requirements
  - F.1.3.2.2 Create subsystem requirements
  - F.1.3.2.3 Review consistency with budgets
  - F.1.3.2.4 Justify verification methods
- F.1.3.3 Perform (Sub)System Risk Assessment
  - F.1.3.3.1 Perform subsystem risk assessment
  - F.1.3.3.2 Perform system risk assessment
- F.1.3.4 Design Mission
  - F.1.3.4.1 Plan mission overview
  - F.1.3.4.2 Select launch vehicle
  - F.1.3.4.3 Design mission astrodynamics
- F.1.3.5 Design Subsystems
  - F.1.3.5.1 Design power subsystem
  - F.1.3.5.2 Design ADCS subsystem
  - F.1.3.5.3 Design thermal subsystem
  - F.1.3.5.4 Design TT&C subsystem
  - F.1.3.5.5 Design CDHS subsystem
  - F.1.3.5.6 Design structures subsystem
  - F.1.3.5.7 Design payload
  - F.1.3.5.8 Design propulsion subsystem
- F.1.3.6 Perform (Sub)System Verification
  - F.1.3.6.1 Perform unit tests
  - F.1.3.6.2 Perform subsystem tests
  - F.1.3.6.3 Perform system tests
- F.1.3.7 Produce Validation Plan
  - F.1.3.7.1 Select validation methods
  - F.1.3.7.2 Develop validation plan
- F.1.3.8 Produce CAD Model
  - F.1.3.8.1 Produce preliminary CAD model
  - F.1.3.8.2 Produce final CAD model

F.1.4 Design Components in Detail

- F.1.4.1 Investigate Off-the-Shelf Components
  - F.1.4.1.1 Identify component requirements
  - F.1.4.1.2 Search commercial & heritage component options
  - F.1.4.1.3 Document viable components
- F.1.4.2 Investigate Materials & Design Options
  - F.1.4.2.1 Define mission environment
  - F.1.4.2.2 Evaluate candidate materials & design options
  - F.1.4.2.3 Identify material & design option risks
  - F.1.4.2.4 Document viable materials & design options
- F.1.4.3 Perform Component Trade-Offs
  - F.1.4.3.1 Define component trade criteria
  - F.1.4.3.2 Select optimal component
  - F.1.4.3.3 Select optimal material & design option
- F.1.4.4 Model & Design Components
  - F.1.4.4.1 Create 3D component geometry
  - F.1.4.4.2 Integrate component into system model
  - F.1.4.4.3 Iterate based on component design
- F.1.4.5 Perform Component Analysis
  - F.1.4.5.1 Create simulation component model
  - F.1.4.5.2 Execute component analysis
  - F.1.4.4.3 Interpret component analysis results
- F.1.4.6 Perform Component V&V
  - F.1.4.6.1 Define V&V approach
  - F.1.4.6.2 Perform verification
  - F.1.4.6.3 Perform validation
  - F.1.4.6.4 Document V&V results

F.2 Produce Spacecraft

F.2.1 Manufacture Components

- F.2.1.1 Pick Contractor
  - F.2.1.1.1 Define component requirements
  - F.2.1.1.2 Issue request for proposals
  - F.2.1.1.3 Evaluate proposal compliance
  - F.2.1.1.4 Award contract to selected proposal
- F.2.1.2 Get Component Manufactured
  - F.2.1.2.1 Provide production documentation
  - F.2.1.2.2 Initiate component production
  - F.2.1.2.3 Monitor component production
  - F.2.1.2.4 Receive completed component
- F.2.1.3 Assure Quality
  - F.2.1.3.1 Inspect produced component dimensions
  - F.2.1.3.2 Inspect produced component materials
- F.2.1.4 Clean Component
  - F.2.1.4.1 Identify cleaning requirements per component
  - F.2.1.4.2 Perform component cleaning
  - F.2.1.4.3 Verify component cleanliness

F.2.2 Test Components

- F.2.2.1 Perform General Component Tests
  - F.2.2.1.1 Perform component vibration tests
  - F.2.2.1.2 Perform component radiation tests
  - F.2.2.1.3 Perform component thermal tests
  - F.2.2.1.4 Perform component chemical tests
  - F.2.2.1.5 Perform component impact tests
  - F.2.2.1.6 Perform component cleanliness tests
  - F.2.2.1.7 Perform component outgassing tests
  - F.2.2.1.8 Perform component software tests

F.2.3 Assemble Subsystems

- F.2.31 Connect Subsys. Mech. Interfaces
  - F.2.3.1.1 Align components with mounting
  - F.2.3.1.2 Secure component mechanical mounts
- F.2.3.2 Connect Subsys. Elec. Interfaces
  - F.2.3.2.1 Identify electrical interface points
  - F.2.3.2.2 Complete subsystem electrical connections
- F.2.3.3 Verify Subsystem Assembly
  - F.2.3.3.1 Verify subsystem mechanical connections
  - F.2.3.3.2 Verify subsystem electrical connections

F.2.4 Test Subsystems

- F.2.4.1 Perform General Subsystem Tests
  - F.2.4.1.1 Perform subsystem vibration tests
  - F.2.4.1.2 Perform subsystem radiation tests
  - F.2.4.1.3 Perform subsystem thermal tests
  - F.2.4.1.4 Perform subsystem chemical tests
  - F.2.4.1.5 Perform subsytem impact tests
  - F.2.4.1.6 Perform subsystem cleanliness tests
  - F.2.4.1.7 Perform subsystem outgassing tests
  - F.2.4.1.8 Perform subsystem software tests
- F.2.4.2 Demonstrate Subsys. Perf.
  - F.2.4.2.1 Simulate mission conditions
  - F.2.4.2.2 Operate subsystem in demonstration
  - F.2.4.2.3 Verify subsystem functional behaviour
- F.2.4.3 Test Deployment Mechanisms
  - F.2.4.3.1 Prepare deployment test
  - F.2.4.3.2 Activate deployment sequence
  - F.2.4.3.3 Monitor deployment sequence
  - F.2.4.3.4 Verify deployment behaviour

F.2.5 Integrate Spacecraft

- F.2.5.1 Connect Spacecraft Mech. Interfaces
  - F.2.5.1.1 Align subsystems with mounting
  - F.2.5.1.2 Secure subsystems mechanical mounts
- F.2.5.2 Connect Spacecraft Elec. Interfaces
  - F.2.5.2.1 Identify electrical interface points
  - F.2.5.2.2 Complete spacecraft electrical connections
- F.2.5.3 Verify Spacecraft Integration
  - F.2.5.3.1 Verify spacecraft mechanical connections
  - F.2.5.3.2 Verify spacecraft electrical connections
- F.2.5.4 Load Fuel on Spacecraft
  - F.2.5.4.1 Connect spacecraft fueling interfaces
  - F.2.5.4.2 Transfer propellant to spacecraft
  - F.2.5.4.3 Monitor fueling operation
  - F.2.5.4.4 Secure fueling system

F.2.6 Test Spacecraft

- F.2.6.1 Perform General Spacecraft Tests
  - F.2.6.1.1 Perform spacecraft vibration tests
  - F.2.6.1.2 Perform spacecraft radiation tests
  - F.2.6.1.3 Perform spacecraft thermal tests
  - F.2.6.1.4 Perform spacecraft chemical tests
  - F.2.6.1.5 Perform spacecraft impact tests
  - F.2.6.1.6 Perform spacecraft cleanliness tests
  - F.2.6.1.7 Perform spacecraft outgassing tests
  - F.2.6.1.8 Perform spacecraft software tests
- F.2.6.2 Inspect Spacecraft Properties
  - F.2.6.2.1 Inspect spacecraft mass moment of inertia
  - F.2.6.2.2 Inspect spacecraft mass
  - F.2.6.2.3 Inspect spacecraft volume
  - F.2.6.2.4 Inspect spacecraft power
- F.2.6.3 Inspect Spacecraft Alignment
  - F.2.6.3.1 Inspect thruster alignment
  - F.2.6.3.2 Inspect antennae alignment
  - F.2.6.3.3 Inspect mechanical alignment
  - F.2.6.3.4 Inspect payload alignment

F.3 Deploy Spacecraft

F.3.1 Launch Spacecraft

- F.3.1.1 Perform Pre-Launch Activities
  - F.3.1.1.1 Establish launch window
  - F.3.1.1.2 Verify rocket integrity
  - F.3.1.1.3 Attach spacecraft to rocket
  - F.3.1.1.4 Roll out rocket to pad
  - F.3.1.1.5 Monitor launch conditions
- F.3.1.2 Monitor Launch Performance
  - F.3.1.2.1 Cool rocket engines
  - F.3.1.2.2 Startup fuel pumps
  - F.3.1.2.3 Monitor rocket thrust
  - F.3.1.2.4 Monitor launch trajectory
- F.3.1.3 Achieve Initial Orbit
  - F.3.1.3.1 Initiate launch
  - F.3.1.3.2 Separate 1st stage
  - F.3.1.3.3 Separate 2nd stage
  - F.3.1.3.4 Separate fairing
  - F.3.1.3.5 Confirm initial orbit

F.3.2 Commission Spacecraft

- F.3.2.1 Establish Spacecraft Attitude
  - F.3.2.1.1 Detect Sun orientation
  - F.3.2.1.2 Compute current attitude
  - F.3.2.1.3 Correct current attitude
  - F.3.2.1.4 Stabilize current attitude
- F.3.2.2 Start Power Generation System
  - F.3.2.2.1 Deploy mechanical components
  - F.3.2.2.2 Verify power generation
  - F.3.2.2.3 Allocate power to subsystems
- F.3.2.3 Establish Communication Link
  - F.3.2.3.1 Deploy antennas
  - F.3.2.3.2 Align antennas to ground station
  - F.3.2.3.3 Configure frequency and modulation
  - F.3.2.3.4 Verify communication link
- F.3.2.4 Perform Subsystem Checks
  - F.3.2.4.1 Check payload
  - F.3.2.4.2 Check thermal subsystem
  - F.3.2.4.3 Check spacecraft structure
  - F.3.2.4.4 Check propulsion subsystem

F.3.3 Perform Transfer to Science Orbit

- F.3.3.1 Perform Transfer to Mars
  - F.3.3.1.1 Perform Mars injection burn
  - F.3.3.1.2 Monitor transfer trajectory
  - F.3.3.1.3 Perform correction burns
- F.3.3.2 Enter Initial Mars Orbit
  - F.3.3.2.1 Perform Mars capture burn
  - F.3.3.2.2 Verify capture orbital parameters
- F.3.3.3 Perform Mars Orbit Corrections
  - F.3.3.3.1 Change orbital altitude
  - F.3.3.3.2 Change orbital inclination
  - F.3.3.3.3 Change orbital eccentricity
  - F.3.3.3.4 Verify science orbit

F.4 Operate Spacecraft

F.4.1 Protect Spacecraft

- F.4.1.1 Regulate Spacecraft Temperature
  - F.4.1.1.1 Monitor spacecraft temperature
  - F.4.1.1.2 Operate active heating
  - F.4.1.1.3 Implement passive heating
  - F.4.1.1.4 Regulate payload temperature
- F.4.1.2 Protect Spacecraft from Space Debris
  - F.4.1.2.1 Implement debris shielding
  - F.4.1.2.2 Monitor large debris
  - F.4.1.2.3 Manoeuvre around large debris
- F.4.1.3 Ensure Spacecraft Power Supply
  - F.4.1.3.1 Manage power generation
  - F.4.1.3.2 Distribute power to subsystems
  - F.4.1.3.3 Monitor power performance
- F.4.1.4 Protect Spacecraft from Radiation
  - F.4.1.4.1 Monitor radiation environment
  - F.4.1.4.2 Detect radiation-induced anomalies
  - F.4.1.4.3 Reconfigure operations to minimize radiation exposure
  - F.4.1.4.4 Log radiation exposure data
- F.4.1.5 Protect Spacecraft from Atmosphere
  - F.4.1.5.1 Monitor atmospheric conditions
  - F.4.1.5.2 Adjust operations based on atmospheric effects
  - F.4.1.5.3 Assess atmospheric influence
- F.4.1.6 Protect Spacecraft from Vibrations
  - F.4.1.6.1 Monitor on-board vibrations
  - F.4.1.6.2 Isolate vibration sources
  - F.4.1.6.3 Adapt operating procedures to minimize vibrations

F.4.2 Collect Telemetry

- F.4.2.1 Obtain Navigation Data
  - F.4.2.1.1 Retrieve spacecraft attitude
  - F.4.2.1.2 Retrieve spacecraft position
  - F.4.2.1.3 Retrieve spacecraft velocity
  - F.4.2.1.4 Log navigation data
- F.4.2.2 Obtain Subsystem Telemetry
  - F.4.2.2.1 Collect status data from subsystems
  - F.4.2.2.2 Monitor key parameters
  - F.4.2.2.3 Detect anomalies in subsystem telemetry
  - F.4.2.2.4 Store telemetry data

F.4.3 Perform Scientific Measurements

- F.4.3.1 Activate Payload
  - F.4.3.1.1 Power on payload
  - F.4.3.1.2 Initialize spacecraft payload configuration
  - F.4.3.1.3 Confirm payload readiness
- F.4.3.2 Measure Non-Gravitational Disturbances
  - F.4.3.2.1 Take accelerometer measurements
  - F.4.3.2.2 Store accelerometer measurements
- F.4.3.3 Measure Total Disturbances
  - F.4.3.3.1 Take total disturbance measurements
  - F.4.3.3.2 Store total disturbance measurements
- F.4.3.4 Measure with Secondary Payload
  - F.4.3.4.1 Take secondary payload measurements
  - F.4.3.4.2 Store secondary payload measurements

F.4.4 Perform Manoeuvre & Attitude Control

- F.4.4.1 Perform Attitude Manoeuvres
  - F.4.4.1.1 Determine attitude change
  - F.4.4.1.2 Begin attitude manoeuvre
  - F.4.4.1.3 Monitor attitude manoeuvre
  - F.4.4.1.4 Verify final attitude
- F.4.4.2 Perform Orbit Control
  - F.4.4.2.1 Determine orbit deviation
  - F.4.4.2.2 Begin orbital manoeuvre
  - F.4.4.2.3 Monitor orbital manoeuvre
  - F.4.4.2.4 Verify final orbital parameters

F.4.5 Communicate with Earth

- F.4.5.1 Receive Commands
  - F.4.5.1.1 Point antennas towards Earth
  - F.4.5.1.2 Detect command signal
  - F.4.5.1.3 Decode command signal
  - F.4.5.1.4 Acknowledge command signal
  - F.4.5.1.5 Relay received command to subsystem
- F.4.5.2 Prepare Data for Transmission
  - F.4.5.2.1 Select data to be transmitted
  - F.4.5.2.2 Encode data
  - F.4.5.2.3 Store data in transmission queue
- F.4.5.3 Transmit Data
  - F.4.5.3.1 Establish communication link
  - F.4.5.3.2 Send encoded data
  - F.4.5.3.3 Monitor transmission status
- F.4.5.4 Receive Data on Ground
  - F.4.5.4.1 Read incoming transmission
  - F.4.5.4.2 Process received data
  - F.4.5.4.3 Store received data

F.4.6 Recover Spacecraft from Hazardous Situation

- F.4.6.1 Disable Non-Critical Subsystems
  - F.4.6.1.1 Identify non-critical subsystems
  - F.4.6.1.2 Place non-critical subsystems in standby
  - F.4.6.1.3 Isolate non-critical subsystem interfaces
  - F.4.6.1.4 Monitor system stability
- F.4.6.2 Regain Attitude Control
  - F.4.6.2.1 Determine current attitude
  - F.4.6.2.2 Determine recovery attitude target
  - F.4.6.2.3 Perform attitude recovery manoeuvre
  - F.4.6.2.4 Verify attitude stability
- F.4.6.3 Regain Power Supply
  - F.4.6.3.1 Assess power availability
  - F.4.6.3.2 Reactivate power supply
  - F.4.6.3.3 Monitor power stability
- F.4.6.4 Correct Orbit
  - F.4.6.4.1 Assess current orbit
  - F.4.6.4.2 Determine orbital corrections
  - F.4.6.4.3 Execute orbit recovery manoeuvre
  - F.4.6.4.4 Verify post-recovery orbital parameters
- F.4.6.5 Reestablish Communication
  - F.4.6.5.1 Determine communication status
  - F.4.6.5.2 Point antennas to Earth
  - F.4.6.5.3 Attempt communication link reinitialization
  - F.4.6.5.4 Confirm communication link

F.5 Decommission Spacecraft

F.5.1 Perform Decommission Manoeuvre

- F.5.1.1 Receive Decommission Trajectory
  - F.5.1.1.1 Receive trajectory data
  - F.5.1.1.2 Store trajectory data
  - F.5.1.1.3 Confirm trajectory data received
- F.5.1.2 Execute Decommission Manoeuvre
  - F.5.1.2.1 Confirm readiness for decommission manoeuvre
  - F.5.1.2.2 Orient spacecraft for decommission manoeuvre
  - F.5.1.2.3 Initiate decommission manoeuvre
  - F.5.1.2.4 Monitor decommission manoeuvre
- F.5.1.3 Confirm Decommission Manoeuvre
  - F.5.1.3.1 Acquire new orbital data
  - F.5.1.3.2 Compare new orbital data to target
  - F.5.1.3.3 Transmit decommission manoeuvre confirmation
  - F.5.1.3.4 Verify receival of decommission manoeuvre confirmation

F.5.2 Configure Spacecraft for Decommissioning

- F.5.2.1 Shut Down Non-Critical Subsystems
  - F.5.2.1.1 Identify non-critical subsystems
  - F.5.2.1.2 Issue shut down commands to non-critical subsystems
  - F.5.2.1.3 Confirm deactivation of non-critical subsystems
  - F.5.2.1.4 Monitor stability post-shutdown
- F.5.2.2 Safe Critical Subsystems
  - F.5.2.2.1 Disable pressurized systems
  - F.5.2.2.2 Reconfigure subsystems to passive state
  - F.5.2.2.3 Confirm safing complete
- F.5.2.3 Confirm Decommissioning
  - F.5.2.3.1 Generate final status report
  - F.5.2.3.2 Transmit decommissioning confirmation

Legend

- Mission
- Function
- Sub-Function
- Sub-Sub-Function
- Logical Block

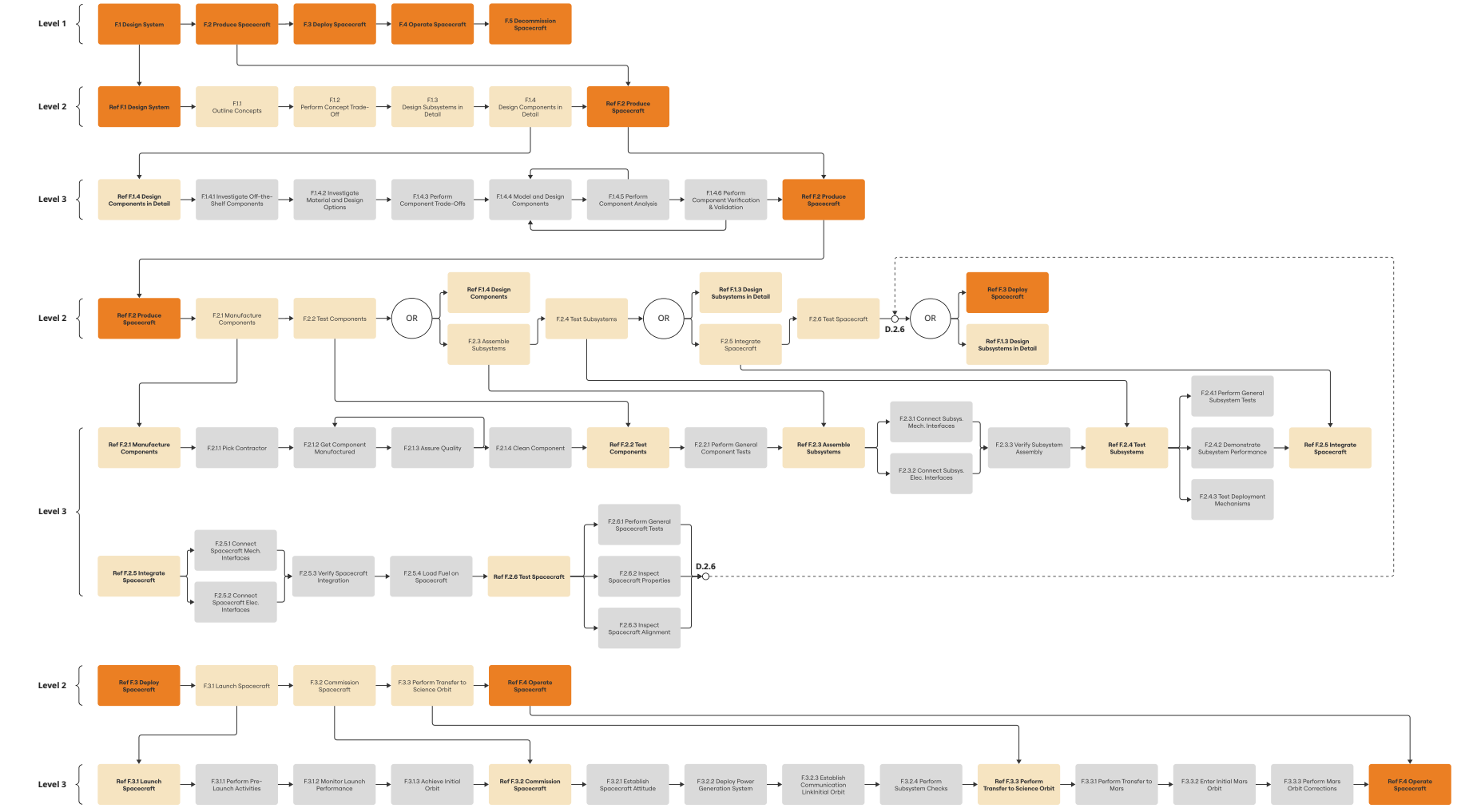
Level 1
F.1 Design System
F.2 Produce Spacecraft
F.3 Deploy Spacecraft
F.4 Operate Spacecraft
F.5 Decommission Spacecraft
Level 2
Ref F.1 Design System
F.1.1 Outline Concepts
F.1.2 Perform Concept Trade-Off
F.1.3 Design Subsystems in Detail
F.1.4 Design Components in Detail
Ref F.2 Produce Spacecraft
Level 3
Ref F.1.4 Design Components in Detail
F.1.4.1 Investigate Off-the-Shelf Components
F.1.4.2 Investigate Material and Design Options
F.1.4.3 Perform Component Trade-Offs
F.1.4.4 Model and Design Components
F.1.4.5 Perform Component Analysis
F.1.4.6 Perform Component Verification & Validation
Ref F.2 Produce Spacecraft
Level 2
Ref F.2 Produce Spacecraft
F.2.1 Manufacture Components
F.2.2 Test Components
OR
Ref F.1.4 Design Components
F.2.3 Assemble Subsystems
F.2.4 Test Subsystems
OR
Ref F.1.3 Design Subsystems in Detail
F.2.5 Integrate Spacecraft
F.2.6 Test Spacecraft
D.2.6
OR
Ref F.3 Deploy Spacecraft
Ref F.1.3 Design Subsystems in Detail
Level 3
Ref F.2.1 Manufacture Components
F.2.1.1 Pick Contractor
F.2.1.2 Get Component Manufactured
F.2.1.3 Assure Quality
F.2.1.4 Clean Component
Ref F.2.2 Test Components
F.2.2.1 Perform General Component Tests
Ref F.2.3 Assemble Subsystems
F.2.3.1 Connect Subsys. Mech. Interfaces
F.2.3.2 Connect Subsys. Elec. Interfaces
F.2.3.3 Verify Subsystem Assembly
Ref F.2.4 Test Subsystems
F.2.4.1 Perform General Subsystem Tests
F.2.4.2 Demonstrate Subsystem Performance
F.2.4.3 Test Deployment Mechanisms
Ref F.2.5 Integrate Spacecraft
Ref F.2.5 Integrate Spacecraft
F.2.5.1 Connect Spacecraft Mech. Interfaces
F.2.5.2 Connect Spacecraft Elec. Interfaces
F.2.5.3 Verify Spacecraft Integration
F.2.5.4 Load Fuel on Spacecraft
Ref F.2.6 Test Spacecraft
F.2.6.1 Perform General Spacecraft Tests
F.2.6.2 Inspect Spacecraft Properties
F.2.6.3 Inspect Spacecraft Alignment
D.2.6
Level 2
Ref F.3 Deploy Spacecraft
F.3.1 Launch Spacecraft
F.3.2 Commission Spacecraft
F.3.3 Perform Transfer to Science Orbit
Ref F.4 Operate Spacecraft
Level 3
Ref F.3.1 Launch Spacecraft
F.3.1.1 Perform Pre-Launch Activities
F.3.1.2 Monitor Launch Performance
F.3.1.3 Achieve Initial Orbit
Ref F.3.2 Commission Spacecraft
F.3.2.1 Establish Spacecraft Attitude
F.3.2.2 Deploy Power Generation System
F.3.2.3 Establish Communication LinkInitial Orbit
F.3.2.4 Perform Subsystem Checks
Ref F.3.3 Perform Transfer to Science Orbit
F.3.3.1 Perform Transfer to Mars
F.3.3.2 Enter Initial Mars Orbit
F.3.3.3 Perform Mars Orbit Corrections
Ref F.4 Operate Spacecraft
Legend
Mission
Function
Sub-Function
Sub-Sub-Function
Logical Block

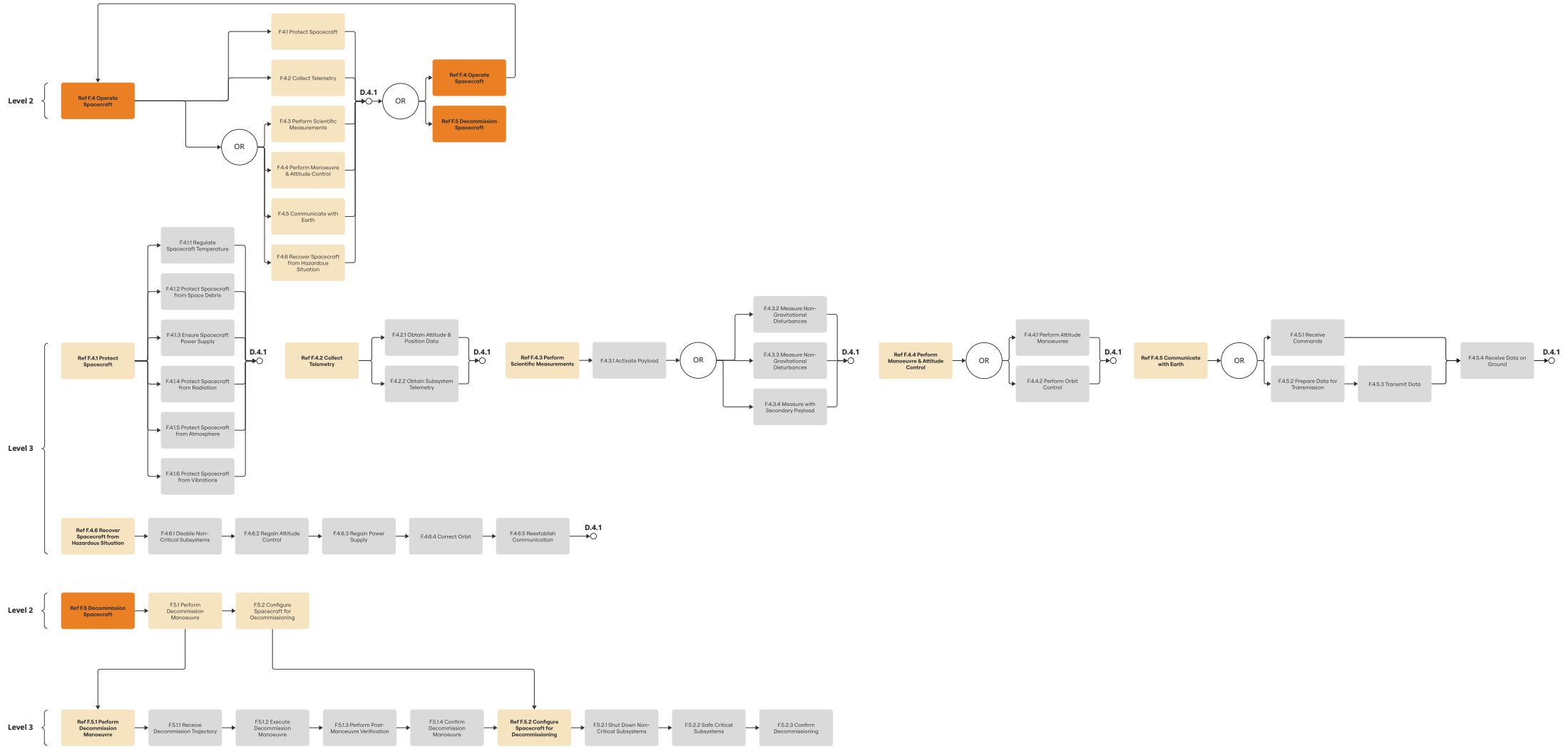
Level 2
Ref F.4 Operate Spacecraft
F.4.1 Protect Spacecraft
F.4.2 Collect Telemetry
F.4.3 Perform Scientific Measurements
F.4.4 Perform Manoeuvre & Attitude Control
F.4.5 Communicate with Earth
F.4.6 Recover Spacecraft from Hazardous Situation
OR
D.4.1
OR
Ref F.4 Operate Spacecraft
Ref F.5 Decommission Spacecraft
Level 3
Ref F.4.1 Protect Spacecraft
F.4.1.1 Regulate Spacecraft Temperature
F.4.1.2 Protect Spacecraft from Space Debris
F.4.1.3 Ensure Spacecraft Power Supply
F.4.1.4 Protect Spacecraft from Radiation
F.4.1.5 Protect Spacecraft from Atmosphere
F.4.1.6 Protect Spacecraft from Vibrations
D.4.1
Ref F.4.2 Collect Telemetry
F.4.2.1 Obtain Attitude & Position Data
F.4.2.2 Obtain Subsystem Telemetry
D.4.1
Ref F.4.3 Perform Scientific Measurements
F.4.3.1 Activate Payload
OR
F.4.3.2 Measure Non-Gravitational Disturbances
F.4.3.3 Measure Non-Gravitational Disturbances
F.4.3.4 Measure with Secondary Payload
D.4.1
Ref F.4.4 Perform Manoeuvre & Attitude Control
OR
F.4.4.1 Perform Attitude Manoeuvres
F.4.4.2 Perform Orbit Control
D.4.1
Ref F.4.5 Communicate with Earth
OR
F.4.5.1 Receive Commands
F.4.5.2 Prepare Data for Transmission
F.4.5.3 Transmit Data
F.4.5.4 Receive Data on Ground
D.4.1
Ref F.4.6 Recover Spacecraft from Hazardous Situation
F.4.6.1 Disable Non-Critical Subsystems
F.4.6.2 Regain Attitude Control
F.4.6.3 Regain Power Supply
F.4.6.4 Correct Orbit
F.4.6.5 Reestablish Communication
D.4.1
Level 2
Ref F.5 Decommission Spacecraft
F.5.1 Perform Decommission Manoeuvre
F.5.2 Configure Spacecraft for Decommissioning
Level 3
Ref F.5.1 Perform Decommission Manoeuvre
F.5.1.1 Receive Decommission Trajectory
F.5.1.2 Execute Decommission Manoeuvre
F.5.1.3 Perform Post-Manoeuvre Verification
F.5.1.4 Confirm Decommission Manoeuvre
Ref F.5.2 Configure Spacecraft for Decommissioning
F.5.2.1 Shut Down Non-Critical Subsystems
F.5.2.2 Safe Critical Subsystems
F.5.2.3 Confirm Decommissioning

5 Mission Design

In this chapter, with the mission requirements having been laid out and the payload designed, the flight plan for the mission must be developed. This begins by examining the functions the mission must perform, and then each phase of the mission is characterised. The effects of sustainability and risk are also discussed.

5.1. Mission Functional Analysis

The Mission Functional Analysis is performed with the Functional Breakdown Structure (FBS) and the Functional Flow Diagram (FFD). The FBS presents all functions to be performed throughout the mission hierarchically, whereas the FFD presents them chronologically. These are included in the previous two pages. The mission functional analysis is referred to at the beginning of every subsystem section to list the functions relevant to that subsystem.

5.2. Launcher selection

The most critical decision to be made about the launch phase is the selection of the launch vehicle. For easier integration with the launcher, and to reduce reliance on external parties, only ESA launchers were considered, following the requirements from ESA and MIS-ESA-2.4 [51]. According to requirement MIS-ESA-2.1, the launch date will be no earlier than 2041. The ESA launchers expected to operate at this time are Ariane 62, Ariane 64, Vega-C, and Vega-E. The Vega-C rocket is not able to launch a payload onto an Earth escape trajectory, so its use in the mission is not considered. Although the Vega-E is expected to improve on the performance of the Vega-C, and does not yet have detailed information available, it is assumed that the performance improvement will not be enough to make it a viable option for the mission. That leaves the two variants of the Ariane 6 rocket, the 62 and the 64.

The Ariane 62 has two fewer solid rocket boosters than its counterpart, but it is preferred if its performance is adequate due to its cost being lower by 28 million euros and its lower emissions [51]. To send the spacecraft on a Mars transfer trajectory, the rocket must inject it with a V_∞ of 2.9 km/s. The cheaper variant can inject 2250 kg of wet mass with this required velocity. According to the launch mass estimate of 2126 kg from the Midterm report [2], this fits the needs of the mission. To ensure the spacecraft stays within the limitations of the launcher, both in terms of mass and the conditions of launch, several system requirements are derived, with codes starting with SYS-LNCH-5.

5.3. Mission Phases

To examine the requirements of the system at every phase of the mission, each phase is separately analysed.

Launch phase

As explained in the Midterm Report [2], the primary objective of the launch phase is to deliver the MarsExplore spacecraft from Earth's surface into a heliocentric transfer orbit toward Mars, using a Hohmann transfer for energy efficiency.

To begin its journey toward Mars after a launch from Guiana Space Centre, the spacecraft must increase its speed through a Mars Transfer Injection (MTI) burn. The change in velocity required, referred to as ΔV_1 and computed using Equation 5.1, is assumed to be impulsive and provided by the launcher.

$$\Delta V_1 = \left| \sqrt{\frac{2\mu_E}{r_{LEO}} + v_\infty^2} - \sqrt{\frac{\mu_E}{r_{LEO}}} \right| \tag{5.1}$$

Where:

$$v_\infty = v_{\text{helio,LEO}} - v_{\text{Earth,orbit}} \tag{5.2}$$

$$v_{\text{helio,LEO}} = \sqrt{\mu_{\text{Sun}} \left(\frac{2}{r_{\text{Earth}}} - \frac{1}{a_{\text{trans}}} \right)} \tag{5.3}$$

$$v_{\text{Earth,orbit}} = \sqrt{\frac{\mu_{\text{Sun}}}{d_{\text{Earth}_{\text{Sun}}}}} \tag{5.4}$$

$$a_{\text{trans}} = \frac{d_{\text{Earth}} + d_{\text{Mars}}}{2} \tag{5.5}$$

This leads to $\Delta V_1 = 14.404$ km/s.

However, the launch date still needs to be computed. This is determined by computing the planetary positions and corroborating that they align with the optimal phase angle. To accurately assess the feasibility of a Hohmann transfer in the 2041-2043 time frame, the relative positions of Earth and Mars are retrieved from NASA JPL's HORIZONS System. Using vector ephemerides for the heliocentric positions of both planets on January 1, 2041, the initial Earth-Sun-Mars angle is restabilised. The initial condition also served as a reference point for the propagation of the launch window determination. At this time, the Earth-Sun-Mars angle was found to be approximately 173.4 degrees.

Thus, to compute the optimal launch window, a subsequent analysis is conducted where the evolution of the relative phases is determined. For a Hohmann transfer, such a phase angle ϕ is derived from the geometry of the elliptical transfer orbit as shown in Equation 5.6.

$$\phi = 180^\circ \left(1 - \sqrt{\left(\frac{(r_E + r_M)^3}{8 r_M^3} \right)} \right) \tag{5.6}$$

where: r_E is Earth's heliocentric distance and r_M is Mars' heliocentric distance. This gives an ideal phase angle of $\phi = 44.336^\circ$.

To determine the phase evolution, an iteration loop was modelled dynamically. The true phase is time dependent and as such, was modelled as shown in

$$\phi(t) = (\theta_M(t) - \theta_E(t)) + \phi_0 \tag{5.7}$$

Assuming constant angular velocities (mean motion), this is simplified as:

$$\phi(t) = (n_M - n_E)t + \phi_0 \tag{5.8}$$

Where ϕ_0 refers to the phase angle at January 1st 2041 (reference epoch), which was as previously explained set to be 173.4 degrees.

The difference in angular velocities leads to a synodic period S, or better said, the time between successive launch windows. This is computed with the following equation:

$$\frac{1}{S} = \left| \frac{1}{T_E} - \frac{1}{T_M} \right| \implies S \approx 780.21 \text{ days} \tag{5.9}$$

Iteratively solving the phase equation $\phi(t) = 44.33^\circ$ within the synodic window yields the target alignment. This results in the optimal launch window occurring on 2041-10-12, with a tolerance margin of ±2 days. Due to this synodic period, this launch date is strict for a launch in 2043 is not acceptable as constrained by **SYS-ASTRO-3.7**.

Transfer phase

Once the spacecraft is injected into its interplanetary transfer trajectory it arrives at Mars on the 24th of June 2042. This transit time was computed using Kepler's Third Law and taking have of the orbital period, as shown in Equation 5.10.

$$T = \frac{1}{2} \cdot 2\pi \sqrt{\frac{a^3}{\mu_M}} \tag{5.10}$$

During such cruise phase, one planned mid-course manoeuvre is required to adjust the orbital inclination to the final 92.44° as required for our sun-synchronous orbit [2]. This change in inclination is to 20 m/s and planned during the transfer to minimize the required delta-v. This manoeuvrer is performed shortly after launch, and when it is complete, the two spacecraft will sequentially separate from the launch vehicle. Following this the deployment and checkout of the critical spacecraft subsystems will be performed. This operation will include the deployment of the solar panels, testing the pointing of any antennas, and examining telemetry to assess the health of spacecraft.

Insertion and aerobraking phase

Upon arrival at Mars on 2024-06-24, the MarsExplore spacecraft begins its orbital insertion phase. The spacecraft needs to be captured and circularized into the final science orbit. A key mission design choice is the implementation of aerobraking for circularization rather than a full propulsive insertion. This decision was motivated, as explained in the Midterm Report, primarily by the significant propellant saving (approximately 1 km/s of delta-v) [2].

When the spacecraft approaches Mars on a hyperbolic trajectory with the pericenter altitude of approximately 120 km, a small retrograde manoeuvre may be executed before atmospheric entry. Thus, the spacecraft does not immediately enter a circular orbit but instead captured into a highly elliptical orbit (eccentricity of around 0.85) with an apocenter of around $r_{apo} = 24620.5$ km.

Moreover, for the capture manoeuvre into such elliptical orbit 1.263 km/s delta-v is required. This is derived from the difference between the spacecraft's velocity at periapsis on the hyperbolic arrival trajectory and the velocity required to achieve the 0.85 eccentric orbit, as shown in Equation 5.11.

$$\Delta V_2 = v_{\text{hyp}} - v_{\text{pericenter}} \tag{5.11}$$

Where:

$$v_{\text{pericenter}} = \sqrt{\mu_M \left(\frac{2}{r_p} - \frac{1}{a} \right)} \tag{5.12}$$

$$v_{\text{hyp}} = \sqrt{v_\infty^2 + \frac{2\mu_M}{r_p}} \tag{5.13}$$

The selection of the 120 km as the initial periapsis was made after iterative simulations balancing three constraints: minimizing total aerobraking duration, ensuring circularization before solar conjunction and thermal safety margins of the spacecraft. Altitudes 110 km or lower provided rapid but extremely risky orbital decay with extreme dynamic pressures and frictional heating, threatening the integrity of the spacecraft. Above 130 km extended exponentially the aerobraking period, dangerously pushing orbital circularization phase to the TT&C communications blackout, as will be explained in Section 6.3.

The simulation performed is based on orbital energy analysis, where the change in specific orbital energy, determined in Equation 5.14, due to the work done by the atmospheric drag is computed per orbit and used to update the semi-major axis and apoapsis. Before diving into how the iteration is performed, an important note to take is that the atmospheric density as a function of altitude was obtained from the tabulated data in Mars-GRAM's first 2 years of data collection and was processed to

cover up to 250 km of altitude. Linear interpolation was applied and is visualized in Figure 5.1, where a logarithmic scale is used for better interpretation.

$$E = -\frac{\mu_M}{2a} \tag{5.14}$$

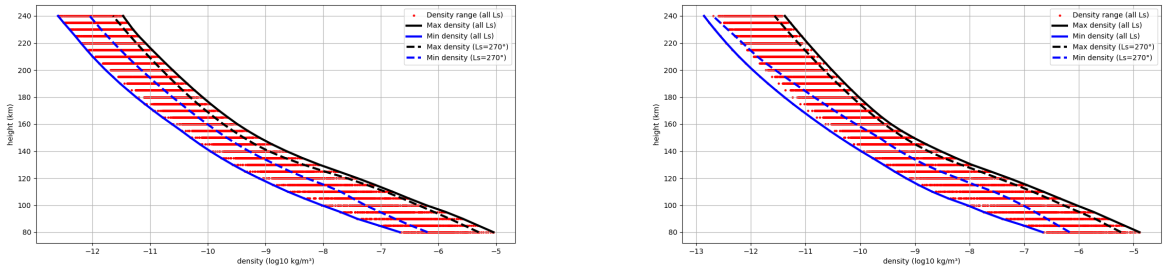

(a) Density Year 1 MarsGRAM

(b) Density Year 2 MarsGRAM

Figure 5.1: Density variations for Year 1 and Year 2 according to MarsGRAM.

Now, onto the orbital decay computation following a energy analysis simulation. For every orbit, firstly the drag force is computed using Equation 5.15.

$$F_D = \frac{1}{2}\rho V^2 C_D S \tag{5.15}$$

- ρ is atmospheric density at 120 km and equals $5.224 \cdot 10^{-8} kg/m^3$ (from Mars-GRAM).
- V is orbital velocity at pericenter.
- C_D is the drag coefficient ($\sim$ 2.7) where such aerodynamic parameter is computed in Section 7.4.
- A is the cross-sectional area of the spacecraft ($\sim$ 2.04 m^2) (1.7 m x 1.2 m).

Then the drag force is integrated along a quarter of the orbital path, at which the spacecraft is assumed to be at periapsis. This assumption is conservative for it essentially allocates 90 degree phase transition which is more than required. Thus the work done by drag is:

$$\Delta E = -F_D \cdot s \tag{5.16}$$

This work down reduces the specific orbital energy and results in an updated orbital energy and new semi-major axis, as shown below:

$$E_{n+1} = E_n + \Delta E \tag{5.17}$$

$$a_{n+1} = -\frac{\mu_M}{2E_{n+1}} \tag{5.18}$$

Finally, from this new semimajor axis, a new apoapsis is found:

$$r_{\text{apo}} = 2a_{n+1} - r_{\text{per}} \tag{5.19}$$

From this value the radial decrease in the apoapsis height is computed. Additionally, an important point to mention is that every epoch the new orbital period is determined and added to the overall time. This subsequently allows a computation of the total aerobraking time. Taking a conservative approach and using the MarsGRAM density values for the Martian Year 2, the simulation predicted

a successful circularization after 572 orbits, which corresponds to approximately 3.6 months. The orbital radius decreases initially at a rate of 178 km/orbit to a rate of 7 km/orbit.

Nevertheless, as previously explained in the midterm report, the science orbit was designed at an altitude of 212.48 km, where the orbital geometry coincides with the required sun-synchronous dawn-dusk orbit with 30 sol ground-track repeat.

To achieve this, requires two post-aerobraking burns: one to raise apoapsis from 120 km to 212.48 km (22.65 m/s), and one to then circularize the orbit into the final science altitude (22.5 m/s). Thus, the bi-propellant propulsion system is required to provide an additional 45.14 m/s to successfully perform this manoeuvre.

Commissioning Phase

In order to achieve an accurate mission timeline, the time allocated for starting up and assessing the health of the science instruments has to be estimated. To do this, a number of comparable missions were investigated, and a commissioning time was selected.

The missions selected to be compared are the Mars Reconnaissance Orbiter, the Trace Gas Orbiter and MAVEN, all three being Mars missions launched within the last two decades. A table summarising the commissioning times of these spacecraft can be seen in Table 5.1 [1] [2] [3] [4]. It appears that these missions all have a commissioning time of around 2 months, so that was selected as the nominal time for this mission as well.

Table 5.1: Commissioning time of comparable Mars missions

	Arrival in science orbit	Science operations start	Commissioning time
MRO	30 August 2006[52]	November 7 2006[52]	69 days
TGO	February 20 2018[1]	April 21 2018[2]	60 days
MAVEN	September 21 2014[3]	November 16 2014[4]	66 days

Science Phase

Following commissioning, the spacecraft will begin normal science operations. To be able to observe temporal changes in the Martian gravity field, the spacecraft have to be taking science measurements for at least one Martian year, which equates to roughly 1.9 years on Earth.

For this phase, a sun-synchronous dawn-dusk 30 sol repeat polar orbit was selected, at an orbital altitude of 212.5 km and an inclination of 92.4432°. Such an orbit passes over the poles, and uses the oblateness of the planet to rotate the orbit around, and ensure that the orbital plane faces the Sun throughout the year. Such an orbit has several advantages and disadvantages that must be taken into account in the design process. First and foremost, the temperature fluctuations of the payload have to be kept at a minimum, and using an orbit that remains as close to constant sunlight will minimise the load on the thermal subsystem. It is also hugely beneficial for power generation, as eclipse times are minimised. Another consideration is the fixed orientation of the spacecraft relative to the general directions of the Earth and the Sun. This is not such an important consideration for most missions, as they are free either to turn the entire spacecraft in the desired direction for communications or solar power generation, or to employ actuators to orient specific components. But due to the unique requirement of the mission to minimise the movement of the centre of gravity, actuators with large ranges of motion cannot be implemented, and due to the fixed orientation of the spacecraft relative to each other, turning the entire spacecraft comes at the cost of the cessation of science operations

[1] https://issfd.org/ISSFD_2019/ISSFD_2019_AIAC18_Bellei-Gabriele.pdf?

[2] https://www.marsdaily.com/reports/ExoMars_Trace_Gas_Orbiter_ready_to_start_sniffing_the_methane_999.html

[3] https://lasp.colorado.edu/maven/about/mission-timeline/

[4] https://www.nasa.gov/missions/nasas-maven-celebrates-one-year-at-mars/

for the duration. Being on an orbit where these operations can be kept to a minimum thus provides a great advantage to the mission. Nonetheless, such an orbit also comes at a cost. Orbits that are both sun-synchronous and repeat only exist at specific altitudes and inclinations, and moving out of these will introduce a drift away from the desired orbit. Also, as an inherent property of dawn-dusk orbits, only the two times of day in their name will be flown above, meaning that no daily variations in gravity between day and night can be measured.

During the science phase, orbit maintenance is critical for it is essential that the spacecraft operates a in a nearly circular Sun-synchronous orbit at 212.48 km. Despite the thin Martian atmosphere, residual drag causes continuos orbital energy loss, which leads to gradual orbit decay. To maintain ground-track repeatability, regular orbit manoeuvres must be performed. The cumulative delta v required for these corrections over the mission lifetime is computed as follows.

Firstly, the atmospheric drag force experiences by the spacecraft is computed using Equation 5.15. However, this time the velocity and atmospheric density are appropriate to the science orbit configuration. This results in a total velocity loss due to drag of around 54.76 m/s for the total mission operational lifetime, as shown in .

$$\Delta v_{\text{drag}} = a \cdot \Delta t = \frac{F_D}{m} \cdot \Delta t \tag{5.20}$$

This $\Delta v_{\text{drag}} = 54.76$ m/s value directly represents the station-keeping ΔV required throughout the 2.04 years of spacecraft operations. In case fuel reserves are left at the end of the science mission, these can be used for an extended science mission, if funds are available. This is also discussed in Section 6.1.

Due to the inversely proportional correlation between altitude and atmospheric density as shown in Figure 5.1, the delta v required for orbit maintenance increases exponentially with a decrease in altitude. Thus, choosing a 188.10 km altitude sun-synchronous dawn-dusk orbit was discarded for the orbital maintenance input is exponentially higher.

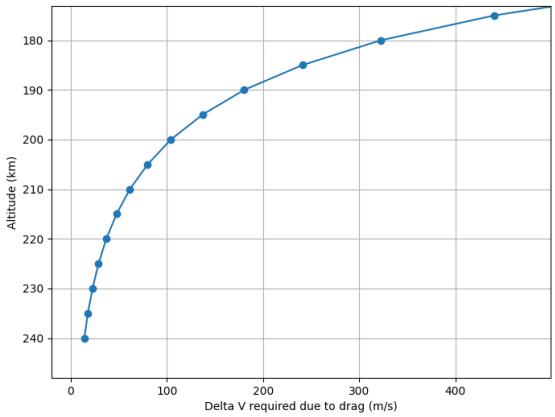

Figure 5.2: ΔV required to counteract atmospheric drag

Decommissioning Phase

Especially at such a low orbit as is chosen for this mission, it is important to consider the fate of the satellites at the end of operational life. The most important aspects are the planetary protection of Mars from contamination by human introduced lifeforms, and ensuring that no space debris is left in frequently used orbits around Mars. The two considered options are leaving the spacecraft in stable graveyard orbits, and letting them re-enter and crash into the Martian surface. A trade-off was performed between these two options.

Decommissioning Trade-Off and Result

Three criteria were chosen for the decommissioning trade-off. These are cost, additional ΔV and sustainability. These were all given weights from 1 to 5, and both options, reentry and graveyard orbit were given scores from 1 to 5 in all criteria. The weights assigned to the criteria and their justifications can be seen in Table 5.2. The result of the trade-off can be seen in Table 5.3. Placing the satellites on a graveyard orbit is the clear winner. To ensure that the spacecraft remain in stable orbit for at least 200 years without interfering with frequently used altitudes or re-entering, they have to be placed in a 660 km altitude polar orbit [53]. To accomplish this, the spacecraft has to be able to provide 200 m/s of ΔV at the end of the mission.

Table 5.2: Justification of decommissioning trade-off weights

Criterion	Weight assigned	Justification
Cost	5	The cost of the mission, and by extension the decommissioning is a driving consideration of the overall mission, and thus receives the highest weight, 4.
Additional ΔV	3	The additional ΔV drives the design, increasing complexity and weight, but does not drive the budgets directly, so it is given a weight of 3.
Sustainability	3	Sustainable exploration is very important to the mission, but has to be balanced with mission success. For this reason it is given a weight of 3.

Table 5.3: Graphical decommissioning trade-off matrix: orbit options vs criteria. Colors reflect performance: green = excellent, blue = good, yellow = correctable, red = poor.

Criterion	Cost (5)	Additional ΔV (3)	Sustainability (3)	Total
Graveyard orbit	3	2	4	**30**
Reentry	1	5	2	25

5.4. Astrodynamic Parameters

The astrodynamic characteristics obtained are summarised here in Table 5.4.

Table 5.4: Astrodynamic parameters

Parameters	**Satellite separation**	**Spacecraft ΔV**	**Aerobraking time**	**Orbit altitude**
Result	58 km	1561.524 m/s	3.5 months	212.48 km
Parameters	**Orbit inclination**	**Period**	**Orbit type**	**Sols-to-repeat**
Result	92.44 degrees	109.39 minutes	Polar dawn-dusk SSO	30 sols

5.5. Mission Operations

Mission operations are a significant part of any space mission. Mission operations can influence spacecraft design, and contribute to cost. In order to account for these effects, an operations and logistics concept description was developed that details all mission operations functions. This figure can be seen in Figure 5.3.

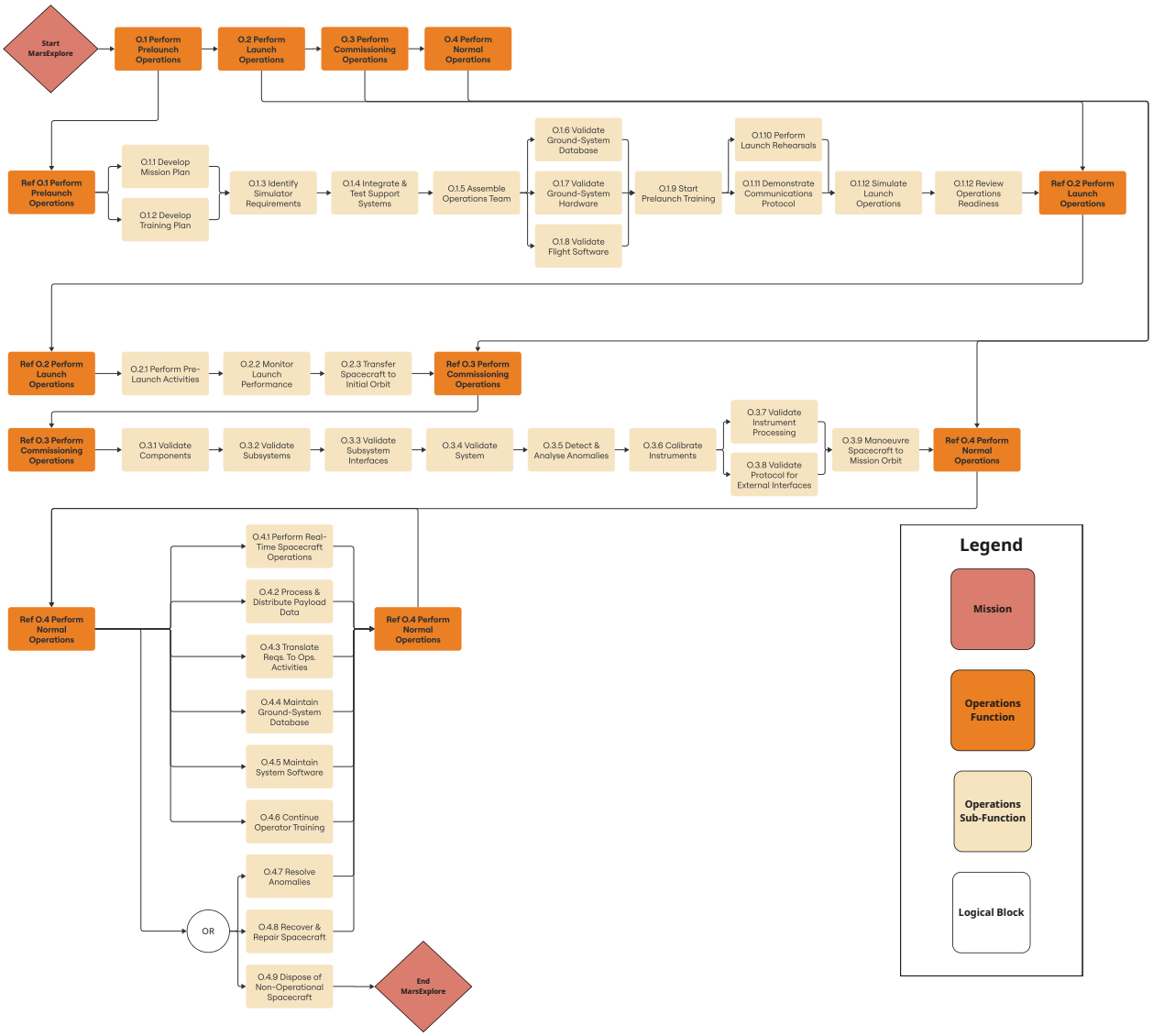

Figure 5.3: Operations and Logistics Concept Description

In order to account for the cost of mission operations in the cost budget two comparable Mars missions with publicly available funding data were examined. The yearly operational costs for the primary mission of MAVEN amounted to 14 million euros[5], while MRO's were 48 million euros[6]. Taking the average of these two values, a yearly operational cost of 28 million euros is obtained. With a nominal mission lifetime of 3.16 years, this amounts to a value of 88.5 million euros for operations costs for the mission.

5.6. Mission Timeline

It is also important to lay out the future of the mission, including the design phases to be undertaken, and the manufacturing of the spacecraft. This can be seen in Figure 5.4. Phase 0 is the initial design phase outlined by this report. The following phases from A to D align with the mission selection and definition phases outlined by the M-class mission call from ESA [51]. Phases E to G contain the mission flight phases outlined in this chapter.

[5] `https://www.planetary.org/space-policy/maven-cost`
[6] `https://www.planetary.org/space-policy/cost-of-the-mars-reconnaissance-orbiter`

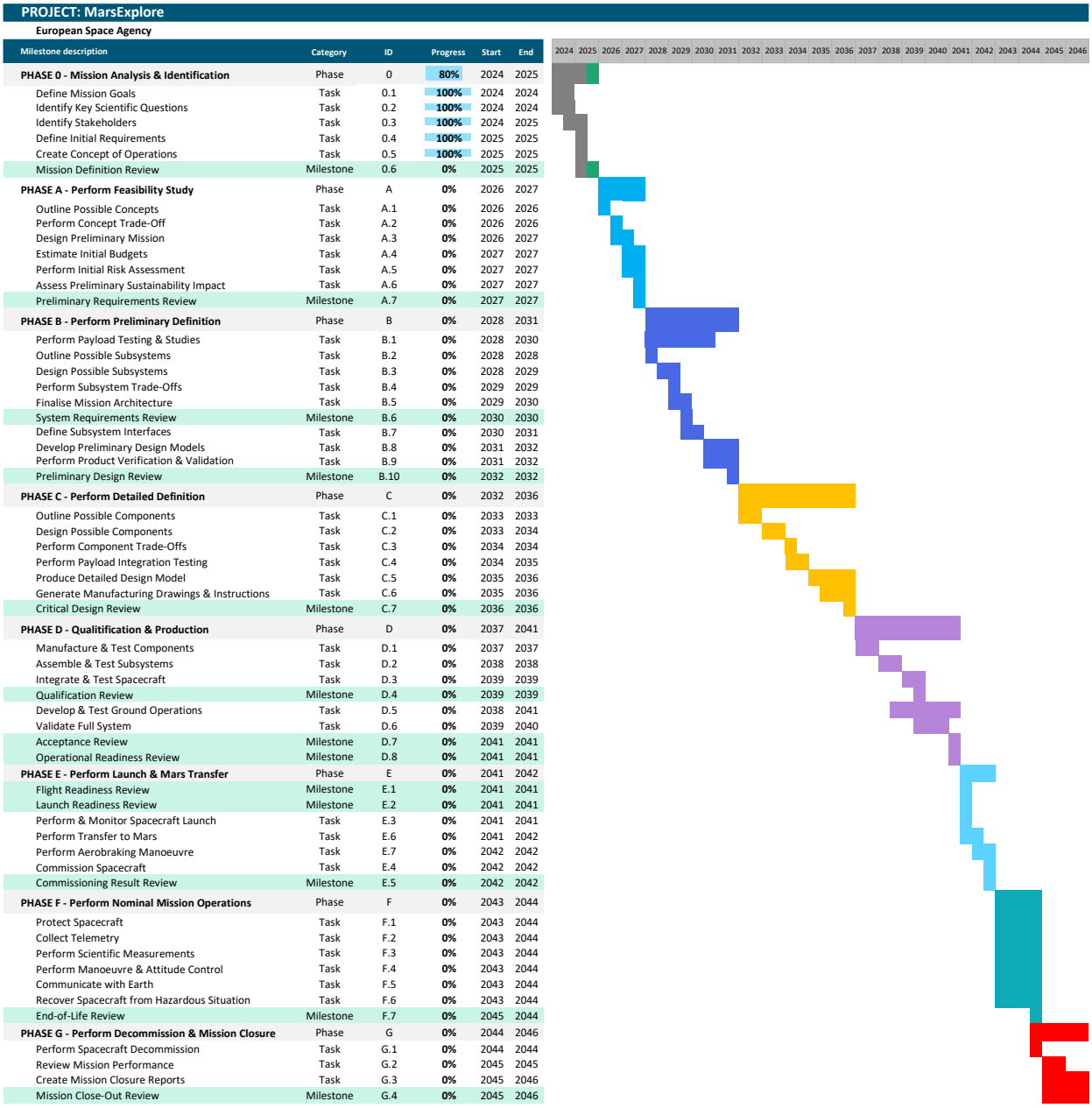

PROJECT: MarsExplore

European Space Agency

Milestone description	Category	ID	Progress	Start	End
PHASE 0 - Mission Analysis & Identification	Phase	0	80%	2024	2025
Define Mission Goals	Task	0.1	100%	2024	2024
Identify Key Scientific Questions	Task	0.2	100%	2024	2024
Identify Stakeholders	Task	0.3	100%	2024	2025
Define Initial Requirements	Task	0.4	100%	2025	2025
Create Concept of Operations	Task	0.5	100%	2025	2025
Mission Definition Review	Milestone	0.6	0%	2025	2025
PHASE A - Perform Feasibility Study	Phase	A	0%	2026	2027
Outline Possible Concepts	Task	A.1	0%	2026	2026
Perform Concept Trade-Off	Task	A.2	0%	2026	2026
Design Preliminary Mission	Task	A.3	0%	2026	2027
Estimate Initial Budgets	Task	A.4	0%	2027	2027
Perform Initial Risk Assessment	Task	A.5	0%	2027	2027
Assess Preliminary Sustainability Impact	Task	A.6	0%	2027	2027
Preliminary Requirements Review	Milestone	A.7	0%	2027	2027
PHASE B - Perform Preliminary Definition	Phase	B	0%	2028	2031
Perform Payload Testing & Studies	Task	B.1	0%	2028	2030
Outline Possible Subsystems	Task	B.2	0%	2028	2028
Design Possible Subsystems	Task	B.3	0%	2028	2029
Perform Subsystem Trade-Offs	Task	B.4	0%	2029	2029
Finalise Mission Architecture	Task	B.5	0%	2029	2030
System Requirements Review	Milestone	B.6	0%	2030	2030
Define Subsystem Interfaces	Task	B.7	0%	2030	2031
Develop Preliminary Design Models	Task	B.8	0%	2031	2032
Perform Product Verification & Validation	Task	B.9	0%	2031	2032
Preliminary Design Review	Milestone	B.10	0%	2032	2032
PHASE C - Perform Detailed Definition	Phase	C	0%	2032	2036
Outline Possible Components	Task	C.1	0%	2033	2033
Design Possible Components	Task	C.2	0%	2033	2034
Perform Component Trade-Offs	Task	C.3	0%	2034	2034
Perform Payload Integration Testing	Task	C.4	0%	2034	2035
Produce Detailed Design Model	Task	C.5	0%	2035	2036
Generate Manufacturing Drawings & Instructions	Task	C.6	0%	2035	2036
Critical Design Review	Milestone	C.7	0%	2036	2036
PHASE D - Qualification & Production	Phase	D	0%	2037	2041
Manufacture & Test Components	Task	D.1	0%	2037	2037
Assemble & Test Subsystems	Task	D.2	0%	2038	2038
Integrate & Test Spacecraft	Task	D.3	0%	2039	2039
Qualification Review	Milestone	D.4	0%	2039	2039
Develop & Test Ground Operations	Task	D.5	0%	2038	2041
Validate Full System	Task	D.6	0%	2039	2040
Acceptance Review	Milestone	D.7	0%	2041	2041
Operational Readiness Review	Milestone	D.8	0%	2041	2041
PHASE E - Perform Launch & Mars Transfer	Phase	E	0%	2041	2042
Flight Readiness Review	Milestone	E.1	0%	2041	2041
Launch Readiness Review	Milestone	E.2	0%	2041	2041
Perform & Monitor Spacecraft Launch	Task	E.3	0%	2041	2041
Perform Transfer to Mars	Task	E.6	0%	2041	2042
Perform Aerobraking Manoeuvre	Task	E.7	0%	2042	2042
Commission Spacecraft	Task	E.4	0%	2042	2042
Commissioning Result Review	Milestone	E.5	0%	2042	2042
PHASE F - Perform Nominal Mission Operations	Phase	F	0%	2043	2044
Protect Spacecraft	Task	F.1	0%	2043	2044
Collect Telemetry	Task	F.2	0%	2043	2044
Perform Scientific Measurements	Task	F.3	0%	2043	2044
Perform Manoeuvre & Attitude Control	Task	F.4	0%	2043	2044
Communicate with Earth	Task	F.5	0%	2043	2044
Recover Spacecraft from Hazardous Situation	Task	F.6	0%	2043	2044
End-of-Life Review	Milestone	F.7	0%	2045	2044
PHASE G - Perform Decommission & Mission Closure	Phase	G	0%	2044	2046
Perform Spacecraft Decommission	Task	G.1	0%	2044	2044
Review Mission Performance	Task	G.2	0%	2045	2045
Create Mission Closure Reports	Task	G.3	0%	2045	2046
Mission Close-Out Review	Milestone	G.4	0%	2045	2046

Figure 5.4: Mission Gantt Chart Detailing All Mission Phases

5.7. System Requirements

A number of system requirements were derived from mission design. These are listed below.

Updated ID	Old ID	Description	Verification
SYS-ASTRO-3.1		The spacecraft shall provide 1308 m/s of ΔV for Mars orbit injection and maneuvers during aerobraking.	Analysis
SYS-ASTRO-3.2		The spacecraft shall provide 49 m/s of ΔV for stationkeeping.	Analysis
SYS-ASTRO-3.3		The spacecraft shall provide 196 m/s of ΔV for decommissioning.	Analysis
SYS-ASTRO-3.4		The spacecraft shall be able to perform its Mars orbit injection burn in less than 1 hour.	Analysis

SYS-ASTRO-3.5		The spacecraft shall be able to perform a complete revolution around their y axis every orbit during science operations.	Analysis
SYS-ASTRO-3.6		The spacecraft shall be able to store the scientific data generated during the conjunctions of the Sun and Mars, lasting 24 days.	Testing
SYS-ASTRO-3.7		The spacecraft systems shall be compatible with a launch date between 2041 October 6–10.	Review of Design
SYS-ASTRO-3.8		The spacecraft shall be able to perform multiple burns during insertion.	Review of Design
SYS-LNCH-5.1		Each spacecraft shall have a maximum launch mass of 1450 kg.	Inspection
SYS-LNCH-5.2		The undeployed spacecraft shall fit within the payload compartment of the Ariane 62 Short Dual Launch Structure configuration.	Inspection
SYS-LNCH-5.2.1	UR-SYS-2.1.1.3	The undeployed spacecraft shall have a maximum height of 4.30 m.	Inspection
SYS-LNCH-5.2.2	UR-SYS-2.1.1.4	The undeployed cross section of each spacecraft shall allow the 2 spacecraft to fit within a circular cross-sectional diameter of 4.6 m.	Inspection
SYS-LNCH-5.3		The spacecraft shall be able to withstand the mechanical environment of launch aboard an Ariane 62 launch vehicle.	Testing
SYS-LNCH-5.3.1	SUB-STRUC-2.1.2.1.2.1	The spacecraft shall withstand a maximum axial g load of magnitude 6 without failing in Euler buckling.	Testing
SYS-LNCH-5.3.2		The spacecraft shall withstand a maximum axial g load of magnitude 6 without failing in yielding.	Testing
SYS-LNCH-5.3.3		The spacecraft shall withstand a maximum axial g load of magnitude 6 without failing at the ultimate load limit.	Testing
SYS-LNCH-5.3.4	SUB-STRUC-2.1.2.1.2.2	The spacecraft shall withstand a maximum lateral g load of magnitude 2 without failing in Euler buckling.	Testing
SYS-LNCH-5.3.5		The spacecraft shall withstand a maximum lateral g load of magnitude 2 without failing in yielding.	Testing
SYS-LNCH-5.3.6		The spacecraft shall withstand a maximum lateral g load of magnitude 2 without failing at the ultimate load limit.	Testing
SYS-LNCH-5.3.7	SUB-STRUC-2.1.2.1.2.3	The spacecraft shall have a fundamental axial natural frequency greater than 20 Hz.	Testing
SYS-LNCH-5.3.8	SUB-STRUC-2.1.2.1.2.4	The spacecraft shall have a fundamental lateral natural frequency greater than 6 Hz.	Testing

5.8. Sustainability

MarsExplore is dedicated to designing a sustainable space mission to Mars in compliance with ESA's standards and future goals. The mission aims to contribute to humanity's knowledge and education. Sustainability has been defined in accordance with the United Nations' Committee on the Peaceful Uses of Outer Space (UN COPUOS), which defines long-term space sustainability as: "[. . .] the ability to maintain the conduct of space activities indefinitely into the future in a manner that realises the objectives of equitable access to the benefits of the exploration and use of outer space for peaceful purposes, in order to meet the needs of the present generations while reserving the outer space environment for future generations." [54].

Sustainability has been considered throughout the full mission design and spacecraft design, from the selection of the launcher, the compliance with ESA and UN standards, and the end-of-life.

Launcher impact

The Ariane 6 launcher, specifically the 62 configuration, has been selected for the MarsExplore mission. This next-generation launcher has been developed to meet the needs of European institutional missions and to work towards a more sustainable future.

In order to asses the environmental impact of the launcher, the propellants emissions of the three different stages have been analysed. The three stages (first, core and upper stage) together with the emission products have been summarized in Table 5.6[7].

Table 5.6: Ariane 62 Launch Vehicle Emissions by Stage

Stage	Propellant Mass (kg)	Emission Products
Solid Rocket Boosters (P120C)	142,000 each Total: 284,000	• Hydrogen chloride (HCl): ~79,520 kg; • Alumina particles (Al_2O_3): ~96,560 kg; • Carbon monoxide (CO): ~28,400 kg; • Black carbon (soot): ~5,680 kg; • Carbon dioxide (CO_2): ~86,000 kg; • Water vapour (H_2O), N_2, Cl_2, etc.
Core Stage (Vulcain 2.1 Engine)	154,000	Primarily water vapour (H_2O) from LH_2/LOX combustion.
Upper Stage (Vinci Engine)	30,000	Primarily water vapour (H_2O) from LH_2/LOX combustion.

The primary emission products from the launch contribute to global warming, ozone depletion and acidification or clouds and rains. More specifically, Hydrogen Chloride (HCl) contributes to acid rain in the lower atmosphere, Carbon Dioxide (CO_2) to global warming and Water Vapour (H_2O) can form lucent clouds if deposited at very high altitudes. Moreover, Aluminium Oxide (Al_2O_3) contributes to cloud deformation and can serve as surfaces for ozone-depleting chemical reactions, together with Chlorine gas (Cl_2). [55]. To make the emissions more tangible, if the alumina particles emitted during launch were evenly distributed, they would cover an area equivalent to approximately 1,700 soccer fields (with one soccer field being about 0.007 km^2).

The total kg of CO_2 emissions were estimated by accounting for both direct emissions and the carbon footprint associated by the production of liquid hydrogen LH_2 (2.7 kg of CO_2-eq) and liquid oxygen LOX (23.7 kg of CO_2-eq). This results in an approximated total amount of 1968800 kg of CO_2 emitted per Ariane 62 launch. Moreover, ESA has stated that 12% of the hydrogen required for the yearly nine flights of the Ariane 6 will be provided by the establishment, decreasing more than 3,000 tonnes of carbon dioxide emissions annually [8]. By the projected launch year of 2041, this would translate into more than 300 tonnes of avoided CO_2 emissions per launch. To put this into perspective, considering that an average new car in the EU emits 106.8 g CO_2/km, one Ariane 62 launch in 2041 will be comparable to about 1050 cars driving in a year now, which is about one fifth of the TU Delft staff car emissions.

The Vinci engine, used in the last stage of the Ariane 6 rocket, incorporates controlled reentry capabilities, ensuring a safe disposal of rocket components, significantly reducing the risk of creating space debris. This responsible approach aligns with international efforts to protect the orbital environment, preserving it for future missions and minimizing hazards to current space operations and life on Earth. Through the selection of this launcher, MarsExplore contributes to sustainable space exploration by actively mitigating long-term debris accumulation.

Planetary Protection and long-term sustainability

Planetary Protection refers to a set of policies and requirements aimed at avoiding harmful contamination of the environment of the Earth and other planets. The guidelines are internationally coordinated

[7] https://www.esa.int/Enabling_Support/Space_Transportation/Ariane/The_engines_of_Ariane_6

[8] https://www.esa.int/Enabling_Support/Space_Transportation/Green_hydrogen_for_Ariane_6_and_more

though the Committee on Space Research (COSPAR). These define protocols for sterilization, spacecraft cleaning, mission design, and simple handling to minimize contamination risks. [56]

MarsExplore falls under Category III, which applies to orbital missions around big celestial bodies, such as Mars. Under this category, cleanliness standards are enforced and any intentional impact in Special Mars Regions is prohibited [56]. The presence of groundwater defines a Special Region on Mars and it is possible that groundwater exist in areas beyond the poles. Moreover, accidental contamination could jeopardize potential signs of life. To mitigate the risk, the mission's end-of-life involves placing the spacecraft into a stable parking orbit, which has to be chosen to prevent long-term orbit cluttering and uncontrolled re-entry.

Moreover, if the satellite remains functional at the end of its primary mission, it can continue collecting data from the parking orbit or serve as a communication relay satellite for future missions. In addition, the use of quantum instruments increases the measurement precisions to potentially three time more accurate than current models. This performance could reduce the need for multiple future missions, similar to the three missions already existing around Earth. For Mars, a single high-precision mission like MarsExplore may suffice for many scientific objectives, reducing the potential environmental impact of future space missions.

Life Cycle Assessment and Sustainable Development Goals

Life Cycle Assessment (LCA) is a scientific method used to quantify environmental impact of a product, or in this case of a space mission, over the entire life cycle. Accurate LCA requires detailed knowledge of system components and processes. However, at the current conceptual phase of the MarsExplore mission, such specific data is not yet available, but for future design, the calculation of the LCA is recommended.

As an alternative, an estimate of the mission's emission factor can be derived using a cost-based method, as proposed in [57]. The emission factor of space missions (per mission full cost) is estimated to be 140 tCO_2 per M€ and the ground-based operations emissions are 250 tCO_2 per M€ [57]. Given the estimated cost of the MarsExplore mission, 717.74 M€, the carbon footprint is approximately 280000 tCO_2. To contextualize this figure, the emissions from MarsExplore would be equivalent to those generated by around 180,000 cars driving for one year. This is equivalent to the emissions produced if every single person in Eindhoven drove a car, over an entire year.

The use of LCA alone does not fully capture the broad sustainability concept proposed by the 2030 Agenda for Sustainable Development. This encourages to consider three dimensions of sustainable development: the economic, social, and environmental, as reflected in the 17 Sustainable Development Goals (SDGs), Figure 5.5[9].

Figure 5.5: United Nations Sustainable Development Goals, https://sdgs.un.org/goals

[9] https://sdgs.un.org/goals

MarsExplore contributes to multiple SDGs, specifically to:

- **SDG 4 - Quality Education**: the mission supports lifelong learning opportunities for all, by making all collected scientific data publicly available. This will maximize the mission's outcome, promoting collaboration and ensuring that the entire scientific community, and humanity at large, benefits directly.
- **SDG - 9, Industry, Innovation, and Infrastructure**: the mission fosters innovation though the utilization of quantum technology in a space mission.
- **SDG - 12, Responsible Consumption and Production**: the mission contributes to sustainable development by prioritizing resource-optimal choices, including launch vehicle selection and mission planning, and minimizing waste.
- **SDG - 14, Life Below Water and SDG - 15, Life on Land**: the mission minimizes harm to terrestrial and marine ecosystems though the usage of a sustainable launcher which avoids space debris.
- **SDG - 17, Partnerships for the Goals**: the mission follows from an ESA proposal, which represents a collaborative and international environment.

5.9. Risk Analysis

The technical risk assessment consists of three steps: identifying potential risks, developing mitigation strategies and setting up contingency plans in the case that the risks materialize. These risks are separated based on the mission phases as defined in Section 5.6. Once the risks are identified, the worst-case impact of each risk is assessed across three categories, namely, Mission, Cost, and Schedule. The risks are then evaluated based on two factors: the consequence, which quantifies the severity of the impact, and the likelihood of occurrence. Risk levels are normalised from 0 to 1, and based on standard engineering practices, these levels are classified as: Low (< 0.14), Moderate ($0.14 - 0.41$) and High (> 0.41) [58].

Regarding consequence, the impact category ratings are defined as follows: mission impact is quantified in Table 4.7, while cost and schedule impacts are presented in the tables below.

Table 5.8: Schedule and Cost Impact Ratings

Rating	Schedule Impact	Rating	Cost Impact
0	No schedule impact	0	None
0.1	Possible minor slip, non-critical path	0.1	Negligible
0.2	Minor subsystem slip	0.2	Minor
0.3	Subsystem slip requires workaround	0.3	Within budgeted range
0.4	Serious subsystem slip with alternatives	0.4	Within acceptable range
0.5	Potential project threat	0.5	Within uncertainty range
0.6	Serious project slip	0.6	Large cost increase
0.7	Probable project threat	0.7	Probable project threat
0.8	Extensive, project threatening	0.8	Project threatening
0.9	Certain, project threatening	0.9	Project threat certain
1	Unacceptable schedule slip	1	Unacceptable cost increase

In terms of likelihood, the definitions are presented in Table 5.9 and are based on occurrence of risks on past deep space missions. It is important to note that likelihood does not refer to the general chance of a risk occurring, but to the probability of the risk negatively impacting mission success.

The following table groups and summarises the most important risks while additional ones documented along the design process can be found in Appendix C.

Figure 5.6 visualise the updated risks before and after mitigation strategies are proposed.

Table 5.9: Likelihood Ratings

Rating	Likelihood
0.1	**Rare:** Risk never materializes
0.3	**Unlikely:** Has occurred in previous missions
0.5	**Moderate:** Has occurred in multiple previous missions
0.7	**Likely:** Has occurred in most missions
0.9	**Almost Certain:** Practically guaranteed

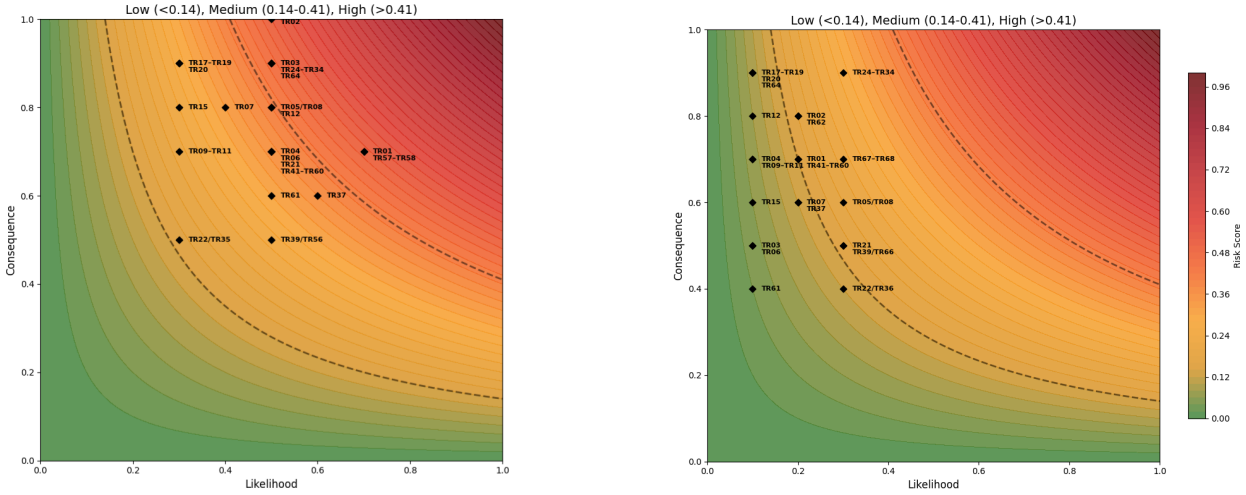

(a) Pre-Mitigation **(b)** Post-Mitigation

Figure 5.6: Risk Maps Before and After Mitigation

Figure 5.6 shows a clear improvement of the risk profile with a substantial shift towards the lower-left after implementing the mitigation strategies. Although the consequence of some risks has also decreased, the visual representation indicates the primary effect of the mitigation efforts in reducing the probability of occurrence. In addition, some risks such as TR24-TR34, TR67-TR68, TR02, TR62 and TR05/TR08 still remain in the lower end of the medium-risk category. This indicates that complete elimination of these risks is not possible. For this reason, continuous monitoring is required along with effective contingency plans.

5.10. Risk Requirements

Having identified the technical risks involved in the mission and their severity, a set of requirements was derived to ensure that mitigation measures are implemented throughout all phases of the mission. A list of risk requirements is documented to ensure mitigation is addressed within spacecraft design and that contingency actions can be executed if necessary. These requirements were determined from a risk analysis at functional level and flow down to subsystem level. These requirements are presented in the table below.

Updated ID	Old ID	Description	Verification
SYS-RISK-8.1	SUB-STRUC-2.6.2.6	The spacecraft shall withstand a dynamic pressure up to TBD Pa during the aerobraking manoeuvrer.	Testing
SYS-RISK-8.2	SUB-STRUC-2.6.2.7	The spacecraft shall withstand a surface temperature of TBD K during the aerobraking manoeuvre.	Testing
SYS-RISK-8.3	SUB-STRUC-2.6.2.8	The spacecraft shall survive a peak total heat load of TBD MJ/m^2 during aerobraking manoeuvre.	Testing
SYS-RISK-8.4	SUB-STRUC-2.6.2.9	The spacecraft's structural components shall be structurally qualified to withstand TBD mechanical loads during aerobraking.	Testing
SYS-RISK-8.5	SUB-CDHS-2.2.4.1.9	The spacecraft shall include software to update trajectory predictions according to real-time data.	Review of Design
SYS-RISK-8.6	SUB-CDHS-2.2.4.1.10	The spacecraft shall include logic to abort the aerobraking sequence and switch to propulsion-based orbital insertion.	Review of Design
SYS-RISK-8.7	SUB-CDHS-2.2.4.1.11	The spacecraft shall perform autonomous command validation to detect and reject incorrect or unsafe command sequences.	Review of Design
SYS-RISK-8.8	MIS-2.6.5.3	The spacecraft shall employ double redundancy for inter-satellite communication.	Review of Design
SYS-RISK-8.9	SUB-ADCS-2.5.2.3	The spacecraft shall be capable of restoring nominal attitude control after an unintended transition to safe mode.	Review of Design
SYS-RISK-8.10		The spacecraft critical surfaces and subsystems shall withstand MMOD impacts from particles of up to 0.01 kg mass, 2700 kg/m^3 density, and 20 km/s relative velocity without loss of structural integrity or functionality.	Review of Design
SYS-RISK-8.11		The spacecraft critical surfaces and subsystems shall withstand a TID of 10.95 rad without degradation in functionality.	Testing

ID	Technical Risk (TR)	Worst Case Impact	Likeli-hood	Conse-quence	Risk	Mitigation Action	Likeli-hood 2.0	Conse-quence 2.0	Risk 2.0	Contingency Action	Responsible Member
Phase 0 – Mission Analysis and identification											
TR01	Inadequate stakeholder alignment	Schedule	0.7	0.7	0.49	Conduct regular reviews of stakeholder requirements	0.2	0.7	0.14	Resolve misalignment	Project Manager
TR02	Overlooked constraints, killer requirements and mission objectives	Schedule	0.5	1	0.5	Perform requirement analysis, validation and assure compliance	0.2	0.8	0.16	Restructure scope and timeline of project	Systems Engineer
Phase A - Feasability											
TR03	Unrealistic concept selection	Schedule	0.5	0.9	0.45	Conduct feasibility and technology readiness assessment	0.1	0.5	0.05	Use another (back-up) concept	Systems Engineer
TR04	Poor risk assessment	Mission	0.5	0.7	0.35	Use a structured risk register	0.1	0.7	0.07	Perform risk review	Risk Manager
Phase B & C - Preliminary and Detailed Design											
TR05/TR08	Incompatibility between subsystems	Schedule	0.5	0.8	0.4	Perform early iteration and concurrent design sessions	0.3	0.6	0.18	Redesign interface between subsystems	System Engineer
TR06	Single points of failure and insufficient redundancy	Mission	0.5	0.7	0.35	Check deisgn for redundancy periodically	0.1	0.5	0.05	Include redundancy in critical components	Chief Engineers
TR07	Design estimate does not fall mass, volume and power budgets	Cost	0.4	0.8	0.32	Close collaboration between budget officer and subsystem engineers	0.2	0.6	0.12	Update and re-iterate design and request looser constraints if possible	Budget Officer
TR09-TR11	A legal, financial or technical requirement is not met	Schedule	0.3	0.7	0.21	Review legal compliance with laws	0.1	0.7	0.07	Review mission to comply with regulations	Project Manager
Phase D – Qualification and Production											
TR12	Manufacturing defects	Schedule	0.5	0.8	0.4	Conduct quality inspections	0.1	0.8	0.08	Repair or replace defective parts	Systems Engineer
TR15	Insufficient system verification	Mission	0.3	0.8	0.24	Ensure verifcation completeness and sufficient testing of critical systems in simulated conditions	0.1	0.6	0.06	Increased redundancy of affected parts	Systems Engineer
Phase E - Launch and Mars Transfer											
TR17-TR19	Launch vehicle, stage and fairing seperation failure	Mission	0.3	0.9	0.27	Use reiable launch vehicle	0.1	0.9	0.09	-	Project Manager
TR20	Orbital collision	Mission	0.3	0.9	0.27	Monitor space environment on Earth and avoid regions with high propability of impact	0.1	0.9	0.09	-	Astrodynamics Chief
TR21	Micrometeoroid impact	Mission	0.5	0.7	0.35	Install a MMOD bumper and select orbit trajectory with low probability of impact	0.3	0.5	0.15	Switch to redundant systems or activate safe mode	Astrodynamics Chief
TR39/TR66	Mars gravity field model uncertainties	Schedule	0.7	0.5	0.35	Use real-time atmospheric data, continuous monitoring of S/C	0.3	0.5	0.15	Perform maneuvers to fix trajectory	Astrodynamics Chief
TR67-TR68	Failure to handle thrermal and structural loads in aerobraking	Mission	0.5	0.7	0.35	Conduct testing of full system	0.3	0.7	0.21	Abort aerobraking sequence, switch to propulsion-based orbital insertion	Systems Engineer
TR24-TR34	Spacecraft commissioning	Mission	0.5	0.9	0.45	Ensure reliability through testing and verification, implement redundancy, monitor operations	0.3	0.9	0.27	Re-attempt comissioning, perform autonomous and ground commanded recovery procedures, use redundancy	Systems Engineer and Chiefs
Phase F – Operation											
TR22/TR36	Dust storm/ Solar flare event	Mission	0.3	0.5	0.15	Monitor weather conditions	0.3	0.4	0.12	Activate safe mode	Astrodynamics Chief
TR37	Resource depletion	Mission	0.5	0.6	0.3	Design with a margin and track fuel consumption and memory	0.2	0.6	0.12	Reduce mission objectives and switch to operating essential systems only	Budget Officer
TR64	Intersatellite communication failure	Mission	0.3	0.9	0.27	Implement redundant communication methods	0.1	0.9	0.09	-	TT&C Chief
TR41-TR60	Subsystem failures	Mission	0.6	0.7	0.42	Ensure subsystem reliability through extensive testing and verification, implement redundancy	0.2	0.7	0.14	Rely on backup systems, reboot respective subsystem and use redundancy	Systems Engineer and Chiefs
Phase G – Decommission and Project Closure											
TR61	Failure to downlink all data before decommissioning	Mission	0.5	0.6	0.3	Plan sufficient downlink sessions before mission completion	0.1	0.4	0.04	Use compromised high-rate transmission mode before shutdown	TT&C Chief
TR62	Incomplete disposal of spacecraft system	Mission	0.5	0.8	0.4	Design autonomous de-orbit	0.2	0.8	0.16	Avoid debris around Mars	Systems Engineer

6 Spacecraft Design

This chapter describes the design process of each subsystem, and their results. The spacecraft subsystems were designed employing concurrent design and systems engineering principles. Results were shared among the team as the design progressed, and an N2 chart was used to keep track of design dependencies between subsystems. This chart can be seen in Table 6.1. As the propellant mass and structural mass both affected each other, an iteration loop was run between them to converge to an accurate value. These boxes are shown in blue.

Table 6.1: System design N2 chart

Science & Mission Design	Satellite separation	Science orbit requirements	Science measurement duration						Launch load & Launch vibrations
Payload performance	**Payload**			Payload pointing accuracy	Payload data output rate	Payload data output rate	Payload operational temp. range	Payload power req.	Payload mass & Dimensions
Orbital altitude & Repeat & Coverage		**Astrodynamics**	Transfer Δv req. & Station keeping Δv req.		Earth visibility		Solar coverage	Solar coverage	
			Propulsion	Manoeuvre pointing accuracy			Prop. operational temp. range	Propulsion power req.	Spacecraft thrust & Propulsion mass & Dimensions
				ADCS			ADCS operational temp. range	ADCS power req.	ADCS mass & Dimensions
					TT&C	Max. time between communications		TT&C power req.	TT&C mass & Dimensions
						CDHS	CHDS operational temp. range	CDHS power req.	CDHS mass & Dimensions
							Thermal	Thermal power req.	Thermal mass & Dimensions & S/C Temp. range
							Power operational temp. range & S/C power	**Power**	Power mass & Dimensions
			S/C mass	Mass moment of inertia					**Structures**

6.1. Propulsion

The propulsion subsystem's main goal is to perform the required manoeuvrers to achieve the mission objectives.

Requirements and Functional Analysis

The design was driven by system and payload requirements as listed below.

Relevant Mission and System Requirements – Propulsion	
SYS-ASTRO-3.1	The spacecraft shall provide 1308 m/s of ΔV for Mars orbit injection and manoeuvrers during aerobraking.
SYS-ASTRO-3.2	The spacecraft shall provide 49 m/s of ΔV for station-keeping.
SYS-ASTRO-3.3	The spacecraft shall provide 196 m/s of ΔV for decommissioning.
SYS-ASTRO-3.4	The spacecraft shall be able to perform its Mars orbit injection burn in less than 1 hour.
SYS-ASTRO-3.8	The spacecraft shall be able to perform multiple burns during insertion.
SYS-PAY-4.13	The CoM of the spacecraft shall not change more than 300 micrometres over the course of a six-month period of science operations.
SYS-PAY-4.14	The spacecraft shall not produce vibrations that render science data unusable for more than 1% of science operations.
SYS-LNCH-5.1	Each spacecraft shall have a maximum launch mass of 1450 kg.

The functions to be performed by the propulsion subsystem, identified in the mission functional analysis of Section 5.1 are the following:

- F.3.3 Perform Transfer to Science Orbit
  - F.3.3.2 Enter Initial Mars Orbit
  - F.3.3.3 Perform Mars Orbit Corrections
  - F.4.3.3 Measure Total Disturbances
  - F.4.3.4 Measure with Secondary Payload
- F.4.4 Perform Manoeuvre & Attitude Control
  - F.4.4.2 Perform Orbit Control
- F.4.6 Recover Spacecraft from Hazardous Situation
  - F.4.6.4 Correct Orbit
- F.5.1 Perform Decommission Manoeuvre
  - F.5.1.2 Execute Decommission Manoeuvre

Analysis

Orbit capture is the largest required manoeuvre, involving multiple high-thrust burns. By using aerobraking, the required ΔV is reduced to 1308 m/s. Nonetheless, according to standard engineering practices outlined in SMAD, manoeuvrers requiring a ΔV of over 1000 m/s typically use bipropellant systems [59] (**SYS-ASTRO-3.1**). This is primarily due to the higher thrust capabilities and greater specific impulse, which are crucial aspects for executing multiple near-impulsive burns required for orbit capture [59] (**SYS-ASTRO-3.4**, **SYS-ASTRO-3.8**). Consequently, a bipropellant system was chosen. This selection is also consistent with prior successful missions involving similar orbital insertion manoeuvrers, such as the Mars Reconnaissance Orbiter [60].

Table 6.3: Properties of MON-3 and MMH Propellants

Property	Value
MON-3/MMH Combination	
O/F Ratio	2.27
Combustion Temp.	3455 K
Mixture Density	1020 kg/m^3
Isp (Vacuum)	340 s
MON-3	
Density	1370 kg/m^3
Freezing Temp.	-15 °C
Boiling Temp.	21 °C
MMH	
Density	880 kg/m^3
Freezing Temp.	-52 °C
Boiling Temp.	87 °C

In terms of propellants, Mars missions make use of hypergolic propellants due to their reliability, ignition and storage characteristics. While the combination of monomethyl-hydrazine (MMH) and nitrogen tetroxide (N_2O_4) has been extensively used in past deep space missions, active thermal systems are needed to maintain a narrow temperature of 15-27°C [61]. Substituting N_2O_4 with Mixed Oxides of Nitrogen (MON-3), which consists of 97%N_2O_4 and 3%NO significantly lowers the freezing point to -15°C allowing for less stringent thermal requirements, while maintaining comparable performance [61]. As such, the MON-3/MMH combination was selected, together with a pressure-fed propulsion system that utilizes helium as pressurant. The properties of this combination are summarised in Table 6.3 [1].

While bipropellant systems are ideal for large manoeuvrers, their use for orbital maintenance pose significant challenges. The payload requires the spacecraft's centre of mass (CM) to remain stable within 300 micrometers over a six-month period, imposing strict constraints on system level (**SYS-PAY-4.13**) . To meet this level of precision, the number of propellant tanks would need to be doubled and arranged symmetrically. Propellants would also have to be drawn simultaneously from each tank to prevent a shift in the centre of mass, similarly to the cold gas system used for GRACE [62]. However, even with this configuration and diaphragm tanks, known to minimise sloshing, residual sloshing would still occur in response to disturbances [63]. This could shift the centre of mass by up to a few millimetres

[1] http://www.astronautix.com/m/monmmh.html

upon every disturbance [64]. Although minor, such sloshing-induced deviations are inherently unpredictable and thus cannot be managed with a mass trimming mechanism, compromising scientific performance [64].

For this reason, a hybrid propulsion system was deemed necessary, despite its weak design heritage. At first, cold gas propulsion was considered for station-keeping. While cold gas thruster burns also generate disturbances, their duration, timing, and magnitude are planned and can therefore be effectively removed [65]. Yet, it's low specific impulse ($I_{sp} = 50 - 80s$) led to a high propellant mass of over 300 kg and volume demands incompatible with the launcher constraints [2].

In contrast, electrostatic propulsion utilizing xenon propellant offered a significantly more mass efficient solution, with an estimated propellant mass around 10 kg [59]. Propellant characteristics used are noted in Table 6.4.Moreover, electric propulsion also supports sustainable space operations with fewer emissions and a smaller carbon footprint being created [3], quantified in Section 7.8. These differences led to the selection of electric propulsion for station-keeping manoeuvres.

Table 6.4: Properties of Xenon Propellant

Property	Value
Specific Impulse	1700 s
Efficiency	0.5
Propellant Density	1350 kg/m^3
State	Compressed gas

To maintain the required 212.48km sun-synchronous orbit using electric propulsion requires an orbit maintenance strategy. Due to continuous drag at low Mars altitude, the orbit gradually decays as explained in Section 5.3 and as previously calculated requires an approximate 54 m/s over the operational lifetime.

Rather than continuous thrusting, a discrete burn strategy is adopted to leverage the payload and data acquisition performance and therefore satisfy **SYS-PAY-4.14** . The spacecraft monitors its altitude and executes correction burns only when the orbital decrease exceeds a defined tolerance margin of $\Delta h = \pm 131$ meters. This being said, the control cycle is as follows:

- First allow a natural decay the optimal orbital altitude, 212.48km, to 212.349km making use of the atmospheric drag.
- When altitude reaches lower bound, initiate burn to restore altitude to the upper margin.
- Finalise manoeuvre and allow atmospheric drag to resume, restarting the cycle.

The strategy ensures that the spacecraft orbit will remain in an almost 212.48 km sun-synchronous dawn-dusk orbit, preserving its ground-track repeatability and science return.

As can be deduced from the control cycle, in order to raise the altitude of the spacecraft two burns are completed; one to raise the apoapsis, and another to circularise the orbit into the upper bound altitude. Thus, the delta-v required per cycle to perform these burns is shown in the equation below:

$$\Delta v_{\text{cycle}} = (v_{\text{trans, per}} - v_{\text{circ, min}}) + (v_{\text{circ, max}} - v_{\text{trans, apo}}) = 0.125 m/s \tag{6.1}$$

Where,

$$v_{\text{trans, per}} = \sqrt{\mu_M \left(\frac{2}{r_{\min}} - \frac{1}{a_t}\right)} \tag{6.2}$$

$$v_{\text{trans, apo}} = \sqrt{\mu_M \left(\frac{2}{r_{\max}} - \frac{1}{a_t}\right)} \tag{6.3}$$

$$v_{\text{circ, min}} = \sqrt{\frac{\mu_M}{r_{\min}}} \tag{6.4}$$

$$v_{\text{circ, max}} = \sqrt{\frac{\mu_M}{r_{\max}}} \tag{6.5}$$

[2] https://www.moog.com/products/propulsion/space-propulsion/spacecraft-propulsion/thrusters/cold-gas-thruster.html

[3] https://industrywired.com/electric-satellite-propulsion-systems-advantages-and-use-cases/

To determine the frequency at which these burns must be performed, Kepler's third law is applied to calculate the orbital period. The decay rate is fixed at $\delta h_{\textbf{per orbit}} = 8.37m$ as previously calculated using the MarsGRAM density models. Combining these parameters, the number of orbits required to drop from h_{max} to h_{min} is:

$$N_{\text{orbits}} = \frac{2\Delta h}{\delta h_{\text{per orbit}}} = 426.3$$

and the time between burns is:

$$\Delta t_{\text{sols}} = \frac{N_{\text{orbits}} \cdot T}{t_{\text{sol}}} = 1.58$$

Therefore, during the operational lifetime of the spacecraft, the electric thrusters shall complete non-continuous burns to provide 0.125 m/s per 1.58 sols to counteract the 54m/s delta-v required.

System Sizing

A hybrid system was selected with both a bipropellant and an electric system on board. While composing one subsystem, these systems perform during different mission phases and can be designed separately. To define the architecture of each system, a first level sizing is documented and then components are included in the analysis.

A first-level sizing was put together for the design of the propulsion subsystem. While an iterative process is adopted, the propellant mass for each manoeuvre is calculated by subtracting the final mass from the initial mass, as determined by Tsiolkovsky's rocket equation. In the case of the bipropellant option, the fuel and oxidiser mass breakdown and their respective tank volume are computed using Table 6.3. This is done assuming spherical tanks for simplified structure and maximum storage efficiency. For an estimation of the pressurant mass and volume a backwards approach is adopted using the end-of-life operating pressure and temperature [59]. Equation 6.6 calculates the mass of pressurant gas required to fill the propellant tank volumes V_{prop} at the final pressure P_{final} using the ideal gas law, assuming all propellants have been expelled and the tank is now filled with pressurant [59]. Equation 6.7 then, calculates the volume required to store the pressurant gas at its initial storage pressure $P_{storage}$ and temperature $T_{storage}$, again using the ideal gas law. In both equations, R_{gas} refers to the specific gas constant equal to 2,077 $J/kg \cdot K$ for helium [59].

$$M_{\text{press}} = \frac{P_{\text{final}} \cdot V_{\text{prop}}}{R_{gas} \cdot T_{\text{storage}}} \tag{6.6}$$

$$V_{\text{press}} = \frac{M_{\text{press}} \cdot R_{gas} \cdot T_{\text{storage}}}{P_{\text{storage}}} \tag{6.7}$$

Next, the average thrust is calculated using Newton's second law, based on the required ΔV, spacecraft mass, and burn duration for each manoeuvre. The burn duration is treated as an independent variable and is adjusted for the requirements of each manoeuvre and the feasibility of the selected system.

Lastly, for the electric propulsion system, the required electrical power is derived from the average thrust T, exhaust velocity v_e, and overall system efficiency η:

$$P = \frac{T \cdot v_e}{2 \cdot \eta} \tag{6.8}$$

For more detailed design, the selection of propulsion components was guided by commercial availability, system-level requirements, and performance trade-offs.

In terms of thruster selection, a trade-off was conducted between thrust level and burn duration for both systems, while also considering mission heritage and commercial availability. For the bipropellant

system, based on mission heritage, the total burn duration is chosen to be 30 minutes for the orbit insertion manoeuvre [4]. This duration, combined with the required delta-v, drove the need for a thruster selection with a 750 N of thrust capability. Specifically, two 400N bipropellant apogee motors by arianegroup were selected [66].

For the electric propulsion subsystem, the system shall be able to perform both orbit keeping and the end of life manoeuvrers. A trade-off was conducted involving altitude loss, required ΔV, burn time duration and power required to reach a certain thrust level. Hall-effect thrusters (HET) were selected due to the higher thrust-to-power ratio compared to ion gridded thrusters. The specific thrust level and burn duration were limited by power subsystem constraints. Based on a feasible thrust range of 50-100mN, the ST-100 Hall-effect thruster by SETS was selected [5]. Figure 6.1 illustrates the design space of the selected hall thrusters, made using manufacturer specifications and guidelines from SMAD [59]. The end-of-life manoeuvre was considered and was determined feasible, but was not explicitly taken into account in the design.

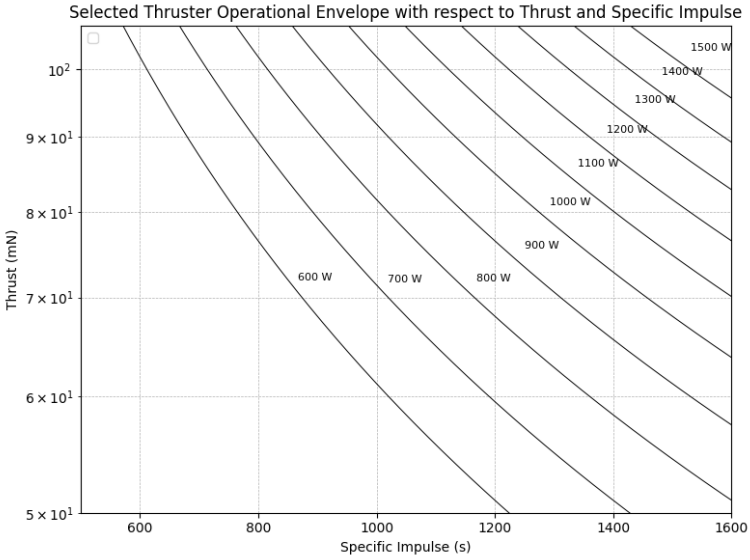

Figure 6.1: Design Space of ST-100 Hall Thruster

Tank sizing was driven by commercial availability. Through iterative design, it was ensured that the tanks had sufficient tank capacity including the selected margin. For the bipropellant system used during the orbit capture phase, a 15% propellant margin has been included. This margin primarily addresses uncertainties inherent in the aerobraking process, such as unpredictable variations in atmospheric density and potential deviations in aerodynamic performance. Similarly, a 20% propellant margin has been applied to the electric propulsion primary due to the uncertainty associated with current atmospheric density models of Mars at low altitudes. In addition, this margin can also be used to extend the lifetime of the mission. Propellant masses and respective volumes and tank capacities are shown in Table 6.5, arriving at a total propellant mass is 432.5 kg [67] [68].

[4] https://www.msss.com/mars/global_surveyor/mgs_msn_plan/section5/section5.html
[5] https://sets.space/st100/

Table 6.5: Propellant Masses, Volumes, Tank Capacities, and Volume Margins

Propellant	Mass [kg]	Volume [L]	Tank Capacity [L]	Volume Margin [L]
MMH	138.5	157.4	198.0	40.6
MON-3	228.5	166.8	198.0	31.2
Helium	1.8	31.2	40.0	7.6
Xenon	14.4	10.0	12.0	2.0

The component selection and mass breakdown of the bipropellant propulsion subsystem is presented in Table 6.6. In short, key elements of the feed system are isolation valves used to isolate section of the feed system in the event of failure, pyrotechnic valves which are one-time use valves that isolate components during launch and ground operations, and fill and drain valves used to load and remove propellants from the tanks [59]. Moreover, parallel redundancy check valves allow flow towards one direction only, filters reduce particulate contamination and lastly, the dual stage regulator regulates gas pressure and minimises fluctuations [59]. While specific dimensions for the feed lines and fittings were not explicitly determined at this stage, titanium and stainless steel materials are commonly used [59]. A 10% mass margin was applied to account for the mass of these components.

Table 6.6: Estimated Dry Mass of Bipropellant Propulsion System

Component	Amount	Mass per Unit [kg]	Total Mass [kg]
Main Components			
Thruster	2	4.30	8.60
Fuel Tank	1	21.00	21.00
Oxidizer Tank	1	21.00	21.00
Pressurant Tank	1	8.00	10.00
Feed System Components			
Isolation Valve [69]	8	0.545	4.36
Pyrotechnic Valve [69]	12	0.160	1.28
Fill and Drain Valve (Propellants) [66]	2	0.090	0.18
Fill and Drain Valve (Helium) [70]	9	0.060	0.54
Parallel Redundant Check Valve [71]	4	0.040	0.16
Dual Stage Regulator [72]	2	5.90	11.80
Filter [69]	3	0.567	1.70
Pressure Transducer [73]	7	0.25	1.75
		Lines and Fittings (10%)	8.30
		Total Propulsion System Dry Mass	**91.31**

The diagram of the system architecture is presented in Figure 6.2. The architecture has been selected following standard practices ensuring double redundancy to enhance performance and reliability. Specifically, each main thruster can independently execute the required manoeuvres in case of failure of the other. Two dual-stage regulators are installed in parallel to ensure uninterrupted pressurization. Check valves are paired redundantly to prevent backflow, and pyrotechnic valves are configured such that either of the two in parallel can complete the required flow path if activated.

Similarly, the component selection and mass breakdown of the electric propulsion section of the subsystem is shown in Table 6.7 [74]. For this design, off-the-self components are used simplifying manufacturability and integration [6]. Two xenon tanks are installed symmetrically to maintain the centre of mass of the spacecraft within accepted limits. As no additional components are accounted for this integration, a 15% margin was applied.

[6] https://www.airbus.com/sites/g/files/jlcbta136/files/2024-06/Datasheet%20ELEKTRO%20PPU%20NG1.pdf

Table 6.7: Estimated Dry Mass of Electric Propulsion System

Component	Amount	Mass per Unit [kg]	Total Mass [kg]
Main Components			
Hall-effect thruster [75]	2	3	6
Power Processing Unit (PPU) [74]	2	20.5	41
Xenon Feed System (XFS) [76]	2	1.1	2.2
		Lines and Fittings (15%)	7.38
		Total Electric Propulsion Dry Mass	**56.58**

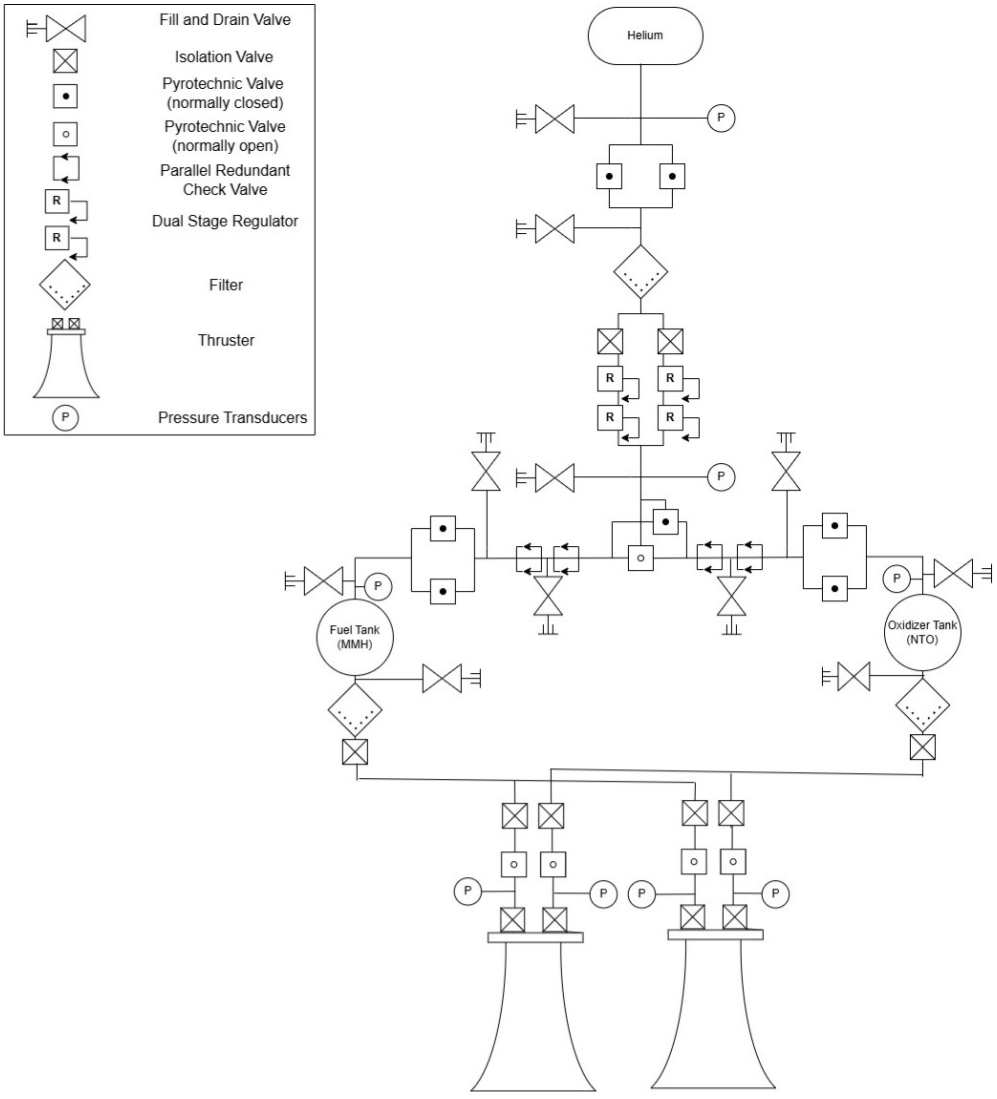

Figure 6.2: Bipropellant System Architecture

Figure 6.3 presents the diagram of the electric system architecture, comprising of two parallel, redundant paths, where power is processed in the power processing unit before arriving at the thrusters. This layout draws from the architecture used in previous missions such as GOCE. On the spacecraft, the thrusters are placed on each side of the spacecraft complementing the redundancy of the LRI (Section 4.1).

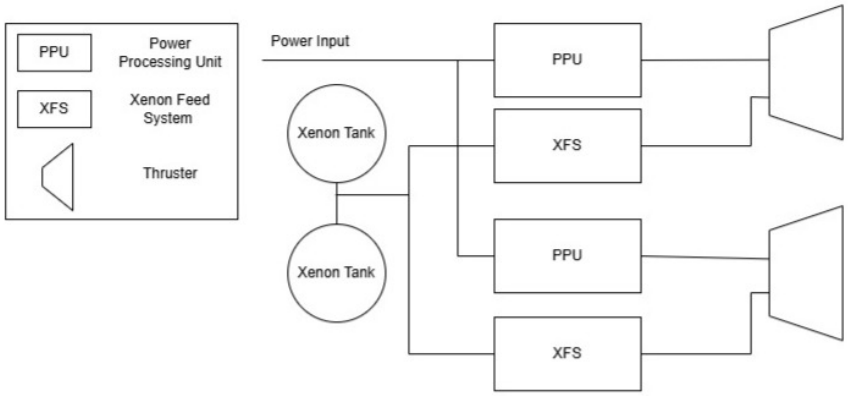

Figure 6.3: Electric System Architecture

During these process python codes were created as documented:

Table 6.8: Propulsion Tool Breakdown

File Name	Description	Main Inputs	Main Outputs
`propulsion.py`	Conducts a first-level estimation of the hybrid system	DeltaVs, burn durations, propulsion parameters, dry mass	Propellant mass and volume, thrust level, power required
`ComponentSelection.py`	Conducts sizing with all defined components of the hybrid system	DeltaVs, burn durations, dry mass, propulsion parameters, components' mass	Propellant mass and volume, Tank fit check and margin
`MassIterationPart.py`	Conducts sizing ensuring tank sizing is sufficient	DeltaVs, burn durations, dry mass, propulsion parameters	Propellant mass Tank fit check upon iteration

Design Results and Sensitivity Analysis

The propulsion subsystem was used for major manoeuvrers.

The pressure-fed bipropellant system included two tanks for MON-3 and MMH, each one with a capacity of 198 L of useable propellant. Two thrusters each of 425 N were used for orbit insertion, providing the required ΔV of 1308 m/s.

The electrostatic system included two tanks of Xe symmetrically placed with respect to the CoM, each with a capacity of 6 L. Although two ST-100 Hall-effect thrusters (50–107 mN) are integrated into the design, only one is intended for station-keeping, delivering the total ΔV equal to 245 m/s.

The total dry mass of the complete propulsion subsystem, including both chemical and electric propulsion elements, is therefore estimated at 147 kg. In terms of power, electric propulsion made use of 20 minute burns where 1025 W were used during that time. At the end of the spacecraft's operational life, longer burns may be feasible, as most other subsystems would be deactivated. The actual burn duration,and hence total end of life manoeuvre, and thrust level in this phase will depend on the degradation state of the battery and the overall power subsystem. For now, the total end-of-life manoeuvre was estimated to take place in 1.2 months.

To assess the robustness of the propulsion subsystem design, several key parameters were varied by 10%, and the resulting changes in propellant mass and power demand were evaluated. Specifically, a 10% variation in total dry mass resulted in a required chemical propellant mass ranging from 389.2 kg to 475.7 kg. A 10% change in ΔV for chemical propulsion (orbit insertion) led to a propellant mass range of 389.4 kg to 484.6 kg. For the electric propulsion system, a 10% variation in ΔV caused the xenon propellant mass to vary between 10.7 kg and 13.2 kg, with a nominal value of 12 kg. Lastly, a 10% change in electric thruster level, assuming constant specific impulse, resulted in power demand ranging from 835 W to 1,104 W, compared to the nominal 1,025 W. The sensitivity analysis shows that

a ±10% variation in key parameters can significantly impact propellant mass requirements and power demand highlighting of margin allocation.

Subsystem Requirements

The derived propulsion requirements are shown below.

Updated ID	Old ID	Description	Verification
SUB-PROP-1		The propulsion subsystem shall have tanks of minimum capacity of: - 158 L for MON-3 - 167 L for MMH - 32 L for He - 10 L for Xenon	Review of Design
SUB-PROP-2		The propulsion subsystem shall have a propellant mass not exceeding 760 kg.	Review of Design
SUB-PROP-3		The bipropellant thrusters shall provide a minimum thrust of 750 N.	Testing
SUB-PROP-4		The bipropellant system shall have a specific impulse in vacuum of at least 340 s.	Testing
SUB-PROP-5		The electric thrusters shall provide a minimum thrust of 50 mN during station-keeping.	Testing
SUB-PROP-6		The electric system shall have a specific impulse of at least 1200 s.	Testing
SUB-PROP-7		The electric system shall be able to perform at least 500 burns.	Testing
SUB-PROP-8		The propellants shall be stored in tanks within their operational temperatures.	Testing

6.2. Attitude Determination and Control Subsystem (ADCS)

The main function of the Attitude Determination and Control Subsystem (ADCS) is to determine the attitude of the spacecraft and orient it according to the needs of the other subsystems. In this section the ADCS will be designed to perform these functions and meet system and mission requirements

Requirements and Functional Analysis

The previously defined requirements that are relevant for the design of the ADCS is listed below.

Relevant Mission and System Requirements – ADCS	
MIS-UR-3.1	All normal subsystems of the mission shall incorporate double redundancy.
SYS-ASTRO-3.5	The spacecraft shall be able to perform a complete revolution around their y axis every orbit during science operations.
SYS-PAY-4.7	The spacecraft shall provide at least 0.1 mrad pointing accuracy in pitch when in nominal science mode.
SYS-PAY-4.8	The spacecraft shall provide at least 0.1 mrad pointing accuracy in yaw when in nominal science mode.
SYS-PAY-4.9	The spacecraft shall provide at least 0.25 mrad pointing accuracy in roll when in nominal science mode.
SYS-PAY-4.14	The spacecraft shall not produce vibrations that render science data unusable for more than 1% of science operations.
SYS-CONT-7.1	The spacecraft shall be able to maintain a coarse pointing accuracy of 40 mrad.
SYS-CONT-7.2	The spacecraft shall be able to recover from a 5 degree per second tumble.

The functions to be performed by the ADCS, identified in the mission functional analysis of Section 5.1 are the following:

- F.4.4 Perform Manoeuvre & Attitude Control
  - F.4.4.1 Perform Attitude Manoeuvres
- F.4.6 Recover Spacecraft from Hazardous Situation

  - F.4.6.2 Regain Attitude Control
- F.5.1 Perform Decommission Manoeuvre
  - F.5.1.2 Execute Decommission Manoeuvre

Analysis

Sensors

Science Mode The driving requirements for the ADCS are **SYS-PAY-4.7**, **SYS-PAY-4.8**, and **SYS-PAY-4.9**, which specify the pointing requirements from the payload. In order to achieve these stringent pointing requirements in science mode, star trackers will need to be used as both sun sensors and horizon scanners lack the accuracy to achieve this. When selecting the specific components, their accuracy, power, and mass must be weighed against each other. Whilst high accuracy is desirable, it is not ideal to pick a star tracker that is much more accurate than required, resulting in a heavier and more power intensive design than necessary. With these considerations in mind, the Terma T1 Star Tracker was chosen as it is lightweight and low power whilst still being sufficiently accurate [7]. The Terma T1 Star Tracker has an accuracy of 10 arcsec = 0.048 mrad, a mass of 0.763 kg, and a power requirement of 3.3 W. In order to conform to **MIS-UR-3.1**, two of these star trackers will be used. This component has a technology readiness level (TRL) of 9.

There are going to be times where the star sensors are unusable during science mode, either due to them having the sun in their field of view or some other unforeseen disturbance. For this reason, a means of maintaining pointing knowledge between star sensor readings is necessary. To accomplish this, gyroscopes are used. In order to not be in violation of **SYS-PAY-4.14**, traditional mechanical gyroscopes will not be used. Instead optical gyroscopes are used. Specifically EMCORE's CIRUS-A was chosen as it features high stability whilst still being relatively light weight and low power[8]. The CIRUS-A has a bias stability of 0.0001 deg/hr = 0.0017 mrad/hr, a mass of 8.165 kg and a power requirement of 10 W. As was the case with the star trackers, two of these gyroscopes will be used for redundancy. This component also has a TRL of 9.

Safe Mode Beyond science mode, the spacecraft also has to be able to orient itself during safe mode. The accuracy to which the spacecraft shall be able to do this is given by **SYS-CONT-7.1**. In this operational mode the spacecraft might be tumbling and the star trackers can therefore not be assumed to give accurate measurements. To ensure pointing knowledge in safe mode, other less sensitive sensors must be used. For this purpose sun sensors are the immediate first choice. However, unless a very high accuracy sun sensor is used, sun sensors provide two axis attitude knowledge. Thus, to have three axis attitude knowledge, a horizon scanner will be used in addition to the sun sensor. The chosen sun sensor is Bradford Space's Fine Sun Sensor, featuring an accuracy of 0.3 deg = 5.24 mrad, a mass of 0.375 kg and a power requirement of 0.25 W [9]. The chosen horizon scanner is Meisei Electric's Earth Sensor, featuring an accuracy of 1 deg = 17.5 mrad, a mass of 0.25 kg and a power requirement of 1 W. Whilst this is an earth sensor and can not be used directly on earth, it can be tuned to the infrared signature of mars. As was the case with the star trackers and gyroscopes, two each of the sun sensor and horizon scanner will be used for redundancy. They also both have a TRL of 9.

Actuators

Dynamic Model

For the high pointing accuracy required, the only feasible actuators are thrusters, reaction wheels and control moment gyroscopes. However, to not disturb the science measurements as stipulated by **SYS-PAY-4.14**, control moment gyroscopes and reaction wheels will not be used as the constant rotation of their wheels would lead to substantial vibrations. That leaves thrusters as the only feasible actuator

[7] https://satsearch.co/products/terma-t1-star-tracker
[8] https://www.emcore.com/products/post/8439/cirus-a-high-performance-fog-inertial-measurement-unit-imu
[9] https://satsearch.co/products/bradford-fine-sun-sensor

alternative. Choosing the type of thruster and the supplier is more complex than choosing sensors as control accuracy depends not only on the thruster used, but also on the spacecraft architecture and control scheme. Thus, to size and select a thruster a spacecraft dynamics model is developed. With this model, the maximum and minimum thrust as well as the thruster bit size can be varied to find the required thruster parameters, after which a specific thruster and supplier can be chosen. This model is based on the following equation [77].

$$\mathbf{J}\dot{\omega}_I = -\omega_I \times (\mathbf{J}\omega_I) + t_d + \mathbf{u} \tag{6.9}$$

In Equation 6.9 **J** is the inertia matrix of the spacecraft, $\dot{\omega}_I$ is the angular acceleration vector of the spacecraft, ω_I is the angular velocity vector of the spacecraft, t_d is the disturbance torques and **u** is the control torque. Beyond this, the subscript I indicates that the value is with respect to the inertial frame, expressed in the spacecraft body frame.

Disturbance Torques

With Equation 6.9 as a basis, the only other thing that needs to be modelled to simulate the spacecraft is the disturbance torques. The main disturbance torques acting on any spacecraft are aerodynamic torques, solar radiation torques, gravity gradient torques and internal torques.

Aerodynamic torques are calculated by first calculating the drag by means of the following formula[59].

$$D = \frac{1}{2}\rho V^2 C_D A \tag{6.10}$$

In Equation 6.10 D is the drag force, ρ is the atmospheric density, V is the velocity of the spacecraft, C_D is the drag coefficient and A is the frontal area of the spacecraft. Following the drag calculation the centre of area is taken as the centre of pressure. Finally the aerodynamic torque is found by multiplying the drag by the displacement of the centre of pressure from the centre of mass.

Next the solar radiation torque is calculated in a similar way to that of aerodynamic torque. The solar pressure force is given by the following formula [59]

$$F = \frac{F_S}{c} A_S (1 + q) cos(i) \tag{6.11}$$

In Equation 6.11 F is the solar pressure force, F_S is the solar constant, c is the speed of light, A_S is the surface area, q is the reflectance factor and i is the angle of incidence of the sun. Following the calculation of this force, it is multiplied by the displacement of the centre of solar pressure, which is taken as the centre of area, and the centre of mass to arrive at the solar radiation torque.

Next, the gravity gradient torque is given by the following equation [59].

$$T_g = \frac{3\mu}{2R^3} \left| I_z - I_y \right| sin(2\theta) \tag{6.12}$$

In Equation 6.12, T_g is the gravity torque, μ is the gravity constant of the planet, R is the distance from the spacecraft to the planet's centre, I_z and I_y are the moments of inertia about z and y, and θ is the deviation of the z axis from the local vertical. Due to the fact that the two spacecraft always have to be aligned, the z axis will always align with the local vertical, meaning that gravity torques can be neglected.

Lastly, Internal torques need to be considered. Due to **SYS-PAY-4.14**, all subsystems will minimise the use of moving parts and thus internal torques, however, there are still two major internal torques that need to be considered. As will be further explained in Section 6.3, the high gain antenna will utilise a gimbal to point the antenna. This will move from one side to the other over the course of one Martian year and will be quite small, however for the purpose of this model a worst case scenario

where the gimbal will have to be moved from one side to the other in one hour is considered. The other considerable internal torque is thruster misalignment. Here the worst case misalignment of 1 deg is used as described in *Space Mission Analysis and Design*[59].

In addition to disturbance torques, the spacecraft also has the opportunity to exert control torques by means of the ADCS control system. As thrusters have been identified as the only feasible option, they can be added to the model with a PD controller to regulate them.

Thruster Selection Finally, with all the parameters of the system defined, it is solved using scipy's solve_ivp function. The result of this is then plotted to see the response of the spacecraft to the disturbance torques. Such a response can be seen over one orbit in Figure 6.4, where only aerodynamic torques and solar disturbance torques are considered.

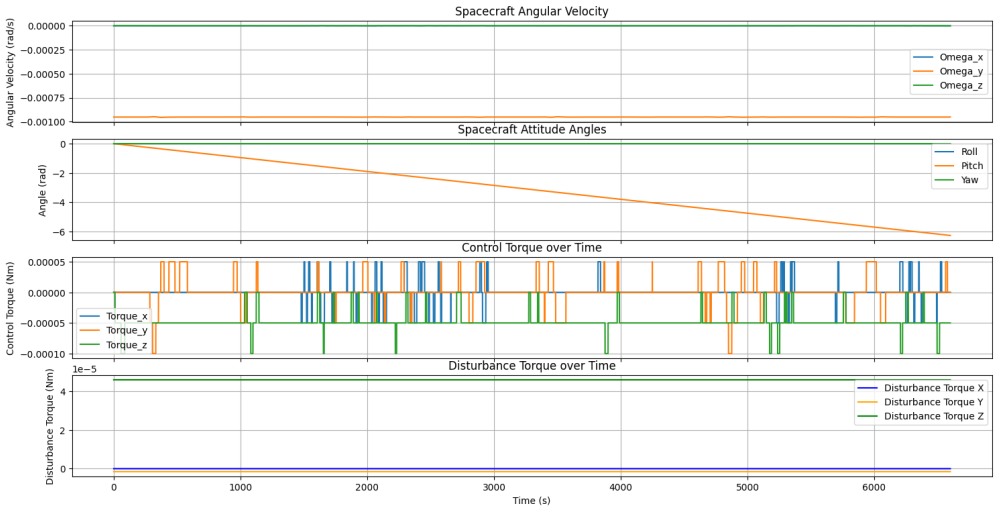

Figure 6.4: Example Dynamic Model Response

By trying various thruster parameters, the ideal thruster bit size is found to be 10 to 100 μNs. It is further found that the maximum torque of the entire system has to be in the order of 10 to 100 mNm. In order to achieve both of these simultaneously, 24 thrusters can be used. This gives up to 8 thrusters per direction per axis, which allows for fine control and small bit sizes by using few thrusters in short bursts whilst also allowing for higher torques by using more thrusters for longer bursts. Based on these parameters, the only feasible thruster types are electric and cold gas. Of these two, cold gas is both lighter, but also simpler, leading to higher reliability and lower risk. Based on this cold gas thrusters are chosen for the present design. One thruster that is found to fit the parameters needed for this mission is Nammo's cold gas thruster[10]. By selecting the 10 mN variant a minimum burn time of 5 ms leads to a bit size of 50 μNs. Further, by burning 8 at the same time and with an average thrust arm of 1 m, a max torque of 80 mNm is achieved. This component, like previous components has a TRL of 9.

With a chosen thruster, the propellant also needs to be chosen. Nammo's cold gas thruster can be used with gaseous N_2, CN_4, and gaseous Xe. Of these gaseous N_2 is both the most sustainable, accessible and the one with the highest specific impulse. Thus, gaseous N_2 is chosen as the propellant for the ADCS cold gas system.

Propellant Sizing To estimate the amount of propellant needed, the total control torques will be simulated for all mission phases, yielding a total impulse. This can then be translated to propellant

[10] `https://www.nammo.com/product/cold-gas-thruster/`

mass with the following equation[11].

$$m_p = \frac{I_{tot}}{g_0 \cdot I_{sp}} \tag{6.13}$$

In Equation 6.13 m_p is the propellant mass, I_{tot} it the total impulse, I_{sp} is the specific impulse, and g_0 is the standard acceleration of gravity. By applying this to what is seen in Figure 6.4, it becomes evident that the aerodynamic torque of the present configuration is quite high, it is a constant $4.6 \cdot 10^{-5}$, leading to 2.7 kNms that need to be counteracted by the ADCS over the science operations. Even more importantly, during the aerobraking manoeuvre, the spacecraft will fly at an altitude with much higher drag, leading to around 15 kg of propellant needed for the aerobraking manoeuvre. Normally this would be reduced by making the spacecraft more symmetric, however due to the LRI taking up the face of the spacecraft that is facing in the flight direction, the antenna has to be placed on one of the faces perpendicular to the flight direction. This leads to an asymmetry in the area about the centre of mass (CoM) that cannot be rectified by moving the solar panels to the opposite side. Thus, to reduce this imbalance, a 40x50 cm flap is added to the opposite side of the spacecraft. This is sketched in Figure 6.5 for clarity. For all mission phases except for launch, this flap is beneficial. As such it will be folded during launch and a mechanical hinge spring hinge will be used that will passively open after launch.

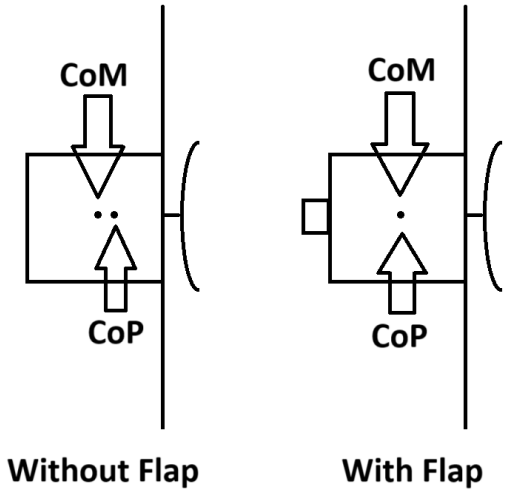

Figure 6.5: Illustration of Effect of Adding Flap to Balance Aerodynamic Torque

By adding the flap as shown in Figure 6.5, the propellant needed during aerobraking is reduced from 15 kg to 0.74 kg, whilst only adding 1 kg to the structural mass.

Following the redesign of the aircraft geometry to reduce disturbance torques, the required propellant mass for the entire mission can be calculated. This is done by considering the functions that the subsystem has to perform. These are maintaining pointing, counteracting displacement due to thruster misalignment, manoeuvres, and maintaining attitude during aerobraking. These are given in Table 6.11.

[11] https://www1.grc.nasa.gov/beginners-guide-to-aeronautics/specific-impulse

Table 6.11: ADCS Propellant Breakdown

Mission Segment	Propellant Needed (kg)
Maintaining Pointing	2.35
Thruster Misalignment	2.23
Antenna Rotation	0.01
Manoeuvres	4.73
Aerobraking	0.74
SUM	**10.06**

The last thing to be selected for the ADCS are the propellant tanks. When storing the propellant at 320 bar it has a density of 325.6 $\frac{kg}{m^3}$. leading to a propellant volume of 28.6 L. To keep the centre of mass from moving as the propellant is drained, it will be stored in two different tanks. To fit this, the PEPT-330, which fits 17.5 L per tank, is chosen [12].

As previously mentioned, a spacecraft dynamic model was made during the design of the ADCS. The files of this model as well as their inputs and outputs are given in Table 6.12. It should be noted that this is a simplified model, however, cold gas thrusters were used aboard GRACE and GRACE-FO and they managed to maintain pointing within their strict pointing requirements [37]. Further, a more sophisticated controller would likely lead to lower propellant usage.

Table 6.12: ADCS Tool Breakdown

Document Name	Model Description	Input	Output
`AerodynamicTorque`	Calculates the aerodynamic torque acting on the spacecraft	C_D, ρ, frontal area, orbit altitude, centre of mass, centre of pressure	Aerodynamic torque
`SolarRadiationTorque`	Calculates the solar radiation torque acting on the spacecraft	Reflectance factor, surface area perpendicular to the sun, centre of mass, centre of solar pressure	Solar radiation torque
`ModelConstants`	Stores all the constants used in the dynamic model	N/A	All model constants
`DynamicModelV3`	Models the response of the spacecraft to disturbance torques	Aerodynamic torque, solar radiation torque, other model constants	control torques over one orbit, attitude pointing accuracy

Design Results and Sensitivity Analysis

The design from the previous subsection is summarised in Table 6.13.

Table 6.13: ADCS Component Summary

Number	Sensor type	Accuracy [mrad](/hr)	Power [W]	Mass [kg]	TRL
2	Star Tracker	0.048	3.3	0.76	9
2	Sun Sensor	5.24	0.25	0.38	9
2	Horizon Scanner	17.45	1	0.25	9
2	Gyroscope	0.0017	10	8.17	9
24	Cold Gas Thruster	0.027	0.35	0.06	9
2	GN_2 Tank			3.1	9

With these components defined, a few performance metrics of the ADCS are also listed as follows:

- Roll pointing accuracy: 0.15 mrad
- Pitch pointing accuracy: 0.078 mrad

[12] `https://satsearch.co/products/rafael-pept-330`

- Yaw pointing accuracy: 0.072 mrad
- Coarse pointing accuracy: 17.5 mrad
- 90° attitude change settle time: 500 s

Following the definition of the ADCS components and their performance, plots of how the spacecraft reacts to the various disturbance torques will be shown here.

Firstly, in Figure 6.6, the response of the ADCS to the external disturbance torques are shown. These are largely constant over one orbit and here a worst case scenario is considered for all disturbances. As can be seen in Figure 6.6, the spacecraft is able to maintain pointing throughout the orbit. It is also able to maintain the constant angular velocity needed to perform one full revolution about it's y axis as stipulated by **SYS-ASTRO-3.5**.

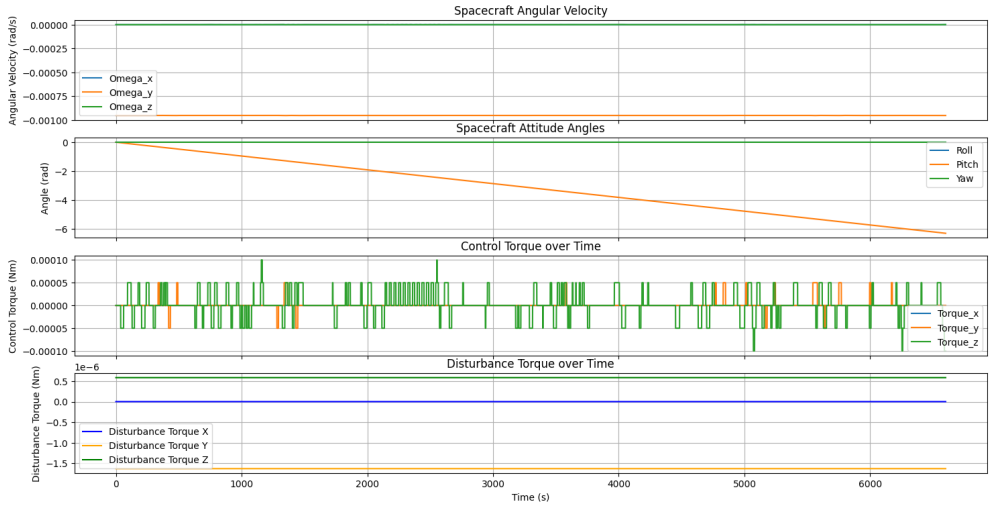

Figure 6.6: Model response to external disturbance torques over one orbit

Next, in Figure 6.7, the response of the ADCS to thruster firing can be seen. Here the external disturbance torques are again taken at a worst case value. Additionally, a worst case thruster misalignment is considered. As is seen, the spacecraft is able to maintain pointing also during this disturbance.

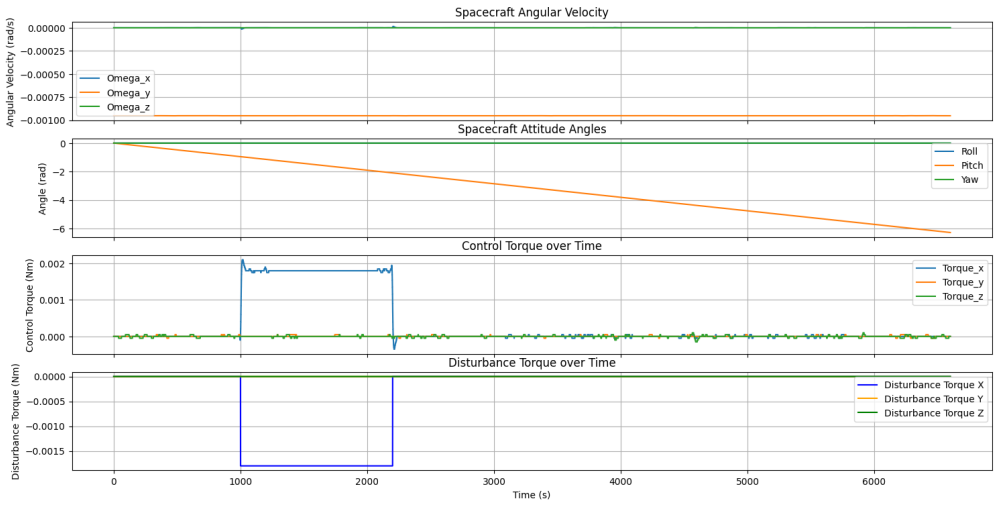

Figure 6.7: Model response to external disturbance torques with thruster firing for orbit raising

Lastly, in Figure 6.8, it is shown that the spacecraft is capable of recovering from a 5 deg/s tumble. It does, however, not maintain its fine pointing requirement during this manoeuvre

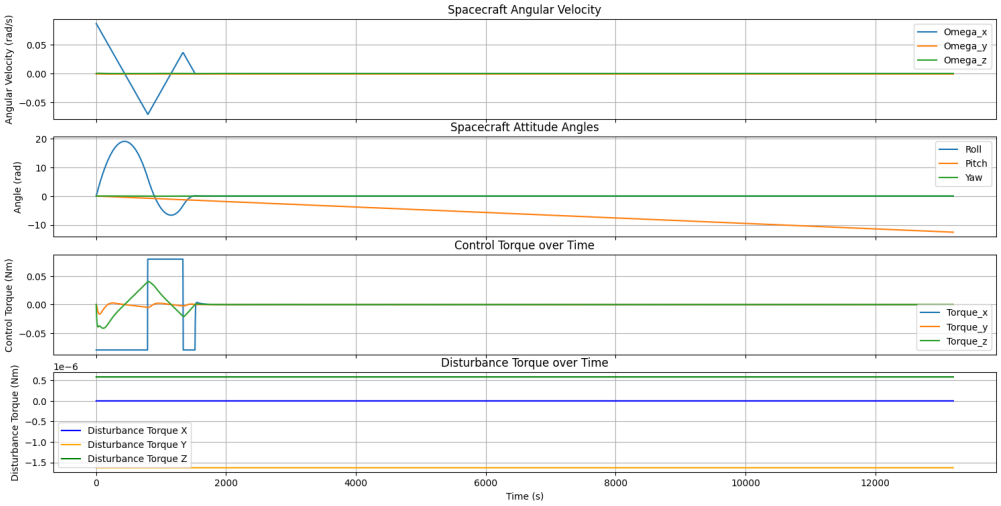

Figure 6.8: Spacecraft recovery from 5 deg/s tumble

Now that all the mission and system requirements have been met, a sensitivity analysis has to be performed to see whether the design is robust or if a small change in input has a big effect on the output. As has been evident through the design, the parameter that the subsystem is most sensitive to is the aerodynamic torque. Thus, this sensitivity analysis will recalculate all how the system would look if the spacecraft flew 30 km higher or lower, resulting in different densities. This will give a good idea of the sensitivity of the subsystem as it covers both the sensitivity to changes in altitude, but also to inaccurate Martian density models. It was found that the component selection would stay the same if the altitude was changed, but that the propellant mass and thus the tank size would change. For the case where the spacecraft were to fly 30 km lower than the current altitude, the dry mass increased by 1.6 kg, an increase of 6 %. Further, it led to an increase in wet mass of 4 kg, an increase of 10.9 %. For the case where the spacecraft were to fly 30 km higher, it did not change the dry mass as the same tanks were optimal. However, the wet mass was decreased by 2 kg, a decrease of 5.4 %. Based on this it can be concluded that the ADCS is not overly sensitive to changes in altitude, but it is nevertheless a significant change.

Subsystem Requirements

The design of the ADCS has led to several subsystem requirements. These can be seen in the following table.

Updated ID	Old ID	Description	Verification
SUB-ADCS-3.1		The ADCS shall make use of star trackers for attitude determination during science mode	Review of Design
SUB-ADCS-3.2		The ADCS shall make use of optical gyroscopes to maintain pointing knowledge between star tracker measurements	Review of Design
SUB-ADCS-3.3		The ADCS shall make use of a combination of sun sensors and horizon scanners for attitude determination in science mode	Review of Design
SUB-ADCS-3.4		The ADCS shall make use of cold gas thrusters for attitude control at all mission stages	Review of Design
SUB-ADCS-3.5		The ADCS shall make use of gaseous nitrogen as propellant	Review of Design

SUB-ADCS-3.6	The ADCS sensors used during science mode shall have a pointing knowledge of at most 0.05 mrad	Testing
SUB-ADCS-3.7	The ADCS sensors used during safe mode shall have a pointing knowledge of at most 20 mrad	Testing
SUB-ADCS-3.8	The ADCS actuators shall have a pointing accuracy of at most 0.03 mrad	Analysis
SUB-ADCS-3.9	The ADCS shall have a dry mass of at most 30 kg	Inspection
SUB-ADCS-3.10	The ADCS shall have a wet mass of at most 42 kg	Inspection
SUB-ADCS-3.11	The ADCS shall have an average power draw of at most 35 kg	Testing

6.3. Telemetry, Tracking and Command (TT&C)

Requirements and Functional Analysis

The TT&C subsystem design has to comply with the following requirements:

Relevant Mission and System Requirements – TT&C Subsystem	
MIS-UR-3.1	All normal subsystems of the mission shall incorporate double redundancy.
MIS-UR-3.2	All critical subsystems of the mission shall incorporate triple redundancy.
SYS-PAY-4.17	The spacecraft shall be able to downlink all of the 3.7 Gbits of payload data generated every day.
SYS-LNCH-5.2	The unemployed spacecraft shall fit within the payload compartment of the Ariane 62 Short Dual Launch Structure configuration.
SYS-LNCH-5.2.2	The unemployed cross section of each spacecraft shall allow the 2 spacecraft to fit within a circular cross-sectional of diameter 4.6 m.
SYS-COMM-6.9	The spacecraft shall be able to establish communications with Earth under all conditions excluding the conjunction of the Sun and Mars, and while in eclipse relative to the Earth.
SYS-COMM-6.1	The spacecraft shall be able to downlink all of the 22 Mb of telemetry data generated every day.
SYS-COMM-6.2	The two spacecraft shall be able to communicate with each other at all times.
SYS-COMM-6.3	All link margins shall close with at least 3 dB clearance.
SYS-RISK-08	The spacecraft shall employ double redundancy for inter satellite communication.

The functions to be performed by the TT&C subsystem, identified in the mission functional analysis of Section 5.1 are the following:

- F.3.2 Commission Spacecraft
  - F.3.2.3 Establish Communication Link
- F.4.5 Communicate with Earth
  - F.4.5.1 Receive Commands
  - F.4.5.2 Prepare Data for Transmission
  - F.4.5.3 Transmit Data
- F.4.6 Recover Spacecraft from Hazardous Situation
  - F.4.6.5 Re-establish Communication
- F.5.1 Perform Decommission Manoeuvre
  - F.5.1.1 Receive Decommission Trajectory
  - F.5.1.3 Confirm Decommission Manoeuvre
- F.5.2 Configure Spacecraft for Decommissioning

- F.5.2.3 Confirm Decommissioning

TT&C Subsystem Design Analysis

A Python tool has been developed to assess whether communication links can be established. The tool comes with a set of assumptions that, combined with worst case scenario conditions, make up the assumptions of TT&C design process:

- Rain loss is negligible
- Transmitter line loss: 1 dB
- Science data produced per day: 3.7 Gbits (same as GRACE-FO [78])
- Science downlink occurs during 2.5-hour daily windows
- One HGA is non-operational
- Earth–Mars distance: 2.52 AU
- Pointing loss of low gain antennas is negligible
- All antennas are RHCP [79]

At 3.7 Gbits per day, the science data represents the main bulk of the data to downlink. The data rate is not a design choice i n itself. Rather, it is defined from the amount of science data gathered per day and the downlink time. Windows of 2.5 hours per day have been allocated, which result in a science downlink data rate of 411 kbits. The downlink could also be achieved in longer timespans as, when in science orbit, the spacecraft is in eclipse for 2.4 % of the orbit. However, this would mean more frequent pointing of the High Gain Antenna (HGA) towards Earth. Moreover, choosing a Ka band frequency as opposed to X band, which is commonly used for deep space missions, allows for a higher data rate. This means that the ground station has to be operated for less time and the HGA has to be pointed less frequently.

The ground station signal to noise ratio encompasses all the gains and losses involved from the moment the signal enters Earth's atmosphere to it being received by the ground station. The DSN 34 m BWG antennas in Madrid, Canberra and Goldstone [80] have been selected. These have a gain to loss ration of 61.1 dB [80].

The BER is assumed to be 10^{-5} as in link budgets illustrated for the Mars Global Surveyor (MGS) uplink and downlink [81].

The transmission power required of 70 W is the result of iterating with various power values and checking if the science downlink margin is above 3 dB. The link margin of the science downlink drives the required transmission power as the size of payload data is most significant. The value of 70 W also closely aligned with the transmitter power of the MGA and Mars Reconnaissance Orbiter (MRO), hence are realistic. The inputs for the downlink are shown below in Table 6.16a.

As for the uplink, the data rate is a design choice that purely depends on the required rate to safely relay commands to the spacecraft. According to a TT&C overview of the (MGS) this is 250 bps [81]. The transmitter power is a result of ground station selection. The DSN BWG 34 m antennas have a transmitter power of 300 W. The inputs for the uplink are shown below in Table 6.16b.

Table 6.16: Telecommunication link budget input parameters for downlink and uplink.

(a) Science Downlink Budget Input Parameters

Input Parameters	Unit	Value
Transmission frequency	GHz	32
Transmitter power	W	70
Transmit antenna beamwidth	deg	0.4
Transmit antenna pointing offset	deg	0.15
Ground Station G/T	-	61.1
BER	-	10^{-5}
Data/day	bits	$3.7{\cdot}10^{9}$
Transfer time/day	s	9000

(b) Command Uplink Budget Input Parameters

Input Parameters	Unit	Value
Transmission frequency	GHz	34
Transmitter power	W	300
Receive antenna pointing offset	deg	0.15
Ground Station G/T	-	61.1
BER	-	10^{-5}
Data Rate	bps	3500

Before computing the gains and losses to be accounted for in the link margin, the sizing of the spacecraft antenna dish is carried out. The following empirical antenna sizing relation is used [50]:

$$D = \frac{21}{f_{GHz}\theta} \tag{6.14}$$

To compute the peak transit antenna gain, an empirical relation is used [50]. As a circular transmit antenna is assumed, the beamwidths θ_x and θ_y are identical:

$$G \approx 44.3 - 10\,\log(\theta_x \theta_y) \tag{6.15}$$

To compute the transmit and receive antenna pointing losses, the following empirical relation is used, where e is the antenna pointing offset in degrees [50]:

$$L_\theta = -12\,(\frac{e}{\theta})^2 \tag{6.16}$$

The transmit antenna pointing loss of the HGA is then computed by subtracting the pointing loss from the peak antenna gain. For the uplink, this is not done as the gain to noise ratio already encompasses all losses within Earth's atmosphere. For instance, the atmospheric loss and transmitter line loss.

The biggest loss to be accounted for is due to free space signal propagation. This is computed as follows [50]:

$$L_{path} = (\frac{4\pi d}{\lambda})^2 \tag{6.17}$$

Before estimating the required signal to noise ratio, the modulation and coding are to be defined. As done in most deep space missions such as MGS [81], the signal is going to be BPSK modulated. Moreover, the signal is initially Reed Solomon 255 encoded, then convolution encoded with rate = 1/2 and k = 7, again as in MGS [81]. The decoding is performed by a Viterbi decoder for the inner code and a Reed Solomon decoder for the outer coding layer. As seen in Figure 6.9 this results in one of lowest required signal to noise ratios of approximately 2.7 dB.
All this feeds into the creation of the link budget tool summarised in 6.17.

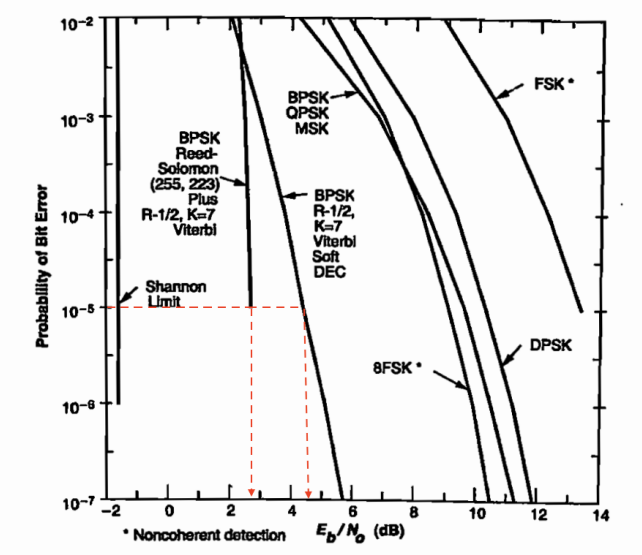

Figure 6.9: Required Eb/N0 [50]

Table 6.17: TT&C Tool Breakdown

Document Name	Model Description	Input	Output
`ephemeris_reader`	Reads ephemeris data to provide solar system geometry over time	Ephemeris file path	Dates, Sun-Earth distance, Sun-Probe-Earth angle
`HGA_downlink`	Calculates downlink link margin using the High Gain Antenna (HGA)	Link budget inputs (see Input Parameters table)	Link margin plot
`LGA_downlink`	Calculates downlink link margin using the Low Gain Antenna (LGA)	Link budget inputs	Link margin plot
`HGA_uplink`	Calculates uplink link margin using the High Gain Antenna (HGA)	Link budget inputs	Link margin plot
`LGA_uplink`	Calculates uplink link margin using the Low Gain Antenna (LGA)	Link budget inputs	Link margin plot

The gains and losses accounted for in the link budget during nominal and emergency operations are shown in Table 6.18 and Table 6.19 respectively. The link margin is computed for the four possible links that have to be established with Earth:

- HGA Downlink
- HGA Uplink: there is an ample link margin of 32.1 dB. However, it is not worth employing a separate ground station solely for this communication mode as it would increase the cost and complexity of mission operations. Moreover, the command data rate could eventually be increased to diminish the link margin and transmit commands faster. In case the availability of the DSN antennas were a problem, this would reduce the required service time.
- LGA Downlink
- LGA Uplink

Table 6.18: High Gain Antenna Link Budgets: Gains and Losses in dB

(a) Downlink

Parameter	Value (dB)
Gains	
Transmitter power (P)	18.45
Transmit antenna gain (G_t)	50.57
Boltzmann constant term	228.6
Losses	
Space loss (L_s)	-294.08
Required data rate (R)	-56.14
Polarisation Loss	-0.18
Transmitter Line Loss	-0.18
Ground Station Parameters	
Ground station E_b/N_0	61.1
Link Parameters	
Received E_b/N_0	*8.32*
Required E_b/N_0	*2.7*
Link Margin	*4.62*

(b) Uplink

Parameter	Value (dB)
Gains	
Transmitter power (P)	24.77
Receive antenna gain (G_t)	50.57
Boltzmann constant term	228.6
Losses	
Space loss (L_s)	-294.61
Required data rate (R)	-35.44
Polarisation Loss	-0.18
Ground Station Parameters	
Ground station E_b/N_0	61.1
Link Parameters	
Received E_b/N_0	*34.8*
Required E_b/N_0	*2.7*
Link Margin	*32.1*

Table 6.19: Low Gain Antenna Link Budgets: Gains and Losses in dB

(a) Downlink

Parameter	Value (dB)
Gains	
Transmitter power (P)	18.45
Transmit antenna gain (G_t)	5.22
Boltzmann constant term	228.6
Losses	
Transmitter line loss (L_l)	-1.00
Space loss (L_s)	-282.47
Required data rate (R)	-23.98
Polarisation Loss (R)	-0.18
Ground Station Parameters	
Ground station E_b/N_0	61.1
Link Parameters	
Received E_b/N_0	*5.72*
Required E_b/N_0	*2.7*
Link Margin	*3.02*

(b) Uplink

Parameter	Value (dB)
Gains	
Transmitter power (P)	24.77
Receive antenna gain (G_t)	5.22
Boltzmann constant term	228.6
Losses	
Space loss (L_s)	-281.13
Required data rate (R)	-31.77
Polarisation Loss	-0.18
Ground Station Parameters	
Ground station E_b/N_0	61.1
Link Parameters	
Received E_b/N_0	*6.62*
Required E_b/N_0	*2.7*
Link Margin	*3.92*

In terms of inter satellite communication, as mentioned in Chapter 2, the maximum separation between the spacecraft is of 58 km. This is far smaller than typical Earth - Mars distances and results in a great reduction of propagation loss. As in MRO, an Ultra High Frequency (UHF) frequency band is used for proximity communications [79]. The data rate is fixed at 20 kbps as this is the data rate that can be achieved through the LRI communication [78]. The UHF LGA link would only serve as redundancy for the laser communication. Moreover, inter satellite communication is continuous so a high data rate is not required.

The signal is BPSK modulated and convolutional encoded at rate = 1/2, k = 7 [79]. The decoding is also convolutional with rate = 1/2, k = 7, accompanied by Viterbi decoding [81]. From Figure 6.9 this leads to a required Eb/N0 of approximately 4.6 dB.

This results in the following inter satellite link budget:

Table 6.20: Inter satellite Link Budget: Gains and Losses in dB

Parameter	Value (dB)
Gains	
Transmitter power (P)	0
Transmit antenna gain (G_t)	0
Receive antenna gain (G_r)	0
Boltzmann constant term	228.60
Losses	
Space loss (L_s)	-122.97
Required data rate (R)	-43.01
Polarisation loss	-0.18
System Noise loss	-17.78
Link Parameters	
Received E_b/N_0	*34.65*
Required E_b/N_0	*4.6*
Link Margin	*39.65*

Design Results

The design of the TT&C subsystem stems from the operational modes in which the spacecraft will communicate with other systems. Each phase requires a different volume of data being relayed to and from the spacecraft. This influences the data rate and signal propagation distance, which are critical parameters in the link budget analysis. The python link budget tool is thus used to produce plots that illustrate the uplink and downlink margins with both antennas at every instance of the mission.

Before illustrating the plots it is important to make a note on solar conjunction. This is when Earth and Mars are on opposite sides of the Sun. More specifically, a conjunction is defined to occur when the Sun - Probe -Earth angle of less than 2 deg [82]. From Horizon's ephemeris database, in the timeline of the mission this results in one 24 day blackout [83]. Throughout this period, the spacecraft will not be able to communicate with Earth and, as such, won't be able to send science data, receive commands or transmit telemetry. Science data will continue to be gathered and, as explained in Section 6.4, will be stored onboard until communication is re-established.

Transfer, Aerobreaking, Commissioning and Decommissioning

When the spacecraft is not in science orbit, no payload data has to be relayed back to Earth. As such, telemetry downlink and command uplink drive the communication. This leads to a downlink data rate of 250 bps, and an uplink data rate of 3500 bps in this missiojn phase[81].

As in MRO, the high gain is to be deployed a few minutes after the launch phase has been completed [79]. This is done when the spacecraft is still close to Earth to ensure commands are real time and less susceptible to errors.

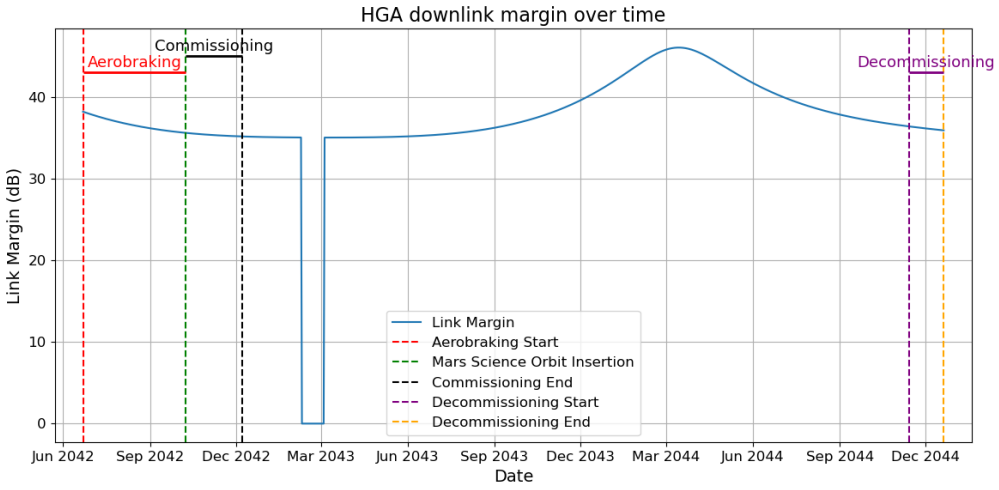

Figure 6.10: HGA Telemetry Downlink Margin over Time

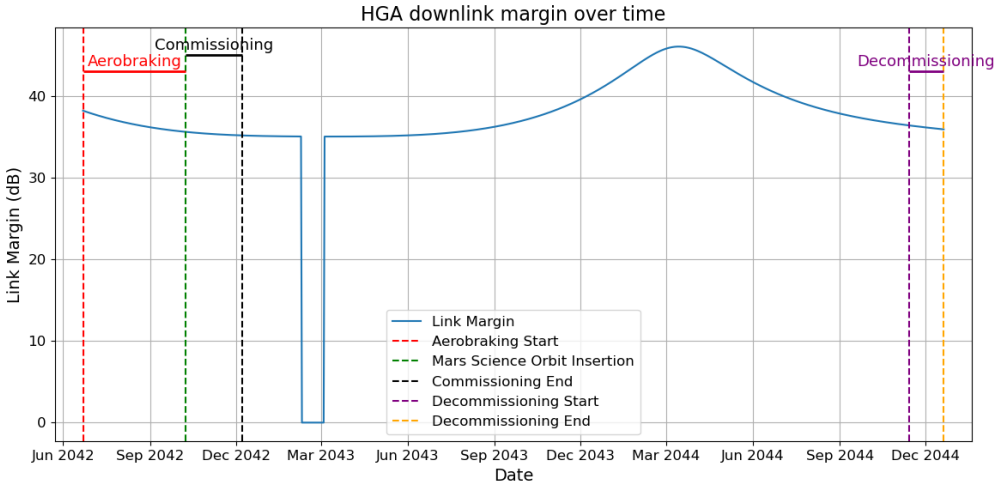

Figure 6.11: HGA Command Uplink Margin over Time

Nominal Science Mode

Once the spacecraft ha been placed in science orbit it will start gathering payload data. This has to be relayed back to Earth together with the spacecraft telemetry through the HGA. The spacecraft must also be able to receive commands from the ground station during this phase.

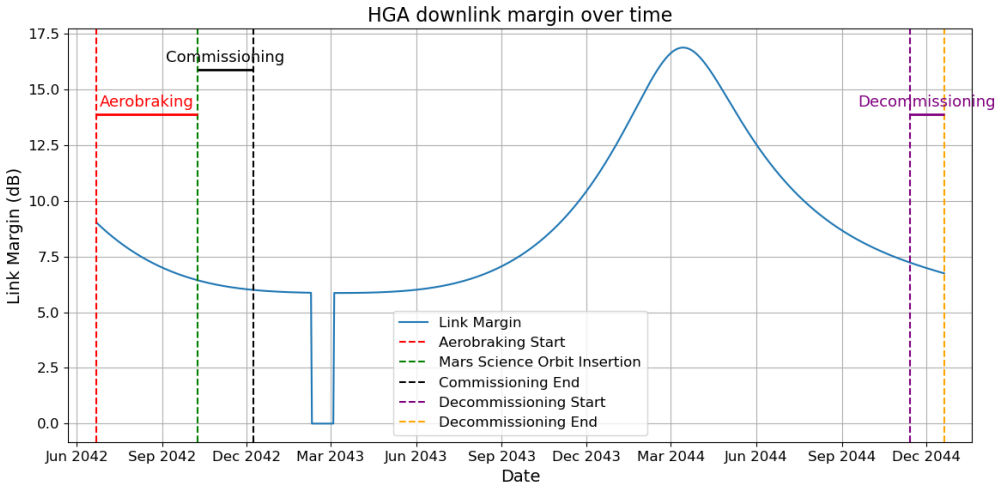

Figure 6.12: HGA Science Downlink Margin over Time

Safe Mode

The spacecraft will enter safe mode if a critical function is compromised. For instance, when pointing control is lost or battery voltage drops below the required level. During these phases, science data will not be relayed back to Earth. However, telemetry downlink and command uplink still has to be possible. When the spacecraft is in safe mode it is likely that the pointing accuracy will not be enough to use the HGA. As such, the low gain antennas are to be used to establish Earth links. These will operate in the X frequency band as high data rates are not required and cannot be sustained when in safe mode. The link margin of these telemetry and command links are shown in Figure 6.13 and Figure 6.14.

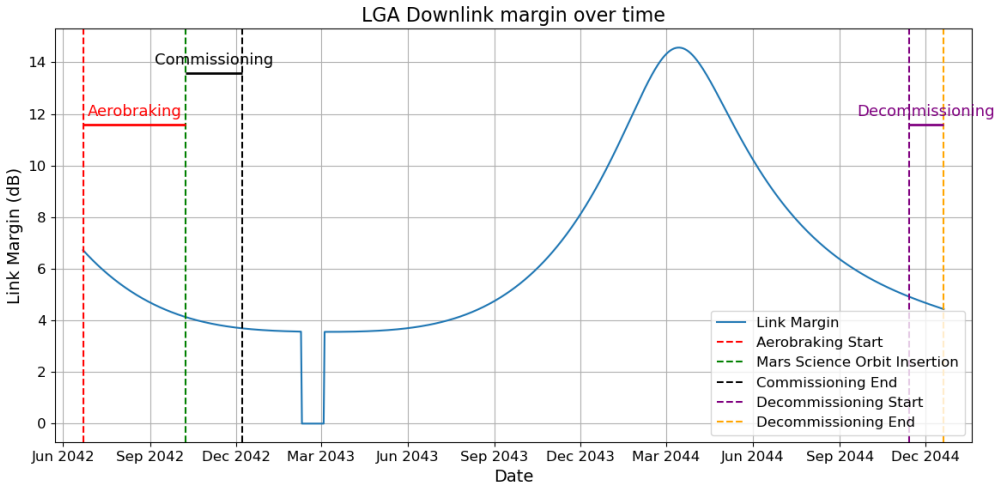

Figure 6.13: LGA Downlink Margin over Time

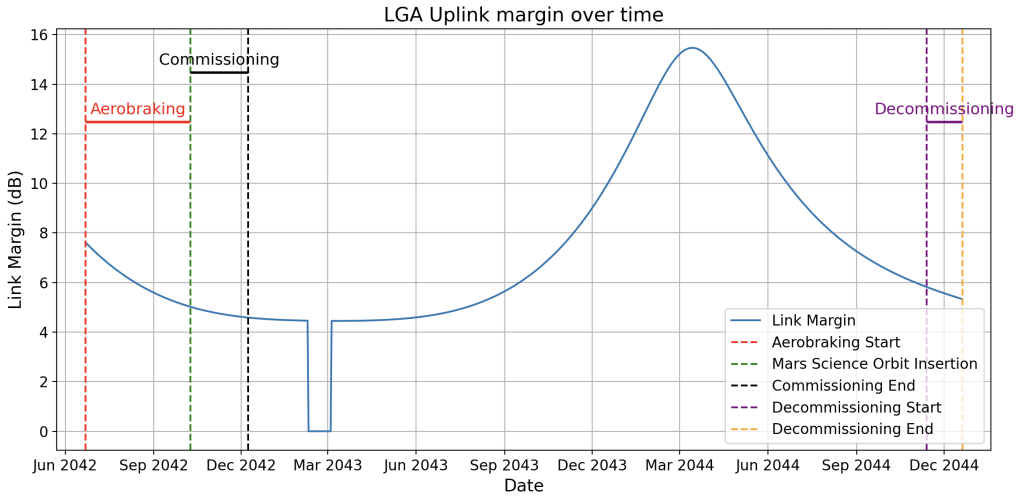

Figure 6.14: LGA Uplink Margin over Time

Having insured that all types of communication links can be established, the components of the TT&C can be defined. The architecture refers to the TT&C architecture of other Mars missions such as MRO and MGS as a guideline [81] [79]. Components are added, removed and adapted from typical Martian telecommunication systems based upon the design choices made. For instance, selecting antennas with appropriate beamwidths and ensuring transponders can handle Ka, X and UHF links.

The following components are per spacecraft. Both spacecraft are equipped with a HGA to ensure redundancy of a critical mission component.

Table 6.21: TT&C comoponent breakdown

Telecom Hardware	**Amount**	**Mass (kg)**	**Power (W)**
Ultra Stable Oscillator (USO)	2	1.7	5
Small Deep Space Transponder (SDST)	2	6.4	16
Band Pass filter	4	0.8	-
Coupler	2	0.4	-
Travelling Wave Tube Amplifier (TWTA)	2	8	140
Isolators	2	0.6	-
Diplexer	3	0.9	-
LGA Microstrip Patch Antenna	2	0.4	-
HGA parabolic reflector	1	12	-
HGA gimbals and drive motors	1	30	14
Waveguide Transfer Switches	4	1.5	-
Cables, harnesses	-	8.3	x
UHF LGA (UHF Antenna III) [84]	1	0.085	-
Electra UHF Transponder (EUT)	1	10	70
Low Noise Amplifier (LNA)	2	-	1
Total	-	81.085	245

The interaction between components and the flow of communication links is illustrated in Figure 6.15.

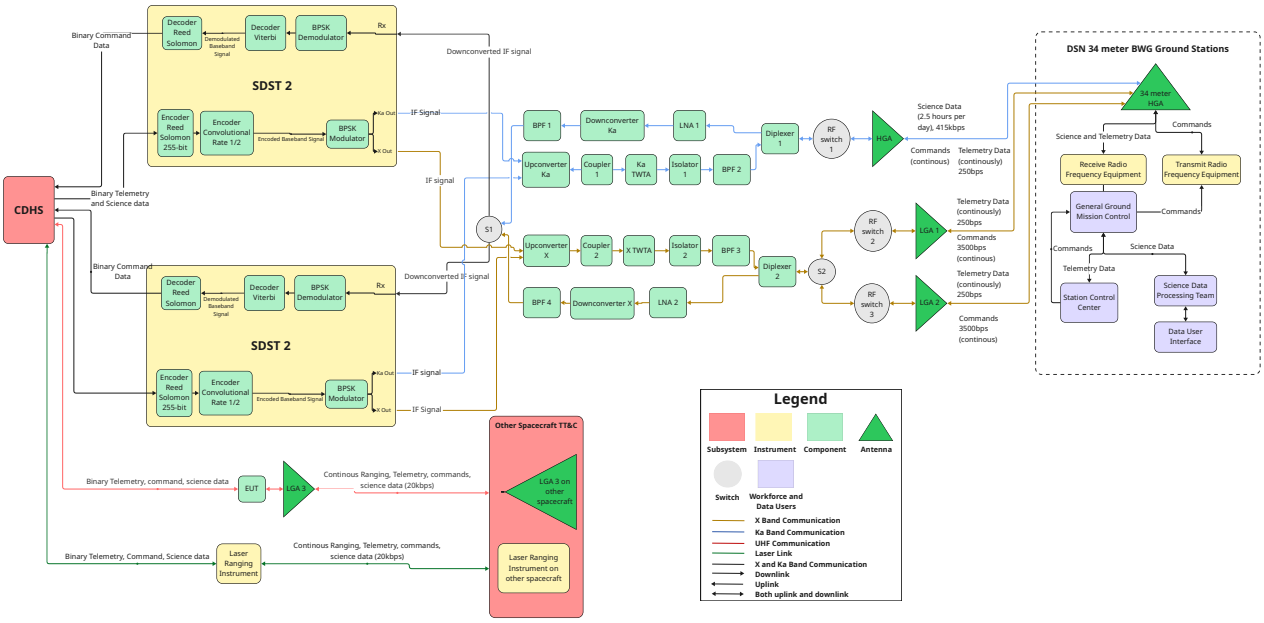

Figure 6.15: Communication Flow Diagram

Subsystem Requirements

The design of the TT&C subsystem leads to defining a set of subsystem requirements to be met.

Updated ID	Old ID	Description	Verification
SUB-TTC-4.1	UR-SUB-TTC-2.6.4.1	The high gain antenna shall have a diameter of 1.64 m	Inspection
SUB-TTC-4.2	UR-SUB-TTC-2.6.4.1	The high gain antenna shall have a a beamwidth of 0.4 deg	Testing
SUB-TTC-4.3	UR-SUB-TTC-2.6.4.1	A downlink with a data rate of 411 kbps shall be established.	Testing
SUB-TTC-4.4	UR-SUB-TTC-2.6.4.1	An uplink with a data rate of 3500 bps shall be established.	Testing
SUB-TTC-4.5	UR-SUB-TTC-2.6.4.1	An emergency downlink with a data rate of 250 bps shall be established.	Testing
SUB-TTC-4.6	UR-SUB-TTC-2.6.4.1	A link with the DSN 34 m BWG ground station shall be established 9000 seconds per day.	Analysis
SUB-TTC-4.7	UR-SUB-TTC-2.6.4.1	A power of 250 W shall be allocated for the TT&C subsystem	Testing
SUB-TTC-4.8	UR-SUB-TTC-2.6.4.1	The low gain antennas shall have a beamwidth of 90 degrees	Testing
SUB-TTC-4.9	UR-SUB-TTC-2.6.4.1	The low gain antennas shall have a gain of 6 dB	Testing
SUB-TTC-4.10	UR-SUB-TTC-2.6.4.1	The high gain antenna shall have a gain of 51 dB	Testing
SUB-TTC-4.11	UR-SUB-TTC-2.6.4.1	The signal shall be BPSK modulated	Testing
SUB-TTC-4.12	UR-SUB-TTC-2.6.4.1	The signal shall be convolutional encoded with k = 7, r = 1/2	Testing
SUB-TTC-4.13	UR-SUB-TTC-2.6.4.1	The signal shall be Reed Slolomon 255 encoded	Testing
SUB-TTC-4.14	UR-SUB-TTC-2.6.4.1	The signal shall be a Viterbi decoded	Testing

Sensitivity Analysis

Varying the input parameters of the link budget tool leads to minimal changes in the TT&C mass, power and volume values. For instance, increasing the data rate will have to be offset by higher antenna gain or higher transmitter power, but these would stem from component selection. Using the upper and lower frequency limits of the Ka band spectrum and sizing the antenna accordingly, the high gain antenna on the spacecraft is between 1.52 - 1.65 m.

6.4. Command and Data Handling Subsystem (CDHS)

Requirements and Functional Flow

The functions to be performed by the CDHS, identified in the mission functional analysis of Section 5.1 are the following:

- F.3.2 Commission Spacecraft
  - F.3.2.4 Perform Subsystem Checks
- F.4.2 Collect Telemetry
  - F.4.2.1 Obtain Navigation Data
  - F.4.2.2 Obtain Subsystem Telemetry
- F.4.3 Perform Scientific Measurements Situation
  - F.4.3.1 Activate Payload
- F.4.6 Recover Spacecraft from Hazardous Situation
  - F.4.6.1 Disable Non-Critical Subsystems
- F.5.2 Configure Spacecraft for Decommissioning
  - F.5.2.1 Shut Down Non-Critical Subsystems
  - F.5.2.2 Safe Critical Subsystems
  - F.5.2.3 Confirm Decommissioning

These functions flow into the following system requirements to be met:

Relevant Mission and System Requirements – CDHS	
SYS-COMM-6.4	The spacecraft shall be able to store commands.
SYS-COMM-6.5	The spacecraft shall be able to distribute commands.
SYS-COMM-6.6	The spacecraft shall be able to gather telemetry data from the spacecraft.
SYS-COMM-6.7	The spacecraft shall be able to store science data.
SYS-RISK-8.10	The spacecraft critical surfaces and subsystems shall withstand a TID of 20.8 rad without degradation in functionality.

CDHS Design Analysis

The design of the CDHS is based upon selecting components that satisfy the system requirements. Due to the high reliability required for the onboard computer, the component selection will be based upon existing space-grade CDHS components [85]. From previous Mars missions, such as MRO and MGS, the required performance of the CDHS can be derived .

SYS-COMM-6.6

The spacecraft will receive commands at a data rate of 3500 bps [81]. Looking at modern CDHS space grade components, the Random Access Memory (RAM) can store up to 36 MBytes of executable code and housekeeping data[85]. This is plenty when compared to the command rate.

SYS-COMM-6.7

An electrical connection to the other subsystems that is able to distribute commands at a rate of 3500

bps is needed. A Space Wire Network has thus been selected. This is capable of high speed data transfer, up to 130 Mbps, within the spacecraft bus [85].

SYS-COMM-6.8
To gather telemetry data from the spacecraft bus, feed it to the CDHS and ultimately relay it back to Earth, the electrical network within the spacecraft has to support telemetry downlink rates of 250 bps [81]. As such, the SpaceWire network is sufficient.

SYS-COMM-6.9
An estimate for the required memory size can be computed from the amount of science data gathered per Earth day and the maximum eclipse time with respect to Earth. This occurs every twenty-six months when Earth and Mars are aligned with the Sun, leading to twenty-four day communication blackout due to solar interference.

Table 6.24: Estimate of the required memory size

Science data per Earth day	3.7 Gbit/day
Worst case communication blackout duration	24 days
Required Memory	88.8 Gbit
Required Memory with 40% margin	124.32 Gbit

As such, when converted to Bytes the spacecraft should posses storage of at least 15.54 GBytes. Due to the triple redundancy required for critical components, the spacecraft is equipped with three storage boards each capable of holding 16 GBytes of data. This results in the total storage capacity of the CDHS subsystem at 48 GBytes.

SYS-COMM-6.10
The radiation level that has to be endured has been estimated in Section 6.7 to be 10.95 rad. Space grade CDHS components of advanced CDHS are able to withstand radiation levels up to 50 krads. This is leaves plenty of margin for unpredictable solar activity throughout the course of the mission Also, the CDHS does not require any additional shielding other than the structural casing and backpane to hold components in place.

Design results

An analysis of the CDHS now leads to component selection. Being a critical component for the spacecraft, the components of the CHDS all employ triple redundancy. There is only one backpane as the connections within it already have redundant pathways within the component [85]. This results in the following component table:

Table 6.25: CDHS Component Breakdown

Component	**Quantity**
Data Storage Boards	3
Housekeeping Input/Output Board	3
Command Detection Unit	3
Multi-function Analog Card	3
Error correction circuitry	3
Low Voltage Power Converter	3
Backpane	1
Enclosure	1
Onboard Computer	3
Total Mass (kg)	**10**

Data and command flows between the CDHS, spacecraft bus and payload are illustrated in Figure 6.16.

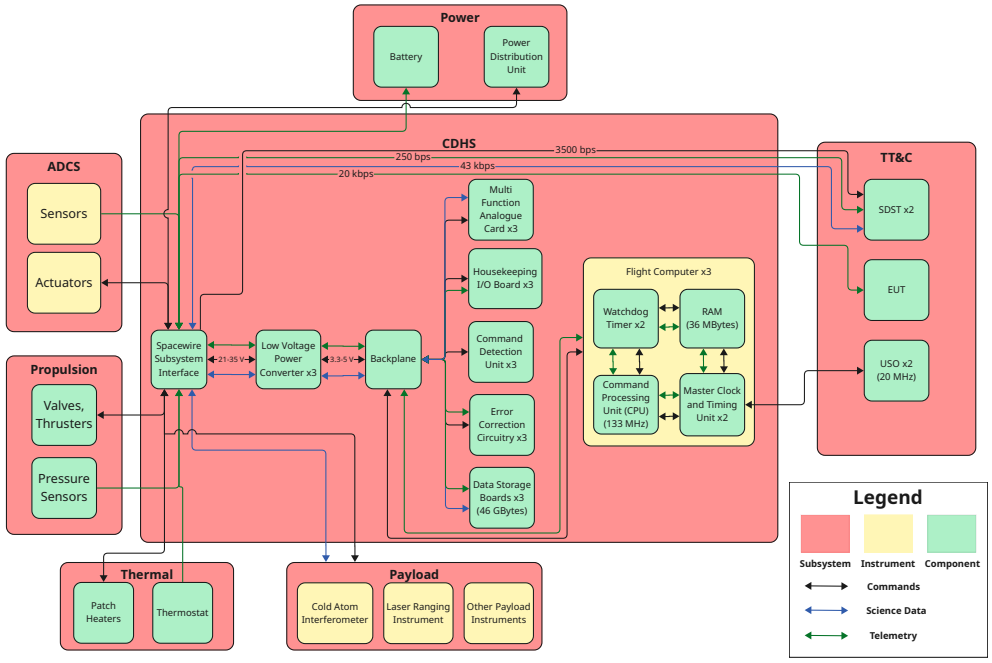

Figure 6.16: Data Handling Block Diagram

Subsystem Requirements

The CDHS design process has led to the establishment of specific subsystem requirements to be meet.

Updated ID	Old ID	Description	Verification
SUB-CDHS-5.1	UR-SUB-TTC-2.6.4.1	The power converter shall decrease the voltage to 3.3 -5 V	Testing
SUB-CDHS-5.2	UR-SUB-TTC-2.6.4.1	A SpaceWire shall be used to connect the spacecraft bus.	Review of Design
SUB-CDHS-5.3	UR-SUB-TTC-2.6.4.1	A power of 30 W shall be allocated to the CDHS at all times.	Testing
SUB-CDHS-5.4	UR-SUB-TTC-2.6.4.1	The CDHS shall distribute commands at 3500 bps	Testing
SUB-CDHS-5.5	UR-SUB-TTC-2.6.4.1	The CDHS shall store science data at a rate of 43 kbps	Testing
SUB-CDHS-5.6	UR-SUB-TTC-2.6.4.1	The RAM size shall be 36 MBytes	Review of Design
SUB-CDHS-5.7	UR-SUB-TTC-2.6.4.1	The command processing unit shall operate at a frequency of 133 MHz	Testing

6.5. Thermal Control Subsystem

Requirements and Functional Analysis

The set of requirements that shaped the thermal control system (TCS) is listed below.

Relevant Mission and System Requirements – CDHS	
SYS-PAY-4.1	The LRI laser source temperature shall not fluctuate by more than 0.1 K per orbit.
SYS-PAY-4.2	The LRI Triple Mirror Assembly temperature shall not fluctuate by more than 0.1 K per orbit.
SYS-PAY-4.3	The LRI cavity temperature shall not fluctuate by more than 1.5 K per orbit.
SYS-PAY-4.4	The CAI temperature shall not fluctuate by more than 0.1 K per orbit.
SYS-PAY-4.5	The LRI temperature shall be kept within the range of 27-33 °C.
SYS-PAY-4.6	The CAI temperature shall be kept within the range of 20-23 °C.
SYS-LNCH-5.1	Each spacecraft shall have a maximum launch mass of 1450 kg.
SYS-THER-9.1	Each spacecraft shall maintain all components within their operational temperature range during operation
SYS-THER-9.2	Each spacecraft shall maintain all components within their survival temperature range during the whole mission

The functions to be performed by the TCS, identified in the mission functional analysis of Section 5.1, are the following:

- F.4.1 Protect Spacecraft
  - F.4.1.1 Regulate Spacecraft Temperature

Analysis

The TCS is based on the methods described by Karam and Versteeg [86, 87]. The tool uses Equation 6.18 to calculate the required radiator area for the input data, assuming the hottest case possible. This is the EOL scenario for the radiator, which has degraded over the mission.

$$A_{\text{rad}} = \left. \frac{\overline{Q}_{\text{int}} + \overline{Q}_{\text{bus}} - \varepsilon_{\text{MLI}}\,\sigma\,T_{\text{set}}^4\,A_{\text{MLI}}}{\varepsilon_{\text{rad}}\,\sigma\,T_{\text{set}}^4} \right|_{\text{hot case data}} \tag{6.18}$$

Here, $\overline{Q}_{int}$ is the average internal dissipated heat, which is equal to the internal power usage, $\overline{Q}_{bus}$ is the average heat due to the heat fluxes present in orbit, which is calculated with Equation 6.19. ε is the emissivity of the respective materials, σ the Boltzmann constant, T_{set} the settling temperature in orbit, and A_{MLI} the area of the spacecraft exterior covered with MLI.

$$Q_{\text{bus}}(t) = \alpha_{\text{MLI}}\left[q_{\text{solar}}(t)\,A_{\text{solar}} + q_{\text{albedo}}(t)\,A_{\text{nad}}\right] + \varepsilon_{\text{MLI}}\,q_{\text{IR}}(t)\,A_{\text{nad}}. \tag{6.19}$$

α_{MLI} is the absorptivity of the MLI, $q_{\text{solar}}(t)$ is the solar flux at Mars as a function of time, A_{solar} is the area of the solar pointing side, $q_{\text{albedo}}(t)$ is the albedo flux as a function of time, A_{nad} is the area of the nadir facing side, and $q_{\text{IR}}(t)$ is the infrared flux from Mars as a function of time.

The solar flux is mostly constant, apart from the 22% dip at one of the poles, depending on the winter or summer solstice. The albedo and infrared fluxes vary sinusoidally over an orbit, with their maxima at the equator being equal to 147.5 W/m^2 and 286.0 W/m^2 respectively [88]. The minima occur at the poles and are equal to 0.0 W/m^2 and 56.0 W/m^2 respectively. The resulting fluxes are shown for three orbits in Figure 6.17.

The chosen radiator finish is silver-lined Teflon, since it has high emissivity ($\varepsilon_{\text{EOL}} = 0.75$) and low absorptivity ($\alpha_{\text{EOL}} = 0.35$). Additionally, silver-lined Teflon has myriad heritage, making it highly reliable [89]. For the MLI, 15 layers of Kapton is chosen, since it has both low emissivity ($\varepsilon_{\text{EOL}} = 0.013$) and low absorptivity ($\alpha_{\text{EOL}} = 0.0035$). Furthermore, the heritage argument also holds for the Kapton MLI [90]. From requirement SYS-THER-9.1, it follows that all components must be kept within their operational temperature range, the most stringent component being the MOM-3 tank, which must stay between 0 and 18.0°C. Henceforth, a design temperature of 13°C is chosen for T_{set}.

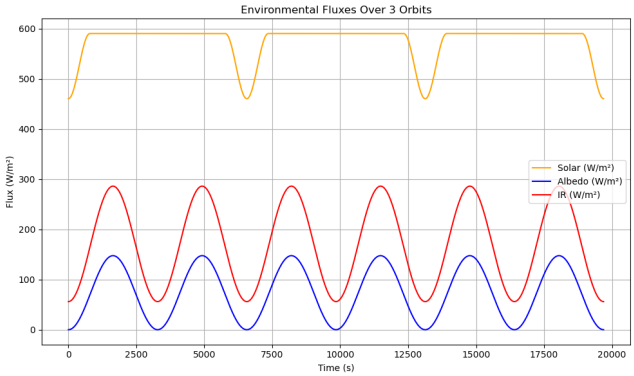

Figure 6.17: Various heat fluxes are computed at three orbits of 212 km altitude and 92.4° inclination.

With the aforementioned variables, the radiator area is calculated to be 2.66 m^2. It is conveniently placed on the shadow side of the spacecraft, opposite to the solar side and not facing Mars. This ensures that practically no albedo and infrared fluxes are absorbed by the radiator, while heat is being ejected to space. The heat flow outwards, Q_{out}, is computed with Equation 6.20. This is used in Equation 6.21 to compute the total heat flow. The internal temperature is then computed over time using Euler's method in Equation 6.22.

$$Q_{out} = \varepsilon_{rad}\,\sigma\,T^4\,A_{rad\_eff} + \varepsilon_{MLI}\,\sigma\,T^4\,A_{MLI} \tag{6.20}$$

$$Q_{net} = Q_{int} + Q_{bus} - Q_{out} \tag{6.21}$$

$$T_{i+1} = T_i + \left(\frac{\Delta t}{m \cdot c_p}\right) Q_{net} \tag{6.22}$$

Here, Δt is the time step, m is the mass, and c_p is the specific heat coefficient, taken for aluminium as it is the structural material. To dampen thermal fluctuations, both long- and short-term, a partial louvre is added onto the radiator. A louvre is a thermostatically actuated set of reflective blades mounted over a spacecraft radiator that automatically opens to shed excess heat and closes to conserve it, passively regulating the vehicle's temperature without consuming electrical power. Consequently, the effective radiator area (A_{rad_eff}) is either increased or decreased, depending on the internal temperature being lower or higher than the design temperature. Only 20% of the radiator is covered by a louvre to save weight. The effect of this addition to the internal temperature is shown in Figure 6.18. It can be seen that without louvres, at BOL, the temperature is 6.4°C, while at EOL it is 12.8°C. With louvres, the temperature is 12.8°C for all cases.

From Figure 6.18, it can also be seen that the temperature variation over one orbit is approximately ±0.01°C, which implies that requirements SYS-PAY-4.1, SYS-PAY-4.2, SYS-PAY-4.3, and SYS-PAY-4.4 are met. To meet requirements SYS-PAY-4.5 and SYS-PAY-4.6, the LRI components as well as the CAI will be encapsulated in MLI and equipped with patch heaters and thermostats. The patch heaters will have triple redundancy for all LRI components and CAI (21 heaters), as well as double redundancy for the propulsion tanks and feed lines (14 heaters), and 16 heaters for redundancy in the spacecraft, resulting in a total of 50 heaters. Owing to the MLI and stable temperature, the nominal power usage of the TCS is 1 W. Finally, the mass is calculated by multiplying the radiator, louvre, and MLI area with their respective densities.

Finally, the temperature in the transfer period is considered and determined to be well within the required survival temperature range. This is due to the louvres being able to change the effective

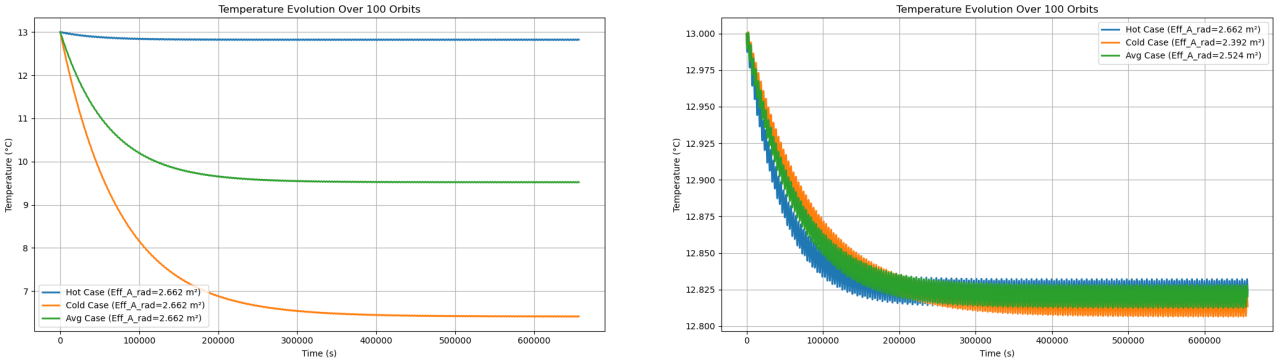

(a) Temperature evolution with no louvres.

(b) Temperature evolution with louvres.

Figure 6.18: Effect of louvres

radiator area to 80%, easily compensating for the lack of albedo and planet infrared radiation.

Table 6.28: TCS Tool Breakdown

Document Name	Model Description	Input	Output
`thermal_final`	Computes all the necessary thermal values and models the internal temperature over time.	Total dry and wet mass and power	Internal temperature, radiator area, TCS mass, and heat fluxes.

Design results

The final TCS design consists of an active thermal system comprising 50 heaters, the majority of which are for redundancy, drawing a nominal power of 1 W. The passive thermal design consists of a 15-layer Kapton MLI with an area of 18.8 m^2, a silver-lined Teflon radiator with an area of 2.7 m^2, and a louvre with an area of 0.5 m^2, which adds up to a total TCS mass of 20.7 kg. The code is analysed for sensitivity by varying the total dissipated power by ±20%, resulting in an internal temperature change of ±2.2%, which indicates sufficient sensitivity.

Subsystem Requirements

Updated ID	Description	Verification
SUB-TCS-1	The TCS shall keep the spacecraft at 13.0 ± 0.1°C in nominal science mode.	Testing
SUB-TCS-2	The TCS shall keep the spacecraft above 0.0°C till the end of the mission.	Analysis
SUB-TCS-3	The TCS shall cover the exterior of the spacecraft with a surface with an absorptance of at most 0.0035 and an emissivity of at most 0.0019.	Inspection
SUB-TCS-4	The TCS shall include a radiator with an absorptance of at most 0.35 and an emissivity of at least 0.75.	Testing
SUB-TCS-5	The TCS shall keep the total spacecraft temperature variation per orbit below 1.0 K	Testing
SUB-TCS-6	The TCS shall keep the temperature variation per orbit for the LRI and CAI below 0.1 K	Testing
SUB-TCS-7	The TCS shall draw no more than 1 W in nominal science mode.	Testing
SUB-TCS-8	The TCS shall provide double redundancy for the propellant tank heating.	Review of Design
SUB-TCS-9	The TCS shall provide triple redundancy for the payload heating.	Review of Design

6.6. Electrical Power Subsystem

The Electrical Power Subsystem (EPS) provides and regulates the power to the spacecraft.

Requirements and Functional Analysis

The preliminary sizing of the EPS had to comply with 6 main requirements:

Relevant Mission and System Requirements – Power Subsystem	
SYS-UR-1.1	Each spacecraft shall have a maximum power generated of 1000W at EOL.
SYS-ESA-2.1	The spacecraft shall not incorporate Radioisotope Thermoelectric Generators.
SYS-PAY-4.15	The spacecraft shall be able to provide 234 W to the payload throughout the mission
SYS-FUNC-7.1	The spacecraft shall be able to provide power to all subsystems during eclipse, with equivalent length of 2.43% of the orbital period.
SYS-FUNC-7.2	The spacecraft shall be able to provide power to all subsystems during power surges.
SYS-FUNC-7.7	The spacecraft shall be able to provide power to all subsystems during all times of the Martian year.

The functions to be performed by the EPS, identified in the mission functional analysis of Section 5.1 are the following:

- F.4.1 Protect Spacecraft
  - F.4.1.3 Ensure Spacecraft Power Supply
- F.4.6 Recover Spacecraft from Hazardous Situation
  - F.4.6.3 Regain Power Supply

Design Analysis

The EPS is divided into three main components, namely:

- Two solar array wings
- The Battery
- The Power Control and Distribution unit (PCDU)

The design of the EPS is driven by the power breakdown of the spacecraft. To get an estimate of the required power, an excel tool is developed. It is shown in Figure 6.19

Spacecraft Power Budget	Voltage (V)	Day/Eclipse/ Both	Day Power (W)	Day Duty Cycle	Day Avg Power (W)	Eclipse Power (W)	Eclipse Duty Cycle	Eclipse Avg Power (W)	Orbit Avg Power (W)	Peak Power (W)	Aerobraking Power (W)
Payload											0
LRI		Both	40	1	40	40	1	40	40	40	
CAI		Both	128.8	1	128.8	128.8	1	128.8	128.8	128.8	
OMIS		Both	4	1	4	4	1	4	4	4	
Iodine Reference Unit		Both	40.8	1	40.8	40.8	1	40.8	40.8	40.8	
MiniCAS		Both	8	1	8	8	1	8	8	8	
CMT		Both	0	1	0	0	1	0	0	0	
ADCS											
Sensors	28	Both	26.6	1	26.6	26.6	1	26.6	26.6	26.6	26.6
Cold Gas Thruster	28	Both	4.2	1	4.2	4.2	1	4.2	4.2	110.6	110.6
Thermal											
Patch Heaters	0	Both	1	1	1	1	1	1	1	1	1
TT&C											80
TWTA		Day	140	1	140	0	1	0	136.598	140	
Transponder		Day	16	1	16	0	1	0	15.6112	16	
Ultra Stable Oscillator		Day	5	1	5	5	1	5	5	5	
Gimball system		Day	16	1	16	0	1	0	15.6112	16	
SSPA		Day	1	1	1	1	1	1	1	1	
EUT		Day	70	1	70	70	1	70	70	70	
CDHS											
OBC	28	Both	30	1	30	30	1	30	30	30	30
Propulsion											
Bipropellant Propulsion		Both	0	1	0	0	1	0	0	50	0
Total Power					531.4			359.4		687.8	
Power Design Margin					0.3			0.3		0.3	
Subtotal Power					690.82			467.22			
					DAY			ECLIPSE		PEAK POWER	AEROBRAKING
Spacecraft Power Required (W)					690.82			467.22		894.14	248.2

Figure 6.19: Spacecraft Power Breakdown

The power for the subsystems is given for nominal science mode, potential peak power bursts and during aerobraking. A 30% margin was added.

Solar Array Design Analysis

Solar array wings were deemed the only suitable option, as due to the chosen orbit only one side of the spacecraft points towards the sun, with the other 5 sides predominantly in shadow. As the antenna also has to point towards the sun, and shadows would even further reduce the limited area available on the body, body-mounted panels were discarded as an option.

To size the solar array, the power required to be generated by the solar array P_{sa} is calculated. The input parameters in Table 6.31 are used. These are the inputs for nominal science mode: during the battery sizing, a significant peak power burst due to the electric propulsion subsystem will be considered as well. This burst is not relevant for the solar array sizing as it is infrequent, therefore the battery will be able to single-handedly meet its power needs.

Table 6.31: Power and Timing Parameters Used in Solar Array Design Analysis

Input	Value	Unit
Daylight Power	690.82	W
Eclipse Power	467.22	W
Daylight Time	6393	s
Eclipse Time	159	s
X_e	0.65	—
X_d	0.85	—

P_{sa} is then given by Equation 6.23:

$$P_{sa} = \frac{\frac{P_e T_e}{X_e} + \frac{P_d T_d}{X_d}}{T_d} \tag{6.23}$$

X_e and X_d are the battery charge efficiency and the distribution efficiency. T_e and T_d are the eclipse time and the time in sunlight respectively.

Then, the ideal solar cell output performance per unit area, P_o can be determined by multiplying the solar flux at Mars with the cell efficiency. The realistic solar cell output is lower due to factors like shadowing, temperature variations and other inefficiencies. This inherent degradation I_d was taken to be 0.85. The power at beginning-of-life per unit area is then given by:

$$P_{BOL} = P_o \, I_d \, \cos\theta \tag{6.24}$$

With θ the solar incidence angle, taken to be 30 degrees in the worst case. Now, the degradation over the lifetime over the solar array L_d must be estimated, taking into accounts factors like radiation, micrometeoroid strikes and temperature cycles. It is given by Equation 6.25, with the degradation per year estimated to be 1%. The power at end-of-life per unit area is then given by Equation 6.26. Finally, the solar array area can be calculated with Equation 6.27.

$$L_d = (1 - \text{degradation/yr})^{\text{satellite life}} \tag{6.25}$$

$$P_{EOL} = P_{BOL} \, L_d \tag{6.26}$$

$$A_{sa} = \frac{P_{sa}}{P_{EOL}} \tag{6.27}$$

The nominal power drop per degree above reference operating temperature is about 0.1%/C for triple-junction GaAs cells [91]. The power required during aerobraking is 248.2 W. However, due

to the solar arrays not being oriented toward the direction of aerobraking, the percentage drop per degree being very small, and the relatively low aerobraking power required, aerobraking was not deemed critical for the sizing process.

Furthermore, regarding the aerodynamic characteristics of the solar array, as they are almost perpendicular to the flight direction, they can be neglected.

Battery Design Analysis

The battery design is driven by the power required during eclipse, but mainly due to the peak power burst required by the electrical propulsion used for station keeping.

The first step in sizing the battery is to determine the voltage of the spacecraft bus. This was chosen to be 28V, due to it being the standard for satellites of MarsExplore's power range [92]. The battery is sized in two ways, the number of cells in a string determines the voltage of the battery, whereas the cell strings in parallel give the required capacity. The number of cells in sting can then be calculated as:

$$N = \frac{V_{bus}}{V_{cell}} \tag{6.28}$$

The chosen cells are the ABSLTM Cell 18650 E35, with a nominal voltage and capacity of 3.7 V and 3.5 Ah respectively, leading to a requirement of 8 cells per battery string. The required capacity C_{req} is then calculated with:

$$C_{req} = P_e T_E + P_{burst} T_{burst} \tag{6.29}$$

The left term represents the power required during eclipse, and the right term represents the power burst of the electrical propulsion system. The total capacity at EOL is then:

$$C_{EOL} = \frac{C_{req}}{DOD \eta_{battery}} \tag{6.30}$$

With DOD the maximum depth-of-discharge, 30%, and $\eta_{battery}$ the battery efficiency, 80%. Over the lifetime (n years) of the battery, it will degrade by a fading factor F_{fading}. The battery capacity at BOL is then given by:

$$C_{BOL} = \frac{C_{EOL}}{F_{fading} n} \tag{6.31}$$

This leads to a total battery capacity requirement of 1840.58 Wh. The number of cell strings in parallel is then given by:

$$p = \frac{C_{BOL}}{V_{cell} C_{cell}} \tag{6.32}$$

This leads to a requirement of 18 strings in parallel. The final battery configuration is thus 8s18p, leading to a total capacity of 67 Ah. With a specific mass and energy density of 210 Wh/kg and 400 Wh/L respectively, this leads to a battery mass and volume of 8.9 kg and 0.26 L. As the battery is critical to mission success, three of these batteries are installed for redundancy.

The cycle of the battery charge over two power bursts is shown in Figure 6.20. As can be seen, the battery never dips below the 30% DOD limit. Furthermore, the battery will be able to power the spacecraft during launch and during the transfer to Mars.

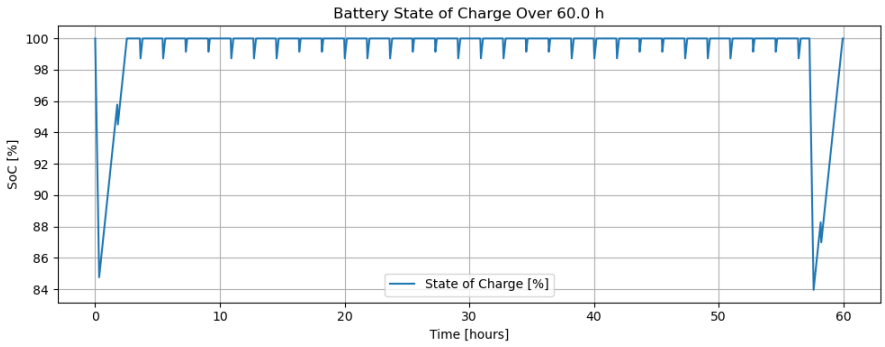

Figure 6.20: Spacecraft Power Breakdown

Power Control and Distribution Unit Design Analysis

The MarsExplore electrical block diagram is provided in Figure 6.21.

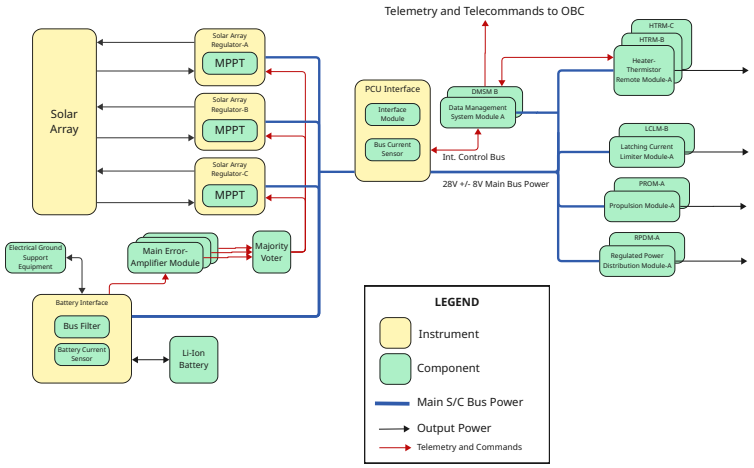

Figure 6.21: Electrical Block Diagram

As was the case for GRACE-FO, CHAMP, GRACE and SWARM, MarsExplore's bus is positively grounded, due to the strong heritage and improved spacecraft charging [93].

The PCDU can be split into two main parts, the power control unit, and the power distribution unit. The power control unit consists of 4 main modules.

- 3 Solar Array Regulator Modules (SARMs), one for each solar array wing, and one for redundancy. 2 out of 3 are able to convert the full power required. The energy transfer scheme chosen is peak-power tracking, therefore each SARM is equipped with a maximum peak power tracker (MPPT), ensuring that each panel is operating at its maximum power generation point.
- Main Error Amplifier Module, which controls the SARM power. Tells the MPPT channels how much current to draw so that the battery charges correctly, and ensures the bus voltage stays within limits.
- Majority Voter, compares the three error amplifier outputs and forwards the majorit value, even if one amplifier fails.
- The Battery Interface consists of:

  Bus Filter, A capacitor that damps high-frequency noise and keeps the 28 V voltage stable when loads or array output fluctuate suddenly

Battery Current Sensor, measures the charge and discharge current so the OBC can estimate the DOD

Li-Ion Battery, the battery of the spacecraft

- The PCU Interface consists of:

  Interface module, which handles all low-level telemetry/telecommand lines in the PCDU

  Bus Current Sensors, which measurs the total spacecraft bus current delivered by the PCDU, so that the OBC can spot any eventual shorts or load growths.

The power distribution unit can be divided into 5 main modules:

- Redundant Data Management System Modules (DMSM-A/B), presents all the power distribution telemetry and command data to the OBC, furthermore, it also converts the raw 28 V bus voltage to the auxilary voltages needed by the smaller PCDU modules.
- Heater-Thermistor Remote Modules (HTRM-A/B/C), responsible for keeping the power subsystem "quiet", ensuring that the 'bang-bang' shocks that disrupted previous gravity missions are eliminated
- Redundant Latching Current Limiter Modules (LCLM-A/B), supply unregulated power to most of the platform units from the power bus.
- Redundant Regulated Power Distribution Modules (RPDM-A/B), supply regulated power to give stable power to sensitive electronics, e.g. the payload instruments.
- Redundant Propulsion Modules (PROM-A/B), drives the ADCS cold gas thrusters, and the propulsion system.

Design Results and Sensitivity Analysis

The final EPS design consists of two solar array wings, each consisting of 317 AZUR Space Triple Junction Solar Cell Assembly 3G30A, with integral bypass diode, interconnectors and cover glass, resulting in a total solar array area of 8.14 m^2. They are mounted on a conventional aluminium CFRP panel, with a highly insulating 40mm foam layer on top to keep temperature consistent. The solar arrays are mounted to the spacecraft with a hinge, allowing the panels to fold flush to the spacecraft to fit inside the launcher. Three 67 Ah batteries are installed, with an 8s18p configuration consisting of ABSL 18650 E35 Li-Ion cells. The total mass of the battery is 8.9 kg. On average, it only draws 17.5 W to charge itself due to the spacecraft being in sunlight almost continuously. The total mass of the EPS is 49.35 kg.

This design allows the EPS to provide the spacecraft with an average continuous power of 830 W during nominal science mode at end-of-life, comfortably satisfying the spacecraft's power demands. At beginning-of-life, the solar arrays are able to generate 910 W. Furthermore, the battery is sized such that during peak power bursts, when the spacecraft requires an additional 1025 W, the battery will be able to power the burst without dipping below 30% DoD. One thing to note for future iterations is that this is a very conservative value, as this burst occurs less than 300 times during the missions operations, a more lenient DoD limit can be considered. However, as the battery does charge/discharge over 9000 times during the entire mission, and an in-depth battery health analysis was not performed at this stage, the 30% limit was considered as a conservative value because it is the standard limit used in battery design.

A sensitivity analysis is performed on two main inputs, the required solar array power, and the peak power burst required by the electrical propulsion. These parameters were varied by +/- 20% each. This resulted in the solar array area varying between 6.5 and 9.8 m^2, and the battery capacity varying between 55.74 and 81.71 Ah.

Subsystem Requirements

Updated ID	Old ID	Description	Verification
SUB-POW-1	UR-SUB-PW-2.6.4.1	The power subsystem shall provide the spacecraft with an average continuous power of at least 830 W.	Testing
SUB-POW-2	SUB-PW-2.6.4.2	The power subsystem shall be able to provide peak power loads of 1507 W for 0.33 hr.	Testing
SUB-POW-3		The power subsystem shall provide 420 W in nominal science mode during eclipse to the S/C bus.	Testing
SUB-POW-4	SUB-PW-2.6.4.3	The power subsystem shall provide an energy storage capacity of at least 66.85 Ah.	Review of Design
SUB-POW-5	SUB-PW-2.6.4.5	The power subsystem shall provide a nominal output voltage of 28 V with a tolerance of 8 V.	Testing
SUB-POW-6	SUB-PW-2.6.4.6	The energy storage subsystem shall support up to 9145 charge/discharge duty cycles at 30% DoD.	Testing
SUB-POW-7	SUB-PW-2.6.4.7	The energy storage subsystem shall have a maximum DoD of 30%.	Testing

6.7. Structures

The primary function of the Structures Subsystem is to provide a physical framework that houses and protects all spacecraft components. It ensures structural integrity and shields the spacecraft from mechanical loads, radiation, magnetic fields, and space debris encountered throughout the mission. This section outlines the procedure with which the structures subsystem is designed such that it can meet its system and mission requirements.

Requirements and Functional Analysis

The previously-defined requirements relevant to the structures subsystem design are listed below.

Relevant Mission and System Requirements – Structures Subsystem	
SYS-LNCH-5.2	The undeployed spacecraft shall fit within the payload compartment of the Ariane 62 Short Dual Launch Structure configuration.
SYS-LNCH-5.2.1	The undeployed spacecraft shall have a maximum height of 4.30 m.
SYS-LNCH-5.2.2	The undeployed cross-section of each spacecraft shall allow the 2 spacecraft to fit within a circular cross-section of diameter 4.6 m.
SYS-LNCH-5.3	The spacecraft shall be able to withstand the mechanical environment of launch aboard an Ariane 62 launch vehicle.
SYS-LNCH-5.3.1	The spacecraft shall withstand a maximum axial g load of magnitude 6 without failing in Euler buckling.
SYS-LNCH-5.3.2	The spacecraft shall withstand a maximum axial g load of magnitude 6 without failing in yielding.
SYS-LNCH-5.3.3	The spacecraft shall withstand a maximum axial g load of magnitude 6 without failing at the ultimate load limit.
SYS-LNCH-5.3.4	The spacecraft shall withstand a maximum lateral g load of magnitude 2 without failing in Euler buckling.
SYS-LNCH-5.3.5	The spacecraft shall withstand a maximum lateral g load of magnitude 2 without failing in yielding.
SYS-LNCH-5.3.6	The spacecraft shall withstand a maximum lateral g load of magnitude 2 without failing at the ultimate load limit.
SYS-LNCH-5.3.7	The spacecraft shall have a fundamental axial natural frequency greater than 20 Hz.
SYS-LNCH-5.3.8	The spacecraft shall have a fundamental lateral natural frequency greater than 6 Hz.
SYS-RISK-8.10	The spacecraft critical surfaces and subsystems shall withstand MMOD impacts from particles of up to 0.01 kg mass, 2700 kg/m^3 density, and 20 km/s relative velocity without loss of structural integrity or functionality.
SYS-RISK-8.11	The spacecraft critical surfaces and subsystems shall withstand a TID of 10.95 rad without degradation in functionality.
SYS-PAY-4.14	The spacecraft shall not produce vibrations that render science data unusable for more than 1% of science operations.
SYS-PAY-4.16	The magnetic field external to the CAI shall be less than 10 mT.

The functions to be performed by the structures subsystem, developed from the mission functional analysis of Section 5.1 are the following:

- F.4.1 Protect Spacecraft
  - F.4.1.1 Protect Spacecraft from Micrometeoroid and Orbital Debris (MMOD) impacts
  - F.4.1.2 Protect Spacecraft from Radiation
  - F.4.1.3 Protect Spacecraft from Magnetic fields
  - F.4.1.4 Protect Spacecraft from Mechanical Loading and vibrations
- F.4.2 Be compatible with volume constraints
  - F.4.2.1 Be compatible with launcher volume constraints
  - F.4.2.2 Be compatible with internal component volumes

Analysis

As seen from the functional analysis above, the sizing of the structures subsystem considers volume compatibility functions and requirements (**SYS-LNCH-5.2 to SYS-LNCH-5.2.2**), and then protection functions and requirements (**SYS-LNCH-5.3 to SYS-PAY-4.16**) , especially from mechanical loading and vibrations.

The equations employed for the analysis assume the following:

- The spacecraft can be reasonably modelled as a uniform beam. This assumption is valid considering the lack of information on precise mass distribution at this time; additionally, the accelerometer measurements require a fixed center of mass (CoM) throughout the spacecraft lifetime [78], resulting in a uniform and "symmetrical" placement of subsystems around the CoM (see Section 7.3).
- The beam is modelled as a cuboid to facilitate the subsystems' symmetrical accommodation.
- A thin-walled semi-monocoque structure, i.e., stiffened panel, is assumed as the spacecraft structure. This is because a semi-monocoque structure offers an optimal balance between strength and weight, modularity for subsystem integration, and compatibility with modern manufacturing methods such as friction stir welding.
- In terms of mechanical loading, this sizing only accounts for frequencies and loads during launch and their effect on rigidity, strength and stability. This is because launch loads are the most limiting load case in almost all mission cases [59]; additionally, more complex loads such as acoustic loads, shock loads and in-orbit loads would require additional resources, such as FEM, currently not available.

Volume Function

The volume function analysis is performed before the mechanical function analysis since structural dimensions are a necessary input for the latter. The volume fitting procedure considers the following: firstly, the accommodation of all relevant spacecraft subsystems within, and on, the spacecraft structure; secondly, the accommodation of the spacecraft structure within the launch vehicle fairing (**SYS-LNCH5-5.2 to SYS-LNCH-5.2.2**).

Thanks to volume estimates of all volume-driving subsystems, 3D CATIA models for the spacecraft internal and external configurations are produced at the beginning of each iteration, based on previous iteration values. This procedure provides a preliminary estimate of the spacecraft dimensions, which serves as inputs for the protective function analysis at Table 6.7. The dimensions are then again updated following the configuration results (panel thickness, stringer configuration, internal casings) of the protective functions analysis.

It is then ensured that these dimensions fit in the chosen "short dual launch structure" configuration of the Ariane 62 fairing [94]). A further visualisation and justification of this procedure's results, i.e., the dimensions, internal layout and external layout of the chosen spacecraft configuration, deployed and undeployed configurations, are found at Section 7.3.

Protection Function
After having established the preliminary dimensions of the spacecraft structural box and internal components, they can be used as inputs for the protective function calculations.

As is explained more in detail at the bottom of this chapter, the tool (code) performing the structural sizing optimisation iterates through various different design parameters to optimise the configuration for minimal structural mass (weight of 0.6), cost (weight of 0.3) and manufacturability (weight of 0.1). Due to the semi-monocoque structure chosen, the design parameters being iterated through are the following: skin panel and stringer material, skin thickness, stringer dimensions (element thicknesses and lengths), stringer geometry, stringer number and layout. As is seen below, these parameters play a critical role in sizing calculations.

Firstly, the mechanical analysis is performed (**SYS-LNCH-5.3 to SYS-LNCH-5.3.8**). The tool calculations for this consist of sizing for rigidity, strength, and stability, through a method based on that of *Space Mission Analysis and Design* [59].

Rigidity sizing Firstly, the rigidity sizing involves calculating the structural inertia [13] and area values that ensure spacecraft natural frequencies above launcher fundamental frequencies. This is done by rearranging the lateral and axial frequency equations for a uniform beam case into Equation 6.33 and Equation 6.34 respectively. As can be seen, this calculation imposes constraints on the cross-sectional area and inertia of the panel and stringers combination.

$$A_{min} = \frac{\left(\frac{f_{\text{nat,ax}}}{0.25}\right)^2 \cdot m_b \cdot h}{E} \tag{6.33}$$

$$I_{min} = \frac{\left(\frac{f_{\text{nat,lat}}}{0.56}\right)^2 \cdot m_b \cdot h^3}{E} \tag{6.34}$$

where A_{min} is the minimum stiffened panel cross-sectional area (panel and stringer) required to meet the axial frequency constraint, I_{min} is the minimum polar inertia moment required to meet the lateral frequency constraint, m_b is the total spacecraft mass, h is the height of the spacecraft and E is the elastic modulus of the structural material. Additionally, $f_{\text{nat,ax}}$ is the launcher axial frequency and $f_{\text{nat,lat}}$ is the launcher lateral frequency, which are 20Hz and 6Hz respectively in the Ariane 62 launcher [94].

Thanks to these minimum area and inertia requirements, the corresponding minimum skin thicknesses and stringer cross-sectional area can be calculated. This is seen in Equation 6.35 and Equation 6.36.

$$t_{ax,min} > \frac{A_{min} - n_{str}A_{str}}{2l + 2w} \tag{6.35}$$

$$t_{lat,min} > 3 \cdot \frac{I_{min} - n_{str}I_{str}}{l^2w + w^2l} \tag{6.36}$$

where $t_{ax,min}$ and $t_{lat,min}$ are the minimum skin thicknesses corresponding to the area (axial) and inertial (lateral) requirements respectively, A_{str} is the cross-sectional area of each stiffener, I_{str} is the polar inertia of each stiffener, n_{str} is the number of stiffeners, l is the length of one of the sides of the rectangular cross-section and w is the "width" of the cross-section, i.e., the length of the other side of the rectangular cross-section.

Strength sizing Secondly, the sizing for strength is performed. These calculations ensure that the material's ultimate and yield strength is sufficiently high in withstanding the maximum equivalent axial load. As seen in Equation 6.37, the equivalent axial load accounts for the axial, (lateral) and bending moment loads all at once, where these loads must all belong to the same lifetime phase of the spacecraft. Additionally, an Ultimate Factor of Safety (UFoS) of 1.25 is used for the equivalent load calculation [59].

[13] `https://www.structx.com/Shape_Formulas_025.html`, accessed 20/05/2025

$$P_{eq} = \left(P_{ax} + 2\frac{P_{lat} \cdot \frac{h}{2}}{d_{1/2}} \right) \cdot 1.25 \tag{6.37}$$

where P_{eq} is the equivalent launch load, P_{ax} is the corresponding axial g-load, P_{lat} is the corresponding lateral g-load, and $d_{1/2}$ is half of the longest diagonal of the polygon's cross-section. In the case of the Ariane 62 launcher, the axial and lateral g-loads corresponding to the maximum equivalent launch load have a magnitude of 6g and 1g respectively, occuring at End of Flight [94].

As mentioned above, this equivalent load must be lower than both the yield and ultimate load capabilities of the material and structure. This is shown in Equation 6.38 and Equation 6.39. For the skin thickness dictated by the yield strength requirement ($t_{y,req}$), a Factor of Safety (FoS) of 1.10 is used [59].

$$t_{y,\min} > \frac{1.10}{2l + 2w} \left(\frac{P_{eq}}{\sigma_y} - n_{str} A_{str} \right) \tag{6.38}$$

$$t_{ult,\min} > \frac{1}{2l + 2w} \left(\frac{P_{eq}}{\sigma_{ult}} - n_{str} A_{str} \right) \tag{6.39}$$

where $t_{y,min}$ and $t_{ult,min}$ are the minimum skin thicknesses corresponding to the yield and ultimate strength requirements respectively, and σ_y and σ_{ult} are the yield and ultimate strength respectively.

Stability sizing Lastly, the sizing for stability involves ensuring the prevention of buckling. Firstly, local compressive buckling of the stiffened panel is considered. Then, global buckling of the stringers due to their slenderness (slenderness ratio) is considered. The procedure followed is that of the *AE2135-I Structural Analysis & Design* course [14].

Local compressive buckling To begin the local compressive buckling calculation, the stiffener crippling stress, unique to its geometry, is calculated. This includes initially applying Equation 6.40 to obtain the crippling stress of each element of the stringer geometry.

$$\frac{\sigma_{cc}^{(i)}}{\sigma_y} = \alpha \left[\left(\frac{C}{\sigma_y} \cdot \frac{\pi^2 E}{12(1-\nu^2)} \left(\frac{t}{b} \right)^2 \right)^{1-n} \right] \tag{6.40}$$

where σ_{cc} is the crippling stress of the i-th stiffener element, σ_y is the yield stress of the material, C is the stiffener buckling coefficient varying between 4 to 6.98 depending on clamping conditions, α is a constant with a value of 0.8, n is a constant with a value of 0.6, ν is the Poisson's ratio, E is the modulus of elasticity, t is the thickness of the stiffener element, and b is the width of the stiffener element.

Based on the above result, each element of the stringer geometry is awarded a load-bearing capability equal to σ_{cc} in the case that $\frac{\sigma_{cc}^{(i)}}{\sigma_y} < 1$, or equal to σ_y in the case that $\frac{\sigma_{cc}^{(i)}}{\sigma_y} > 1$. This allows a conservative estimate of the stringer strength to be made, since each element is checked against -and limited to- its limiting failure mode out of the yielding or crippling failure modes.

Then, the weighted sum of is applied to obtain the crippling stress of the entire stringer geometry.

$$\sigma_{cc} = \frac{\sum \sigma_{cc}^{(i)} A_i}{\sum A_i} \tag{6.41}$$

where A_i is the area of the i-th stiffener element. As evident, the above calculation varies depending on the geometry of the stringer (eg. hat, Z, I stringer etc.). Therefore, during the iteration over stringer shapes, the calculation is uniquely developed for each stringer shape considered.

[14] https://brightspace.tudelft.nl/d2l/le/content/612268/viewContent/3326875/View

Secondly, the effective sheet width is calculated through Equation 6.42. This quantity measures the portion of the skin adjacent to the stiffener, which via its proximity to the stiffener has the same load-bearing capabilities as the stiffener itself.

$$2w_e = t_{pan}\sqrt{\frac{C_{we}\pi^2}{12(1-\nu^2)}}\sqrt{\frac{E}{\sigma_{cc}}} \tag{6.42}$$

where $2w_e$ is the effective width, C_{we} is the panel buckling coefficient, taken as 4 for a conservative estimate, and t_{pan} is the thickness of the skin panel.

Thirdly, the buckling stress of each inter-stringer panel element -taking into account the effective width of the stringers- is calculated through Equation 6.43.

$$\sigma_{cr} = C_{we} \cdot \frac{\pi^2 E}{12(1-\nu^2)}\left(\frac{t_{pan}}{b_{pan}-2w_e}\right)^2 \tag{6.43}$$

where b_{pan} is the inter-stiffener distance. The same area-weighted sum stress calculation as in Equation 6.41 is repeated for each of the four panels.

Lastly, the total buckling stress of the stiffened panel (panel plus stiffeners) is calculated thanks to Equation 6.44. Through the area-weighted sum, the buckling stress of the panel and the crippling stress of the stiffeners are accounted for.

$$(\sigma_{cc})_{\text{stiff panel}} = \frac{\sum \sigma_{each}^{(i)} A_{i,each}}{\sum A_{i,each}} \tag{6.44}$$

where $\sigma_{each}^{(i)}$ is the stress of each i-th stiffener and panel comprising the stiffened panel, and the $A_{i,each}$ is their respective areas.

The resulting total load-bearing capability of the stiffened panel is then as written at the LHS of Equation 6.45. This capability is checked against the equivalent load P_{eq} resulting from the axial and lateral launch loads, to ensure that the spacecraft does not fail in local compressive buckling, as seen at the equation's RHS.

$$P_{\text{stiff panel}} = (\sigma_{cc})_{\text{stiff panel}} A_{\text{stiff panel}} > P_{eq} \tag{6.45}$$

Global buckling of stringers The global buckling of the stringers due to their slenderness (slenderness ratio) can now be addressed. The column-like nature of the stiffeners lead to their failure in either crippling at low slenderness ratios or in Euler buckling at high slenderness ratios. The transition between these two regimes is marked by the Johnson parabola and the stiffeners' critical slenderness ratio.

Considering the large length of the longest side of the spacecraft compared to its other dimensions, this will translate to an equal, long length of the stiffeners. It is thus imperative to check whether Euler buckling as a result of the high slenderness ratio is limiting.

Firstly, the critical slenderness ratio for each stiffener configuration (geometry and material) is calculated through Equation 6.46

$$\left(\frac{L_e}{\rho}\right)_{crit} = \sqrt{\frac{2\pi^2 E}{\sigma_{cc}}} \tag{6.46}$$

where $\left(\frac{L_e}{\rho}\right)_{crit}$ is the critical slenderness ratio, and just as for the local buckling analysis, E is the modulus of elasticity and σ_{cc} is the crippling strength of the stiffener.

Then, the actual slenderness ratio for each configuration (geometry, dimensions and material) is calculated through .

$$\left(\frac{L_e}{\rho}\right)_{str} = \frac{L_e}{\sqrt{\frac{I_{xx}}{A_{str}}}} \tag{6.47}$$

where $\left(\frac{L_e}{\rho}\right)_{str}$ is the actual slenderness ratio of the stringer, L_e is the longest length ("height") of the stiffener, ρ is the radius of gyration of the stiffener, I_{xx} is the second moment of area of the stiffener and A_{str} is the cross-sectional area of the stiffener.

In the case that $\left(\frac{L_e}{\rho}\right)_{str} < \left(\frac{L_e}{\rho}\right)_{crit}$, then crippling-driven failure is the limiting failure mode, and the failure stress is determined based on the slenderness ratio through the Johnson parabola, Equation 6.7.

$$\sigma_{cr} = \sigma_{cc}\left[1 - \frac{\sigma_{cc}\left(\frac{L_e}{\rho}\right)^2_{str}}{4\pi^2 E}\right] \tag{6.48}$$

where σ_{cr} is the crippling strength of the stringer based on the Johnson parabola.

In the case that $\left(\frac{L_e}{\rho}\right)_{str} > \left(\frac{L_e}{\rho}\right)_{crit}$, Euler buckling is the limiting failure mode and and the failure stress is determined based on the slenderness ratio through the Euler buckling curve, Equation 6.49.

$$\sigma_{cr,Euler} = \pi^2 E\left(\frac{\rho}{L_e}\right)^2 \tag{6.49}$$

where $\sigma_{cr,Euler}$ is the crippling strength of the stringer based on the Euler curve.

For all stringer configurations tested -and as expected from the long length of the stringers- the Euler buckling mode is the dominant failure mode, as opposed to local compressive buckling of the stiffened panel. This is better exemplified by Figure 6.22a, where it is clear that a total of 8 stringers is required to bear the launchload in Euler buckling, whereas even 4 are sufficient for the local compressive buckling. Hence, the load-bearing capability of the stringer based on the Euler buckling failure mode, at the LHS of Equation 6.50, is checked against the equivalent load P_{eq} at the RHS. This ensures that the spacecraft does not fail in Euler buckling during launch.

$$P_{\text{Euler}} = (\sigma_{cr})_{\text{Euler}} A_{\text{str}} n_{\text{str}} > P_{eq} \tag{6.50}$$

As can be seen from the equation, the Euler capability is dependent only on the cross-sectional area of each stringer and on the number of stringers. Hence, the structural tool minimizes the mass of the required stringers by iterating through varying stringer cross-sectional dimensions (stringer element lengths and thickness) and number of stringers, all whilst ensuring Euler buckling is prevented. An example of how the stringer geometrical parameters -in this case thickness- vary the loadbearing capacity is seen in Figure 6.22b.

Additional protection considerations Below are additional protection considerations concerning the secondary structure. They make use of some of the optimisation results at Table 6.7. However for clarity, the explanation behind these considerations' rationale are included in this section. All of these components are included within the structural mass calculation of the code.

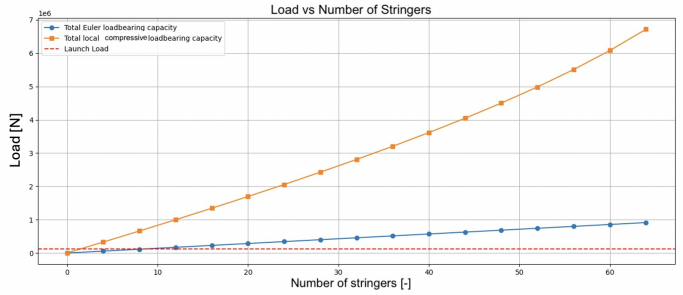

(a) Structure load-bearing capacity vs. number of stringers, for local compressive buckling and Euler buckling

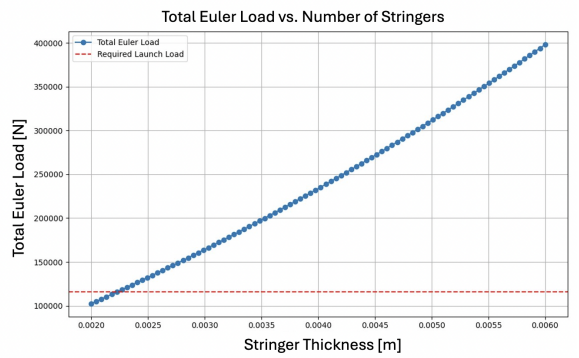

(b) Structure loadbearing capacity in Euler buckling as a function of stringer thickness

Figure 6.22: Effect of varying structural parameters on structural load-bearing capacity, compared to the required launch load.

Magnetic Shielding In accordance with **SYS-PAY-4.16**, the magnetic field external to the CAI shall be less than 10 mT [44]. The largest contributing factor to magnetic interference inside the spacecraft are the HETs. Given that the magnetic field at the HET channel exit is 30 mT in the worst case scenario, and the CAI would be placed around 1.25 m, an additional suppression factor of at least 20 is needed, given that the magnetic field gets weaker with distance. Thus, magnetic shielding must be incorporated into the HET. For this, an iron-based alloy is selected[15], with density of 7.18 g/cm^3. According to [95], this should be possible to be achieved with a thickness of 7 mm surrounding the HETs.

Radiation To comply with the radiation requirement **SYS-RISK-11**, the structure shall protect electronics and other radiation-sensitive components from a TID of 10.95 rad, the radiation experienced at the chosen orbit altitude on Mars.

Considering that each of the 1.5 mm aluminium panels reduces the incoming radiation by 35% [16], the spacecraft internal components experience a TID of 8.37 rad. The majority of the electronics in the spacecraft, such as the CDHS, batteries and part of the payload are space-grade components which are radiation-hardened. Radiation-hardened components can withstand the 8.37 rad TID without additional shielding, seen their ability to withstand TID up to 300 krad(Si), i.e., 180 rad [96]. Hence, the majority of the electronic components do not require additional shielding.

However, the LRP and OBE components of the payload are not radiation-hardened, thereby requiring additional shielding. It is assumed that they can handle the same doses as Commercial Off-The-Shelf (COTS) electronics, an average of 10 krad (Si) [97], i.e, 6 rad. Thereby to reduce the received TID of 8.37 rad to that of 6 rad, a percentage reduction of 29% is required. This percentage reduction is achievable through 1 cm of High-density polyethylene (HDPE) with density of 900 kg/m^3. The mass corresponding to this radiation shielding is calculated to be 8.37 kg.

MMOD protection To comply with the requirement **SYS-RISK-10**, the structure shall protect the spacecraft from MMOD particles of up to 0.01 kg mass, 2700 kg/m³ density, and 20 km/s relative velocity. Therefore, a whipple shield is implemented on the frontal area of the spacecraft, which is most at risk from the impacts. Compared to alternative MMOD solutions, the whipple shield is advantageous as it is lightweight, simple and highly effective against the high-velocity micrometeoroids and orbital debris encountered in Martian orbit.

To calculate the required whipple shield rear wall thickness, the below equation is utilised [98].

[15] `https://metglas.com/magnetic-materials/` (accessed June 17, 2025)
[16] `https://patents.google.com/patent/EP0356488A4/zh` (accessed June 17, 2025)

$$t_w = \frac{C\, m_p^{1/3} V}{S^{1/2}} \tag{6.51}$$

where t_w is the required rear wall thickness, $C = 0.055(\rho_p \rho_b)^{1/6}$ is an empirical constant, m_p is the projectile mass in kg, V is the projectile velocity in km/s, S is the standoff distance in cm, ρ_p is the density of the projectile, ρ_b is the density of the whipple shield rear wall.

Considering a rear wall made of aluminium of 2800 kg/m^3, a 1.5mm thickness requirement results. This means that the aluminium panels of the primary spacecraft structure are sufficient at performing the rear wall function. Hence, no additional material nor mass is required for the rear wall.

For the bumper wall, inherently additional to the (rear wall) aluminium panels, the thickness has a ratio of 0.2 with the rear wall thickness [99]. This equates to a 0.3 mm bumper wall thickness. The additional mass corresponding to the MMOD shielding, i.e., the bumper wall, then corresponds to 1.67 kg. It is important to note that although the MLI does provide partial MMOD shielding [99], the MLI contribution is difficult to estimate and its exclusion allows for a conservative estimate of the bumper wall thickness required.

CAI vibration platform Following the same resonant frequency analysis as in Equation 6.34 and Equation 6.36, a platform thickness of 1 cm for the CAI vibration platform (measuring 1.1 m x 1.7 m) was deemed sufficient: it can prevent the resonant lateral frequencies below 100 Hz, which the instrument is prone to [100]. This adds 3.3 kg to the structural mass.

Antenna boom skin thickness Following the same resonant frequency analysis as in Equation 6.34 and Equation 6.36, but for a cylindrical cross-section, a minimum antenna boom thickness was determined. Considering an antenna boom measuring 30 mm in diameter, 0.6 m in height, supporting a total mass of 42 kg, and manufactured out of Uni-directional Carbon Fibre Reinforced Polymer (CFRP) with E-modulus of 250 GPa [101], the minimum boom skin thickness amounts to 4.4 mm. This thickness is determined by the lateral frequency requirement of the boom, which due to the boom's perpendicularity with the launcher, corresponds to the launcher's axial frequency of 20 Hz.

Internal mountings A margin of 1.15 as stated by SMAD [59] was used to account for internal mountings, joints, discontinuities, etc. This contributes to the total structural mass.

Optimisation loop

The tool, summarized at Table 6.34 performs the structural sizing optimisation by iterating through all possible combinations of the possible parameter values:

- Skin and stiffener material: Aluminium, CFRP, Titanium, Stainless Steel
- Skin thickness: 0.0015 m to 0.0023 m
- Stringer number: 0 to 65
- Stringer element lengths: 0.015 m to 0.05 m
- Stringer thickness: 0.002 m to 0.006 m
- Stringer Type: hat, Z, I

It optimizes for structural mass (weight of 0.6), cost (weight of 0.3) and manufacturability (weight of 0.1), all whilst ensuring that all requirements are met. The structural mass was weighted most highly due to the criticality of this parameter within the entire design and its respective budget. As for cost, despite being an important consideration, it is secondary to structural integrity and performance. For manufacturability, although it is important to reduce its complexity, aerospace structures are

often custom-built and can accommodate complex manufacturing if the resulting configuration offers significant performance or mass advantages.

Table 6.34: Structures Tool Breakdown

Document Name	Model Description	Input	Output
Structure2_optimal_-current2.py	Calculates optimal structural configuration by iterating through skin panel/stringer material, skin thickness, and stringer layout on panels.	Spacecraft wet mass, spacecraft dimensions, launch loads and frequencies; stringer properties from test_johnson.py	Optimal structural mass, skin panel/stringer material, skin thickness, stringer layout
test_johnson.py	Calculates optimal stringer properties (thicknesses, lengths, shape/type, number) to avoid Euler buckling.	Spacecraft dimensions, launch load	Stringer geometry: element sizes and types
magnetic_calculation.py, whipple_shield.py, radiation_calcs.py	Compute mass and dimensions for shielding against magnetic fields, MMOD, and radiation.	Component dimensions, material properties	Shielding mass, dimensions

Design Results and Sensitivity Analysis

The results of the most optimal configuration in terms of mass (weight of 0.6), cost (weight of 0.3) and manufacturability (weight of 0.1) is summarised at Table 6.35.

Table 6.35: Resulting Structural Configuration Breakdown

Category	Value
Skin and Stiffener Material	Aluminium 7075-T6
Panel Skin Thickness	0.0015 m
Total Number of Stringers	8
Stringer Placement	2 stringers, equidistant, on each of -Z, +Z, -Y, +Y panels (see Figure 7.6)
Stringer Type	Z
Stringer Cross-section Element Lengths	0.05 m each
Stringer Cross-section Element Thicknesses	0.003 m each
Structural Mass (prior to iteration with propulsion mass)	138.5 kg +/- 10 %
Structural Mass (following iteration code with propulsion mass)	140 kg +/- 15%
Structural cuboid volume	3 m (height) x 1.2 (width) x 1.7 (length) (see Section 7.3)

The winning semi-monocoque, thin-walled, cuboid configuration measures 3 m in height, 1.2 m in width and 1.7 m in length (see Section 7.3). Note that care was taken to limit the spacecraft height due to the criticality of the Euler buckling mode, as identified in the "Global Buckling of Stringers" section. Overall, this configuration strikes an excellent balance between strength, mass, manufacturability and cost. Aluminium 7075-T6 outperformed CFRP, Titanium, and Stainless Steel due to its optimal balance of high strength-to-weight ratio, low cost, and excellent manufacturability. These are also the same reasons for which the Z stringer type outperformed the I and hat stringer types.

The stringer dimensions and number are driven by the Euler buckling case under the launcher g-load. In fact, since Euler buckling is limiting (rather than local compressive buckling of the stiffened panel), a skin panel thickness of 1.5 mm is sufficient. This is the minimum manufacturable thickness for aerospace applications [17]. Redundancy is considered in that the stringer dimensions are sized with a knockdown factor of 0.75: for example, as seen in Figure 6.22b, a 0.0022 m stringer thickness would be sufficient to bear the launch load - but the chosen 0.003 m thickness allows redundancy.

This all amounts to a cuboid structural mass of 138.5 kg prior to iteration with the propulsive wet mass (see Table 6.1). The uncertainty of +/- 10% in this value is explained the "Sensitivity Analysis" section below. After iteration with the propulsive wet mass, the structural mass amounts to 140 kg,

[17] https://kdmfab.com/zh/aluminum-sheet-thickness/

for which the uncertainty is +/- 15% considering the cumulative uncertainty in the structural and propulsive masses independently (see Section 6.1).

Sensitivity Analysis The sensitivity analysis results for the structural tool agree with structures theory. They are summarised below.

- Structural mass showed low sensitivity to spacecraft wet mass, changing by only ±0.8-1.2% for a ±5% variation. This is reasonable since the wet mass increase does not have a one-to-one relationship with the structural mass by virtue of their governing equations. In fact, since in the present case, Euler buckling (as opposed to local buckling) is the limiting failure mode, the one-to-one relationship is even less marked. Since Euler buckling is limiting, thicker stringers must be employed to handle the heavier g-load from the heavier spacecraft mass. Hence, only the stringers are modified and not the panel underneath, of which the modification would instead occur in the case of limiting local buckling. Since the stringers constitute only a small fraction of the total structural mass, increasing their size does not lead to a marked one-to-one increase in structural mass with spacecraft mass. Thus, the lack of direct proportionality is reasonable.
- Variations in width/length had a moderate impact (± 1-2% mass change for ± 5%), while height had a strong influence (-5.67% , - +6.68%). As the overall cross-sectional dimensions increase, more material is required, increasing the structural mass. (The increased cross-sectional area from the increased dimensions would actually offer an additional advantage for local buckling, leading to a smaller panel thickness and less mass. However, this latter consideration is not relevant in the current case, since local buckling is not limiting and the panel thickness is already at its minimum manufacturable thickness.) This effect is less marked than that of increasing the height because Euler buckling is limiting as opposed to compressive buckling.

Overall, accounting for the most limiting case in which the spacecraft dimensions and mass all simultaneously increase by 5%, an increase in the structural mass of 10% is observed.

Sustainability Considerations In order to comply with the ESA Green Agenda, a number of sustainable choices are implemented into the structural design itself as well as into its related manufacturing, assembly and integration process (also see Section 7.6). These are listed as below.

- The tool's optimisation for minimal mass, such as through the prioritisation of high strength-to-weight materials, low stringer thicknesses, low stringer number, etc., inherently contributes to a more conscious and minimal consumption of materials. This additionally translates to lower required launch energy, and material minining, processing, and transport, which would otherwise have adverse effects on the environment.
- Recycled titanium is used for the bolts connecting secondary structures. Recycled titanium maintains the same excellent mechanical properties, durability, and lightweightedness as its virgin counterpart, whilst requiring 95% less energy for manufacturing [18]. Similarly, the PEEK and HDPE employed for radiation shielding can be obtained from recycled sources, with the latter being extremely readily available and particularly low energy in production [102].
- CNC nesting software and Friction stir welding are employed for the nesting (pre-processing) and joining of the aluminium panels respectively. The former process ensures minimal error and thus minimal material waste; the latter ensures less energy consumption, no fumes or filler materials, as compared to alternative processes such as fusion welding [103].
- The contractors selected for the stringer and internal mounts are carrying out additive manufacturing of the parts to ensure topology optimisation and less material waste.
- The modular assembly of the secondary structures (internal mounts), through their bolted joints, allows for easy disassembly if required, repair, inspection and non-destructive testing. These

[18] https://www.aeroproind.com/post/stages-of-recycling-titanium-explained

all contribute to less waste production. In fact, non-destructive testing is carried out wherever possible to avoid part waste.

- Anodising is the preferred surface treatment over plating, painting, etc. due to its non-toxic nature and durability. [104]

Subsystem Requirements

Below are the resulting subsystem requirements for Structures.

Updated ID	Old ID	Description	Verification
SUB-STRUC-1		All structural panels shall be manufactured out of Aluminium 7075-T6 with density of 2800 kg/m^3.	Inspection
SUB-STRUC-2.1		The +ve X and -ve X skin panels shall have dimensions of 1.7 m x 1.2 m.	Inspection
SUB-STRUC-2.2		The +ve Y and -ve Y panels shall have dimensions of 3 m x 1.2 m.	Inspection
SUB-STRUC-2.3		The +ve Z and -ve Z panels shall have dimensions of 3 m x 1.7 m.	Inspection
SUB-STRUC-2.4		All structural panels shall have a skin thickness of 1.5 mm	Inspection
SUB-STRUC-3		The aluminium structural box shall be fabricated using CNC nesting software and friction stir welding along designated joints.	Inspection
SUB-STRUC-4		All stringers shall be manufactured out of Aluminium 7075-T6 with density of 2800 kg/m^3.	Inspection
SUB-STRUC-5.1		All stringers shall be Z stringers.	Inspection
SUB-STRUC-5.2		All 3 of the element lengths comprising each Z stringer cross-section shall be 5 cm x 0.23 cm in dimension.	Inspection
SUB-STRUC-6		All stringers shall be manufactured through additive manufacturing.	Inspection
SUB-STRUC-7		2 stringers shall be bolted onto each of the +ve Y, -ve Y, +ve Z, -ve Z spacecraft panels.	Inspection
SUB-STRUC-8		The 2 stringers shall be mounted onto each of the panels such that each of the stringers is equidistant from its nearest panel edge and from the other adjacent stringer.	Inspection
SUB-STRUC-9		Bolts out of recycled titanium Ti-AI6-V4 shall be used to fasten internal secondary structural components.	Inspection
SUB-STRUC-10		The structure shall incorporate 1 cm thick HDPE (High-Density Polyethylene) surface radiation shielding for the LRP and OBE payload components.	Inspection
SUB-STRUC-11		The structure shall incorporate 7mm thick METGLAS® 2605S3A Alloy magnetic shielding for the HETs.	Inspection
SUB-STRUC-12		A PEEK platform with a thickness of 1 cm shall prevent CAI vibrations below 100 Hz from triggering resonant frequency within the spacecraft structure.	Analysis or Test
SUB-STRUC-13.1		The structure shall include an external aluminium bumper wall with thickness of 0.3 mm for micrometeoroid and debris protection.	Inspection
SUB-STRUC-13.2		The external bumper wall shall be mounted at a standoff distance of 10 cm from the structural panel.	Inspection
SUB-STRUC-13.3		All external aluminium panels shall be anodised to a minimum coating thickness of 25 μm unless mission-specific requirements dictate an alternative treatment.	Inspection

7 Design Overview

7.1. Spacecraft System Characteristics

Table 7.1: Mission and Subsystem Parameters

Type of parameter	Parameter	Value
Mission parameters	General Payload Arrangement	LRI-CAI
	Launcher	Ariane 62
	Planned Total Mission Lifetime	3.16 years
	Science Operation Duration	1 Martian year
	Decommissioning	Deorbiting and functioning as relay satellite
System parameters	Dry Mass (with margin)	691.7 kg
	Launch Mass (with margin)	1124.2 kg
	Nominal Power	842 W
	Cost (with margin)	717.7 M euros
Astrodynamics	Solar Incidence Angle	±27°
	Orbit Insertion Method	Mid-course inclination and aerobraking
	Orbit Type	Polar dawn-dusk SSO
	Total DeltaV	1.56 km/s
	Period	109.39 minutes
	Science Orbit Inclination	92.44 deg
	Science Orbit Altitude	212.48 km
	Orbit Repeat Interval	30 sols
ADCS	Course Pointing Accuracy	17.5 mrad
	Fine Pointing Accuracy	0.078 mrad
	Propellant Type and Mass	Nitrogen, 10kg
	Slew Rate	0.11-0.3 (depending on axis)
TT&C	Ground Station Location(s)	Madrid, Canberra, Goldstone
	HGA Downlink Frequency	32 GHz
	HGA Uplink Frequency	34 GHz
	LGA Downlink Frequency	8.42 GHz
	LGA Uplink Frequency	7.2 GHz
	Telemetry Data Rate	31.25 kbit/s
	Science Data Rate	411 kbit/s
	Command Data Rate	3500 kbit/s
	Inter satellite Data Rate	20 kbit/s
	Downlink Science Link Margin	3.74 dB
	High-Gain Antenna Pointing Accuracy	0.15 deg
	Visiting Frequency	Once p.d.
	Coverage	9.5 hours p.d.
CDHS	Memory size (40% margin)	46 GBytes
Propulsion	Capture Type of Propulsion	Bipropellant
	Capture Propellant Type and Mass	MMH/MON-3 , 416.95 kg
	Capture Thrust Level	750 N
	Station-keeping Type of Propulsion	Electric
	Station-keeping Propellant Type and Mass	Xenon, 14.35 kg
	Station-keeping Thrust Level	50-170 mN
Structures	Spacecraft Dimensions	3 m (height) x 1.7 m (width) x 1.2 m (length)

Type of parameter	Parameter	Progress
	Structural Mass	140 kg
	Material	Aluminium 7075-T6
	Stringer configuration	2 stringers on each of the following panels: -ve Z, +ve Z, -ve Y, +ve Y panels; 8 stringers in total
Thermal control	Radiator Material	127 μm silver-lined Teflon
	MLI	15 Kapton layers
	MLI Area	18.8 m^2
	Radiator Area	2.67 m^2
	Temperature Range	12.8 ± 0.1°C
	Number of heaters	50
Power	Solar Array Area	8.14 m^2
	Battery Capacity	67 Ah
Payload	Mass	143.5
	Power	234
	Dimensions	See Table 4.4
	Temporal Field Error	10^(-19)
	Static Field Resolution	380 d/o

7.2. Budgets

Throughout the design process, the budgets have been constantly changing. However, the budgets have been a key driver during the design process and it has been a goal to reduce them throughout. In the following subsection, the different budgets will be discussed, with an explanation both of how they were derived, and of big changes in the budgets. Ideally all budgets would have been plotted with an uncertainty that was found during the design, but unfortunately this was not deemed feasible in the time frame of the present design. Thus, to still give a certain confidence interval, statistical confidence intervals from literature based on design maturity is used instead[105].

Mass Budget

The evolution of the mass budget can be seen in Figure 7.1a. For the baseline, the mass budget was entirely based on statistical relationships, but all subsequent mass estimates are based on subsystem mass estimates. From the final report and onwards these subsystem mass estimates are based on actual component masses. The mass budgets have not changed much throughout the design. The biggest change occurred from the last midterm iteration to the first final iteration. The reason for this was that the configuration of the spacecraft changed quite substantially between these two.

Beyond the mass evolution seen in Figure 7.1a, the mass can be broken down into the various subsystems as seen in Figure 7.1b as a pie chart and in Table 7.2.

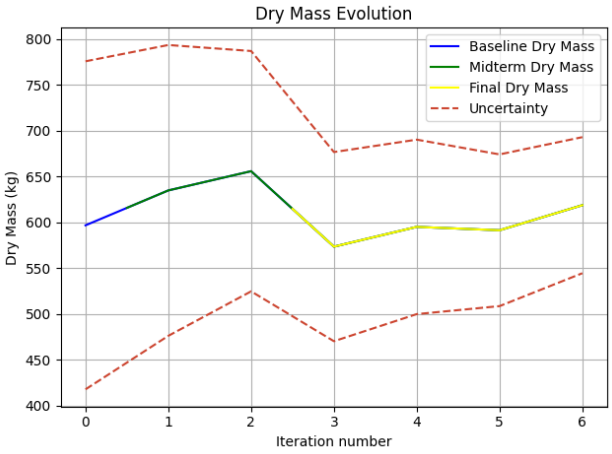

(a) Evolution of dry mass throughout the design process

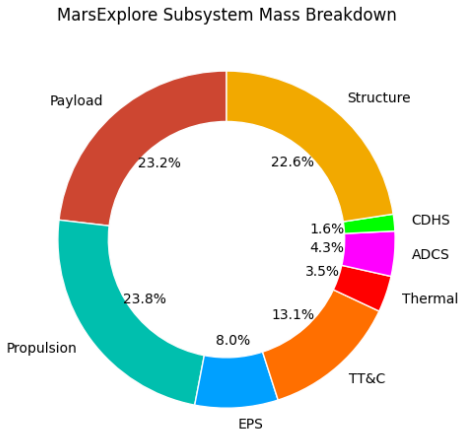

(b) Mass breakdown of each spacecraft

Figure 7.1: Dry mass analysis during the MarsExplore project: (a) Mass evolution over design iterations and (b) Subsystem breakdown of final design

Table 7.2: Subsystem Mass Breakdown

Subsystem	Mass (kg)	Percentage (%)
Payload	143.5	27.2%
Propulsion	147.7	28.0%
EPS	49.35	9.3%
TT&C	81.0	15.3%
Thermal	21.6	4.1%
ADCS	26.7	5.1%
CDHS	10.0	1.9%
Structure	140.0	26.5%
Total	**619.85**	**100.0%**

Power Budget

The evolution of the power budget can be seen in Figure 7.2. As was the case for the mass budget, the first iteration was entirely based on parametric models. Further iterations after this were based on subsystem level estimates and from the final and onwards, the power estimate was based on component power consumption. The component level power distribution, as well as the power consumption in different mission phases, can be found in Section 6.6.

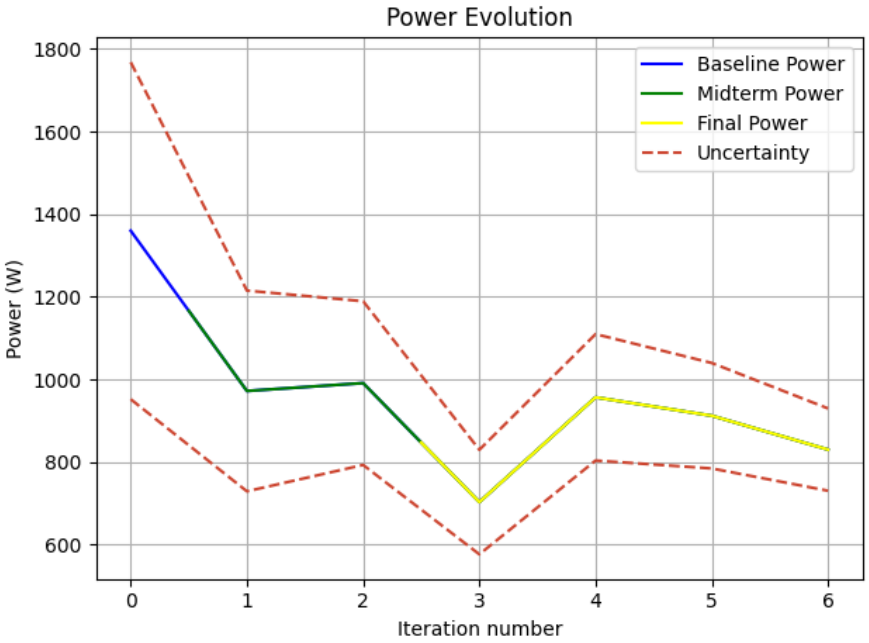

Figure 7.2: Evolution of power mass throughout the design process

Cost Budget

The last budget to consider is the cost budget. This is one of the most important budgets as it is a big factor in whether the mission is accepted or not. The evolution of the cost budget can be seen in Figure 7.3a.

The baseline cost budget was entirely parametric, based on previous mars missions. It was also for just one spacecraft and did not take into account launch or operations. This has since been added to make the baseline budget comparable to the ones from later iterations.

Following this, in the midterm, the estimation method was improved. Here the percentage wise contribution of the payload was removed and replaced by a cost estimate for the payload that was derived from the cost of similar components. The cold atom interferometer was estimated to cost 60 M€ [48] and the laser ranging instrument was estimated to cost 25 M€ [49]. In addition to the more accurate payload cost being added, margins were applied to each subsystem based on TRL as described in *Space Mission Analysis and Design*[59]. All subsystems except for the payload was given a 5 % TRL margin, whereas the payload was given a 20% TRL margin. A learning curve of 80 % is then applied to find the cost of the second unit. Lastly, to arrive at a full cost at completion (CaC), the launch cost of 107.2 M€ [106] as well as the operational cost of 88.5 M€ as described in Section 5.5. Lastly a system level margin of 7.5 % was applied. This is quite a low system margin, however this is made up for by the fact that the payload cost is likely overestimated. It is based on the cost of the cold atom laboratory that was sent to the international space station. Beyond the fact that the technology has matured and thus become cheaper since then, the cold atom laboratory is far more complex and has more functionalities than the cold atom interferometer needed for this mission. Additionally, by using the system margin of 7.5%, the effective margin makes up 12.8% as can be seen in Figure 7.3b. This is slightly higher than the 12% prescribed by ESA in [106].

Next, in the final, the method did not change significantly. The only change in method that occurred happened in iteration 5 where an outlier in the dataset used to arrive at a parametric relationship was removed. This resulted in a reduction in cost.

Following the cost evolution as seen in Figure 7.3a, a breakdown of the cost into the various activities of the mission lifetime has been made. This can be seen in Figure 7.3b. Further a table of how the cost

of the first unit breaks down into the various subsystem can be seen in Table 7.3. It should be noted that the subsystem costs as described here include both development and design, and the production of that subsystem.

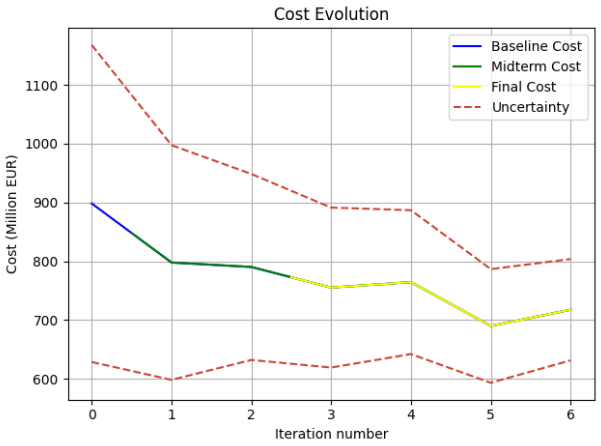

(a) Evolution of cost at completion throughout the design

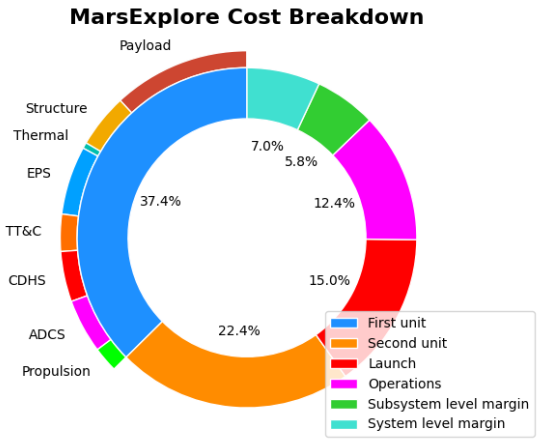

(b) Cost breakdown into all mission activities

Figure 7.3: Cost analysis of the Mars Explore mission

Table 7.3: Subsystem Cost Breakdown

Subsystem	Cost (M€)	Percentage (%)
Payload	102.00	33.3%
Structure	37.29	12.2%
Thermal	4.08	1.3%
EPS	47.48	15.5%
TT&C	25.67	8.4%
C&DH	34.84	11.4%
ADCS	37.49	12.2%
Propulsion	17.52	5.7%
Total	**306.37**	**100.0%**

In addition to the breakdown of the cost into various activities, it can also be broken down into annual cost. This has been done according to *Space Mission Analysis and Design*[59]. In Figure 7.4, the annual cost per year of the mission throughout it's lifetime can be seen. Additionally, the cost of potentially extending the mission has been added in blue. In Figure 7.5, the cumulative cost over the mission lifetime is displayed. Here the additional cost of extending the mission duration has also been added.

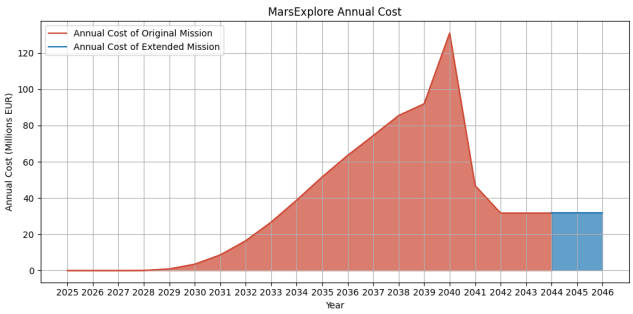

Figure 7.4: Annual cost per year over the project lifetime

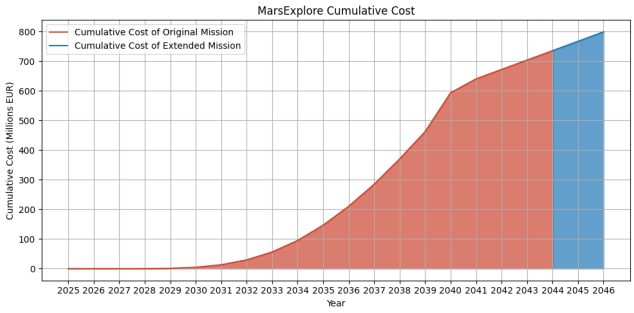

Figure 7.5: Cumulative cost per year over the project lifetime

It should be noted that the current CaC is over the requirement, in fact it exceeds it by 46 M€. As such additional funding will likely be required to pay for operations. It is not unlikely that government agencies like NLR and DLR would be interested in partnering with ESA on this mission. DLR in particular is already involved in cold atom research aboard the ISS and are likely to want to continue their research into this [1].

7.3. Internal and External Configuration

The internal configuration is sketched in Figure 7.6. The symmetrical placement of subsystems and tanks about the CAI ensures a constant alignment of the spacecraft CoM with the CAI location. The drawback of this tank placement, as seen in the sketch, is that the tanks are the dimension-constraining component in all directions. This however has the following benefit: the resulting empty volume naturally encompasses a margin for integration elements such as feed lines, other internal mountings, etc. that are hard to quantify at this stage.

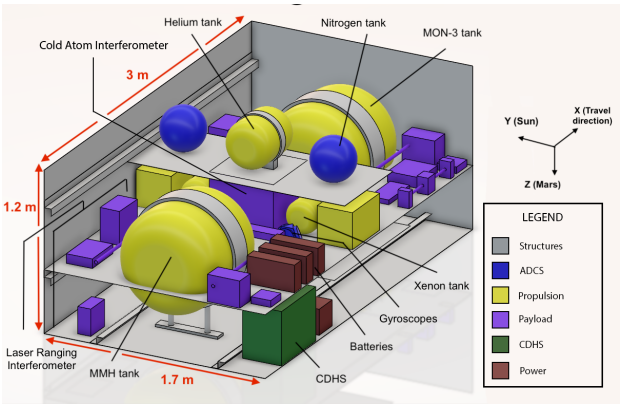

(a) Internal configuration viewed isometrically

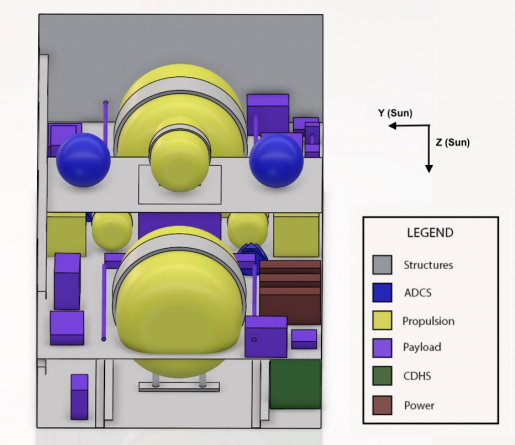

(b) Internal configuration viewed in the flight direction

Figure 7.6: Comparison of internal configurations from two viewpoints

As seen in Figure 7.7b, the spacecraft are fitted in a planar side-by-side configuration within the top compartment of the "Ariane 62 Short Dual Launch Structure" payload fairing. A shared payload adapter plate -such as the Multi-Satellite Adapter Plate (MSAP) RUAG 937/1194- houses both spacecraft using independent clampband adapters and supports their dedicated low-shock separation systems [94]. This setup allows easy mechanical integration, mass balance, and separate deployment of each

[1] "Bose Einstein Condensate and Cold Atom Laboratory," *drl.de*, accessed May 21, 2025. `https://www.dlr.de/en/qt/research-transfer/projects-missions/beccal`

spacecraft. The solar arrays, antenna boom and ADCS flap are folded flush to the spacecraft. An overview of the deployed external configuration is shown in Figure 7.7a.

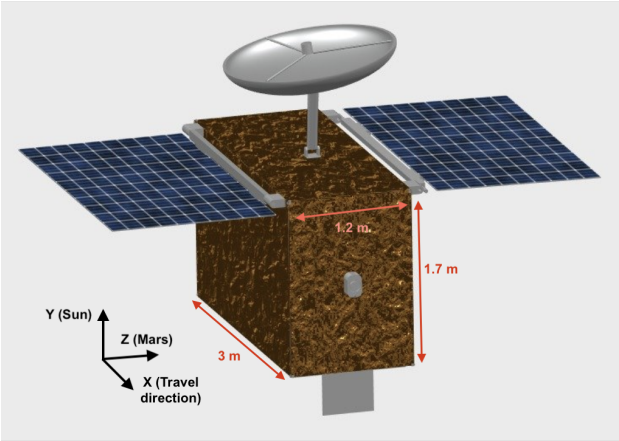

(a) External configuration viewed isometrically

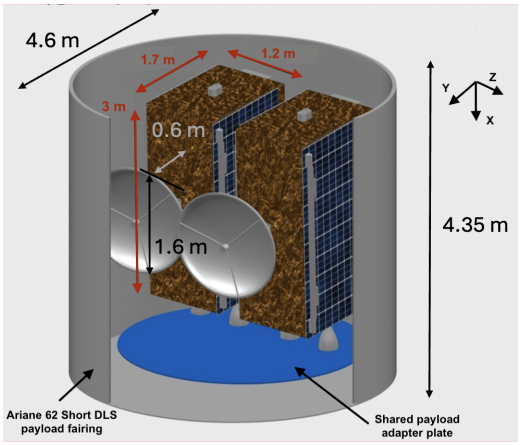

(b) External configuration viewed in the Ariane 62 launcher, undeployed

Figure 7.7: Comparison of external configurations, deployed and undeployed in launcher

7.4. Aerodynamics

As previously explained in Section 5.3, the drag coefficient used is $C_D = 2.705$. This results from the interaction between incident Martian atmospheric molecules (CO_2 primarily) and the spacecrafts MLI outer surface (out of Kapton). The methodology for this computation adheres to that of Cook [107] for drag coefficient determination in free-molecule flow.

This methodology starts with the computation of how much of the incoming Martian CO_2 molecules have collided with the Kapton surface. This is done by calculating a mass ratio, also referred to as μ, with the equation below:

$$\mu = \frac{m_{i,CO_2}}{m_{s,Kapton}} = \frac{44.01 \text{ amu}}{398.41 \text{ amu}} \approx 0.11046 \tag{7.1}$$

Next, it is determined how much energy and momentum the incident molecules transfer to the surface molecules. This is described by the accommodation coefficient, α. This is calculated with two theories: Baule's theory, which assumes average particle collisions, and another accounting for head-on collision energy transfers. These two theories lead to two different accommodation coefficients as shown in Equation 7.2 and Equation 7.3.

$$\alpha_{\textbf{head-on}} = \frac{4\mu}{(1+\mu)^2} = 0.96 \tag{7.2}$$

$$\alpha_{\textbf{Baule's}} = \frac{2\mu}{(1+\mu)^2} = 0.48 \tag{7.3}$$

Because μ is quite small, it is suggested that the accommodation factor is taken as an average of the previously computed factors, leading to $\alpha = 0.72$. This value is relatively small as well, which means that the incident molecules do not stick frequently with Kapton surface, and thus still preserve high kinetic energy and momentum.

Once the accommodation coefficient is determined, it can be used to compute the ratio of the speed of the re-emitted molecule to the speed of the incident molecule, denoted as r. Conceptually, this value indicates how much deflection of a molecule is retained after it strikes the surface. It is determined as follows:

$$r = \sqrt{1 - \alpha} = 0.53 \tag{7.4}$$

Finally, this is the key parameter that allows us to determine the drag coefficient, which in turn arises from the net change in momentum of the incident particles as they interact with the spacecraft. This momentum change has two components: the momentum of the incoming carbon dioxide molecules (incident momentum), and the momentum of the molecules that leave the surface (re-emitted momentum).

The C_D accounts for both thanks to the use of the r factor. This is shown in Equation 7.5.

$$C_D = 2 \cdot (1 + \frac{2}{3} r) \tag{7.5}$$

Overall, this results in the above-mentioned value of $C_D = 2.705$.

7.5. Hardware and Software Diagrams

The hardware block diagram is included in Figure 7.8. This details the subsystems of the spacecraft, and their division into instruments and components. Moreover, the relationship between said elements is depicted, and several connections are shown, including the flow of commands, telemetry, power and standard connections. The flow of the laser throughout the LRI payload instrument is also depicted for illustrative purposes. All the hardware is encompassed by the structures subsystem, which integrates the spacecraft.

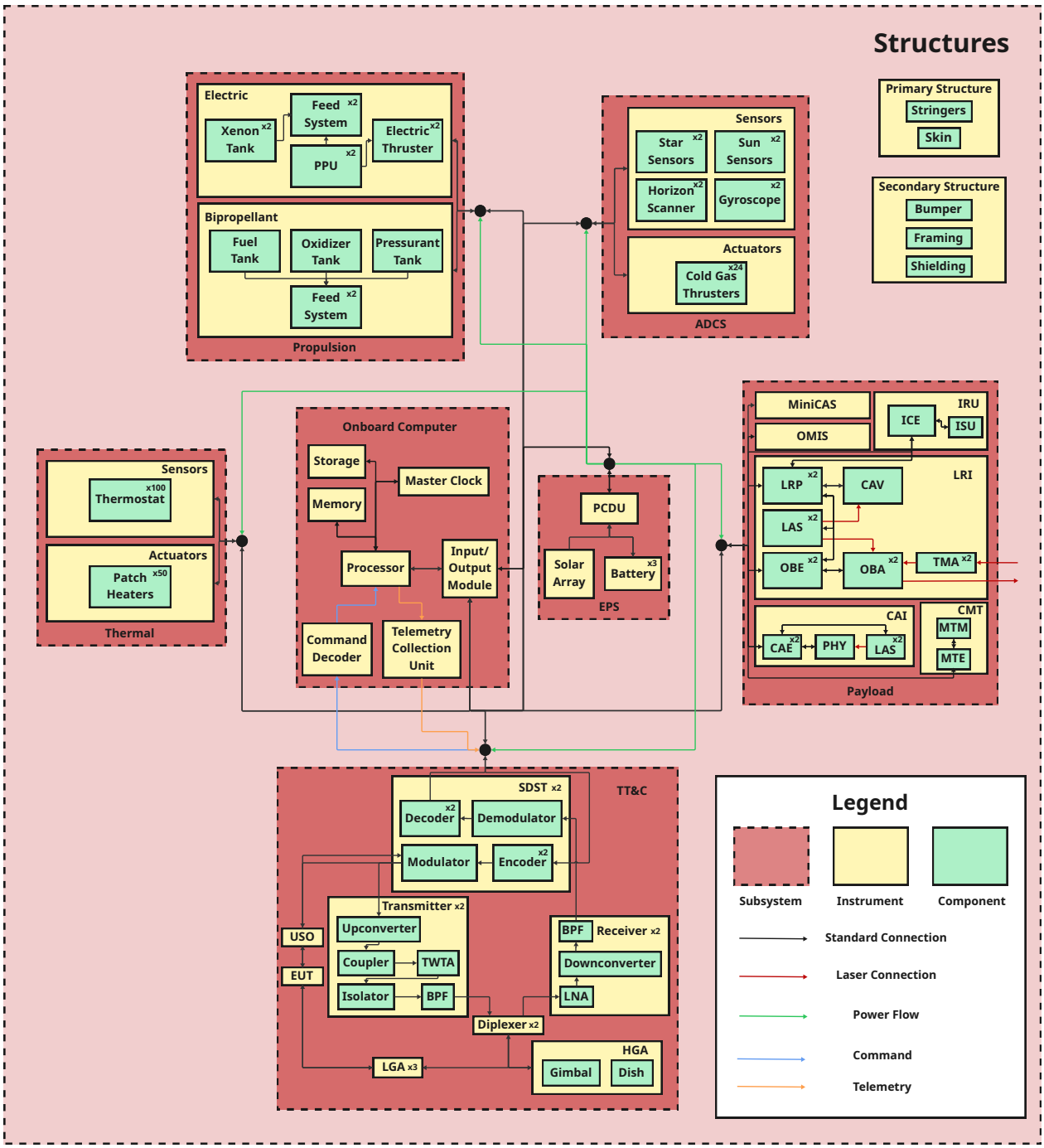

Figure 7.8: Hardware Block Diagram for MarsExplore

The software block diagram is included in Figure 7.9. This details the logic of the spacecraft, how the subsystems interact with each other, and how the spacecraft uses logic to switch between its different modes. Moreover, the power lines and connections to the onboard computer are shown.

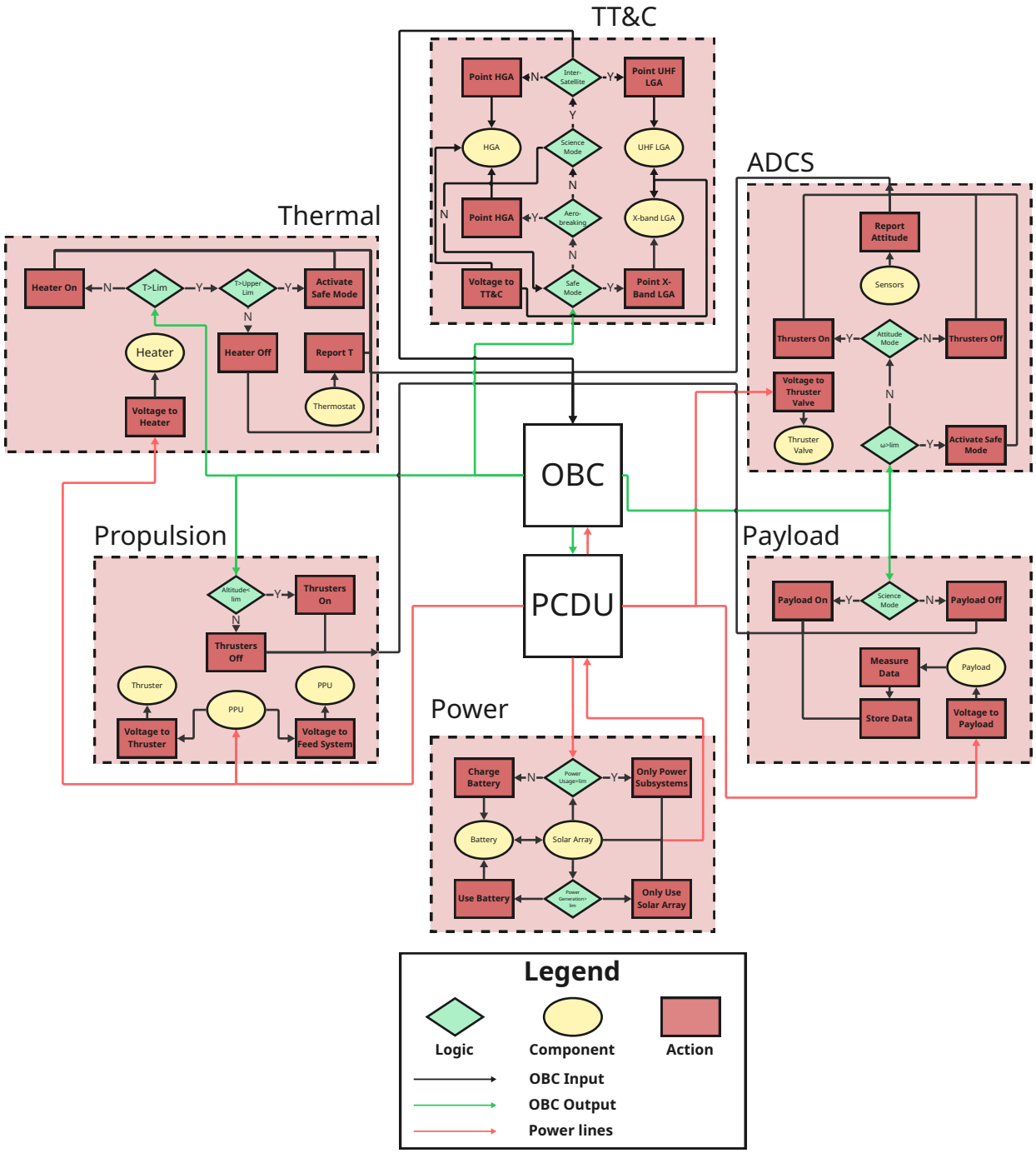

Figure 7.9: Software Block Diagram for MarsExplore

7.6. Manufacturing, Assembly & Integration Plan

The manufacturing, assembly and integration plan is portrayed in Figure 7.10. This details the steps to be taken in the production of the spacecraft, including the testing of components, subsystems and the system. A timeline, in compliance with the Mission Gantt Chart of Figure 5.4, is included for reference. To better understand the references to specific subsystem components and structural panels, see Figure 7.6.

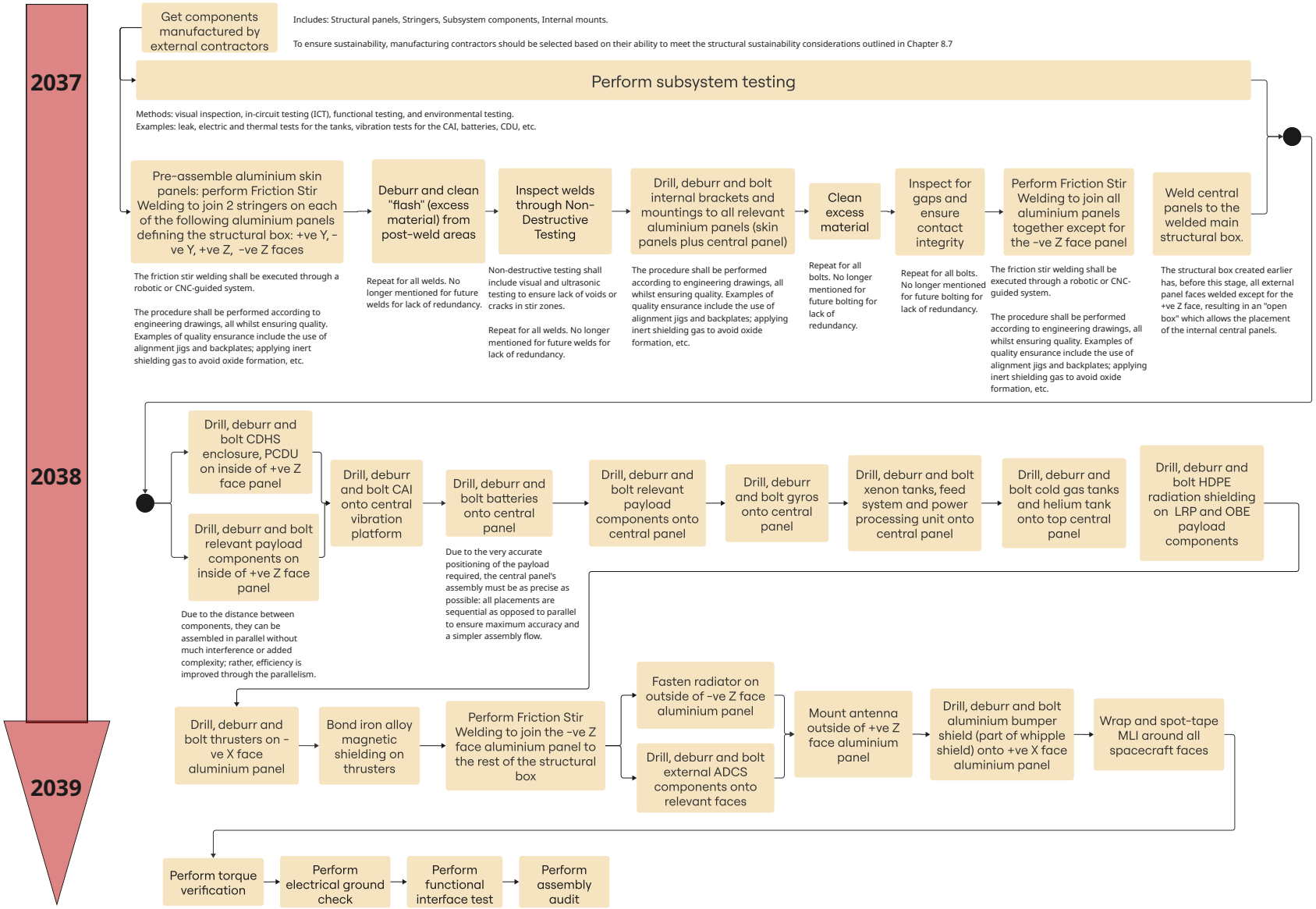

Figure 7.10: Manufacturing, Assembly & Integration Plan for MarsExplore

7.7. Performance Analysis

MarsExplore's performance is evaluated based on how effectively the mission meets its defined requirements.The primary objective of the mission is to answer the science questions, stated in Chapter 2. Evaluating the mission's science return helps determinate not only which questions can be answered but also the degree of resolution with which they can be addressed.

The performance estimation methodology is based on the estimated measurement error equations detailed in Section 2.1, where it is shown that the optical link error is the most critical parameter influencing science outcomes. An optical link error of 10^{-12} $\mathrm{m}/s^2/\sqrt{(Hz)}$ is considered the most realistic value achievable for the LRI+CAI measurements. With this precision, the mission can achieve a gravity field resolution of about 28 km (380 d/o) and a minimum RMS value close to 10^{-19} m^2/s^2 over the mission duration of one Martian year. These values can be observed in Figure 7.11, where the spatial resolution in km can be found from the intersection of the green line with the power signal law (in d/o, n) though: $\frac{\pi \cdot R_{Mars}}{n}$. The temporal resolution describes the ability to detect changes over time in the gravity anomalies detected in the static measurements, and it is 360 d/o, significantly better than 30 d/o required in **MIS-SCI-1.3**. This can be observed in the 30 Sols measurements, as the orbits will be repeated every 30 sols. The predicted accuracies and errors also satisfy the core science requirements **MIS-SCI-1.1** and **MIS-SCI-1.2**.

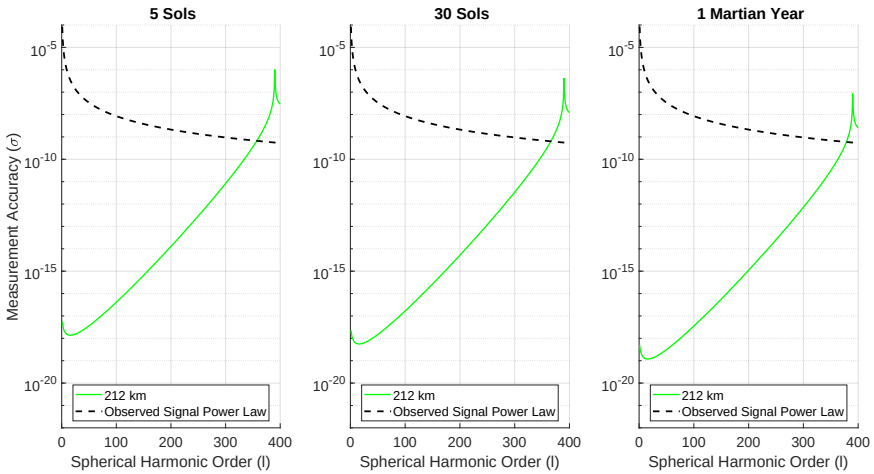

Figure 7.11: Sensitivity MarsExplore Measurements Over Different Periods of Time

These resolutions are around three times better than the current gravity field maps and allows for the detection of deep aquifers, most sQCD, and volatile-rich sediments, with valuable spatial resolution. Furthermore, the high precision at low degrees (particularly degree 2) opens up possibilities to investigate the seasonal cycles of CO_2 and H_2O, which are key to understanding Mars' climate system. However, the current resolution in the temporal measurements, does not meet the sensitivity threshold needed to detect mantle deformation. A precision of 3.734 μGal/yr is achieved, while 0.018 μGal/yr is necessary.

To complement the gravity measurements and improve scientific coverage, four OMIS accelerometers, as described in Chapter 4, have been added to the spacecraft, satisfying requirement **MIS-SCI-1.8**. This allows for measurements of Mars' atmosphere and winds.

The current performance allows the mission to address all the science questions, with some such as **SQ5** (mantle deformation) and **SQ6** (global H_2O cycles) only partially addressed. To enhance the quality of temporal gravity measurements, a lower optical noise level of 10^{-14} $\mathrm{m}/s^2/\sqrt{(Hz)}$ could be pursued. This could be a reasonable value, but it must be requested and confirmed with the payload

providers. It would likely have a significant impact on the mission's cost budget and could also affect the schedule.

With regards to the payload requirements, almost all payload requirements are met to the extent specified. Firstly, individual patch heaters are added to payload instruments requiring strict thermal control, meeting requirements **SYS-PAY-4.1** - **SYS-PAY-4.6**. The ADCS is designed to meet and surpass the pointing requirements indicated in **SYS-PAY-4.7** - **SYS-PAY-4.9**, and similarly with the TT&C and power subsystem, the subsystems are designed to meet their requirements **SYS-PAY-4.17** and **SYS-PAY-4.15**. The structures subsystem incorporates magnetic shielding to meet **SYS-PAY-4.16**.

Moreover, the propulsion subsystem considers non-continuous electric propulsion in compliance with **SYS-PAY-1.14**. The CAI is positioned in an along-track configuration as specified in **SYS-PAY-4.10**.

The performance is slightly undermined by the CoM requirements. Firstly, not all tanks are placed symmetrically, as the fuel and oxidizer tanks are prohibitive in size. Thus, the fuel and oxidizer tanks are placed on opposite sides of the CoM, and the CAI and bipropellant tanks shall be positioned such that the CoM coincides with it after all fuel and oxidizer is consumed, which could potentially compromise the CoM requirements. During science operations, it should be possible to meet **SYS-PAY-4.13**, as all other tanks are placed symmetrically. Finally, it is determined that the antenna dish movement would surpass the trim range of the CMT of GRACE-FO. Hence, **SYS-PAY-4.11** states that this trim range must be improved for MarsExplore's CMT.

Section 7.1 presents the spacecraft characteristics. Considering the mass, power, and cost requirements, namely **SYS-LNCH-5.1**, **SYS-UR-1.1**, and **MIS-ESA-2.1**, all are met. The power and mass requirements are well performed, while the cost is exceeded when a margin is applied. This is still accountable for the current knowledge of the detail of the design. Each single component shall be selected and cost discussed with the provider in order to reliably estimate the cost.

7.8. Design Sustainability

To quantify an estimate of the carbon footprint of the design and make conscious design choices through different iterations, the component material emissions were calculated for the bigger components. The launcher emissions have not been considered throughout the design phase since they are separate and independent from the design.

The major contributors to carbon emissions identified are the CO_2-equivalent contribution of:

- the batteries used;
- the solar arrays used;
- the propellants used, namely Xenon for electric propulsion, MMO-3 for bipropellant propulsion, Nitrogen for ADCS manoeuvres;
- the materials used for the structure of the spacecraft and the antenna, namely Aluminium, Titanium, High Density Polyethylene (HDPE), Cobalt, and Polyether Ether Ketone (PEEK);
- the thermal insulator material, MLI;

The quantitative value for the CO_2-equivalent contributions is computed, using the following equation:

$$m_{CO_2\,\text{eq.}} = m \cdot CO_2\ \text{eq.} \tag{7.6}$$

The values presented in Table 7.4 have been used to compute the CO_2 equivalent mass per kg / m^2 of parameter, obtained from life cycle assessment literature [2].

[2] https://www.ecocostsvalue.com/data-tools-books/

Table 7.4: CO_2 equivalent emissions of selected spacecraft materials

Material	CO_2-eq (kg/unit)	Material	CO_2-eq (kg/unit)
Li-ion battery (kg)	79.4	PV arrays (m^2)	412.9
Xenon (kg)	28.92	MMO-3 (kg)	70
Helium (kg)	0.712	Aluminum (kg)	7.254
Titanium (kg)	37.44	HDPE (kg)	3.258
PEEK (kg)	175.982	Nitrogen (kg)	0.299
PTFE / Teflon (kg)	9.6	MLI (kg)	10
Cobalt (kg)	7.72	–	–

The total CO_2-equivalent impact calculated for the final MarsExplore design amounts to about 35 tonnes for the final design. To put this into perspective, this is roughly equivalent to the annual carbon emissions of 23 average European cars, each driving for one year. Evidently, the calculated emission of a single spacecraft is very small compared to those from the launcher or the overall mission. This discrepancy is likely due to the limited level of detail considered in estimating the spacecraft's carbon footprint.

The carbon footprint emissions value has been fluctuating throughout the different mission design iterations and has been particularly influenced by key design decisions. In particular, the selection of a hybrid propulsion system instead of a purely bi-propellant system, significantly contributed to emission reductions, sice Xenon propulsion produced approximately 60% fewer carbon emissions compared to MMO-3. Additionally, the overall environmental impact was lowered due to the reduction in the power system mass and solar array size as described in Section 6.6, which follows from the selection of a Sun-synchronous orbit. This orbit provides consistent solar illumination, allowing for more efficient energy harvesting and reducing the need for oversized power components.

7.9. System Risk

The risk of each subsystem was defined similarly to the payload risk Section 4.9. Again, the Development Difficulty Index is evaluated using SOT and DED to quantify the risk during the design and development. The scales used can be found in Table 4.5 and Table 4.6. Unlike the payload risk assessment, the consequence is defined as the effect of partial or complete failure of the subsystem during science operations, taking redundancy into account too. Consequence is assessed at mission level as shown in Table 4.7. The results are summarised in Table 7.5.

Table 7.5: SOT/DED Ratings, Resulting Development Difficulty Index and Mission Impact for Subsystems

Item	SOT	DED	Development Difficulty Index	Mission Impact
Payload	4	3	**0.22**	**0.90**
Propulsion	3	2	**0.11**	**0.70**
Power	1	1	**0.02**	**0.90**
Thermal Control	1	1	**0.02**	**0.70**
TT&C	1	2	**0.04**	**0.60**
CDHS	1	1	**0.02**	**0.70**
Structures	1	3	**0.50**	**0.6**
ADCS	1	1	**0.02**	**0.70**

The table presents a high-level risk assessment for each subsystem. Each subsystem has numerous distinct components, each with their own SOT and DED. Therefore, it is important to note that a relatively low overall subsystem score might conceal one or more critical components. For instance,

the propulsion system's overall score averages out the risk of the Hall-effect thruster with the high maturity of the bipropellant system. Nonetheless, these values remain valuable for identifying the primary risk drivers at a subsystem level. These numbers are visualised in Figure 7.12.

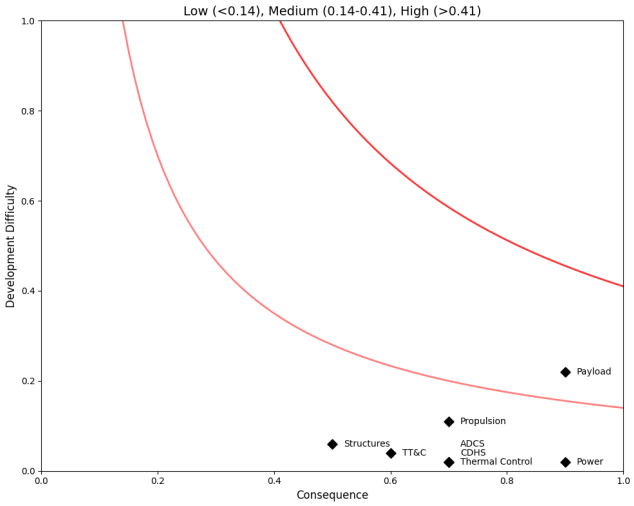

Figure 7.12: Risk Map of Subsystems

As depicted in the figure, the payload is at medium-level risk. However, the risk associated with the payload is balanced by the overall spacecraft design approach. The majority of other subsystems are cluttered in the low risk section, indicating low development difficulty. By minimizing complexity across the subsystems, the overall project risk is kept at an acceptable level, compensating for the inherent risk of the quantum payload instruments.

7.10. Reliability, Availability, Maintainability, and Safety Characteristics

Assuring quality is crucial in space engineering due to the particular difficulty or impossibility in doing so after launch. Reliability, Availability, Maintainability and Safety (RAMS) tools and methodologies should be used from the beginning of the design to end-of-life to support engineering budgets, cost estimates, safety and survivability considerations [108].

Reliability

Reliability of a spacecraft is defined as the probability with which it will successfully complete the specified mission performance for the required mission time. A reliable system minimises critical failures, reduces repair costs, and improves the stakeholders' satisfaction with a successful mission. Reliability is calculated using failure rates, therefore the accuracy of this measurement depends on the accuracy and realism of the knowledge of failure mechanisms and models [109].

An analysis of historical Mars orbiter missions showed that approximately 36% of these have failed. However, since 2001, all Mars orbiter missions have been successful. Most of the failures were attributed to launch vehicle issues and malfunctions in guidance and control systems [110]. The most instructive mission failure for MarsExplore is the aerobraking incident of MRO, which experienced a hardware failure in its telecommunication system [111]. In Section 5.9, aerobraking was identified as one of the major sources of risks, and this incident reiterates the importance of high reliability in aerobraking.

MarsExplore benefits from a robust redundancy strategy to ensure mission success and system reliability. Triple redundancy is implemented on all critical instruments and subsystems, namely CDHS and the batteries, and double redundancy is maintained for all normal subsystems. After 1 year, according to [59], the parts most likely to cause failure are either the TT&C subsystem or the

propulsion subsystem. For TT&C the high gain antenna is deployed close to Earth, in order to achieve real time commands. Moreover, two low gain antennas are included in the mission that can be used for emergency, as explained in Section 6.3. In addition, the low gain antennas have already been used in deep space missions. These factors increase the reliability of the system. The propulsion system has significant redundancy, both in its thrusters and its feed systems, as explained in Section 6.1. Other common causes of failure are the electrical system and attitude control. With regard to attitude control, several redundant components are used. Moreover, all components have a TRL of 9 with plenty of space heritage. Batteries include triple redundancy as they are identified as a critical subsystem.

With regards to the payload, redundancy is a key consideration, and it is integrated throughout the payload design. Firstly, a second LRI unit is present on each spacecraft. This allows the spacecraft to switch positions in case of LRI failure, as presented in Figure 4.1 and Figure 4.2. As a result, all LRI components are cold redundant, as two are found per spacecraft, with the exception of the optical cavity. Only one cavity needs to be included in the constellation, so by including one per spacecraft, this is already redundant. The same can be said about the iodine reference unit, of which one is included per spacecraft. The QPR of the OBA is also hot redundant per OBA unit.

Moving on to the CAI, the strict placement of the physics package on the spacecraft CoM limits the ability to include a redundant unit. However, its other components are all cold redundant, and the redundancy for accelerometers is improved with the addition of four OMIS accelerometers, of which two are included in along-track configuration like the CAI. Finally, the MiniCAS is fully redundant. In principle, one emitter and one receiver must be included in the constellation, but instead one emitter and one receiver is found in each spacecraft.

In the worst-case scenario where both instruments fail, Ka-band Doppler tracking enables continued gravity field measurements with higher accuracy than X-band, which has been used in previous Mars missions. Additionally, the inclusion of numerous accelerometers allows for far more precise determination of the disturbances on the spacecraft, in comparison with previous Mars missions. Consequently, meaningful scientific return is ensured even under failed payload performance.

On the other hand, some components exhibit difficulty in implementing redundancy, and are thus inherently risky. This is the case with the tanks and the solar array. In case of solar array hinge failure, for example during the aerobraking manoeuvre, or anything causing prevention of solar array deployment, would compromise the mission. This is not the case with the high-gain antenna, as there is one per satellite, and the low-gain antennas can also communicate with Earth in the worst case scenario.

With regards to the tanks, it is required that these are placed symmetrically about the CoM, according to **SYS-PAY-4.13**. The tanks are already the most driving components in terms of volume along all dimensions, complicating the inclusion of redundant tanks. Leakage in a tank could compromise the compliance of **SYS-PAY-4.13**, deteriorating the scientific return, whereas complete tank outburst would result in mission failure.

Quantifying the reliability is very complicated for space missions, but given previous Mars missions and the robust redundancy approach, it can be estimated that the reliability of MarsExpore is around 97%.

Availability

Availability is the ”Ability of an item to be in a state to perform a required function under given conditions at a given instant of time or over a given time interval, assuming that the required external resources are provided” [112]. This is a proportion of how much time the system is operational and follows the following equation:

$$A = \frac{Uptime}{Total\_time} \tag{7.7}$$

Availability is a percentage and can be enhanced by ensuring efficient maintenance procedures and having readily spare part.

NASA has estimated that the Mean Time Between Failure (MTBF) in a satellite can be from 20000 to 25000 hours, but an efficient redundant system can have a MTBF of 623301 hours, so 25 times higher. [113] On Mars most of the failures result then in permanent capability loss due to communication delays and impossible in-situ repairs.

Availability has also been a key consideration in the payload design. As discussed in Section 4.6, the inclusion of the MiniCAS brings down the link acquisition time from 9 hours (as in GRACE-FO) to a few minutes. The consideration of this instrument in the design phase greatly increases the spacecraft's capability to enter and exit science mode, should it be required, without compromising the mission operations, thus improving availability.

Maintainability

Maintainability is the simplicity with which maintenance can be performed on the spacecraft such that it returns to its normal operating conditions. The spacecraft is physically isolated from the ground station, making it impossible to perform maintenance on the hardware after launch. Errors in the software can be present and stay undetected until after the launch or can be introduced by the space environment. The ground station can send data to the spacecrafts to check, repair, or update the software[3].This includes non-scheduled maintenance that reduces the probability of failures.

Physical maintenance of the hardware is possible while on Earth. During the assembly process, the system performance must be verified, as explained in Chapter 8. Regular maintenance of components enables early detection of damage, allowing for timely replacement and the avoidance of delays during and after the verification process.

Safety

Safety ensures that the system operates without harming operators and the environment, aiming to ensure that accidents are prevented and all hazards identified and controlled. Possible risks for the spacecraft and how that can be mitigated are discussed in Section 5.9. However, the spacecraft itself could pose risks to the environment as well. If a launch failure would occur, the negative effects of debris would fall into water or areas with low population density. To prevent contamination of other celestial bodies, the spacecraft is carefully sterilized, following Planetary Protection regulations [56].

The main components that could cause harm to the environment, other than the propellants of the launcher, are the propellants of MarsExplore and the CAI, which contains toxic materials. A failure in the aerobraking phase could lead to the crash into Mars surface, which could jeopardize possible life and damage the planet, as discussed in Section 5.8. This critical orbit insertion has already been done in previous Mars missions. To further reduce the risk of failure, both the commissioning of the spacecraft and the deployment of the solar arrays will occur only after the spacecraft reach a stable orbit.

Spacecraft safety includes protecting the spacecraft from internal failure. For example, software safety can be implemented through fault detection, isolation and recovery (FDIR) techniques that range from the protection of individual electronic components to the safeguarding of the entire spacecraft. This allows the spacecraft to enter safe mode, should it be needed, as portrayed in the software diagram of Figure 7.9. ESA uses guidance and navigation FDIR designed to identify errors in real time through ongoing sensor cross-checks and to isolate them in order to trigger sensor or actuator reconfigurations[4]. Safety in the propulsion system is introduced through isolation of valves and burst discs prevent overpressure Section 6.1.

[3] https://www.esa.int/esapub/bulletin/bullet91/b91deni.htm

[4] https://www.esa.int/Space_Safety/Hera/Fault_detection_isolation_and_recovery

8 Verification and Validation

The verification and validation strategy is closely aligned with the V-model [114]. In this context, the product refers to the spacecraft. Product verification ensures that each design element on subsystem and system level meets its specified requirements, while product validation confirms that the final system fulfils the mission objectives and stakeholder needs. Within this process, model verification and validation are important during the preliminary and detailed design phases. Here, model refers to the tools and models developed during the design process.

8.1. Model Verification

A structured verification process takes place to ensure tool and model correctness and reliability. At first, to ensure correct formulation in the tools, the code is peer-reviewed by multiple team members. Then unit tests for functions, and system tests for larger pieces of code ensures that the model outputs what is required. This step confirms the correct output return for a range of test cases, including boundary and undefined cases. Moreover, integration tests are used to verify that modules work together. Results are compared to expected values derived from simplified hand calculations or previous design iterations if applicable. The Python tool *Pytest* complements these procedures for testing and debugging, helping identify and resolve issues more efficiently. For external tools and existing models, the outputs are cross-validated against independently calculated reference cases and respective literature.

Unit Tests and Integration Tests

To verify the tools already created in the design process of Chapter 6, unit and system tests carried out are summarised in Table 8.1.

Table 8.1: Summary of unit and integration tests performed during the design process

ID	File Name	Function Name	Test Description - Expected Result	P/F	Cov.
VER-ASTRO-01	mars_delta_v_functions	compute_dir_tranfer_injection	T1: Check output values manually. T2: velocity positive	P	100%
VER-ASTRO-02	mars_delta_v_functions	compute_capture_orbit	T1: Check output values manually	P	100%
			T3: Velocity at pericenter > apocenter	P	100%
VER-ASTRO-03	mars_delta_v_functions	compute_mars_inclination	T1: Check output values manually	P	100%
VER-ASTRO-04	mars_delta_v_functions	compute_mars_circularization	T1: Check output values manually	P	100%
VER-ASTRO-05	mars_delta_v_functions	compute_mars_period	T1: Check output values manually	P	100%
			T2: Time threshold positive	P	100%
VER-ASTRO-06	complex_drag_v.py	orbital_decay	T1: Check output values manually	P	100%
			T2: Altitude displacement negative	P	100%
VER-ASTRO-07	complex_drag_v.py	compute_atmospheric_drag	T1: Check literature values match	P	100%
VER-ASTRO-08	complex_drag_v.py	plot_delta_v_vs_altitude	T1: Plot runs without error	P	100%
			T2: Exponential delta-v increase	P	100%

VER-ASTRO-09	mars_delta_v_functions	plot_comparison_deltav	T1: Plot runs without error	P	100%
VER-ASTRO-10	mars_delta_v_functions	Simulate_and_plot	T1: Plots run without error	P	100%
VER-ASTRO-11	mars_delta_v_functions	Simulate_and_plot2	T1: Plots run without error	P	100%
VER-ASTRO-12	sso_repeat.py	Repeat_sso	T1: Orbits match literature	P	100%
VER-ASTRO-13	sso_repeat.py	Plot_repeat_curves	T1: Visual inspection	P	100%
VER-ASTRO-14	aerobraking_time.py	compute_transfer_time	T1: Check output values manually	P	100%
VER-ASTRO-15	aerobraking_time.py	simulate_aerobraking	T1: Check output values manually	P	100%
			T2: Time threshold positive	P	100%
VER-ASTRO-16	launch_window.py	compute_synodic_period	T1: Check output values manually	P	100%
VER-ASTRO-17	launch_window.py	compute_phase_angle	T1: Check literature values match	P	100%
VER-ASTRO-18	launch_window.py	compute_launch_window	T1: Check dates match porkchop plots	P	100%
VER-ASTRO-19	marsdensity.py	plot_mars_density	T1: Visual inspection	P	100%
			T2: Check output values manually		
VER-ASTRO-20	penumbra.py	penumbra_one	T1: Check values match hand calcs	P	100%
VER-ASTRO-21	penumbra.py	solar_coverage	T1: Check values match hand calcs	P	100%
			T2: Coverage between 0 and 1	P	100%
VER-ADCS-01	AerodynamicTorque.py	aerodynamic_torque	T1: Check against hand calcs	P	100%
VER-ADCS-02	SolarRadiationTorque.py	solar_radiation_torque	T1: Check against hand calcs	P	100%
VER-ADCS-03	DynamicModelV3.py	disturbance	T1: Correct external torque sum	P	100%
			T2: Correct internal torque sum	P	100%
VER-ADCS-04	DynamicModelV3.py	controller	T1: Torque clamped correctly	P	100%
			T2: Torque matches hand calcs	P	100%
			T3: Correct discretisation	P	100%
VER-ADCS-05	DynamicModelV3.py	dynamics	T1: System created correctly	P	100%
VER-ADCS-06	DynamicModelV3.py	plot	T1: Visual inspection	P	100%
VER-ADCS-07	DynamicModelV3.py	desired_attitude	T1: Attitude computed correctly	P	100%
VER-BUDG-01	CostBudget.py	linear_regression	T1: R^2=1.0, coef=2.0, intercept=0.0	P	100%

VER-BUDG-02	CostBudget.py	dry_mass_vs_cost	T1: Returns correct keys	P	100%
VER-BUDG-03	CostBudget.py	calculate_total_cost	T1: Cost >0, correct structure	P	100%
			T2: Unit cost = sum subsys costs	P	100%
			T3: Cost increases with margin	P	100%
VER-BUDG-04	CostBudget.py	run_cost_budget	T1: 6 elements, no negatives	P	100%
VER-BUDG-05	CostOverTime.py	N/A	T1: Visual inspection	P	100%
VER-BUDG-06	MassPowerCost.py	N/A	T1: Visual inspection	P	100%
VER-PROP-01	propulsion.py	compute_mass_after_deltav	T1: Check output values manually	P	100%
			T2: Zero deltav → no propellant	P	100%
			T3: m_initial > m_final	P	100%
			T4: Higher Isp → less propellant	P	100%
VER-PROP-02	propulsion.py	compute_mass_fuel	T1: Check output values manually	P	100%
			T2: Masses > m_prop	P	100%
VER-PROP-03	propulsion.py	compute_tank_volume	T1: Check output values manually	P	100%
			T2: Zero density → error	P	100%
VER-PROP-04	propulsion.py	compute_spherical_tank_mass	T1: Check output values manually	P	100%
			T2: Mass scales linearly	P	100%
VER-PROP-05	propulsion.py	compute_exhaust_velocity	T1: Check output values manually	P	100%
VER-PROP-06	propulsion.py	compute_average_thrust	T1: Check output values manually	P	100%
			T2: Double duration → half thrust	P	100%
VER-PROP-07	propulsion.py	compute_power_required	T1: Check output values manually	P	100%
			T2: Double efficiency → half power	P	100%
VER-PWR-01	Power Budget Tool.xslx	Average Day Power	T1: 40W	P	100%
VER-PWR-02	Power Budget Tool.xslx	Average Eclipse Power	40W	P	100%
VER-PWR-03	Power Budget Tool.xslx	Average Orbit Power	40W,40W,1.82h,39.514W	P	100%
VER-PWR-04	Power Budget Tool.xslx	Cell Power	0.4335A,1.311W	P	100%
VER-PWR-05	Power Budget Tool.xslx	Required solar power	P_e=467.22W, 830.63W	P	100%
VER-PWR-06	Power Budget Tool.xslx	Perf per area	590W/m2,147.5W/m2	P	100%
VER-PWR-07	Power Budget Tool.xslx	BOL power	147.5W/m2,0.85	P	100%
VER-PWR-08	Power Budget Tool.xslx	EOL power	111.81W/m2,102W/m2	P	100%
VER-PWR-09	Power Budget Tool.xslx	Solar array area	830.63W,8.14m2	P	100%
VER-PWR-10	Power Budget Tool.xslx	Battery Capacity	482.2W,1025W,1844.1Wh	P	100%
VER-PWR-11	Power Budget Tool.xslx	EOL capacity	21.35Wh,0.3,0.889Wh	P	100%
VER-PWR-12	Power Budget Tool.xslx	BOL capacity	0.889Wh,1.0095, 0.196Wh	P	100%
VER-PWR-13	Battery_Cap.py	battery_capacity	T1: Visual inspection of plot	P	100%
VER-TTC-01	dB_conversions.py	conv_to_dB	Convert 100 to dB	P	100%
VER-TTC-02	ephemeris_reader.py	ephemeris_reader	912 dates parsed	P	100%

VER-TTC-03	ephemeris_reader.py	ephemeris_reader	912 deltas parsed	P	100%
VER-TTC-04	ephemeris_reader.py	ephemeris_reader	912 STO angles parsed	P	100%
VER-TTC-05	ephemeris_reader.py	ephemeris_reader	First date: 2042-06-22	P	100%
VER-TTC-06	ephemeris_reader.py	ephemeris_reader	First delta: 1.64 AU	P	100%
VER-TTC-07	ephemeris_reader.py	ephemeris_reader	First sto_angle: 36.2°	P	100%
VER-TTC-08	HGA/LGA files	HGA/LGA functions	Return type: Dictionary	P	100%
VER-TTC-09	HGA/LGA files	HGA/LGA functions	Default SNR: 5dB	P	100%
VER-TTC-10	HGA/LGA files	HGA/LGA functions	Default wavelength: 0.0093685m	P	100%
VER-TTC-11	HGA/LGA files	HGA/LGA functions	Space losses < 200dB	P	100%
VER-TTC-12	HGA_downlink.py	trasnmit_antenna_diameter	T1: Compare to reference	P	100%
VER-TTC-13	HGA/LGA files	Transmitter power	1W→0dB	P	100%
VER-TTC-14	HGA_downlink.py	Peak transmit gain	T1: Crosscheck reference	P	100%
VER-TTC-15	HGA_downlink.py	Transmit gain	T1: No loss = peak gain	P	100%
VER-TTC-16	HGA_uplink.py	Peak receive gain	T1: Compare reference	P	100%
VER-TTC-17	HGA_uplink.py	Receive gain	T1: No loss = peak gain	P	100%
VER-TTC-18	link_analysis	Boltzmann term	1J/K→0dB	P	100%
VER-TTC-19	HGA/LGA files	Space losses	T1: Zero length→zero loss	P	100%
VER-TTC-21	HGA_downlink.py	Transmit point loss	T1: Compare reference	P	100%
VER-TTC-22	HGA_uplink.py	Receive point loss	T1: Compare reference	P	100%
VER-TTC-23	HGA/LGA files	Required data rate	1bit/s→0dB	P	100%
VER-STRUC-01	Structure2.py	Polygon_lengths	T1: Compare manual result	P	100%
VER-STRUC-02	Structure2.py	Stringer_stress	T1: Compare manual value	P	100%
VER-STRUC-03	Structure2.py	Stringer_area	T1: Compare manual value	P	100%
VER-STRUC-04	Structure2.py	Load_launcher	T1: Compare manual value	P	100%
VER-STRUC-05	Structure2.py	calculate_poly_loads	T1: Compare manual value	P	100%
			T2: Compare buckling stress	P	100%
			T3: Compare area	P	100%
VER-STRUC-06	Structure2.py	calculate_weight	T1: Compare manual result	P	100%
VER-STRUC-07	Structure2.py	calculate_thickness	T1: Compare Excel value	P	100%
VER-STRUC-08	Structure2.py	max_diagonal	T1: Compare manual value	P	100%
VER-STRUC-09	Structure2.py	radius_of_gyration	T1: Compare manual value	P	100%

VER-STRUC-10	Structure2.py	check_frequency	T1: Raise errors correctly	P	100%
			T2: Calculate area/inertia	P	100%
VER-STRUC-11	Structure2.py	calculate_t_min	T1: Compare manual value	P	100%
VER-STRUC-12	Structure2.py	structural_mass	T1: Returns expected tuple	P	100%
VER-STRUC-13	test_johnson.py	calculate_r	T1: Compare manual value	P	100%
VER-STRUC-14	test_johnson.py	determine_stringer	T1: Best config matches	P	100%
VER-STRUC-15	test_johnson.py	find_combinations	T1: Symmetrical only	P	100%
VER-STRUC-16	test_johnson.py	test_johnson	T1: Returns expected tuple	P	100%
VER-STRUC-17	CAI_vibration.py	-	T1: Mass matches manual	P	100%
VER-STRUC-18	radiation_calcs.py	shielding_mass	T1: Mass matches manual	P	100%
VER-STRUC-19	magnetic_calc.py	-	T1: Mass matches manual	P	100%
VER-STRUC-20	whipple_shield.py	rear_wall_thickness	T1: Thickness matches manual	P	100%
VER-STRUC-21	whipple_shield.py	rear_wall_thickness	T1: Mass matches manual	P	100%
VER-SCI-01		do_model_sst	T1: Test math formulas	P	100%
			T2: Signal power law correct	P	100%
			T3: Visual plot inspection	P	100%
			T4: Satellite separation correct	P	100%
VER-SCI-02-05	plot files	plot functions	T1: Visual inspection	P	100%
VER-SCI-06	expected_signals		T1: Array values in range	P	100%
VER-SUST-01		Calculate_sustainability	T1: Visual inspection	P	100%
			T2: Hand calculations	P	100%
VER-THER-01	Thermal.py	compute_orbit_period	T1: Manual calculation	P	100%
VER-THER-02	Thermal.py	generate_flux	T1: Correct array outputs	P	100%
VER-THER-03	Thermal.py	compute_radiator	T1: Monotonic behavior	P	100%
VER-THER-04	Thermal.py	generate_flux_n	T1: T>0K, correct length	P	100%
VER-THER-05	Thermal.py	compute_temp	T1: T>0K, correct length	P	100%
			T2: Manual T final check	P	100%
VER-THER-06	Thermal.py	plot_all_cases	T1: Visual inspection	P	100%
VER-THER-07	Thermal.py	compute_TCS_mass	T1: Manual calculation	P	100%

External Tools & Models

It should be noted that, while an attempt to use Mars-GRAM was done, the tool was not used directly. Instead, density data were extracted from Mars-GRAM and implemented in Python scripts to generate

independent atmospheric density models. This data was provided in a state that has already been verified. Specifically, Mars-GRAM has previously supported missions such as MGS, Mars Odyssey, MRO, and MAVEN, and has been validated against MGS thermal emission spectrometer Radio Science data [115].

8.2. Model Validation

After completing the code and verifying that it is implemented correctly, model validation takes place.

Generally, model validation follows these steps:

1. Define validation criteria and pass\fail thresholds
2. Choose test cases and datasets used for cross validation
3. Use models to predict test outcome
4. Compare model predictions to the real life test outcomes using statistical methods
5. Perform sensitivity analysis to ensure test integrity

As dedicated datasets for direct validation are not available for the design of a spacecraft, model validation ensures that the output data are consistent and comparable with the performance and design parameters of heritage missions. Relevant heritage missions, depending on the specific application or subsystem being validated, include Mars orbital missions such as Mars Global Surveyor and Mars Odyssey, as well as gravity missions like GRACE-FO and GOCE. Table 8.2 structures this comparison. Data derived from these heritage missions are utilized as inputs to the tools created and any discrepancies between the model's predictions and the known heritage data is discussed.

Table 8.2: Model Validation

ID	File Name	Mission Used	Input	Output	Expected Output	Actual Output	Diff	Reasoning
VAL-PROP-01	ComponentSelection.py	Mars Global Surveyor	Bipropellant System, Dry mass: 1,062 kg, Δv: 977 m/s	Propellant mass [kg]	389	393.4	0.01	Minor deviation due to assumptions
VAL-PROP-02	propulsion.py	Mars Reconnaissance Orbiter	Monopropellant system Dry mass of 1031 kg, DeltaV of 1400 m/s	Propellant mass [kg]	1187	1020.82	0.14	Mass calculation uses ideal conditions, gravity losses and inefficiencies not explicitly defined
VAL-SCI-01	do_model_sst.m	Mars Reconnaissance Orbiter	400 km altitude, X-band measurement, 3 Earth year mission duration	Degrees and Order accuracy	70	67	0.04	Slight difference might be caused by error and frequencies of measurements
VAL-PWR-01	Power Budget Tool.xslx	Mars Express	Orbital period 6.7 hr, eclipse 95 min, solar flux 490 W/m², 20% efficiency, 1.88 yr lifetime, 400 W eclipse, 550 W daylight	Solar array area [m²]	11.42	11.72	0.03	Slightly different efficiencies and small differences in assumptions
VAL-PWR-02	Power Budget Tool.xslx	Mars Express	Creq = 350 Wh, Voltage = 3.5 V, Capacity = 1.5 Ah, Energy = 5.25 Wh, DOD = 30%, Efficiency = 0.6	Battery Capacity [Ah]	72	70.5	0.02	Different DOD and efficiency assumptions
VAL-PROP-03	DynamicModelV3.py	GRACE-FO	Ixx = 110.5, Iyy = 580.7, Izz = 649.7, min torque = 0.05 mNm, max torque = 0.02 Nm, disturbance = [4.6e-6, -1e-5, 0], Isp = 72	Propellant mass per day [g]	1.3	1.7	0.308	GRACE uses magnetorquers, model uses simplifications
VAL-STRUC-01	Structure2_optimal _current2.py	GRACE-FO	Wet mass = 607 kg, h = 3.12 m, l = 0.72 m, w = 0.87 m	Structural mass [kg]	105	96.97	-0.076	FEM not implemented, uses 17.5% structural mass estimate
VAL-BDG-01	CostBudget.py	MAVEN	Dry mass = 809 kg, Launch = 187 M$, Operational = 28 M$	Total mission cost [M$]	582.5	659	0.131	High margin, early estimate
VAL-THER-01	Thermnal_final.py	MRO	Dry mass = 1031 kg, Wet mass = 2180 kg, Power = 1000 W	Radiator area [m²]	2.7	3.2	0.185	Model assumes 212 km orbit; MRO is at 300 km, reducing albedo/IR
VAL-TTC-01	HGA_downlink.py, LGA_downlink.py	Mars Global Surveyor	Eb/N0 = 68.10 dB, Ant Gain = 7.1 dB, Power = 44.23 dB, Distance = 0.448 AU, Rate = 250 bps, Freq = 8.4 GHz, Req Eb/N0 = 27.94	Link Margin (dB)	4.76	3.17	1.59	Different margin setup, includes waveguide and noise spectral density
VAL-TTC-02	HGA_uplink.py, LGA_uplink.py	Mars Global Surveyor	Eb/N0 = 67.05 dB, Rec Ant Gain = 0, Distance = 0.448 AU, Rate = 125 kbps, Freq = 7.2 GHz, Req Eb/N0 = 38.13	Link Margin (dB)	5.51	2.95	2.56	Different margin setup, includes waveguide and noise spectral density

While the models show a strong basis with heritage mission data, their applicability to the current mission is influenced by differences in mission parameters such as orbital altitude, spacecraft configuration, and subsystem technologies. In most cases, the validations are based on Mars orbiters and Earth gravity missions, which share a similar environment and system design but may differ in mission objectives and power requirements.

8.3. Product Verification

Product verification is done using five methods. These are Inspection, Analysis, Review of Design, Demonstration and Testing. Tables summarising science requirements (Section 2.8), payload requirements (Section 4.10) risk requirements (Section 5.10) and subsystem requirements (Chapter 6), each include a dedicated column specifying the verification strategy to be applied, selected from one of the aforementioned methods. Additionally, a compliance matrix can be found in Appendix A set up to show the extent that each requirement has been met during the design process.

Inspection involves direct observation and qualitative assessment of components and the spacecraft. Facilities required for inspection include clean rooms, such as ISO Class 8, equipped with lighting and magnifications tools. The cost of using such facilities typically ranges from 500-1000€ per day, depending on the specific location.[1]. In addition to physical inspection, review of design documentation is also conducted. This method establishes that the product satisfies most of the driving requirements by directly tracking these requirements with respect to design elements and specifications.

Analysis employs models and software and are mainly used when testing is not feasible due to financial and/or engineering constraints. On the subsystem level, analysis will be used as the main verification method of astrodynamics characteristics, as well as for the TT&C and the payload. It will also be used on the subsystem level in conjunction with testing. Analysis activities require access to computational facilities and specialised software tools such as ANSYS and MATLAB/Simulink. Access to such commercial licenses can largely vary.

Review of design is established by examining design documentation to confirm that the product meets specified requirements.

Demonstration is effective for showing basic functionality and will mainly be used in CDHS to verify that command sequences are correctly interpreted and executed. For instance, a FlatSat setup shows the basic operability without collecting extensive telemetry data. The specific pricing can vary based on system complexity and vendor, but values are between 20000-50000€ [2].

For verification by test, a comprehensive list was made for system and subsystem level defining the purpose of each test and the respective facilities to be used. This method is preferred rather than relying only on analysis. The final column lists the requirements to be verified per test.

Type	Test	Description	Facility	Requirements to be Verified
System Level Tests				
Structural	Vibration Test	Demonstrates structural integrity under simulated launch loads	HYDRA multi-axis vibration test facility[3]	SYS-LNCH-5.3, SUB-STRUC-12
Structural	Acoustic Test	Confirms spacecraft withstands required noise levels from engine and boundary layer	HYDRA multi-axis vibration test facility	SYS-LNCH-5.3
Structural	Shock Test	Demonstrates resistance to required acceleration shock loads	HYDRA multi-axis vibration test facility	SYS-LNCH-5.3

Continued on next page

[1] https://torontech.com/tvac-thermal-vacuum-test-chamber/

[2] https://www.satelliteevolution.com/post/endurosat-launches-next-gen-flatsat-to-scale-critical-missions-testing

[3] https://www.esa.int/Enabling_Support/Space_Engineering_Technology/HYDRA_multi-axis_vibration_test_facility

Type	Test	Description	Facility	Requirements to be Verified
Functional	Deployment Test	Ensures deployment of antennas and solar arrays within timing requirements	Large Space Simulator (LSS)	SYS-2.2.2.1, SYS-2.2.3.1
Functional	CoM Balance Test	Ensures the Center of Mass trim capability	Mass Properties Measurement Facility [4]	SYS-PAY-4.11, SYS-PAY-4.12
Thermal	Thermal Vacuum Test	Verifies equipment operation in vacuum and temperature range	Large Space Simulator (LSS)[5]	SYS-PAY-4.1 to SYS-PAY-4.6, SUB-PROP-8
Thermal	Thermal Vacuum Cycling	Simulates rapid temperature shifts due to sunlight transitions and aerobraking	Large Space Simulator (LSS)	SYS-RISK-8.1-SYS-RISK-8.4, SYS-RISK-8.11
Integration	Mechanical Integration Test	Verifies fit and interface integrity through assembly	Clean Room Complex[6]	UR-SYS-2.1.1.3, UR-SYS-2.1.1.4
Integration	Electrical Integration Test	Checks signal and power interfaces and electromagnetic compatibility	Materials and Electrical Components Laboratory[7]	SUB-ADCS-3.11, SUB-TCS-7, SUB-TTC-4.7, SUB-POW-1
Integration	Software Integration Test	Verifies software functionality on simulated hardware	Software Systems Laboratory[8]	SUB-CDHS-2.2.4.1.9, SUB-PAY-2.4.2.2.8
Subsystem Level Tests				
ADCS	Actuator Performance Test	Verifies actuator capability, response time, and behaviour	GNC, AOCS & Pointing Laboratory[9]	SYS-PAY-4.7 to SYS-PAY-4.9, SUB-ADCS-3.6, SUB-ADCS-3.7
Power	Solar Array Illumination Test	Demonstrates power generation under solar conditions	Space Power Laboratory[10]	TBD
Power	Power Load Test	Demonstrates continuous, peak, and eclipse-mode power delivery under operational conditions	Space Power Laboratory[11]	SUB-POW-1, SUB-POW-2, SUB-POW-3
Power	Energy Storage Capacity and Cycles Test	Demonstrates energy storage, voltage regulation, and charge/discharge cycling behaviour	Space Power Laboratory[12]	SUB-POW-5, SUB-POW-6, SUB-POW-7

Continued on next page

[4] https://technology.esa.int/page/combined-cog-and-moi-measurement-unit-w50m6

[5] https://www.esa.int/Enabling_Support/Space_Engineering_Technology/Test_centre/Large_Space_Simulator_LSS

[6] https://technology.esa.int/lab/test-centre

[7] https://technology.esa.int/lab/materials-electrical-components-laboratory

[8] https://technology.esa.int/lab/software-systems-laboratory

[9] https://technology.esa.int/lab/gnc-aocs-pointing-laboratory

[10] https://technology.esa.int/lab/ESPL-european-space-power-laboratory

[11] https://technology.esa.int/lab/ESPL-european-space-power-laboratory

[12] https://technology.esa.int/lab/ESPL-european-space-power-laboratory

Type	Test	Description	Facility	Requirements to be Verified
Propulsion	Hot Fire Test	Confirms thrust, specific impulse, and burn duration	DLR Institute of Space Propulsion[13]	SUB-PROP-3, SUB-PROP-4
Propulsion	Cold Flow Test	Evaluates valve timing and flow integrity	DLR Institute of Space Propulsion	SUB-PROP-4
Propulsion	Electric Thrusters Performance Test	Verifies thrust, Isp, and power efficiency	Propulsion Laboratory[14]	SUB-PROP-5, SUB-PROP-6, SUB-PROP-7
Payload	Performance Test	Verifies resolution, sensitivity, and signal-to-noise ratio	RF Payload Systems Laboratories[15]	
Payload	Electromagnetic Compatibility Test	Verifies magnetic field does not interfere with payload components	Maxwell EMC[16]	SYS-PAY-4.16
TT&C	Communication Test	Confirms uplink/downlink communication with ground stations	Communication and TT&C Laboratory[17]	SYS-PAY-4.17, SUB-TTC-4.3, SUB-TTC-4.4, SUB-TTC-4.5
TT&C	RF Performance Test	Checks transmitter frequency/power and receiver sensitivity	Maxwell EMC[18]	SYS-PAY-4.18, SYS-PAY-4.19, SYS-PAY-4.20, SUB-TTC-4.2, SUB-TTC-4.11
TT&C	Modulation and Coding Test	Verifies that the signal is modulated,encoded, and decoded.	RF Payload Systems Laboratories[19]	SUB-TTC-4.11, SUB-TTC-4.12, SUB-TTC-4.13, SUB-TTC-4.14
TT&C	Antenna Performance Test	Measures gain, polarisation, and switching performance	Compact Payload Test Range	SUB-TTC-4.9, SUB-TTC-4.10, SUB-TTC-4.11
CDHS	Processor Functionality Test	Verifies processor performance and timing	Data Systems and Microelectronics Lab[20]	SUB-CDHS- 5.7
CDHS	Command Execution Test	Ensures execution of onboard and uplinked commands	Data Systems and Microelectronics Lab	SUB-CDHS-5.4, SUB-CDHS-5.1
CDHS	Memory Functional Test	Confirms data integrity and access speed	Data Systems and Microelectronics Lab	SUB-CDHS-5.5, SUB-CDHS-5.7, SYS-ASTRO-3.6

Continued on next page

[13] https://www.dlr.de/en/ra/about-us
[14] https://technology.esa.int/lab/tec-m-epl-esa-propulsion-laboratory
[15] https://www.esa.int/Enabling_Support/Space_Engineering_Technology/RF_Payload_Systems_Laboratories
[16] https://technology.esa.int/page/maxwell-emc
[17] https://technology.esa.int/lab/communication-and-ttc-laboratory
[18] https://technology.esa.int/page/maxwell-emc
[19] https://www.esa.int/Enabling_Support/Space_Engineering_Technology/RF_Payload_Systems_Laboratories
[20] https://technology.esa.int/lab/Data-Systems

Type	Test	Description	Facility	Requirements to be Verified
Thermal	Heater Functionality Test	Verifies heater activation and deactivation behavior	Large Space Simulator (LSS)	SUB-TCS-5,SUB-TCS-6
Thermal	Radiator Emissivity Test	Verifies radiator heat rejection capacity	Large Space Simulator (LSS)	SUB-TCS-4
Structures	Limit Load Test	Validates strength at design load limits	HYDRA multi-axis vibration test facility	SYS-LNCH-5.3
Structures	Stiffness Test	Measures deformation under expected load	HYDRA multi-axis vibration test facility	SYS-LNCH-5.3
Structures	Modal Test	Captures frequency response and modal shapes	HYDRA multi-axis vibration test facility	SYS-LNCH-5.3.7, SYS-LNCH-5.3.8

The detailed price breakdown for conducting a test campaign at ESA's ESTEC Test Centre, is not publicly available and direct communication is necessary. Costs are highly dependent on mission and system requirements such as the type and number of tests, duration of campaign, spacecraft specifications, and facility usage.

8.4. Product Validation

In the final stages of the detailed design, the emphasis shifts from the verification of the design compliance with the requirements to the validation of scientific and stakeholder objectives.

The validation is centred on several mission objectives: detecting and mapping the static gravity to identify subsurface structures (e.g. water and sediments), and observing the temporal gravity field. These needs are linked with the resolution in spherical harmonics (D/O), temporal sampling frequency, and sensitivity to gravitational perturbations. Therefore, the main priority of the validation plan is to corroborate that the spacecraft is capable of resolving these phenomena under real operational constraints.

In order to accomplish this, several tests will be conducted. A structured approach will be followed using two validation environments: Integrated Mission System Simulator (IMSS) and Ground Segment Testbed (GST). Both IMSS and GST will be designed to precisely replicate and test the complex interactions between the mission and systems.

- Integrated Mission System Simulator (IMSS): Simulates the spacecraft, its subsystems (ADCS, CDHS, TT&C, EPS, Thermal...) and LRI/CAI payloads. It models how the data will flow through the various subsystems corroborating with the interaction at system level.
- Ground Segment Testbed (GST): Simulates the ground segment data distribution, including the data reception processing and command updates.

To set up the environment, the approach consists of the following steps:

1. Validation Environment Setup: Configure IMSS and GST.
2. Scenario Generation: create 'truth' data and operational conditions
3. Simulate Data flow: Run IMSS to simulate on-board data generation and storage
4. Simulate Communication: simulate data downlink and command uplink via TTC
5. Ground Processing: Run GST processing.

E2E testing Two main End-to-End tests will be performed to trace and validate the performance in accomplishing the mission objectives:

- E2E Test 1: Nominal Static Gravity Field Mapping: Validates the instantaneous interaction between; ADCS, LRI/CAI, CDHS and TTC in producing high resolution static gravity field map product under nominal operations. The procedure will be as follows:
  1. IMSS simulates ADCS maintaining precise attitude. Its stability directly interacts with LRI range and CAI acceleration sensitivity, generating instrument data. This validates the payload-to-CDHS interface, including time for CDHS to compress and store the data without loss or corruption.
  2. CDHS prepares data for downlink. TTC simulates transmission. This validates the CDHS-TTC interface.
  3. GST receives data from IMSS's TTC, validating the ground reception.

  Once the methodology has been executed, the generated gravity product accuracy should meet the requirements, achieving static gravity determination success.
- E2E Test 2: Temporal Gravity Mapping: Validates the long-term interaction between IMSS and GST to acquire and determine temporal gravity changes. The procedure will be as follows:
  1. Repeat step 1 from the E2E Test 1 over a simulated Martian year. This ensures the data quality over extended periods.
  2. Repeat step 1 & 2 from the E2E Test 1 over a simulated year. This validates the robustness of the TTC-GST link and ground station command scheduling over time.

  This iteration can be simulated for longer periods of time, ensuring temporal change determination effectiveness.

Detailed Scenario-Based Testing Nevertheless, E2E tests do not ensure challenging conditions validation. This will be therefore corroborated with scenario testing for challenging or unusual conditions, specially to account for total blackout scenarios due to solar conjunction and high atmospheric drag scenarios.

- Scenario Test 1: This will ensure the spacecraft system interaction (ADCS-CDHS-EPS) during a prolonged communication blackout and its ability to acquire data and store it properly. The methodology is as follows:
  1. IMSS simulates the solar conjunction where TTC will be blocked for a predefined time (2-3 weeks).
  2. CDHS will manage LRI/CAI data acquisition in its memory. This will validate the CDHS's storage capacity.
  3. ADCS must maintain attitude autonomously, executing programmed manoeuvres.

  Therefore, by following this procedure, the spacecraft capability to meet science objectives and acquire data autonomously will be validated.
- Scenario Test 2: This test will ensure the spacecraft capability to interact with unprecedented changes in atmospheric density. The methodology is as follows:
  1. Firstly, IMSS introduces localised, higher atmospheric drag regions (e.g. simulating atmospheric density variations) along the spacecrafts orbit.
  2. ADCS must respond to the increased drag to maintain the precise attitude required for LRI/CAI measurements. This corroborates ADCS's interaction with varying external forces.

  By following these steps, the spacecrafts dynamics would be validated.

9 Conclusion and Future Outlook

The mission objective is to design an ESA M-Class-compliant mission to map the static and dynamic gravity field of the planet Mars, demonstrating the effectiveness of novel quantum sensing instruments, with a group of 10 people over 10 weeks. The mission shall launch in 2041 on a European launcher, with a total cost of 670 million euros. This report aimed to justify the final detailed spacecraft design as well as the final mission design.

MarsExplore focuses on the presence of subsurface liquid water, buried impact craters, volatile-rich sediments, the influence of Phobos, mantle deformation (estimated at 0.13 mm/year), dust storms, atmospheric winds, and seasonal polar cap changes. Compared to past missions, MarsExplore significantly improves spatial resolution from 96 km to less than 30 km, significantly enhancing the scientific return. This leads to a deeper understanding of the planet's formation history and enables better modelling and prediction of atmospheric dynamics on both Mars and Earth. The mission aims at detecting gravity signals ranging from 0.0182 to 2400 μGal, capturing key variations that are critical to understanding Mars' geophysical processes.

The market analysis justified a dominant market position of MarsExplore. The primary stakeholder is Assistant Professor Bart Root. The secondary stakeholders are TU Delft, EU, NASA, the scientific community, the quantum technology industry, and the general public. The main competing stakeholders are other proposal teams entering the ESA M-Class M8 Mission call. MarsExplore justified its strong position through its unique use of quantum technology, which the European Commission and NASA have shown interest in. The Total Available Market, Serviceable Available Market, and Serviceable Obtainable Market have been estimated, respectively, as 130 B€, 1.7 B€, and 940 M€, accounting for funding from NASA, the European Union, and industries from the gravity sensor market, showing realistic feasibility of the mission.

MarsExplore justified obtaining both static and temporal gravitational field data through Satellite-to-Satellite Tracking with a payload, which consists of a Laser Ranging Interferometer (LRI) and a Cold Atom Interferometer (CAI). Said components enable the current best precision, with the LRI reaching a Technology Readiness Level (TRL) of 8, others, such as the CAI and MiniCAS, remaining at TRL 5, reflecting the balanced approach between innovation and feasibility.

MarsExplore's launch will be performed using the Ariane 62, offering a total ΔV capacity of 14.404 km/s for interplanetary injection. Following a three-month aerobraking phase, the spacecraft transitions into a stable quasi-polar orbit at 212.48 km altitude. Science operations commence after a two-month commissioning phase, with the mission concluding in a designated graveyard orbit, where the spacecraft may serve as a communications relay. The overall trajectory design reflects a commitment to sustainability through compliance with ESA's Green Agenda and Planetary Protection policies.

The technical risk assessment systematically evaluated risks across all mission phases, addressing potential impacts on performance, cost, and schedule. Most were mitigated through design adaptations and contingency planning, though several moderate-level risks persist, necessitating continued monitoring throughout implementation. Overall, the risk is sufficiently low to justify performing the mission.

The detailed design analysis converged to a dry mass of 691.7 kg and a total launch mass of 1124.2 kg per spacecraft. Sustainability shaped the spacecraft's design, influencing choices in propulsion, orbit selection, structure, and power. Nominal operations require 842 W, delivered by two deployable solar arrays, a battery, and a Power Control and Distribution Unit. The hybrid propulsion system delivers 425 N with a bipropellant thruster for orbit insertion, with Hall-effect thrusters (50–170 mN) for fine orbit control. The required precision pointing is achieved through a robust ADCS using star trackers,

sun sensors, gyroscopes, and cold gas thrusters. Communications are done by a high-gain and dual low-gain antennas, while a triply-redundant CDHS controls all spacecraft operations. The Thermal Control Subsystem maintains a design temperature of 13°C, balancing propellant tank constraints and payload thermal stability requirements through 50 heaters, a 15-layer Kapton MLI, and Teflon-coated radiators. Structurally, the spacecraft is built from aluminium T6 alloy to withstand radiation and micrometeoroid impacts, with final dimensions of 3.0 m height, 1.7 m width, and 1.2 m length. Internal and external configurations are shown in Figure 9.1.

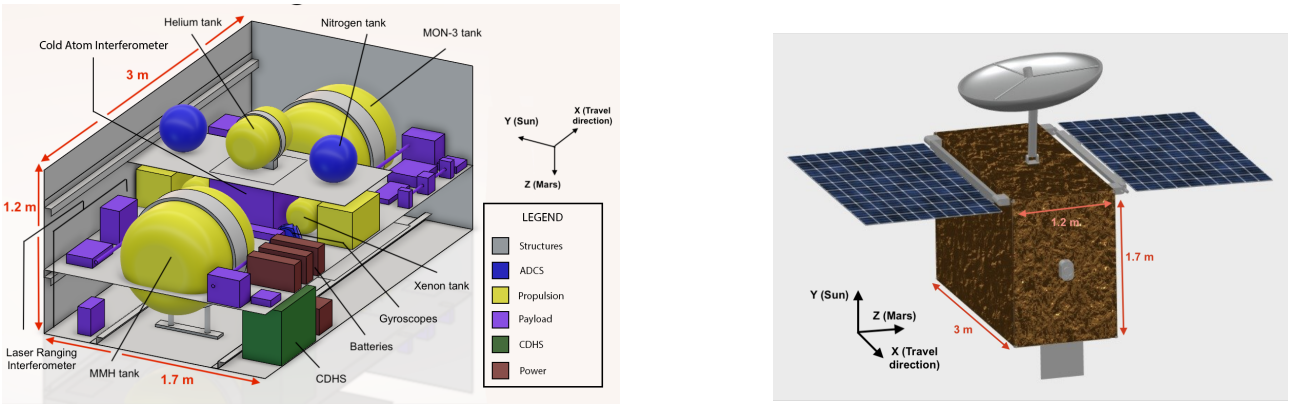

(a) Internal configuration

(b) External configuration

Figure 9.1: Internal and External Configuration

To comply with the given cost requirement of €670 million from ESA, the cost budget was estimated and justified. The cost budget was progressively refined—from early parametric estimates to a comprehensive subsystem-level breakdown with applied margins—yielding a final estimate of €717.7 million, being justified by available funding. Supporting this, the hardware and software block diagrams provided a structured overview and justification of subsystem interactions and operational logic. A dedicated manufacturing and integration plan further established a clear pathway from component procurement to final spacecraft assembly.

To conclude the detailed design, a verification and validation plan was produced. Product verification ensured that each design element met its specified requirements, while product validation confirmed that the final system fulfilled the mission objectives and stakeholder needs. Finally, model verification and validation were outlined to ensure that the tools were correctly implemented and accurately represent real-world behaviour. Ultimately, the presented detailed spacecraft design as well as the final mission design are adequately justified, and MarsExplore is ready to move on to the next stage of development.

Recommendations

The MarsExplore mission meets its primary science and operational goals. Improvements can be made to enhance its overall reliability, efficiency, and sustainability. In particular, the aerobraking phase has not been fully accounted for in the current spacecraft design. The spacecraft was not specifically designed to comply with requirements coming from this critical phase or shaped to optimize atmospheric drag. In the same vein, vibrations induced by aerodynamic loads on the boom mounted solar panels have not been currently investigated. This is due to the fact that the solar panel surface area is perpendicular to the flight direction, meaning the solar panels do not add “frontal area” to the drag experienced. Regardless, unexpected vibrations could be critical to structural integrity. Thus, a dedicated design iteration is recommended to account for these aerobraking effects, i.e.: to accurately estimate deceleration time, assess thermal protection, and the structural response of the booms. Performing detailed simulations to evaluate how long the aerobraking phase would take will

also ensure better timeline control.

Additionally, the mass and volume constraints resulting from the bipropellant tanks makes the idea of a kickstage a worthwhile future consideration. This would have the additional benefit of optimising the Ariane 62's performance, by separating high-energy maneuvers from the primary stage, enhancing mission versatility and injection accuracy.

With regards to the payload, the required optical link error for the LRI remains to be estimated. Discussions must take place with planetary scientists and payload manufacturers to determine the optimal required optical link error, taking into consideration the increase in science return and development efforts.

Further design iterations are recommended to reduce complexity and increase mission reliability and robustness. The current concept involves multiple mission phases, each requiring distinct system modes and ground intervention strategies. More detailed planning of operational timelines, fault detection and recovery procedures, and ground segment coordination will be essential to ensure smooth transitions between mission phases. In particular, automating certain spacecraft functions during high-risk phases could reduce reliance on Earth-based commands and minimize response delays caused by communication latency. Moreover, the mission's end-of-life strategy should be strengthened to calculate orbital decay times from the final orbit and ensure sufficient propellant is allocated for a final manoeuvrer. The current cost estimation approach can be improved by adopting a bottom-up methodology, allowing for more accurate budgeting based on subsystem-level inputs. Additionally, incorporating Monte Carlo simulations would enhance the understanding of uncertainties and risks associated with key cost drivers.

Code Repository and Statement on AI Usage

The code for the tools and trade-off considered in this report can be found in `https://github.com/sarmadagamboa/DSE-VS`. Moreover, the MarsExplore team's statement on Artificial Intelligence (AI) usage in this report will be provided in a separate deliverable. Large Language Models, such as ChatGPT, were used to assist in the formatting and proofreading of text, such as formatting LaTeX tables. Moreover, it has also been used to help in debugging code and to assist with code documentation, such as the inclusion of docstrings.

Acknowledgements

DSE Group 10 would firstly like to acknowledge Bart Root, Francesco Orefice and Sasha Vlaskin for their continued support throughout the DSE, as well as invaluable contributions to the project and learning experience.

We would also like to thank DLR for their extensive support on the MarsExplore mission, namely: Lisa Wörner, Alexander Koch, Christian Schubert and Julia Desirée van den Toren. Their contributions to the team were very significant, ranging from help on the cost estimation procedures to answering numerous questions on the several payload instruments.

Finally, we would like to thank the staff of TU Delft's Aerospace Engineering Faculty, namely Dominic Dirkx, for his help on quantum clock spacecraft, Stefano Speretta, for his help with the link budget tool, and João Encarnação, for his help with penumbra calculations.

Reference List

[1] L. Wörner et al. "MaQuIs—Concept for a Mars Quantum Gravity Mission". In: *Planetary and Space Science* (2023). DOI: 10.1016/j.pss.2023.105660.

[2] Yasmine Mafoutsis et al. *MarsExplore: Designing a Mars Gravity Mission Using Quantum Technologies*. Midterm Report. Project Coordinator: Bart Root; Project Coaches: Sasha Vlaskin, Francesco Orefice. Delft University of Technology, Faculty of Aerospace Engineering, 2025.

[3] Carl A. Heiland. *Geophysical Exploration*. New York: Prentice-Hall, 1940.

[4] Bruce G. Bills and Alexander I. Ermakov. "Simple models of error spectra for planetary gravitational potentials as obtained from a variety of measurement configurations". In: *Planetary and Space Science* 179 (2019), p. 104744. DOI: 10.1016/j.pss.2019.104744. URL: http://dx.doi.org/10.1016/j.pss.2019.104744.

[5] Bert Wouters et al. "GRACE, time-varying gravity, Earth system dynamics and climate change". In: *Reports on Progress in Physics* 77.11 (2014), p. 116801. DOI: 10.1088/0034-4885/77/11/116801.

[6] Bernhard Hofmann-Wellenhof and Helmut Moritz. *Physical Geodesy*. 2nd. Vienna, Austria: Springer, 2006.

[7] Alex S. Konopliv et al. "Mars high resolution gravity fields from MRO, Mars seasonal gravity, and other dynamical parameters". In: *Icarus* 211.1 (2011), pp. 401–428. ISSN: 0019-1035. DOI: https://doi.org/10.1016/j.icarus.2010.10.004. URL: https://www.sciencedirect.com/science/article/pii/S0019103510003830.

[8] Nicolaas Sneeuw. "A Semi-Analytical Approach to Gravity Field Analysis from Satellite Observations". Ph.D. dissertation. Munich, Germany: Institut für Astronomische und Physikalische Geodäsie, Technische Universität München, 2000.

[9] T. Lévêque et al. "Gravity Field Mapping Using Laser Coupled Quantum Accelerometers in Space". In: *Surveys in Geophysics* (2020).

[10] Martino Travagnin. *Cold Atom Interferometry for Earth Observation: Perspectives for Satellite-Based Quantum Gravimetry*. Technical Report EUR 30492 EN. Luxembourg: Joint Research Centre, European Commission, 2020. DOI: 10.2760/225071.

[11] Kolja Nicklaus et al. "Towards NGGM: Laser Tracking Instrument for the Next Generation of Gravity Missions". In: *Remote Sensing* 14.16 (2022), p. 4089. DOI: 10.3390/rs14164089. URL: https://doi.org/10.3390/rs14164089.

[12] Vlada Stamenkovic et al. *Deep Trek: Science of Subsurface Habitability & Life on Mars*. White Paper submitted to the Planetary Science and Astrobiology Decadal Survey 2023–2032. Whitepaper #250, Published in the Bulletin of the AAS, Vol. 53, Issue 4. 2021. URL: https://baas.aas.org/pub/2021n4i250/release/1.

[13] Sebastian Emanuel Lauro et al. "Multiple subglacial water bodies below the south pole of Mars unveiled by new MARSIS data". In: *Nature Astronomy* 5 (2021), pp. 63–70. DOI: 10.1038/s41550-020-1200-6.

[14] Nicky Jenner and Emily Baldwin. *First evidence of planet-wide groundwater system on Mars*. Posted by Nanci Bompey on AGU GeoSpace blog. 2019. URL: https://blogs.agu.org/geospace/2019/03/01/first-evidence-of-planet-wide-groundwater-system-on-mars/.

[15] Isabel Egea-González et al. *Ammonia or methanol would enable subsurface liquid water in the Martian South Pole*. 2024. arXiv: 2401.09873 [astro-ph.EP]. URL: https://arxiv.org/abs/2401.09873.

[16] Debra L. Buczkowski. "Stealth quasi-circular depressions (sQCDs) in the northern lowlands of Mars". In: *Journal of Geophysical Research: Planets* 112.E9 (2007), E09002. DOI: 10.1029/2006JE002836. URL: https://agupubs.onlinelibrary.wiley.com/doi/10.1029/2006JE002836.

[17] D. L. Buczkowski. "Comparing Quasi-Circular Depression (QCD) Locations to Northern Lowland Materials on Mars". In: *Seventh International Conference on Mars*. 1353. Houston, TX: Lunar and Planetary Institute, 2007, p. 3302. URL: https://www.lpi.usra.edu/meetings/7thmars2007/pdf/3302.pdf.

[18] B. M. Jakosky. "Mars: A Volatile Planet". In: *Mars: A Volatile World*. Ed. by B. M. Jakosky. Elsevier, 2021, pp. 1–12. DOI: 10.1016/B978-0-12-820245-6.00002-1. URL: https://www.sciencedirect.com/science/article/pii/B9780128202456000021.

[19] Paul D. Komar. "Modes of sediment transport in channelized water flows with ramifications to the erosion of the Martian outflow channels". In: *Icarus* 42.3 (1980), pp. 317–329. DOI: 10.1016/0019-1035(80)90097-4. URL: https://www.sciencedirect.com/science/article/pii/0019103580900974.

[20] Howard A. Perko, John D. Nelson, and Jacklyn R. Green. "Review of Martian Dust Composition, Transport, Deposition, Adhesion, and Removal". In: *Space 2002 and Robotics 2002: Proceedings of the Conference*. American Society of Civil Engineers, 2002, pp. 176–189. DOI: 10.1061/40625(203)25. URL: https://ascelibrary.org/doi/10.1061/40625(203)25.

[21] Margaret A. Rosenburg, Walter S. Kiefer, and Herbert V. Frey. "Morphometry of Quasi-Circular Depressions in the Southern Hemisphere of Mars: Implications for QCD Formation and Resurfacing History". In: *38th Lunar and Planetary Science Conference*. Houston, TX: Lunar and Planetary Institute, 2007, p. 1460. URL: https://www.lpi.usra.edu/meetings/lpsc2007/pdf/1460.pdf.

[22] James A. Jr. Skinner and Kenneth L. Tanaka. "Evidence for and implications of sedimentary diapirism and mud volcanism in the southern Utopia highland–lowland boundary plain, Mars". In: *Icarus* 186.1 (2007), pp. 41–59. DOI: 10.1016/j.icarus.2006.08.008.

[23] Stuart G. Wakeham and Elizabeth A. Canuel. "The nature of organic carbon in density-fractionated sediments in the Sacramento–San Joaquin River Delta (California)". In: *Organic Geochemistry* 31.4 (2000), pp. 389–407. DOI: 10.1016/S0146-6380(00)00005-5.

[24] D. Dirkx et al. "Phobos laser ranging: Numerical geodesy experiments for Martian system science". In: *Planetary and Space Science* 101 (2014), pp. 108–121. DOI: 10.1016/j.pss.2014.06.020.

[25] V. Lainey et al. "Mars moon ephemerides after 14 years of Mars Express data". In: *Astronomy & Astrophysics* 654 (2021), A113. DOI: 10.1051/0004-6361/202141362.

[26] Antonio Genova et al. "Seasonal and static gravity field of Mars from MGS, Mars Odyssey and MRO radio science". In: *Icarus* 272 (2016), pp. 228–245. DOI: 10.1016/j.icarus.2016.02.050.

[27] M. Baker et al. "Seasonal Variations of Snow Depth on Mars". In: *Science* 294.5549 (2001), pp. 2141–2146. DOI: 10.1126/science.1066556. URL: https://www.science.org/doi/10.1126/science.1066556.

[28] Adrien Broquet et al. *Mars's northern ice cap is young with a cold, stiff mantle beneath*. DLR Press Release. German Aerospace Center (DLR). 2025. URL: https://www.dlr.de/en/latest/news/2025/marss-northern-ice-cap-is-young-with-a-cold-stiff-mantle-beneath.

[29] Scott D. Guzewich et al. "Gravity Wave Observations by the Mars Science Laboratory REMS Pressure Sensor and Comparison With Mesoscale Atmospheric Modeling With MarsWRF". In: *Journal of Geophysical Research: Planets* 126.7 (2021), e2021JE006907. DOI: 10.1029/2021JE006907. URL: https://doi.org/10.1029/2021JE006907.

[30] Özgür Karatekin et al. "Atmospheric angular momentum variations of Earth, Mars and Venus at seasonal time scales". In: *Planetary and Space Science* 59.10 (2011), pp. 923–933. DOI: 10.1016/j.pss.2010.03.013.

[31] Flavio Petricca et al. "Constraining the Internal Structures of Venus and Mars from the Gravity Response to Atmospheric Loading". In: *The Planetary Science Journal* 3.7 (2022), p. 164. DOI: 10.3847/PSJ/ac7878. URL: https://doi.org/10.3847/PSJ/ac7878.

[32] Ellen Van den Acker et al. "Influence of the seasonal winds and the CO2 mass exchange between atmosphere and polar caps on Mars' rotation". In: *Journal of Geophysical Research: Planets* 107.E7 (2002), pp. 9-1-9–8. DOI: https://doi.org/10.1029/2000JE001539. URL: https://agupubs.onlinelibrary.wiley.com/doi/abs/10.1029/2000JE001539.

[33] E. Doornbos et al. "Air Density and Wind Retrieval Using GOCE Data". In: *Proceedings of ESA Living Planet Symposium*. ESA. Bergen, Norway, 2010.

[34] Angelo Bassi et al. "Quantum Technologies in Space". In: *Experimental Astronomy* 51.3 (2021), pp. 1677–1694. DOI: 10.1007/s10686-021-09731-x.

[35] Antonio Genova. "ORACLE: A mission concept to study Mars' climate, surface and interior". In: *Acta Astronautica* 166 (2020), pp. 317–329. ISSN: 0094-5765. DOI: https://doi.org/10.1016/j.actaastro.2019.10.006. URL: https://www.sciencedirect.com/science/article/pii/S0094576519313128.

[36] European Space Agency. *Report on the Space Economy 2025*. Tech. rep. European Space Agency (ESA), 2025. URL: https://space-economy.esa.int/documents/tJMabTj61KkdGVOtF6SKw6wGSxicen6ajUWamCG3.pdf.

[37] Richard P. Kornfeld et al. "GRACE-FO: The Gravity Recovery and Climate Experiment Follow-On Mission". In: *Journal of Spacecraft and Rockets* 56.3 (2019), pp. 931–951. DOI: 10.2514/1.A34326.

[38] Klaus Abich et al. "GRACE-Follow On Laser Ranging Interferometer: German Contribution". In: *Proceedings of the International Conference on Space Optics (ICSO)*. Presented by DLR and partners from AEI and SpaceTech GmbH. European Space Agency (ESA). Antibes Juan-les-Pins, France, 2019.

[39] Jan Wüst et al. "Optical Iodine Clocks for Future GNSS". In: *Proceedings of the European Frequency and Time Forum (EFTF)*. Presented by German Aerospace Center (DLR). DLR, Ulm University, and partners. 2023.

[40] Jose Sanjuan et al. "Simultaneous laser frequency stabilization to an optical cavity and an iodine frequency reference". In: *Optics Letters* 46.2 (2021), pp. 360–363. DOI: 10.1364/OL.413419. URL: https://doi.org/10.1364/OL.413419.

[41] Malte Misfeldt et al. "Scale Factor Determination for the GRACE Follow-On Laser Ranging Interferometer Including Thermal Coupling". In: *Remote Sensing* 15.5 (2023), p. 1304. DOI: 10.3390/rs15051304. URL: https://doi.org/10.3390/rs15051304.

[42] Emily Rose Rees et al. "Absolute frequency readout derived from ULE cavity for next generation geodesy missions". In: *Optics Express* 29.16 (2021), pp. 26014–26025. DOI: 10.1364/OE.429392. URL: https://doi.org/10.1364/OE.429392.

[43] Alireza HosseiniArani et al. "Advances in Atom Interferometry and their Impacts on the Performance of Quantum Accelerometers On-board Future Satellite Gravity Missions". In: (2024). URL: https://arxiv.org/abs/2404.10471.

[44] European Space Agency. *STE-QUEST: Space-Time Explorer and Quantum Equivalence Principle Space Test – Assessment Study Report*. Tech. rep. ESA/SRE(2013)6. Assessment Study Report. Noordwijk, The Netherlands: European Space Agency, 2013. URL: https://sci.esa.int/documents/34375/35992/1567263162847-STE-QUEST%5C_Assessment%5C_Study%5C_Report.pdf.

[45] Marina Rezinkina and Claus Braxmaier. "Designs of Miniature Optomechanical Sensors for Measurements of Acceleration with Frequencies of Hundreds of Hertz". In: *Designs* 8.2 (2024). Accessed 16 June 2025, p. 67. DOI: 10.3390/designs8020067. URL: https://www.mdpi.com/2411-9660/8/2/67.

[46] Lee Kumanchnik, Marina Rezinkina, and Claus Braxmaier. "Choice of the Miniature Inertial Optomechanical Sensor Geometric Parameters with the Help of Their Mechanical Characteristics Modelling". In: *Micromachines* 14.8 (2023), p. 1685. ISSN: 2072-666X. DOI: 10.3390/mi14081685. URL: https://www.mdpi.com/2072-666X/14/8/1685.

[47] Yanwei Ding et al. "Progress on the Use of Satellite Technology for Gravity Exploration". In: *Journal of Geodesy and Geodynamics* 35.3 (2015), pp. 527–534. DOI: 10.1016/S1674-9847(15)30047-2. URL: http://jgg09.com/jweb%5C_ddcl%5C_en/EN/10.1016/S1674-9847(15)30047-2.

[48] Adrian Cho. "Coolest Science Ever Headed to the Space Station". In: *Science* (2017). Article on NASA's Cold Atom Laboratory mission. URL: https://www.science.org/content/article/coolest-science-ever-headed-space-station.

[49] Dr. Benjamin Knispel. *High-tech for surveying the world: funds provided*. Press release on GRACE Follow-On mission and Laser Ranging Interferometer development. 2013. URL: https://www.aei.mpg.de/197581/high-tech-for-surveying-the-world.

[50] James R. Wertz and Wiley J. Larson. *Space Mission Analysis and Design*. 3rd. El Segundo, CA and Dordrecht, Netherlands: Microcosm Press and Kluwer Academic Publishers, 1999. ISBN: 9781881883104.

[51] European Space Agency. *Call for a medium-size and a fast mission opportunity in ESA's science programme*. 2025.

[52] Richard W. Zurek and Suzanne E. Smrekar. "An overview of the Mars Reconnaissance Orbiter (MRO) science mission". In: *Journal of Geophysical Research: Planets* 112.E5 (2007), p. 1. DOI: https://doi.org/10.1029/2006JE002701.

[53] Kapish Aggarwal and Ron Noomen. "Graveyard orbits for future Mars missions". In: *Advances in Space Research* 72.7 (2023). Space Environment Management and Space Sustainability, pp. 2901–2916. ISSN: 0273-1177. DOI: https://doi.org/10.1016/j.asr.2022.07.023. URL: https://www.sciencedirect.com/science/article/pii/S027311772200624X.

[54] United Nations Committee on the Peaceful Uses of Outer Space. *Report of the Committee on the Peaceful Uses of Outer Space, Sixty-first session (20–29 June 2018)*. General Assembly Official Records, Seventy-third Session, Supplement No. 20 (A/73/20). 2018.

[55] Paul Erik Schabedoth. "Life Cycle Assessment of Rocket Launches and the Effects of the Propellant Choice on Their Environmental Performance". Master's thesis. Trondheim, Norway: Norwegian University of Science and Technology, 2020. URL:

https://ntnuopen.ntnu.no/ntnu-xmlui/bitstream/handle/11250/2779647/no.ntnu:inspera:57317890:36141261.pdf?sequence=1.

[56] European Cooperation for Space Standardization. *Space Sustainability: Planetary Protection*. 2019.

[57] Jürgen Knödlseder et al. "Estimate of the carbon footprint of astronomical research infrastructures". In: *Nature Astronomy* (2022). Published online 21 March 2022; originally posted as arXiv:2201.08748. DOI: 10.1038/s41550-022-01612-3. URL: https://arxiv.org/abs/2201.08748.

[58] Robbert J. Hamann. "Risk Assessment Tool for Hardware & Software". In: *Systems Engineering Coaching & Consultancy* ().

[59] Wiley J. Larson and James R. Wertz. *Space Mission Analysis and Design*. Kluwer Academic Publishers, 1992.

[60] Stacia M. Long et al. "Mars Reconnaissance Orbiter Aerobraking Daily Operations and Collision Avoidance". In: *Spacecraft Design, Testing and Performance*. 20th International Symposium on Space Flight Dynamics, 2007. URL: https://ntrs.nasa.gov/citations/20080012690.

[61] Hunter Williams Huu P. Trinh Christopher Burnside. "Assessment of MON-25/MMH Propellant System for Deep-Space Engines". In: *NASA Marshall Space Flight Center* ().

[62] Kelley Case, Gerhard Kruizinga, and Sien-Chong Wu. *GRACE Level 1B Data Product User Handbook*. Tech. rep. JPL D-22027. Version 1.3. Accessed: 2024-03-01. Jet Propulsion Laboratory, California Institute of Technology, 2010. URL: https://earth.esa.int/eogateway/documents/20142/37627/GRACE-L1B-Handbook-v1.3.pdf.

[63] Cornelius J. Dennehy, NASA Engineering, and Safety Center. *Spacecraft Micro-Vibration: A Survey of Problems, Experiences, and Mitigations*. "Propellant sloshing and control-structure interactions may also contribute to the spacecraft's internal disturbance environment". NASA Technical Reports Server, 2018. URL: https://ntrs.nasa.gov/api/citations/20180006315.

[64] Tengjie Gao, Hector Gutierrez, and Daniel Kirk. "Modeling Torsional Stiffness and Damping of Liquid Slosh in Spacecraft Diaphragm Tanks". In: *Journal of Spacecraft and Rockets* 62 (2024), pp. 1–14. DOI: 10.2514/1.A36019.

[65] Beate Klinger and Torsten Mayer-Gürr. "The role of accelerometer data calibration within GRACE gravity field recovery: Results from ITSG-Grace2016". In: *Advances in Space Research* 58.9 (2016), pp. 1597–1609. ISSN: 0273-1177. DOI: https://doi.org/10.1016/j.asr.2016.08.007. URL: https://www.sciencedirect.com/science/article/pii/S0273117716304409.

[66] arianegroup. *CHEMICAL BI-PROPELLANT THRUSTER FAMILY*. URL: https://ariane.group/app/uploads/2024/09/ArianeGroup_Chemical_Bipropellant_Thruster_Family.pdf.

[67] arianegroup. *PROPELLANT TANKS FOR MONOPROPELLANT AND BIPROPELLANT SYSTEMS*. URL: https://www.space-propulsion.com/brochures/propellant-tanks/spacecraft-propellant-tanks.pdf.

[68] MT Aerospace. *Spacecraft Propellant Tanks*. URL: https://www.mt-aerospace.de/files/mta/tankkatalog/MT-Tankkatalog.pdf.

[69] arianegroup. *PYROVALVES FILL, DRAIN AND VENT VALVES LATCH VALVES, FLOW CONTROL VALVE*. URL: https://www.space-propulsion.com/brochures/valves/space-propulsion-valves.pdf.

[70] Nammo. *Fill and Drain Valve*. URL: https://www.nammo.com/product/fdv-fvv/.

[71] Vacco Space Products. *3/8" LOW PRESSURE CHECK VALVE*. URL: https://www.vacco.com/images/uploads/pdfs/V1D10856-02.pdf.

[72] MOOG. *Helium Regulator*. URL: https://www.moog.com/content/dam/moog/literature/sdg/space/propulsion/moog-pneumatic-pressure-control-regulator-datasheet.pdf.

[73] bradford. *Off the shelf propulsion components*. URL: https://www.bradford-space.com/products/pressure-transducers.

[74] Airbus Defence and Space. *Elektro Power Processing Unit (PPU) for Hall Effect Thrusters*. URL: https://www.airbus.com/sites/g/files/jlcbta136/files/2024-06/Datasheet%20ELEKTRO%20PPU%20NG1.pdf.

[75] ST-100 Hall Effect Thruster. *Xenon Feed System*. URL: https://sets.space/wp-content/themes/sets-space/images/product-sheet/2023/ST-100.pdf.

[76] Space Electric Thruster Systems. *Xenon Feed System*. URL: https://sets.space/wp-content/themes/sets-space/images/product-sheet/2023/XFS.pdf.

[77] Yaguang Yang. *Spacecraft Modeling, Attitude Determination, and Control: Quaternion-Based Approach*. Boca Raton, FL; London; New York: CRC Press, Taylor & Francis Group, 2019. ISBN: 9781138331501.

[78] Aerosapce Research Center. *GRACE-FO: The Gravity Recovery and Climate Experiment Follow-On Mission*. 2019. URL: https://arc.aiaa.org/doi/10.2514/1.A34326.

[79] Shervin Shambayati Jim Taylor Dennis K. Lee. *Mars Reconissance Orbiter Telecommunications*. 2006. URL: https://descanso.jpl.nasa.gov/DPSummary/MRO%5C_092106.pdf.

[80] Jet Propulsion Laboratory. *Deep Space Network Antenna Positioning*. 2015. URL: https://deepspace.jpl.nasa.gov/dsndocs/810-005/302/302C.pdf.

[81] NASA. *Mars Global Surveyor Telecommunications*. 2001. URL: https://descanso.jpl.nasa.gov/DPSummary/MGS%5C_07Aug01.pdf.

[82] NASA. *Mars Communications Disruption and Delay*. 2023. URL: https://www.lpi.usra.edu/lunar/strategies/resources/M2M-ACR2023%5C_MarsCommunicationDisruptionDelay.pdf.

[83] NASA. *Horizons System*. URL: https://ssd.jpl.nasa.gov/horizons/tutorial.html.

[84] *UHF Antenna III*. 2025. URL: https://www.endurosat.com/products/uhf-antenna-iii/.

[85] Perot Systems Government Services. *A HIGH PERFORMANCE COMMAND AND DATA HANDLING SYSTEM FOR NASA'S LUNAR RECONNAISSANCE ORBITER*. 2009. URL: https://ntrs.nasa.gov/api/citations/20080032738/downloads/20080032738.pdf.

[86] Robert D. Karam. *Satellite Thermal Control for Systems Engineers*. Progress in Astronautics and Aeronatics. Reston, VA: American Institute of Aeronautics & Astronautics, 1998.

[87] Casper Versteeg and David L. Cotten. *Preliminary Thermal Analysis of Small Satellites*. Technical Report. Athens, Georgia: Small Satellite Research Laboratory, The University of Georgia, 2025. URL: https://s3vi.ndc.nasa.gov/ssri-kb/static/resources/Preliminary_Thermal_Analysis_of_Small_Satellites.pdf.

[88] Martyn J. Fogg. *Chapter 5. The Ecopoiesis of Mars*. SAE International, 1995.

[89] James B. Heaney. *Evaluation of Commercially Supplied Silver-Coated Teflon for Spacecraft Temperature-Control Usage*. NASA Technical Memorandum NASA TM X-70588. Preprint X-765-74-24. Greenbelt, Maryland: NASA Goddard Space Flight Center, 1974.

[90] H. Mesforoush et al. "Experimental and numerical analyses of thermal performance of a thin-film multi-layer insulation for satellite application". In: *Cryogenics* 102 (2019), pp. 77–84. ISSN: 0011-2275. DOI: https://doi.org/10.1016/j.cryogenics.2019.07.005. URL: https://www.sciencedirect.com/science/article/pii/S0011227519301183.

[91] Mukund R. Patel and Omid Beik. *Spacecraft Power Systems*. 2nd. Boca Raton, FL; Abingdon, Oxon, UK: CRC Press, 2024. ISBN: 978-1-032-38348-4 (hardcover), 978-1-032-38352-1 (paperback), 978-1-003-34460-5 (eBook). DOI: 10.1201/9781003344605.

[92] Reshma Ravindran and Ahmed M. Massoud. "State-of-the-Art DC-DC Converters for Satellite Applications: A Comprehensive Review". In: *Aerospace* 12.2 (2025), p. 97. DOI: 10.3390/aerospace12020097. URL: https://doi.org/10.3390/aerospace12020097.

[93] Grant Bonin et al. "Solar Array Arcing Mitigation for Polar Low-Earth Orbit Spacecraft". In: *Proceedings of the 24th Annual AIAA/USU Conference on Small Satellites*. SSC10-X-7. Logan, UT, USA: American Institute of Aeronautics and Astronautics, 2010, pp. 1–9. URL: https://utias-sfl.net/wp-content/uploads/SSC10-X-7.pdf.

[94] Arianespace. *Ariane 6 User's Manual*. Issue 2, retrieved from https://www.arianespace.com/ariane-6/. Arianespace. 2021.

[95] Tsuneji Rikitake. *Magnetic and Electromagnetic Shielding*. Berlin, Heidelberg: Springer-Verlag, 1987. ISBN: 978-3-540-17961-4. DOI: 10.1007/978-3-642-82832-3. URL: https://doi.org/10.1007/978-3-642-82832-3.

[96] Freissinet et al. "Investigating the effects of gamma radiation on selected chemicals for use in biosignature detection instruments on the surface of Jupiter's moon Europa". In: *Planetary and Space Science* 175.1-12 (2019). DOI: https://doi.org/10.1016/j.pss.2019.05.009. URL: https://www.sciencedirect.com/science/article/pii/S0032063318303830?via%3Dihub.

[97] F. Faccio. *COTS for the LHC radiation environment: the rules of the game*. Presentation or Internal Report. CH-1211 Geneva 23, Switzerland, n.d.

[98] S. Ryan and W. P. Schonberg. "A review of Whipple shield ballistic limit equations". In: *International Journal of Impact Engineering* 187 (2024), p. 104899. ISSN: 0734-743X. DOI: 10.1016/j.ijimpeng.2024.104899. URL: https://www.sciencedirect.com/science/article/pii/S0734743X24000241.

[99] Eric Christiansen et al. *Handbook for Designing MMOD Protection*. NASA Technical Handbook JSC-63677. NASA Johnson Space Center, 2009.

[100] Aopeng Xu et al. "Vibration compensation of an atom gravimeter". In: *Chinese Optics Letters* 17.7 (2019), p. 070201. DOI: 10.3788/COL201917.070201.

[101] Sivaganesh Kanmani Selvaraj and Mahendrakumar Mathialagu Madhavan. "Application of low modulus CFRP fabric for steel beams strengthening: Experimental and design validation". In: *Thin-Walled Structures* 208 (2025), p. 112625. ISSN: 0263-8231. DOI: 10.1016/j.tws.2024.112625. URL: https://doi.org/10.1016/j.tws.2024.112625.

[102] Association of Plastic Recyclers. "Life-Cycle Impact Assessment of Recycled HDPE". In: *Recycling Today* (2020).

[103] TRA-C industrie. "What are the ecological benefits of friction stir welding?" In: *TRA-C Industrie Blog* (2024).

[104] Laura Patricia Domínguez-Jaimes et al. "Growth of Anodic Layers on 304L Stainless Steel Using Fluoride-Free Electrolytes and Their Electrochemical Behavior in Chloride Solution". In: *Materials* 15.5 (2022), p. 1892. DOI: 10.3390/ma15051892.

[105] NASA Office of the Chief Engineer. *Expanded Guidance for NASA Systems Engineering: Volume 2 – Crosscutting Topics, Special Topics, and Appendices*. NASA Technical Report NASA/SP-20230009501. Accessed: 2025-06-18. Washington, DC: NASA Headquarters, 2023. URL: https://ntrs.nasa.gov/citations/20230009501.

[106] ESA Future Missions Department (SCI-F) Directorate of Science. *CALL FOR A MEDIUM-SIZE AND A FAST MISSION OPPORTUNITY IN ESA'S SCIENCE PROGRAMME -TECHNICAL ANNEX*. 2025.

[107] M. V. Cook. *The Aerodynamic Characteristics of Slender Bodies of Revolution*. Reports and Memoranda No. 3431, Aeronautical Research Council. London: Her Majesty's Stationery Office, 1965.

[108] A. Cervone et al. "The path towards increasing RAMS for novel complex missions based on CubeSat technology". In: *CEAS Space Journal* 16.2 (2023), pp. 203–224. DOI: 10.1007/s12567-023-00517-9.

[109] John Starl Peter Fortesque and Graham Swinerd. *Spacecraft System Engineering Third Edition*. Wiley, 2003.

[110] Malaya Kumar M Biswal and Ramesh Naidu Annavarapu. *Mars Missions Failure Report Assortment: Review and Conspectus*. arXiv preprint arXiv:1903.02461v2. Submitted 1 Mar 2019, revised 13 Jan 2021. 2021. URL: https://arxiv.org/abs/1903.02461v2.

[111] Roy E. Gladden. "Mars Reconnaissance Orbiter Telecommunications". In: *Proceedings of the AIAA/AAS Astrodynamics Specialist Conference*. 2008. DOI: 10.2514/6.2008-3353. URL: https://arc.aiaa.org/doi/pdf/10.2514/6.2008-3353.

[112] European Cooperation for Space Standardization (ECSS). *ECSS System Engineering – Glossary of Terms*. https://ecss.nl/wp-content/uploads/standards/ecss-s/ECSS-S-ST-00-01C1October2012.pdf. ECSS-S-ST-00-01C Rev. 1. 2012.

[113] Steve Koontz et al. *Safe and Reliable, All the Way to Mars and Back*. NASA Technical Memorandum NASA/TM–2014–08718. Houston, TX, USA: NASA Johnson Space Center, 2014. URL: https://ntrs.nasa.gov/api/citations/20140008718/downloads/20140008718.pdf.

[114] *Systems Engineering and Aerospace Design: Lecture AE3211-I-L02-EngineeringMethods-V19*. 2025.

[115] J. Hoffman H. L. Justh A. M. Dwyer Cianciolo. *Mars Global Reference Atmospheric Model (Mars-GRAM): User Guide*. 2021.

A Compliance Matrix

Table A.1: Compliance Matrix. Blue = Compliant, Green = Acceptable, Orange = Correctable, Red = Unacceptable

ID Old ID	Requirement	Compliance	Explanation
MIS-SCI-1.1 **UR-SUB-PAY-2.4.2.2.1**	The static gravity field of Mars shall be measured to a resolution of at least 360 d/o.	Comp	The static gravity field achieves a resolution of 380 d/o.
MIS-SCI-1.2 **UR-SUB-PAY-2.4.2.2.2**	The temporal gravity field of Mars shall be measured to a resolution of at least 30 d/o.	Comp	The temporal gravity field achieves a resolution of 360 d/o.
MIS-SCI-1.3 **UR-SUB-PAY-2.4.2.2.2**	The temporal gravity field of Mars shall be measured as a 30 sol timeseries.	Comp	The temporal gravity field is can be measured as a 30 sol timeseries because the spacecraft are on a 30 sol repeat orbit.
MIS-SCI-1.3.1 **UR-SUB-PAY-2.4.2.2.2**	The orbiter shall pass over the same points on the surface of Mars at least once every 30 sols.	Comp	The spacecraft are on a 30 sol repeat orbit.
MIS-SCI-1.4 **SUB-PAY-2.4.2.2.3**	The temporal gravity field of Mars shall be measured to a sensitivity of at least 0.0182 µGal/year.	Corr	The temporal gravity field is measured to a sensitivity of 3.73 µGal/year.
MIS-SCI-1.5	The mission shall analyse gravitational fluctuations with periods up to 1 Martian year at least.	Comp	The spacecraft perform science measurements for 1 Martian year.
MIS-SCI-1.5.1	The orbiter shall perform science measurements for at least 1 Martian year.	Comp	The spacecraft perform science measurements for 1 Martian year.
MIS-SCI-1.6	The mission shall gather gravity data on at least 95% of the Martian surface.	Comp	The near-polar orbit and extended mission lifetime ensure almost total coverage.
MIS-SCI-1.6.1	The orbiter shall have an orbital inclination between 85 and 95 degrees.	Comp	The orbit inclination is 92.4 degrees.
MIS-SCI-1.7	The measurements shall have at a minimum root-mean-square amplitude of 10^(-20) .	A	The achieved RMS amplitude is 10^(-19).
MIS-SCI-1.7.1	The optical link error of the measurement shall be at least 10^(-14)	A	A reasonable value of 10^(-12) is assumed, lower value must be requested to payload providers.

Continued on next page

Continued from previous page

ID + Old ID	Requirement	Compliance	Explanation
MIS-SCI-1.7.2	The separation of the two satellites shall be at most 58 km.	Comp	The spacecraft separation is 58 km.
MIS-SCI-1.8	The payload shall be capable of measuring acceleration along three orthogonal axes.	Comp	4 OMIS are included to measure in all directions.
MIS-ESA-2.1 **ESA-SYS-1.3.1.1**	The mission shall have a Cost at Completion ceiling of 670 million euros at 2025 economic conditions.	A	The current Cost at Completion is 715 million euros.
MIS-ESA-2.2	The mission shall launch no earlier than 2041.	Comp	The mission will launch in late 2041.
MIS-ESA-2.3 **ESA-SUB-PW-1.1.1.3**	The mission shall not incorporate Radioisotope Thermoelectric Generators.	Comp	The mission does not incorporate Radioisotope Thermoelectric Generators.
MIS-ESA-2.4 **UR-SYS-2.1.1.1**	Launch shall be performed with an ESA launcher.	Comp	The launcher is ESA's Ariane 62.
MIS-ESA-2.5	The mission shall comply with the COSPAR Policy on Planetary Protection.	Comp	Complied to policy in decommissioning strategy.
MIS-ESA-2.6 **ESA-MIS-1.1.1.1**	All mission activities shall comply with ESA's 2024/2041 Green Agenda standards	Comp	Incorporated sustainability through design process.
MIS-ESA-2.7 **UR-SYS-2.6.8.1.1**	All critical technologies shall be at a Technology Readiness Level of 6 according to the ISO scale by the end of the mission's definition phase.	Comp	The lowest TRL is 5 for the CAI, expected to be improved in the next few years.
MIS-UR-3.1 **UR-MIS-2.6.5.1**	All normal subsystems of the mission shall incorporate double redundancy.	Comp	All normal subsystems incorporate double redundancy.
MIS-UR-3.2 **UR-MIS-2.6.5.2**	All critical subsystems of the mission shall incorporate triple redundancy.	Comp	The batteries and CDHS incorporate triple redundancy.
MIS-UR-3.3 **UR-MIS-0**	The mission shall demonstrate the use of quantum technologies for interplanetary space missions.	Comp	The mission uses quantum sensing technologies.
SYS-UR-1.1	Each spacecraft shall have a maximum power generated of 1000W at EOL.	Comp	The solar arrays produce at most 930 W at EOL.

Continued on next page

Continued from previous page

ID + Old ID	Requirement	Compliance	Explanation
SYS-ESA-2.1	The spacecraft shall not incorporate Radioisotope Thermoelectric Generators.	Comp	The spacecraft do not incorporate Radioisotope Thermoelectric Generators.
SYS-ASTRO-3.1	The spacecraft shall provide 1308 m/s of V for Mars orbit injection and maneuvers during aerobraking.	Comp	Inclusion of a bipropellant propulsion system sized accordingly.
SYS-ASTRO-3.2	The spacecraft shall provide 49 m/s of V for stationkeeping.	Comp	Inclusion of an electric propulsion system sized accordingly.
SYS-ASTRO-3.3	The spacecraft shall provide 196 m/s of V for decommissioning.	Comp	Inclusion of an electric propulsion system sized accordingly.
SYS-ASTRO-3.4	The spacecraft shall be able to perform its Mars orbit injection burn in less than 1 hour.	Comp	Inclusion of a bipropellant propulsion system sized accordingly.
SYS-ASTRO-3.5	The spacecraft shall be able to perform a complete revolution around their y axis every orbit during science operations.	Comp	Inclusion of ADCS sized accordingly, simulation in dynamic attitude model.
SYS-ASTRO-3.6	The spacecraft shall be able to store the scientific data generated during the conjunctions of the Sun and Mars, lasting 24 days.	Comp	Inclusion of CDHS with 48 Gbytes of storage.
SYS-ASTRO-3.7	The spacecraft systems shall be compatible with a launch date between 2041 October 6-10.	Comp	The mission timeline is planned accordingly.
SYS-ASTRO-3.8	The spacecraft shall be able to perform multiple burns during insertion.	Comp	Inclusion of a bipropellant propulsion system sized accordingly.
SYS-PAY-4.1	The LRI laser source temperature shall not fluctuate by more than 0.1 K per orbit.	Comp	Inclusion of patch heaters, MLI and thermostats.
SYS-PAY-4.2	The LRI Triple Mirror Assembly temperature shall not fluctuate by more than 0.1 K per orbit.	Comp	Inclusion of patch heaters, MLI and thermostats.
SYS-PAY-4.3	The LRI cavity temperature shall not fluctuate by more than 1.5 K per orbit.	Comp	Inclusion of patch heaters, MLI and thermostats.
SYS-PAY-4.4	The CAI temperature shall not fluctuate by more than 0.1 K per orbit.	Comp	Inclusion of patch heaters, MLI and thermostats.
SYS-PAY-4.5	The LRI temperature shall be kept within the range of 27-33 °C.	Comp	Inclusion of patch heaters, MLI and thermostats.

Continued on next page

Continued from previous page

ID + Old ID	Requirement	Compliance	Explanation
SYS-PAY-4.6	The CAI temperature shall be kept within the range of 20-23 °C.	Comp	Inclusion of patch heaters, MLI and thermostats.
SYS-PAY-4.7	The spacecraft shall provide at least 0.1 mrad pointing accuracy in pitch when in nominal science mode.	Comp	Inclusion of ADCS sized accordingly, simulation in dynamic attitude model.
SYS-PAY-4.8	The spacecraft shall provide at least 0.1 mrad pointing accuracy in yaw when in nominal science mode.	Comp	Inclusion of ADCS sized accordingly, simulation in dynamic attitude model.
SYS-PAY-4.9	The spacecraft shall provide at least 0.25 mrad pointing accuracy in roll when in nominal science mode.	Comp	Inclusion of ADCS sized accordingly, simulation in dynamic attitude model.
SYS-PAY-4.10	The CAI shall be positioned in a single axis, along-track configuration.	Comp	In accordance with payload design.
SYS-PAY-4.11	The CMT shall provide a spacecraft trim capability of at least +- 5 mm in the X and Y axis.	A	Almost met by GRACE-FO's CMT, some development needed.
SYS-PAY-4.12	The CoM of the spacecraft shall be offset by less than 300 micrometers from integration to transfer orbit acquisition.	Comp	Achieved by GRACE-FO, spacecraft is highly symmetrical.
SYS-PAY-4.13	The CoM of the spacecraft shall not change more than 100 micrometers over the course of a six month period of science operations.	Comp	All tanks are placed symmetrically.
SYS-PAY-4.14	The spacecraft shall not produce vibrations that render science data unusable for more than 1% of science operations.	Comp	Propulsion operation time <1% of science operations.
SYS-PAY-4.15	The spacecraft shall be able to provide 234 W to the payload throughout the mission	Comp	Included in solar array sizing.
SYS-PAY-4.16 SUB-STRUC-2.6.1.3	The magnetic field external to the CAI shall be less than 10 mT.	Comp	Magnetic shielding for Hall Effect Thruster sized.
SYS-PAY-4.17	The spacecraft shall be able to downlink all of the 3.7 Gbits of payload data generated every day.	Comp	Included in TT&C downlink sizing.

Continued on next page

Continued from previous page

ID + Old ID	Requirement	Compliance	Explanation
SYS-PAY-4.18	The payload shall collect science data at a 10 Hz measurement rate.	Comp	In accordance with payload design and science.
SYS-PAY-4.19	The absolute knowledge of laser frequency at time scales greater than 10,000 seconds shall have a fractional sensitivity of 10^-8 or better.	Comp	Inclusion of Iodine Reference Unit.
SYS-PAY-4.20	The spacecraft shall have an absolute frequency reference, with stability of 10^-14 for observation times >100s.	Comp	Inclusion of Iodine Reference Unit.
SYS-LNCH-5.1	Each spacecraft shall have a maximum launch mass of 1450 kg.	Comp	The wet mass per spacecraft is 1124.2 kg.
SYS-LNCH-5.2	The undeployed spacecraft shall fit within the payload compartment of the Ariane 62 Short Dual Launch Structure configuration.	Comp	Launch fit check has been performed.
SYS-LNCH-5.2.1 UR-SYS-2.1.1.3	The undeployed spacecraft shall have a maximum height of 4.30 m.	Comp	The spacecraft height is under 4 m.
SYS-LNCH-5.2.2 UR-SYS-2.1.1.4	The undeployed cross section of each spacecraft shall allow the 2 spacecraft to fit within a circular cross-sectional of diameter 4.6 m	Comp	Dimension fit check has been performed.
SYS-LNCH-5.3	The spacecraft shall be able to withstand the mechanical environment of launch aboard an Ariane 62 launch vehicle.	Comp	Structures sized accordingly.
SYS-LNCH-5.3.1 SUB-STRUC-2.1.2.1.2.1	The spacecraft shall withstand a maximum axial g load of magnitude 6 without failing in Euler buckling.	Comp	Structures sized accordingly.
SYS-LNCH-5.3.2	The spacecraft shall withstand a maximum axial g load of magnitude 6 without failing in yielding.	Comp	Structures sized accordingly.
SYS-LNCH-5.3.3	The spacecraft shall withstand a maximum axial g load of magnitude 6 without failing at the ultimate load limit.	Comp	Structures sized accordingly.

Continued on next page

Continued from previous page

ID + Old ID	Requirement	Compliance	Explanation
SYS-LNCH-5.3.4 SUB-STRUC-2.1.2.1.2.2	The spacecraft shall withstand a maximum lateral g load of magnitude 2 without failing in Euler buckling.	Comp	Structures sized accordingly.
SYS-LNCH-5.3.5	The spacecraft shall withstand a maximum lateral g load of magnitude 2 without failing in yielding.	Comp	Structures sized accordingly.
SYS-LNCH-5.3.6	The spacecraft shall withstand a maximum lateral g load of magnitude 2 without failing at the ultimate load limit.	Comp	Structures sized accordingly.
SYS-LNCH-5.3.7 SUB-STRUC-2.1.2.1.2.3	The spacecraft shall have a fundamental axial natural frequency greater than 20 Hz.	Comp	Structures sized accordingly.
SYS-LNCH-5.3.8 SUB-STRUC-2.1.2.1.2.4	The spacecraft shall have a fundamental lateral natural frequency greater than 6 Hz.	Comp	Structures sized accordingly.
SYS-RISK-8.10	The spacecraft critical surfaces and subsystems shall withstand MMOD impacts from particles of up to 0.01 kg mass, 2700 kg/m^3 density, and 20 km/s relative velocity without loss of structural integrity or functionality.	Comp	Structures sized accordingly.
SYS-RISK-8.11	The spacecraft critical surfaces and subsystems shall withstand a TID of 20.8 rad without degradation in functionality.	Comp	Structures sized accordingly.
SYS-COMM-6.1	The spacecraft shall be able to downlink all of the 22 Mb of telemetry data generated every day.	Comp	TT&C subsystem sized accordingly.
SYS-COMM-6.2	The 2 spacecraft shall be able to communicate with each other at all times.	Comp	TT&C subsystem sized accordingly.
SYS-COMM-6.3	All link margins shall close with at least 3 dB clearance.	Comp	TT&C subsystem sized accordingly.
SYS-COMM-6.4	The spacecraft shall be able to store commands.	Comp	CDHS sized accordingly.
SYS-COMM-6.5	The spacecraft shall be able to distribute commands.	Comp	CDHS sized accordingly.

Continued on next page

Continued from previous page

ID + Old ID	Requirement	Compliance	Explanation
SYS-COMM-6.6	The spacecraft shall be able to gather telemetry data from the spacecraft	Comp	CDHS sized accordingly.
SYS-COMM-6.7	The spacecraft shall be able to store science data during all mission phases.	Comp	CDHS sized accordingly.
SYS-COMM-6.8	The spacecraft shall be able to receive uplink data of 37.8 MB every day.	Comp	TT&C subsystem sized accordingly.
SYS-COMM-6.9	The spacecraft shall be able to establish communications with Earth under all conditions excluding the conjuntion of the Sun and Mars, and while in eclipse relative to the Earth.	Comp	TT&C subsystem sized accordingly.
SYS-FUNC-7.1	The spacecraft shall be able to provide power to all subsystems during eclipse, with equivalent length of 2.43% of the orbital period.	Comp	Power subsystem sized accordingly.
SYS-FUNC-7.2	The spacecraft shall be able to provide power to all subsystems during power surges.	Comp	Batteries sized accordingly.
SYS-FUNC-7.3	Each spacecraft shall maintain all components within their survival temperature range during the whole mission	Comp	Thermal subsystem sized accordingly.
SYS-FUNC-7.4	Each spacecraft shall maintain all components within their operational temperature range during operation	Comp	Thermal subsystem sized accordingly.
SYS-FUNC-7.5	The spacecraft shall be able to maintain a coarse pointing accuracy of 40 mrad.	Comp	ADCS subsystem sized accordingly.
SYS-FUNC-7.6	The spacecraft shall be able to recover from a 5 degree per second tumble	Comp	ADCS subsystem sized accordingly.
SYS-FUNC-7.7	The spacecraft shall be able to provide power to all subsystems during all times of the Martian year.	Comp	Power subsystem sized for maximum Mars-Sun distance.
SYS-RISK-8.8	The spacecraft shall employ double redundancy for inter satellite communication.	Comp	TT&C subsystem sized accordingly.

B Project Design and Development Logic

The Project Design and Development Logic is presented in Figure B.1, detailing the logical order of activities to be performed in the post-DSE phases of the mission.

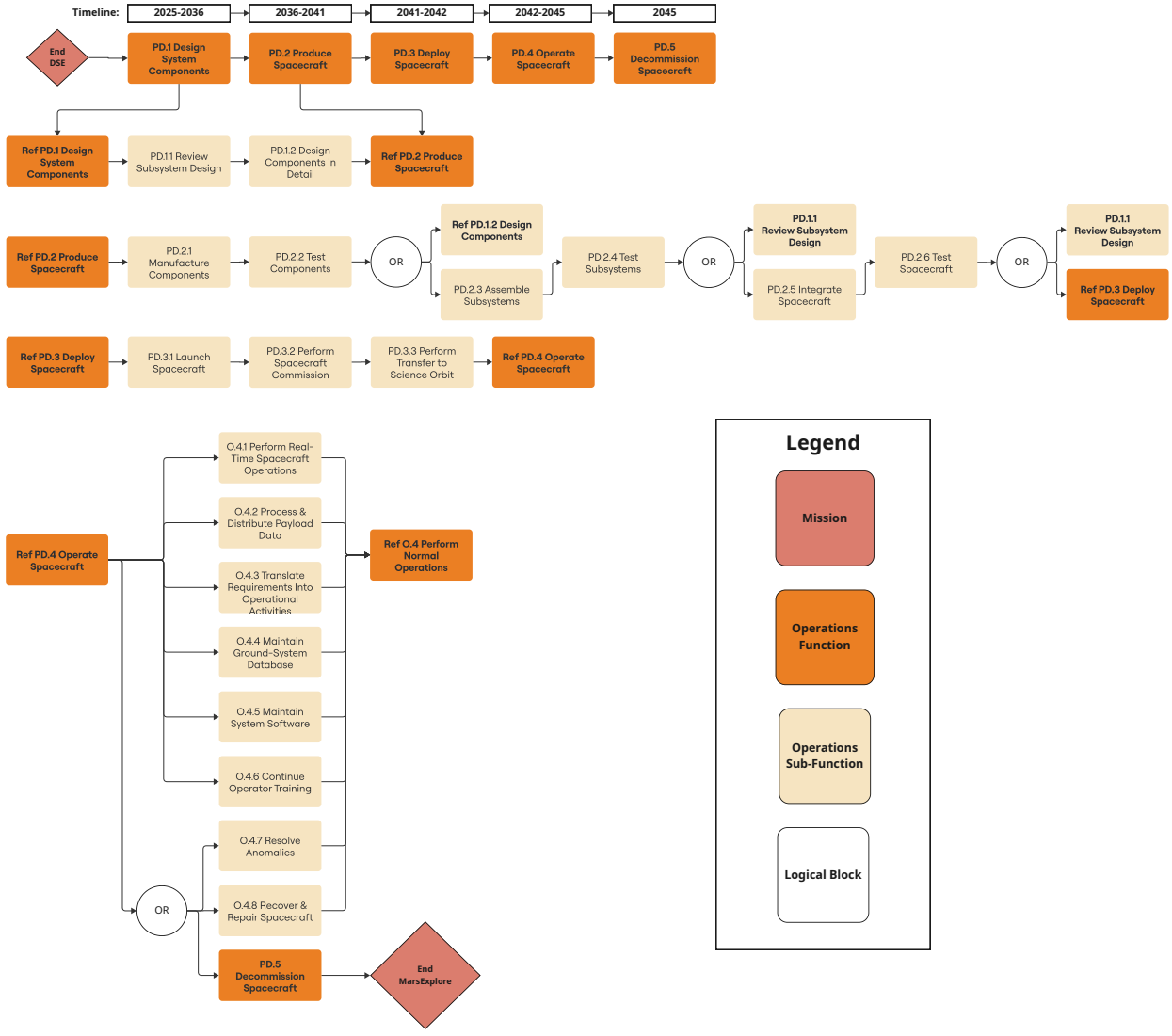

Figure B.1: Project Design and Development Logic

C Additional Risks

Additional risks are presented in the following tables.

Table C.1: Commissioning of Spacecraft

ID	Risk
TR24	Thruster valve failure (inability to actuate burns)
TR25	Fuel leakage
TR26	Pressurization system failure
TR27	Mechanical deployment failure (e.g. solar panels)
TR28	Battery failure
TR29	Antenna deployment failure
TR30	Ground station misalignment
TR31	Incorrect frequency setup
TR32	Inactive heaters or radiators
TR33	Thermal sensors error
TR34	Initial attitude not established

Table C.2: Subsystem failures

ID	Risk
TR41	Engine failure
TR42	Inadequate power generation due to degredation
TR43	Power generation failure
TR44	Power distribution failure/malfunction
TR45	Damaging of antenna
TR46	Temporary loss of communication link
TR47	Degradation of communication hardware
TR48	Data corruption
TR49	Thermal control degradation
TR50	Thermal sensor drifting
TR51	Thermal regulation failure
TR52	Attitude determination failure
TR53	Attitude control failure
TR54	Data handling errors
TR55	Data storage failure
TR56	Payload instrument degradation
TR57	Payload instrument damage (solar flare, radiation...)
TR58	Structural fatigue failure
TR60	Failure of structure to withstand loads

Table C.3: Phase-Specific Risks

ID	Risk	Mission Phase
TR13	Supply chain delays	Phase D
TR14	Delays in verification	Phase D
TR16	Missing launch window	Phase E
TR69	Incorrect communication of commands to SC during aerobraking maneuver	Phase E
TR70	Safe mode activates during aerobraking maneuver	Phase E
TR23	Incorrect trajectory insertion	Phase E
TR38	Degradation of calibration references	Phase F
TR40	Communication failure with subsystems	Phase F
TR63	Lack of feedback for future missions	Phase G